"Temporal coding and cellular synchronisation in the superior colliculus"

Pauluis, Quentin

Document type : *Thèse (Dissertation)*

UNIVERSITE CATHOLIQUE DE LOUVAIN
Faculté de Médecine
Département de Physiologie et de Pharmacologie
Unité de Neurophysiologie

TEMPORAL CODING AND CELLULAR SYNCHRONISATION IN THE SUPERIOR COLLICULUS

by

Quentin PAULUIS, M.D.

Thesis submitted in partial fulfillment of the requirements
for the degree of "Docteur en Sciences médicales"
Preparatory document

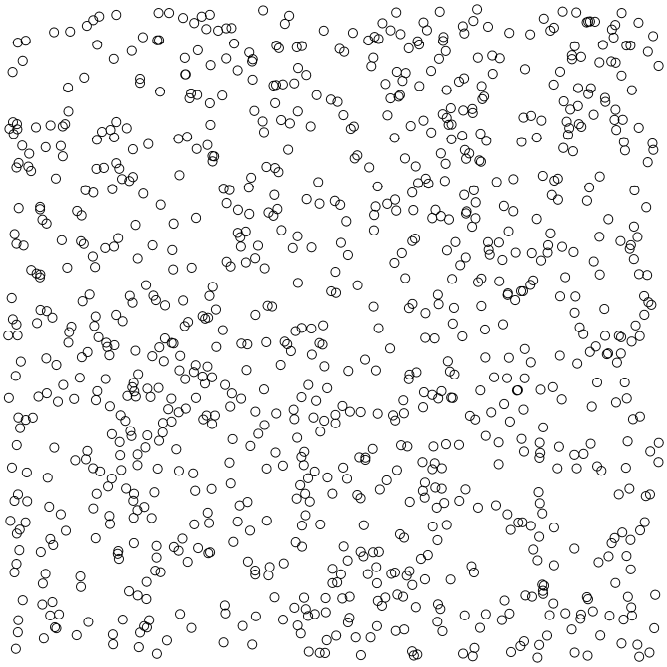

Promoter : Pr Etienne OLIVIER
Co-promoter : Dr Stuart BAKER

1999

UNIVERSITE CATHOLIQUE DE LOUVAIN
Faculté de Médecine
Département de Physiologie et de Pharmacologie
Unité de Neurophysiologie

TEMPORAL CODING AND CELLULAR SYNCHRONISATION IN THE SUPERIOR COLLICULUS

by

Quentin PAULUIS, M.D.

Thesis submitted in partial fulfillment of the requirements
for the degree of "Docteur en Sciences médicales"
Preparatory document

Jury

Pr Marc CROMMELINCK, President
Pr Etienne OLIVIER, Promoter
Dr Stuart BAKER, Co-Promoter
Pr Jean-Michel GUERIT
Dr David HANSEL
Pr Léon PLAGHKI
Dr Pieter ROELFSEMA

1999

CONTENTS

LIST OF ABBREVIATIONS

ACH : auto-correlation histogram

CCH : cross-correlation histogram

CE : coincident event

EEG : electroencephalogram

EMG : electromyogram

GABA : gamma-aminobutyric acid (inhibitory neurotransmitter)

ISI : interspike interval

NMDA : N-methyl-D-Aspartate (excitatory neurotransmitter)

RMA : relative modulation amplitude

SC : superior colliculus

A distinguished theorist has recently written, "no theory or model of brain function has survived its birth by more than a decade, and most die in infancy". I believe this is due to our ignorance of the local cortical operation.

Vernon Mountcastle, 1995.

Chapter 1 Introduction

By studying the dynamics of local neuronal network activity, this thesis considers the controversial hypothesis of "temporal coding", which could be formulated as follows:

Does the precise moment at which a spike occurs mean something in terms of information processing?

After briefly reviewing the history, this introduction develops various hypotheses of temporal coding which are not exclusive. These hypotheses are divided into four classes: namely the binding theory; the synfire chains; the time advance coding scheme; and the timed neuronal selection.

Next comes a survey of some brain areas where synchrony and oscillations were evidenced and where interesting experiments were conducted.

The last part is devoted to the physiology of the superior colliculus where cellular recordings presented in Chap. 4 were made.

1. History and Background

1.1 Neurons

Neurophysiology became a real philosophical theory during the 20th century. This "neurophilosophy" has the advantage of being based on facts and reproducible experiments. Would Plato or Aristotle believe that knowledge of the function of nerves, tendons or ligaments was metaphysics? Although the brain has been thought to be the center of the intelligence since Hippocrates (460-379 B.C.) and Galien (A.D. 130-200), explanations of

brain mechanisms remained inaccurate and even fanciful until the detailed description of the brain cells. The compound microscope was developed in the late 17th century, but methods to harden the brain tissue were discovered only one century later. However, even at that time, brain tissue had a uniform appearance under microscope. At the turn of the 20th century, stains were introduced that could selectively color the neuron nuclei of the brain cells, like the Nissl stain. The Italian histologist Camillo Golgi found another staining technique able to describe neurons in their entirety, that is the cell body – or soma – and some thin tubes that radiate away from the soma, called neurites. He shared the Nobel prize in 1906 with Santiago Ramon y Cajal who worked out the circuitry of many regions of the brain.

1.2 Dynamics

At the same time, the electrical excitability of the cortex was discovered, leading to the description of the reflex organization of the spinal cord by Sir Sherrington and the first ideas about the cortical function. It was understood in terms of successive superimposition of reflex loops (Mountcastle, 1995). First descriptions of the electroencephalogram by Berger were published between 1929 and 1931, showing correlations between EEG patterns and behavioral states. Today the cortex is thought to be a widely distributed system. In the macaque cortex, 72 functionally specialized areas have been identified, and 758 inter-areal connections which represent only 15 % of the theoretical possibilities (Mountcastle, 1995). Sensory and motor areas are organized in a columnar manner. Each column extends over 300 to 600 μm and contains several hundred microcolumns of 80 to 100 neurons, heavily interconnected in the vertical dimension (Mountcastle, 1995).

Neurophilosophy belongs to the monistic theory, called after the "monad", which is an indivisible unit possessing both mental and physical characteristics. It is a complicated way to say that spirit - or soul - cannot be dissociated from the body, and that every thought is the product of brain activity and biophysical laws. However, this does not necessarily mean that the activity is deterministic: indeed, it can be unpredictable because of its complexity.

Brain complexity is astonishing: 10 billion excitatory or inhibitory neurons, each connected to thousands of others and able to discharge and to change their connectivity during tens of years... The properties of such a system are likely to be emergent. The system properties are not the simple result of summing properties over the elements of the population, but emerge from their dynamic interactions.

"Mind and brain are not identical, no more than lung and respiration are identical" (Mountcastle,1995).

1.3 Cerebral code

What is coded by the brain cells ? Where ? When ? All these questions are at stake in today's neurophysiology. Recordings of single cortical neurons in the sixties led to important notions of cell receptive fields and firing rate code. Sensory neurons were characterized by the zone of the visual space, the area on the skin, or the range of sound frequencies within which an adequate stimulus would elicit the maximum number of action potentials. Neurons were also selectively responsive to features of the sensory stimuli that were not signaled by any of their afferent fibers, like orientation and direction of moving bars in the visual cortex. This orientation and direction detection was an emergent feature of the local network and led to the notion of orientation columns. Neurons with the same orientation selectivity are closely localized in a columnar fashion, so that direction selectivity and receptive field do not vary across the different layers of the gray matter. Since cells discharge maximally for a given stimulus orientation, their firing rate is thought to code the correspondence between stimulus and neuronal properties.

A single object will elicit an increase of activity in some cell populations, whose properties correspond best to the object, and an activity decrease in some others. This principle is so general that it is not debated. Next comes the differentiation problem : how will the presentation of an object be different from the presentation of another object ? The existence of specialized areas organized in a somewhat hierarchical fashion led to the idea that groups of neurons are activated sequentially and very specifically, until one cell or a few cells specific to only one object, are finally activated. However this equivalence between one object and one cell is unrealistic, because of the enormous number of cells that would be required to code all the possible combinations of object features. Instead, object coding by groups of neurons is now well accepted. What is specific to the object, is the combination of recruited cells, called the “cell-assembly” by Hebb (1949). In the motor cortex and in the superior colliculus, such ensemble coding is extended by the notion of the population vector (Georgopoulos et al., 1989, 1995; Schwartz 1993, 1994; Lee et al.1988). In a cell population, each cell has a preferred direction. The movement coded by the population is the average of the individual cell preferred directions, weighted by their firing rate. As a consequence, on the motor side as well, there is no specific cell which would code a particular movement.

The second problem is related to the present work. How can two objects be coded separately yet simultaneously by a widely distributed system ? This question would have been answered easily if we had accepted the idea of an object specific cell, but since two objects are coded by two different groups of separated neurons, how can a neuron discharge be referred to one object and not to the other ? This is the binding problem: what glues together hundreds of neurons coding the same object although they are dispersed in various brain areas ? What differentiates them from another cell-assembly that codes a second object ?

The proposed answer is synchrony (Singer et Gray, 1995). All cells coding the same object would discharge at the same time. And if two objects were presented, cells of one group would discharge at different times from cells of the second group. It is like multiplexing information in a unique temporal dimension. This hypothesis will be detailed below. Synchrony could also answer different sorts of problems which will be reviewed : information transfer, learning, timed neuronal selection, and time advance coding schemes.

The notion of a temporal code brings together all these theories and opposes them to the usual firing rate code. All of these temporal coding theories assert that the exact moment at which a cell discharges is not random and contains some kind of information about how the information is processed by the system.

1.4 Synchronization mechanisms

At this stage, it could be interesting to distinguish synchrony and oscillations, and to review briefly how some neurons could synchronize.

Synchrony is the simultaneous occurrence of an action potential in two cells. In this context, when two cell are synchronized, it is supposed that their spikes occur at the same time more often than expected by chance (i.e. the product of their firing rate).

Oscillation refers to the periodic occurrence of synchronized spikes. If the neurons emit synchronous spikes every 25 ms, their relationship is called oscillatory and the oscillation frequency is determined by the reciprocal of the mean interval between synchronous spikes, *1/25 ms = 40 Hz*. If the cells are synchronized at variable intervals, no period emerges and they are just non-oscillatory synchronized cells. A technical background is provided in Appendix to familiarize the reader with the assessment of synchrony and oscillations in the cross-correlation histogram (CCH).

Although Wilson and Cowan (1972) first demonstrated that oscillations could occur when two mathematical variables – representing the population firing rates in excitatory and inhibitory neurons – are coupled, it remained to show that cells which emit discrete action potentials could synchronize and oscillate in the same way.

Theoretical studies demonstrated that excitatory coupling could not stabilize in-phase synchronization (Tsodyks et al. 1993; Hansel et al., 1995), except if the cellular interaction were instantaneous (Mirollo and Strogatz, 1990). Another anecdotal case of synchronization in a network of excitatory cell was synchronization on an identical refractory period. Networks with delayed excitatory coupling could converge to a periodic solution but neurons do not necessarily fire in unison and many different combinations are possible (Gerstner; 1996).

On the contrary, *inhibitory* connections could lead to synchronized firing (van Vreeswijck et al., 1994). It was shown for the first time in the rat hippocampus, that oscillations in the gamma frequency are an emergent property of networks which includes mutually interconnected inhibitory interneurons (Whittington et al., 1995; Traub et al, 1996; Wang an Buszaki, 1996; White 1997). Such oscillations pace the firing pattern of excitatory cells and gate temporally afferent inputs (Burchell et al. 1998). The basic idea is that after the activity in the inhibitory population rose quickly, the network activity was brutally inhibited. If the input is maintained the cycle is repeated.

These models have been applied to the cortical network, each of them including different features and assuming more or less complicated cell model and connectivity (Bush P, Sejnowski T, 1996; Hansel and Sompolinsky, 1996; van Vreeswijck and Sompolinsky, 1998).

Some authors also suggested the possibility that the oscillations observed between cortical cells were driven from oscillatory subcortical inputs (Ghose and Freeman, 1997).

The second chapter of this thesis is devoted to the analysis of the dynamics of a large neural network and explains how changing the parameters related to the inhibitory cells modifies the network oscillations. Indeed, in most cases, the oscillation period depends on the duration of the inhibitory post-synaptic potentials. Some other configurations could exist in the thalamus or in the cerebellum, but they always depend on the population resetting by some inhibitory cells. They will be reviewed in further sections.

2. Temporal Coding Hypotheses

2.1 The binding theory

2.1.1 Gestalt Psychology

One of the most entertaining subjects in neuroscience is image processing by the central nervous system. Everybody has experienced the perception switching which occurs when looking at some ambiguous drawings, like in Fig.1. The perception switches from one subject to the other although the image does not change. This phenomenon has been used by some psychologists to argue that image processing depends on the sensations *and* on subject's expectations. The same principle is applied in the Rorschach test, in which the patient is asked to interpret inkblot figures.

A B

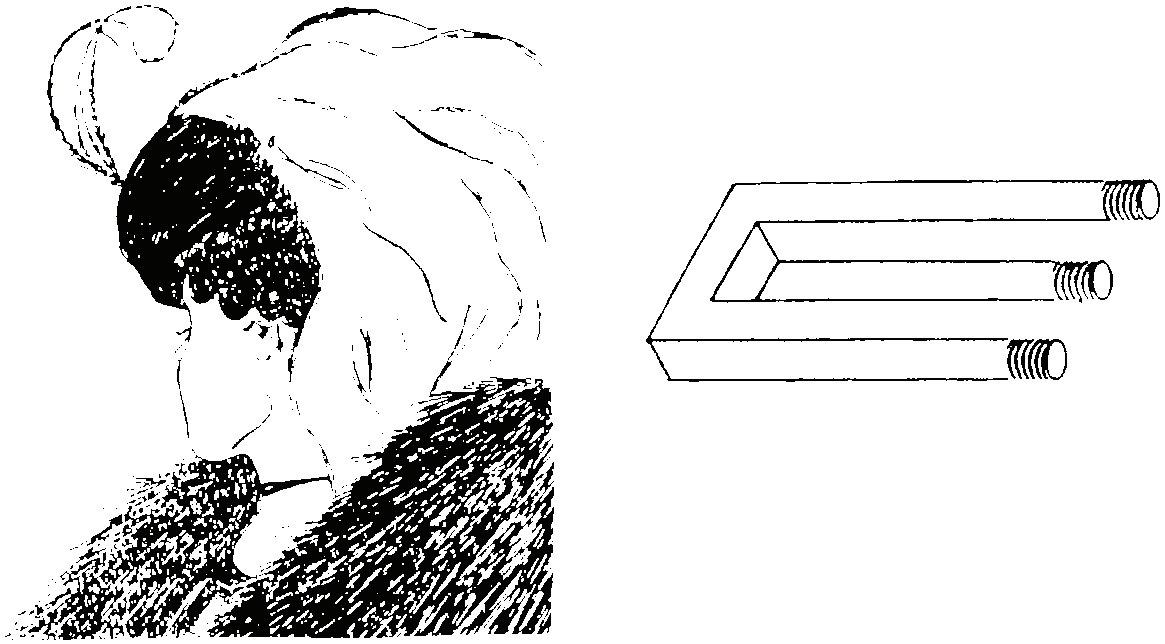

Figure 1. Ambiguous drawings. On the left, you can see a young woman with a necklace, or an old hook-nosed sorcerer (anonymous). On the right, there is another famous illusion. Some small changes in connectivity modify the perception of the number of pegs.

The Gestalt psychologists provided at the beginning of this century a more detailed analysis of the criteria, according to which the visual system groups elements into a coherent image. *Gestalt* is German for "shape" or "pattern", or even "configuration", as suggested by Rock and Palmer (1990). The Gestalt laws of grouping were proximity, similarity, closure, and good continuation. Rock and Palmer also proposed two new laws: connectedness and

enclosure (see Fig. 2). Gestalt psychologists also showed that expectation could help the system to perform correctly. At first sight, Figure 3 is just a spotted area. However, after the recognition of the Dalmatian dog, next readings are dramatically enhanced. Not surprisingly, it was found by the Gestalt physiologists that one of the most important criteria that help the visual system to regroup objects is the connectedness. Figure 3 is difficult to recognize because parts were not connected. Present theory assumes that in order to perform the binding of the different spots into one coherent shape, the visual system has to be primed by higher associative inputs from other cortical areas. Shape recognition would be achieved by the synchronization of cells coding for parts of the dog, and further synchronization with higher brain structure would lead to the dog recognition.

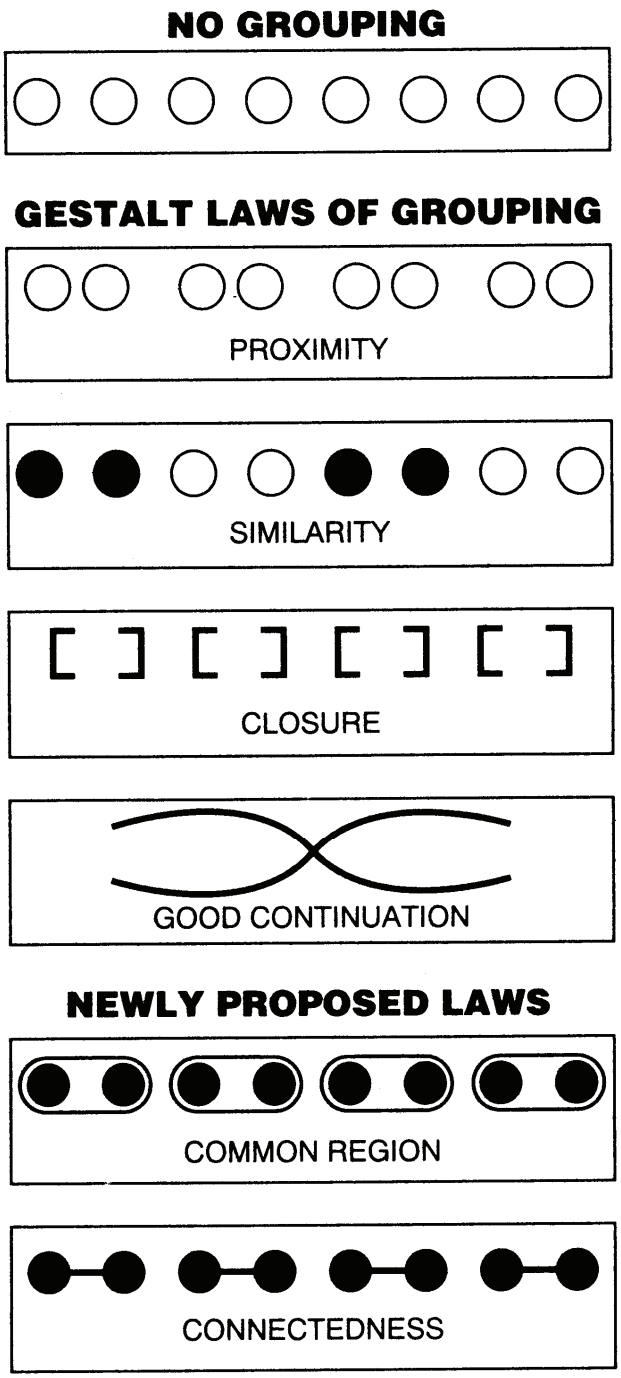

Figure 2. Grouping laws. These laws have been first proposed by Werheimer who launched in 1912 the gestalt psychology at the Institute of Psychology in Frankfurt am Main. Two new laws were introduced recently by Rock and Palmer (from Rock and Palmer, 1990).

Figure 3. After some delay, and especially if it suggested, it is possible to distinguish a Dalmatian dog (from Eckhorn, 1994; modified from James, 1966)

Demonstration of the importance of contour connection is straightforward. Parts of the objects, if not connected, are difficult to bind together. In Fig. 1B, some minor and local changes in connectedness are able to modify completely how a scene is perceived.

Although connectedness is important for scene segmentation and seems a natural process, its implementation on a computer or in an artificial neural network is not simple (Roelfsema and Singer, 1998). A mathematical approach would lead to a precise and extensive calculation of the various possible combinations between each pixel, and then testing the observed pattern with these combinations. A feed-forward artificial neural network would also require a large number of units to store all possible ways by which two pixels could be connected. This combinatorial explosion is akin to the problem of coding for a large panel of various objects, with object specific cells.

Probably the best way to compute connectedness is simply to start looking at one point, check if it has similar neighbors, store the new neighbors in a buffer, and test the buffer points until it is empty. Each time the buffer is empty, one group has been identified, and the algorithm should look at the next unchecked point. This algorithm can easily answer the question of binding between two points (Fig. 4) and is very efficient. Moreover, it is naturally implemented by recurrent neural networks which are able to perform all the local comparisons simultaneously. This is achieved if neighboring units are able to transmit a tag to their neighbors, but only to those representing positive pixels. In both cases, connectedness is naturally implemented as a transitive process: if A is connected to B, and B to C, A should be

connected to C. The idea advanced by Roelfsema and Singer (1998) is that the visual cortex computes connectedness similarly.

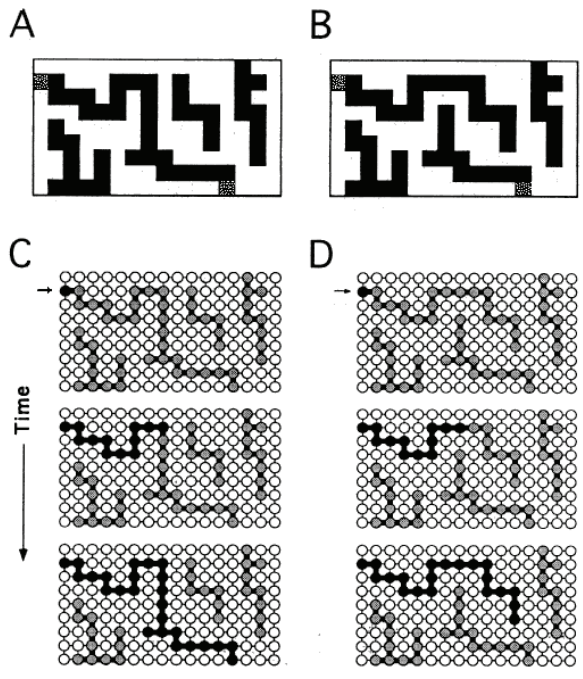

Figure 4. A serial algorithm for connectedness detection. (A) Image in which the two gray tiles are connected. (B) Slightly modified image in which the two gray tiles are not connected. (C) Schematic illustration of the interactions. Neurons that have been activated have been indicated in gray. In order to detect connectedness, a "tag" (black) is spread among activated neurons, starting at the arrow. This tag only propagates to neighboring neurons that are also activated. (D) A local change in the image results in a global change in the tag-spreading process (from Roelfsema and Singer, 1998).

A first possible tag is an enhancement of the neuron response. Two cells would discharge higher if they responded to the same object. The second possible tag is synchronization of cell discharges. Two cells would discharge repetitively exactly at the same time if they were activated by the same object. These two tags are not exclusive but it is important to understand that only synchrony allows a distinction between two different objects. Indeed, if two groups simultaneously increase their firing rate, nothing differentiates them anymore. Enhanced activity would be interesting only to differentiate foreground from background. Moreover, it interferes with the cell ability to code correspondence between the object and cell preferences. For example, a high discharge rate in a cell coding red color could be due to a single red point, or to a large orange object (Roelfsema and Singer, 1998).

Finally, when the problem of natural visual processing is addressed, coherent movement has to be considered as another very potent law of grouping. On the one hand, the movements of two objects are usually not correlated, and on the other hand, some separated points could be grouped together if they move coherently. Look, for example, at the cover figure and slide the bookmark. Professor Ad Aertsen starts talks about binding theory with this amusing experiment. Moreover it is well known that small accelerations elicit locked cell responses that are precisely synchronized (Kruse and Eckorn, 1996). In a natural environment, such

stimulus locked activities are prone to very efficiently separating responding cells into various groups that discharge at different times.

2.1.2 Synchronous neuronal assembly

The statement of the binding theory is : cells that discharge in reference to the same object emit spikes at exactly the same time, with a precision of a few milliseconds, forming a synchronous neuronal assembly. Other active cells tend to discharge at another moment, when the first group is silent.

As long as the neurons were considered as integrators with membrane time constant of tens of milliseconds, such a hypothesis would be inconceivable because neuronal time precision depends directly on the duration of the synaptic integration. Coincidence detection has long been suspected (Abeles, 1982; König et al., 1994) and its advantages for sensory segmentation were first pointed out by von der Malsburg and Schneider (1986). This first theory was termed the Correlation theory, and was illustrated by a simple network of one inhibitory neuron and 20 excitatory cells, which were able to form two coherent groups in response to two different stimuli.

One of the key experiments is shown in Fig. 5 for the anesthetized cat (Engel et al. 1991b), and it has been reproduced in the conscious monkey (Kreiter and Singer 1994). Four groups of cells with similar receptive fields but different preferred orientation are recorded when presenting one or two moving light bars. During the first part of the experiment, only one bar is presented with different orientations. When a vertical moving bar is presented to pair 1-3, the cross-correlation histogram (Fig. 5A) exhibits a central peak which suggests that spikes of group 3 cells tend to occur at the same time as spikes of group 1. In other words, both groups are synchronized. Satellite peaks at +/- 22 ms show that cells synchronize at some regular intervals, that is they are somewhat oscillatory. In Fig. 5B, groups 2 and 4 are synchronized when a horizontal moving bar is presented. When the moving bar is oblique (Fig. 5C), synchronization is demonstrated between groups 2 and 3 although the orientation is not optimal. The second part of the experiment (Fig. 5D) is shown in the right column: a horizontal and a vertical bar are presented simultaneously. The two first pairs of groups are still synchronized but groups 2 and 3 now discharge independently. As a consequence, cells can be described as belonging to two different groups responding to each moving bar. And reciprocally, each group is characterized by the exact moments of constituting cell discharge.

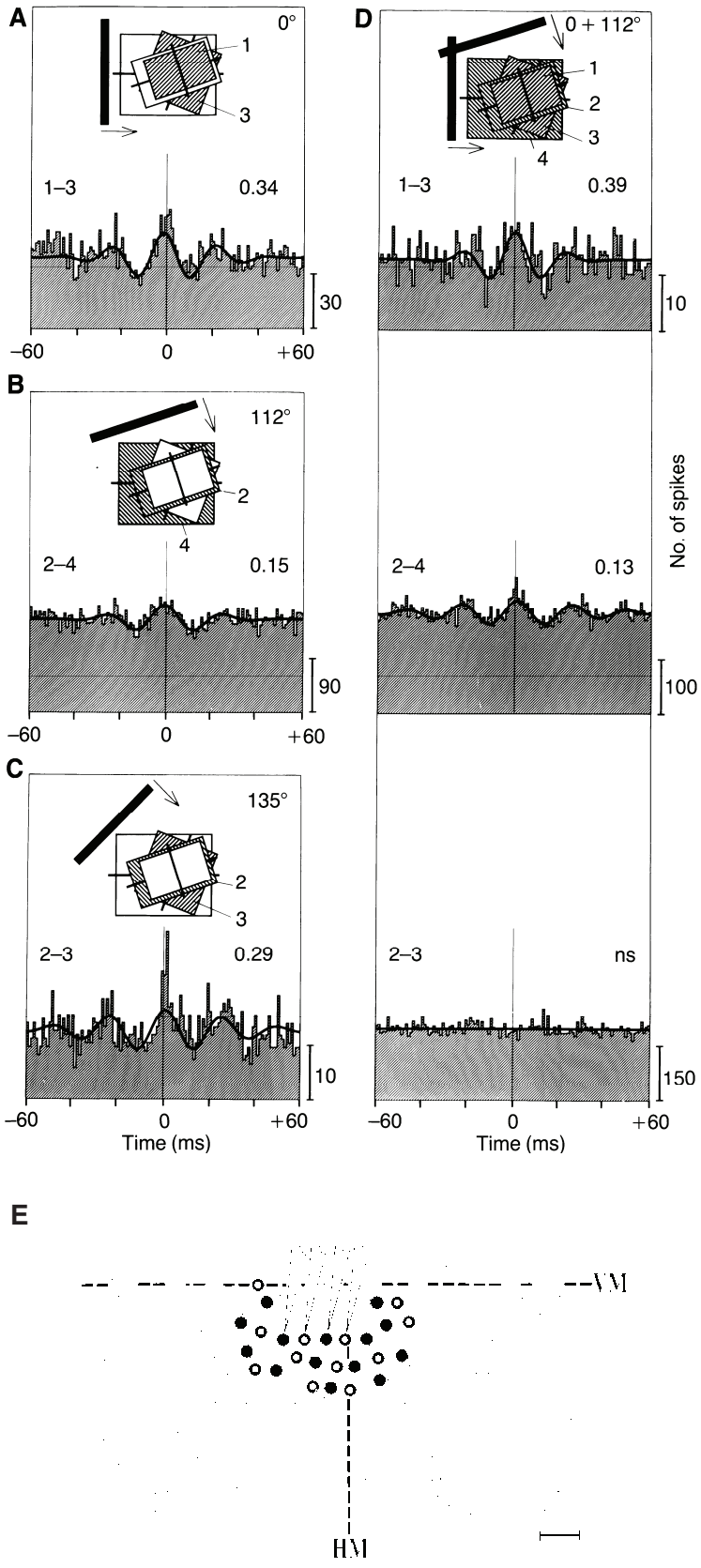

Figure 5. Multiunit activity was recorded from four different orientation columns of area 17 of cat visual cortex separated by 0.4mm. The four cell groups had overlapping receptive fields and orientation preferences of 22° (group1), 112° (group 2), 157° (group 3), and 90° (group 4), as indicated by the thick line drawn across each receptive field in (A)-(D). The figure shows a comparison of the responses to stimulation with single moving light bars of varying orientations (left) with the responses to the combined presentation of two superposed light

bars (right). For each stimulus condition, the shading of the receptive fields indicates the responding cell groups. Stimulation with a single light bar yielded a synchronization between all cells activated by the respective orientation. Thus, groups 1 and 3 responded synchronously to vertically (0°) oriented bar (A), groups 2 and 4 to a light bar at an orientation of 112° (B), and cell groups 2 and 3 to a light bar of intermediate orientation (C). Simultaneous presentation of two stimuli with orientations of 0° and 112°, respectively, activated all four groups (D). However, in this case the groups segregated into two distinct assemblies, depending on which stimulus was closer to the preferred orientation of each group. Thus, responses were synchronized between groups 1 and 3, which preferred the vertical stimulus, and between 2 and 4, which preferred the stimulus oriented at 112°. The two assemblies were desynchronized with respect to each other, and so there was no significant synchronization between groups 2 and 3. The CCH between groups 1 and 2, 1 and 4, 3 and 4 were also flat (not shown). Note that the segregation cannot be explained by preferential anatomical wiring of cells with similar orientation preference (Ts'o et al., 1986) because cell groups can readily be synchronized in all possible pair combinations in response to a single light bar. The number to the upper right of each CCH indicates the relative modulation amplitude. Scale bars indicate the number of spikes (Legend from Engel et al., 1992; experiment from Engel et al., 1991).
Notice that the argument advanced by the authors about the non- involvement of the lateral connections in the synchronization process is not as straightforward.
(E) Assembly formation by cell groups with overlapping receptive fields. Shaded areas represent band of orientation columns responding to vertical contours. If cell groups with overlapping receptive fields are stimulated by two independent objects (D), two spatially overlapping assemblies emerge that are desynchronized relative to each other (indicated by dots and circles). Each of these assemblies comprises synchronously firing cells, which is demonstrated directly by recording from four different sites in the cortex (D). In fact, the two bars activate most of the cells in this region, because the neurons have a limited orientation selectivity. By simply considering mean activity levels, it would only be known that a number of different feature detectors are active, but not whether they actually respond to two different objects or just a single one. However, with evaluation of the temporal relationships the whole set of active cells can be partitioned into two distinct assemblies. Scale bar is 1mm. Abbreviations: HM, representation of the horizontal meridian; VM representation of the vertical meridian. (from Engel et al., 1992)

2.1.3 Oscillations

Initially, synchrony was reported alone as depending on the overlap of cell receptive fields (Toyama et al., 1981a,b; Ts'o et al., 1986). Later, it was emphasized that cells in the visual cortex discharge synchronously at intervals of 15-30 ms and that the local field potential also exhibits oscillations at a frequency in the gamma range (30-70Hz) and of which the negative phase is synchronized with the cell discharge (Gray and Singer, 1989). As shown in Fig. 6, such oscillations are responsible for the satellite peaks in the cross-correlation histogram. Long range synchronization has been found to be accompanied most of the time by oscillations, which also suggests that oscillations could favor synchronous firing among cortical areas (Engel et al., 1992; König at al., 1995).

Neither the onset latency nor the phase are precisely related to the stimulus presentation, as demonstrated by flat shift-predictors (Gray at al., 1990; Jagadeesh et al., 1992, Livingstone 1996; Bringuier at al. 1997, Gray and Viana di Prisco, 1997). Shift predictors are computed as a nromal cross-correlation histogram, except that one spike train is compared to the spike train recorded during the next trial. It allows one to extract the effects locked on the stimulus presentation. A flat shift predictor excludes the possibility that the synchronous firing was due

to some fine spatial structure in the receptive fields of cortical neurons. Indeed, the response due this spatial structure would be reproduced for each trial, and should be reflected in the shift predictor. Such assertions made the origin of the oscillations a matter of debate.

2.1.4 Learning

Hebb postulated in the 1940s : "When an axon of cell A is near enough to excite cell B and repeatedly or consistently takes part in firing it, some growth process or metabolic change takes place in one or both cells such that A's efficiency, as one of the cells firing B, is increased."

Synapse effectiveness increases if both the pre-synaptic and post-synaptic cells fire together. This highlights the importance of synchrony and synchronous assemblies in the learning process. Recent advances in the comprehension of the synaptic plasticity agree with Hebb's rule. Mechanisms involved are long-term potentiation, long term depression, and dendritic back-propagation of the action potential (Stuart and Sakmann, 1994; Larkum et al., 1999). Short-term memory will be discussed in the section devoted to the hippocampus, and we will focus now on long term memory.

Koch (1997) proposed that memory is everywhere. "It resides in the concentration of free calcium in dendrites and the cell body; in the presynaptic terminal; in the density and exact voltage-dependency of the various ionic conductances; and in the density and configuration of specific proteins in the postsynaptic terminals". For the purpose of this introduction, suffice it to say that memory resides mainly in the cortico-cortical connections, which in mammals develop mainly postnatally (Innocenti and Frost, 1979; Price and Blakemore 1985).

These connections have been demonstrated to be the anatomical substrate for interhemispheric synchrony. Indeed, synchronization between neurons in visual area 17 of the right and left hemisphere is abolished by section of the corpus callosum (Engel et al. 1991). Moreover, experiments with strabismic kittens offer direct evidence for experience-dependent modifications of synchrony (Roelfsema et al., 1994). If convergent strabismus is induced in a kitten, binocular fusion becomes impossible. Double vision is then avoided by using one eye at a time, and usually one eye becomes dominant for fixation, whereas the information conveyed by the other eye is suppressed. The non-fixating – amblyopic – eye acquires some perceptual deficits, which become apparent when the normal eye is closed. Visual acuity is reduced, the image is temporally unstable and spatially distorted. In visual area 17, neurons responding to stimulation of the amblyopic eye are as numerous as neurons responding to

stimulation of the normal eye, and they exhibit similar receptive field properties. Usually, some cortical cells can be driven by stimulus of both eyes, they have a "binocular receptive field" and their response to a moving stimulus exhibits some direction selectivity. In the cortex of amblyopic cats, neighboring cells in a column are driven almost exclusively from either the right or the left eye, and cells responding to the same eye are interconnected by horizontal intracortical fibers (Löwel and Singer, 1992). Whereas no apparent anatomical discrepancy could account for the visual deficit of the amblyopic eye, König et al., (1993) and Roelfsema et al. (1994) showed neurons responding to stimulation of the normal eye exhibit stronger synchronized discharges than neurons responding to stimulation of the amblyopic eye. This suggests that reduced synchrony could be the neurophysiological expression of strabismic amblyopia and that synchrony relies on an experience-dependent process.

2.2 Synfire chains and information transfer

Strictly speaking, the synfire chain mechanism is not very different from the binding theory. Both theories assume that information is transmitted by synchronized neurons. But rather than looking at oscillations as a sign of information processing, the synfire chain theory focuses on the conditions required to transmit information synchronously from one group of neurons to the next, and on further evidences of complex temporal patterns in the discharges of simultaneously recorded cells (Dayhoff and Gerstein 1983a,b; Abeles and Gerstein 1988; Abeles et al. 1993. Baker and Lemon, 1999). The oscillations observed in many brain regions may be just a byproduct of the local network dynamics (Abeles 1994). Abeles (1991) presented the synfire chain as the propagation of the synchronized activity successively from one cell group to the other (Fig.6). Each group was called a node, and connections between nodes were diverging or converging; that is one cell connects to few other cells in the next node and receives inputs from few other cells in the preceding node.

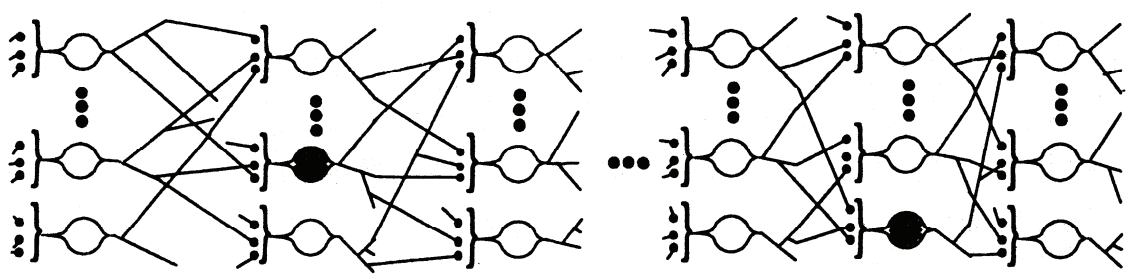

Figure 6. *A chain of diverging/converging connections. Locally these connections look like a multi-layered feed-forward network. However when a long chain is considered the same neuron may take part in more than one link. The neuron marked by gray shading takes part in the two links.* (from Abeles et al., 1994)

2.2.1 Neurons acting as Coincidence detectors

Synfire chain dynamics suppose that information is transmitted synchronously and that neurons discharge at the same time. This latter condition can be fulfilled if neurons act as coincidence detectors, rather than as simple integrator. In 1982, Abeles concluded that cortical cells were more sensitive to synchronous input than to asynchronous excitation. Moreover, cells can exhibit some firing patterns that are very irregular in stable conditions. This variability is evidenced by the distribution of the interspike interval (ISI; quantified by the coefficient of variation, i.e. the standard deviation divided by the mean), and by the Fano factor which is the variance of the spike count during a brief interval divided by the mean (Gabbiani and Koch, 1998). An integrate-and-fire model does not account for large variations since it simply sums up the inputs until a threshold is crossed. But a leaky integrate-and-fire model with a short memory time constant will exhibit much more variable interspike intervals. The condition to get a coincidence detector is that the integration time is shorter than the mean interspike interval (König et al., 1996); precise mathematical statements were provided recently by Kempter et al. (1998).

The integration time constant is thus a crucial parameter to decide whether or not neurons act as coincidence detectors. Assuming that the integration time constant was in the order of 15 ms or more, Shadlen and Newsome (1994,1998) explain the ISI variability by balanced and random fluctuations of the excitatory and inhibitory inputs. In order to produce a graded response to hundreds of excitatory synaptic inputs, these excitatory inputs must be balanced by a precise level of some other inhibitory inputs. The peak in CCH is the consequence of common inputs, but no information about the temporal pattern of synaptic inputs can be recovered from the one spike train because it is mainly determined by random fluctuations of excitatory-inhibitory balance. The information would be coded by the firing rate of neuronal population and could be decoded within 10 to 50 ms. This “random walk”, due to balanced excitation and inhibition, excludes synchrony as an informative component.

But the network dynamics could also achieve the balance between excitation and inhibition if the inhibition depends somehow on the network activity. This could also explain the spike train variability. Van Vreeswijck and Sompolinski (1996) showed that with a large number of random connections, but with a much larger number of neurons, any small change in the external input yields a strong irregular pattern of activities. This is due to the fact that despite the connections being strong, they come from too many separated cells to be synchronized. Interestingly, the balance between excitation and inhibition in such a sparse network occurs

spontaneously. A similar regime called “synchronous chaotic state” was described by Hansel and Sompolinski (1996) in the context of the orientation column and was compatible with sharp orientation tuning in response to a weakly oriented bar. If the excitatory and inhibitory connections were modified, the model also exhibited regular oscillations. Fortunately, van Vreeswijck and Sompoliski (1998) provided further mathematical analysis of such network dynamics.

Since spike train variability can be produced by the network, this argument furnishes no definite proof of the coincidence detection hypothesis. The debate relies mainly on the measurements *in vivo* of the cell membrane time constant and the ability of several synchronous presynaptic spikes to initiate a post-synaptic action potential.

Indeed, the overall network activity may transiently increase the membrane conductance and lower the time constant by an order of magnitude (Bernander et al., 1991; Rapp et al., 1992). This led Koch et al. (1996) to conclude that, under realistic experimental conditions, the measured time constant represents a maximum limit on the actual value, but does not tell us how rapidly the membrane can respond. In their numerical model, the soma of a cortical neuron behaves more as an integrator, whereas distal dendrites behave more like coincidence detectors. It should also be stressed that the dendritic arbors can promote synchrony detection by the activation of low-threshold, voltage-gated dendritic channels (Markram and Sakmann, 1994; Stuart and Sakmann, 1994), which would dramatically reduce the time required to induce a voltage change at the soma. Larkum et al. (1999) showed that in a pyramidal cell a single back-propagating sodium action potential generated in the axon facilitates the initiation of dendritic calcium action potentials when the back-propagated potential is coincident with distal dendritic inputs within several milliseconds. Although, a neuron is still unlikely to respond much faster than a few milliseconds, the coincidence detection at the sub-millisecond time scale could take place in the dendritic arbor (Softky, 1994). Such results could explain the high performance of neurons able to process time differences as small as 15 μs (Moiseff and Koinishi, 1981).

2.2.2 Coincident and unitary events

Since neurons could act as coincident detectors, and since relevant information could be transmitted synchronously, it should be of interest to look at moments when two neurons synchronize more often than by chance. Two synchronous spikes are termed a *coincident event* (CE), and if these coincident events occur at one moment during a trial more often than

expected by chance, each occurrence is called a *unitary event*. The purpose of the study of Rhiele et al. (1997) is to relate these moments to the behavior of a monkey performing a delayed task. The monkey has to touch a circle presented on a video display, but only once the circle is filled. This filling occur randomly 600, 900, 1200, or 1500 ms after the onset of the target. The monkey learns these possible delays and the reaction time decreases as the delay increases. What is shown by Rhiele at al, is an increase of the number of coincident spikes when the monkey expects that the target will be filled and that it will be required to do the movement (Fig. 7&8). However, the method used to assess significance of the coincident spikes is probably flawed. Indeed, it uses the firing rate averaged over all trials to estimate the expected number of coincident spikes. This does not take into account the possible co-variation that could occur between the firing rate of two cells during a single trial. If two cells both have a high firing rate during the same trials, and if both have a low firing rate during the other trials, such a co-variation produces more coincident spikes than if both cells discharged independently (see Fig. 9). The problem is similar if cells increase their firing rate at the same moment. This subject will be developed in Chap. 3, where an original method to alleviate this problem is proposed.

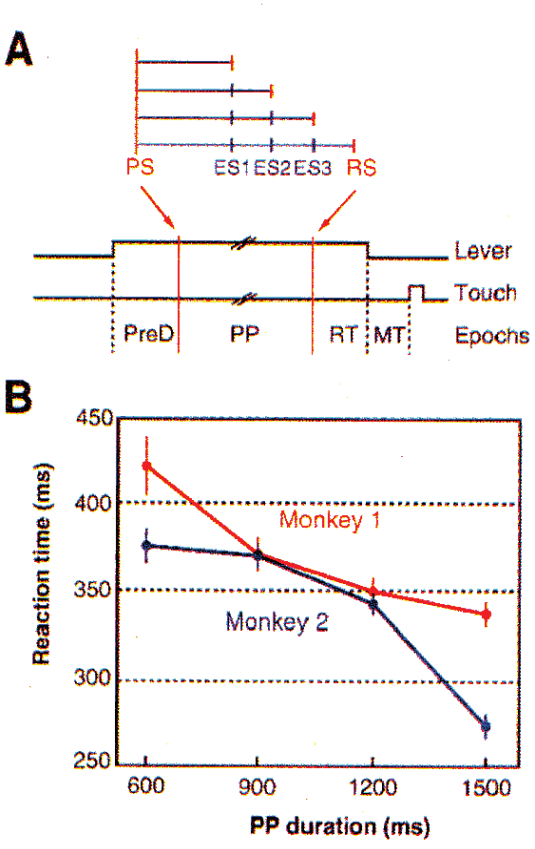

Figure 7. *(A) Two macaque monkeys were trained to touch a target presented on a video display equipped with a capacitive touch screen. To start a trial, the animal had to hold down a switch. After a constant delay of 1 s (PreD), a preparatory signal (PS) forming an open circle (diameter, 3 cm) appeared on the screen, indicating the upcoming target position. after a second delay of variable duration (preparatory period, PP), the response signal (RS), indicated by filling the circle, instructed the animal to move its hand to the target and touch it. The PP could last 600, 900, 1200, or 1500 ms; these intervals were presented in a random order and with an equal probability. Thus, from one possible PP duration (and, hence, expected signal ES) to the next, the conditional probability for the RS to occur increased, reaching values of 0.25, 0.33, 0.5, and 1. The reaction time (RT) and the movement time (MT) were recorded in each trial. Criteria for obtaining the reward were (1) to keep the switch pressed during the PP, (2) to move and to touch the target after RS, and (3) to perform the movement so that neither RT nor MT exceeded 1 s. (B) Behavioral results. For each monkey, mean RTs and standard error in relation to PP duration are shown as recorded during the last training sessions (monkey 1, N=35; monkey 2, N=59) when they performed the task with more than 90% correct trials. By using a two-factor (PP-duration x training session) analysis of variance, changes in RT were found to be highly significant for both monkey [monkey 1; F(3,102)=38.19, P<0.001); monkey 2, F(3,174)=157.81, P<0.001].* (from Rhiele et al. 1997)

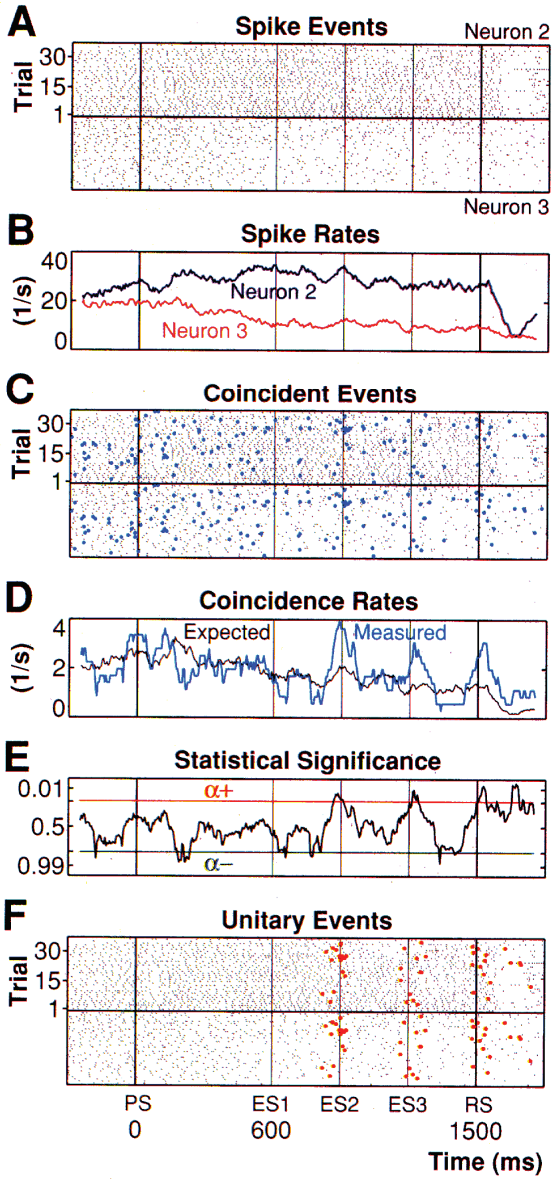

Figure 8. *Unitary event analysis of the spiking activity of two simultaneously recorded single MI neurons. The 36 trials with longest PP duration (1500 ms) were selected in this example. Thus the monkey could expect the RS to occur at three successive moments (ES1, ES2, and ES3) before it actually occurred at RS. Results of UE analysis over a time interval of 2100 ms, starting 300 ms before PS and lasting until 300 ms after RS, are shown. (A) Conventional raster displays of spike discharges of the two neurons (top, neuron 2; bottom, neuron 3). Each dot represents an action potential, and each horizontal line depicts the spiking activity in a single trial. (B) Spike discharge rate for each neuron (normalized to spikes per second) was computed by sliding a boxcar window of 100 ms in steps of 5 ms over the spike events [dots in (A)]. (C) In a copy of the raster displays from (A), spike coincidences of the two neurons within a precision window of 5 ms are indicated by blue dots. (D) Comparison of measured and expected coincidence rates. The measured coincidence rate (blue curve, normalized to coincidences per second) was derived in the same way as the spike rates, by sliding a boxcar window in steps of 5 ms over the coincident events [blue dots in (C)]. The expected coincidence rate (black curve), based on the null hypothesis of independent firing, was calculated as the product of the individual firing rates [curves in (B)]. (E) For each time window, the statistical significance for a positive difference between measured and expected coincidence rates was calculated from a Poisson distribution (with the mean set to the expected coincidence rate) as the cumulative probability P of observing the actual number of coincidences or an even larger one by chance. The larger the number of excessive coincidence, the close P is to zero. Similarly, the larger the number of lacking coincidences, the close its complement, 1-P, is to zero, while P approaches 1. To enhance visual resolution at the relevant low-probability values of P or 1-P, we plotted a logarithmic function of the two: $\log_{10}[(1-P)/P]$. For excessive coincidences, this function is – dominated by P; for lacking coincidences, it is dominated by 1-P. This procedure, derived from the surprise measure (Palm et al., 1988), is comparable to measuring significance on a decibel scale. It yields positive numbers for excessive coincidence (for example, 1 for P=0.1 and 2 for P=0.01) and negative numbers for lacking coincidences, and it changes sign at the chance level (P=0.5).Whenever the significance value of an excess number of observed coincidences exceeded a fixed threshold level α^+ (here P=0.05), this defined an epoch with significantly more coincidences than expected by chance. We marked these significant precise coincidences as UEs, and they are indicated by red dots in the raster display in (F). Occasionally, the significance value dropped below the negative threshold level α^- (here, shortly after PS) . Such cases, defining epochs with significantly fewer coincidences than expected by chance, were more rare because of the generally low expected coincidence rates in these data and are not considered further here. The widths of the coincidence window and of the sliding time window as well as the significance level α^+ could be set to selected (fixed) value in the analysis; values of 5 ms and 100 ms, respectively, and P=0.05 were used throughout the results reported here.* (From Rhiele et al., 1997)

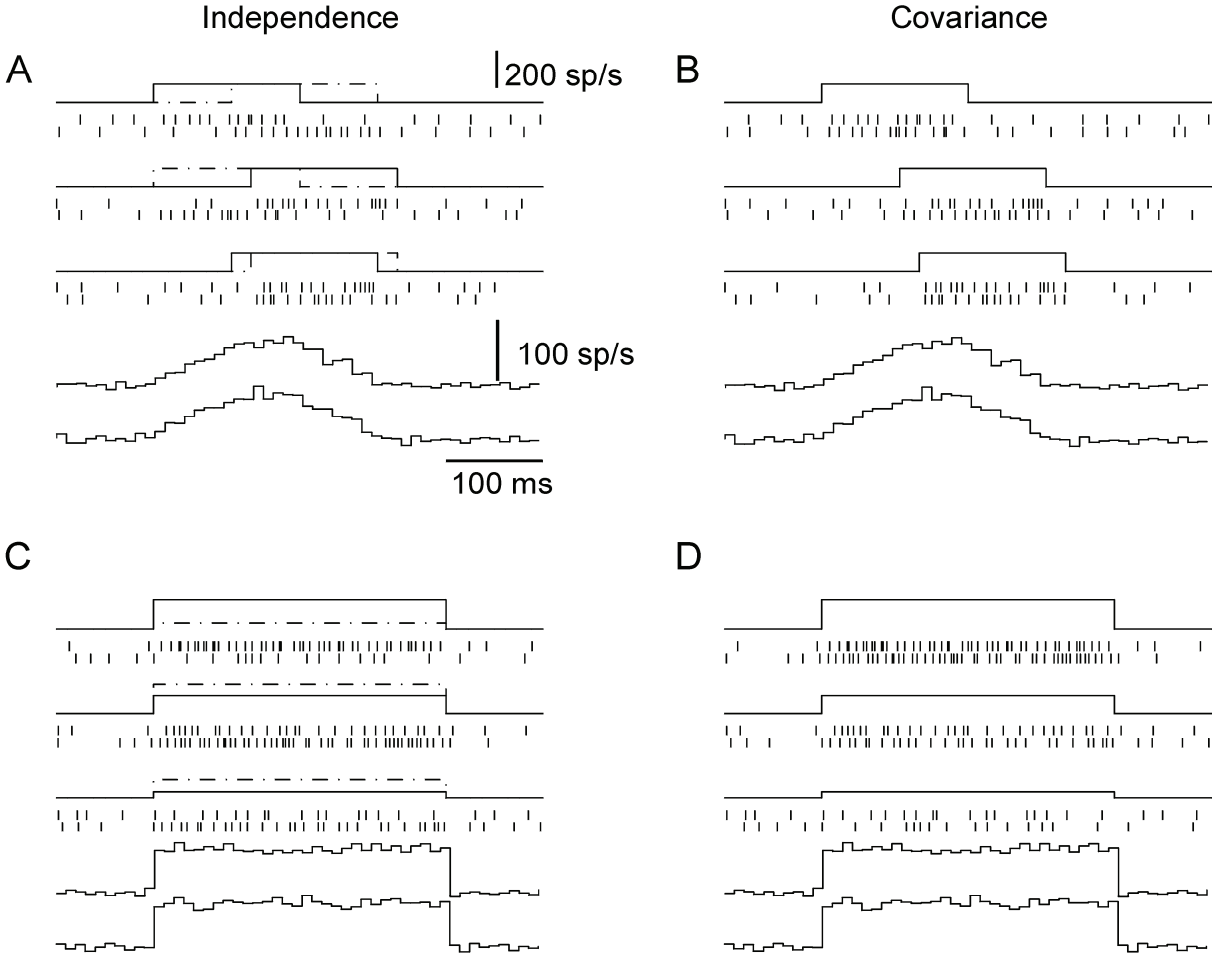

Figure 9. Types of non-stationarity in neuronal firing. (A,B) Variation in onset latency. Three trials are shown, the solid and dotted lines show the underlying firing rate of the two units, whose rasters are shown beneath. The traces at the bottom show the PSTHs, calculated from 100 similar trials (burst of 150 ms with a temporal jitter of 100 ms). In (A), the onset latency of the firing bursts are independent between the two spike trains; in (B), they are the same within each trial. The PSTH smoothes the firing rate changes, and fails to distinguish the independent from covariant situation. (C,D) Variation in firing rate. Same display conventions as (A,B). The magnitude of a burst may vary across trials; this may be independent (C) or covary (D) between the two spike trains. The PSTH represents only the mean firing rate, and is again identical for independent and covariant conditions. To multiply the average firing rates to obtain the number of CEs implies that the cell discharges are not covariant. If the cell discharges covary, CEs are found in excess, despite the absence of short-term synchrony.

The study of Rhiele et al. (1997) was not the first one to attempt a demonstration of the temporal coding in behaving animals. Vaadia et al. (1995) presented a similar analysis, subject to the same drawbacks, but their presentation was fair because they showed the complete JPSTH and the cross-correlation histogram. Indeed, this display elucidates the nature of the central peak, which was composed of a large and very broad peak (>200 ms width) and of a possible narrow one which was not investigated. The problem is that such coincident events are related to the co-activation of both units rather than to precise neuronal synchrony.

2.2.3 Temporal pattern detection

Since the repeated activation of a synfire chain excites the same nodes sequentially, it is expected that some complex patterns will be repeated if some cells belonging to these nodes are recorded. A temporal pattern is thus the determined sequence of activation of one or a few recorded cells. For example, three cells A,B,C could exhibit a four spike patterns A0-B20-C25-B32, standing for the sequential activation of B 20 ms after A, C 25 ms after A, and B again 32 ms after A. As pointed out by Dayhoff and Gerstein (1983a), recurrent patterns may not be exactly the same each time they are produced either because of biological noise, or because variability may be part of the code. Variation could occur in the temporal spacing (B30-34 instead of B32), in the occurrence of extra or missing spikes (sometimes, B could also discharge 5 ms after A), or the pattern could be time-scaled (it would span 45 ms instead of 32 ms). Moreover a pattern could overlap with itself, if the same pattern is started before the previous one is finished. As a consequence the number of possible patterns is enormous. All these considerations make the testing of pattern significance a daunting problem. In the first paper on this topic, no less than three methods were proposed (Dayhoff and Gerstein, 1983a). In order to quantify significance, the number of patterns was compared to the number of similar patterns found in 99 shuffled trains. Abeles and Gerstein (1988) then proposed to calculate significance assuming that each spike train is a Poisson process.

Pattern detection has been applied in few situations, to recordings obtained in the crayfish claw and in the cat visual cortex (Dayhoff and Gerstein, 1983b), and in the frontal cortex of the behaving monkey (Abeles et al., 1993). Recently, Baker and Lemon (1999) reported some patterns in the motor cortex of the behaving monkey, which were highly significant if spike trains were postulated to be equivalent to a Poisson process. They showed that if one assumes a more regular process, like the more realistic gamma process[1], no significant patterns are found. Recordings presented in Chap. 4 exhibit some synchrony whatever the hypothesis on the underlying process regularity, but statistics performed on the coincident events (CEs) depended on the assumptions made about the underlying cell process.

---

[1] A uniform Poisson process describes the occurrence of an event that has a small and constant probability to occur within a time interval. The distribution of the interval between two events is exponential, the maximum number of events occurs in the first time step and decreases in the next ones. A non-uniform Poisson process describes simply such a random process when the probability of occurrence changes with time.

The gamma distribution is closely related to the Poisson distribution. The order a describes the distribution of intervals separating a successive Poisson events. If $a=1$, the gamma distribution is simply the Poisson distribution. When $a>1$, the gamma distribution is narrower than a Poisson distribution and accounts for a refractory period.

Synchrony between two spikes can be viewed as the simplest pattern. The method presented in Chap. 3 to establish significance of CEs could be easily extended to the problem of testing the significance of other simple temporal patterns.

2.3 Time advance coding scheme

Amongst temporal coding theories, the most audacious has been proposed by John Hopfield (1995, 1996; Hopfield et al., ??), and has completely different applications. Indeed, in this system, the ongoing collective oscillatory pattern just provides a temporal frame of reference. Information – the analog strength of a sensory cue – is represented by using the timing of action potentials with respect to this collective 'clock'. The daring touch is to propose a logarithmic encoding: the more a spike precedes the average population, the more it carries information. Action potentials are then transmitted after some delay to other recognition units that respond selectively only for perfect input synchrony. Consequently, the pattern of action potentials has to be compensated exactly by the set of delays. Temporal patterns are stored in the set of conduction delays and validated by a coincidence detector.

Although it highlights the importance of time delay in temporal pattern recognition, requirements for extremely precise coincidence detectors are fulfilled only in specialized auditory cells, or in the bats sonar system. Moreover, this leads one to consider only the spikes which are in advance on the network activity as the most important, and synchronized neurons as receiving only little input. A restrictive coding scheme that wastes so much energy seems unlikely.

From the point of view of synfire chains, spikes in advance on the network activity are important because first cells are probably the most responsive ones and could discharge twice or more. First cells could also prime the propagation of the local activity by exciting or inhibiting some neighboring cells.

2.4 Timed neuronal selection

In this most conservative hypothesis, synchrony is just the result of a timed neuronal selection. Once the network reaches a high level of excitation, a local inhibitory feedback loop resets the network activity to zero. Once the inhibition effect wears off, and if the input is sustained, the network activity bursts once again. Cells that are not responsive enough are not able to fire before the inhibitory feedback and remain silent. Such a timed neuronal

selection is purely local, but could also be viewed as the selection of a node belonging to a synfire chain.

The originality of the hypothesis is that it explains oscillation as a means to transform a continuous flow of information into packets, exactly as if the input was digitalized or discretized. The network acts as a special kind of analog digitalizer, except that the information is coded by a population process rather than by a single variable. Parodi et al. (1996) suggested that in the case of moving targets, periodic resetting avoids information jamming. Indeed, if two neurons responded to the same stimuli with different firing rate intensities, it is easy to understand that in the absence of any resetting, they will desynchronize after a few spikes. (However, they felt justified in attributing the inhibitory reset to feedback projections from other associative areas). Laurent (1996) suggested a very similar hypothesis to explain the advantage of oscillatory dynamics in the insect olfactory system.

From another point of view, the resetting hypothesis emphasizes the winner-takes-all concept which takes place repeatedly during stimulus motion. Strictly speaking, timed neuronal selection does not select a single winner, but a sub-population of winners. Although selective competition is accepted as a ubiquitous phenomenon in the brain, it was studied mainly in the case of the firing rate code, especially in the establishment of self-organizing sensory and motor maps (Kohonen, 1982, 1995, Kohonen et al.,1997; Willshaw et al., 1997; Bishop et al., 1998). Fukai (1996) pointed out that if inhibition strength is fixed, a competitive network of spiking inhibitory cells selects an almost fixed number of winners when stimulated by broad ranges of stimulus patterns. In a further section, we will discuss oscillations in the motor cortex. They are usually found when attention is required during movement preparation or during a holding task. As proposed by Parodi et al. (1996), it could be that these situations – like motion processing – requires a comparison between successive patterns. Therefore, periodic resetting would also be recommended to avoid information jamming.

3. Synchrony in the nervous system

The purpose of this section is to provide the reader with an account of the different brain areas that have been involved in temporal coding. Since this phenomenon is probably ubiquitous amongst vertebrates and insects, the review is oriented on the cognitive process instead of being exhaustive. It is indeed impossible to summarize such a fast expanding field without

restriction. Priority was given to the cellular recordings because information processing can be quantified by discrete action potentials and their time precision is of the order of one millisecond, whereas the local field potentials and electro-encephalographic activities reflect the network mean activity at a time scale of ten milliseconds. However, field potentials allow non-invasive studies in humans, and are an efficient means for the assessment of inter-areal synchronization.

3.1 Visual system

The wealth of knowledge available about the visual system provides an ideal context to test the binding theory. Synchronous oscillations were recorded in a large number of conditions, in anesthetized or conscious animals: cats, monkeys, and even in the three layered cortex of the turtle (Prechtl, 1994).

Synchrony is described as locked on a sudden change in the stimulus presentation or as an oscillatory process when the stimulus has a constant velocity. In all these experiments in the visual system, it was very important to use either an optical bench or a computer screen with a high refresh rate (≥ 100 Hz) because Wollman and Palmer (1995) showed that cortical cells and neurons in the lateral geniculate nucleus could synchronize on the video vertical refresh rate with a frequency of 60 Hz (even 90 Hz, Jones and Berkley, 1983).

Synchronization dependence on the stimulus features has been studied extensively, and the unanimous conclusion is that close cells exhibiting similar responses (receptive fields, preferred orientation, direction, and velocity) have the strongest chance of synchronizing. Moreover, the synchrony is increased between two cells with different receptive fields if they are excited by a single moving bar rather than two separate ones.

When a stimulus moving at a constant velocity is presented, synchrony occurs at regular intervals. The phases of the oscillations are not locked to the stimulus presentation, nor to the movement onset (Eckhorn et al., 1988; Kruse and Eckhorn ,1996; Gray et al. 1989a&b). In the visual cortex and under anesthesia, *oscillations* were always recorded during the presentation of such a moving stimulus. Nelson et al. (1992) recorded most of their cross-correlation histograms during spontaneous activity and even if precise *synchrony* was observed, they never saw 40 Hz oscillations in the absence of visual stimulation with moving light bars.

If the mesencephalic reticular formation is activated, oscillations increase (Munk et al., 1996; Metherate et al. 1992; Steriade et al., 1996a). This supports the fact that in the awake animal, oscillations can be enhanced or evoked by attentive tasks (Roelfsema et al, 1997). As suggested in the previous section, oscillations during attentive state could be required to contrast an expected difference between successive situations.

This brings up the question of the dependence on the firing rate. Are the oscillations simply due to a sustained level of activity? This relationship is poorly illustrated in most of the studies. Formally, the test must involve a comparison between the expected cross-correlation peak due to cell firing-rate and the observed peak amplitude. Such a relationship is difficult to establish, because it must ideally be drawn between the same two cells, or between pairs of cells recorded at equal distance since synchrony depends on the connectivity. Roelfsema et al. (1994) showed in strabismic kittens that amblyopia did not affect the cell firing rate, but only the experience-dependent connectivity, and therefore the synchrony. But most other experimenters do not perform comparisons matched for the firing rate.

If the oscillations are simply related to the activation of a local network, there should be some cells that oscillate continuously in response to the presentation of a stationary point. Indeed there are some! Neuenswander and Singer (1996) demonstrated that stationary squares presented during three seconds evoke in retinal ganglion cells some oscillatory responses in the frequency range of 61 to 114 Hz that could be synchronized over 20 degrees of visual angle. Neurons in the lateral geniculate nucleus (LGN) discharge synchronously with the corresponding ganglion cells of the same retina; that is cells in both LGNs could be synchronized by a stimulus crossing the vertical meridian. As expected from such a high oscillation frequency and long stimulus presentation, oscillations were not phase-locked on the stimulus-onset.

No oscillations were found by Sillito et al. (1994) in extracellular recordings made from two LGN cells while the cells were stimulated with a moving bar, but synchrony was observed and depended on the integrity of the visual cortex. The moving bars were presented only during 150 ms, so that these results describe only the transient response to some new stimuli. Likewise, Alonso et al. (1996) demonstrated that neighboring geniculate neurons with similar overlapping receptive fields could synchronize within 1 millisecond, probably due to common input from the same ganglion cell, and that these synchronized spikes are more efficient at evoking a post-synaptic response.

In a compelling experiment, Amzica et al. (1997) showed that it is possible to instrumentally condition awake cats to generate grouped fast oscillations in the visual cortex (area 17) or even in the motor cortex (area 4). These oscillations were associated with a widespread increase in synchrony between thalamic and cortical field potentials.

Other experiments related to the synchrony between the cortex and the lateral geniculate nucleus will be examined in the section devoted to the thalamo-cortical system

3.2 Auditory system

Although an auditory stimulus could seem very different from a visual one, their cortical processing shares many similarities. Indeed in a natural visual scene, each small movement of an object elicits a synchronous discharge in the corresponding cell-assembly. Complex sounds are represented by cells responding to a characteristic frequency. These cells are grouped and form tonotopic maps. Studying the complex vocalization of the marmoset, Wang et al. (1995) have shown that sound representation is carried out by spatially dispersed and synchronized cortical cell assemblies. Cells are phase-locked to the envelope of a portion of a complex vocalization, according to the cell characteristic frequency. As a consequence, the synchrony between neuronal populations and the stimulus does increase, and the temporal complexity of the signal decreases. Cell-assemblies are reproducibly time-locked on the stimulus, extracting low frequency information by their temporal grouping and coding the high frequency component by their firing rate.

Moreover, it was shown by de Charms and Merzenich (1996), that cortical cells could synchronize their discharge even when the auditory stimulus is constant, in the same way as visual cell synchronize their response when the stimulus moves at constant velocity.

3.3 Motor system

As just explained, cats could be conditioned to produce fast oscillations in the motor cortex (Amzica et al, 1997.). These oscillations were evidenced in the local field potentials which represent an estimate of the average activities of postsynaptic signals on the dendrites and somata within less than 1 mm from the electrode tip (Mitzdorf, 1987). Local field potential (LFP) provides an easy way to sample large groups of neurons since in the motor cortex, it is more difficult to quantify the motor map of a single cell than the receptive field of a visual cell.

As a consequence, most of the experiments performed with behaving animals investigated local field potentials, and fast oscillations were found to be task-related, but they are usually most pronounced within 20 to 35 Hz. As in the visual cortex, it has been shown that cells tend to discharge during the negative phase of fast LFP oscillations (Muthy and Fetz, 1992). Auto- and cross-correlation histograms of multi-unit or single-unit activities exhibit similar fast oscillatory patterns when the LFP is also oscillatory (Murthy and Fetz, 1996b).

Fast oscillations in the motor cortex were reported to be strongest with attentive task engagement and to be disrupted by movement onset, except during the initial phases of fine digital movement. Unanimous agreement seems to be reached about the presence of oscillations during movement preparation (Murthy and Fetz, 1992, 1996a,b; Sanes and Donoghue, 1992; Donoghue et al., 1998) but the question remains about the influence of the movement. Murthy and Fetz (1992, 1996a) showed that episodes of fast oscillations occur often and became synchronized over large areas of the sensori-motor cortex during exploratory forelimb movement, like retrieving raisins from a box slot (Klüver board). Indeed, such exploratory tasks require sensory feedback to guide precise movements, and synchronized LFPs could be a substrate for sensori-motor integration. During these experiments, no precise relationship between synchronization of LFPs and the occurrence of movements or bursts of EMG activity could be evidenced. But no oscillations were found during repetitive and overtrained wrist movements. Donoghue et al. (1998) observed that LFP oscillations occurred in nearly all trials at the beginning of the task, when the hand reaches into a bowl, but when the monkey grasps the food reward they were present only in 10-20% of the trials.

These results are consistent with the oscillation task-dependence reported by Baker et al. (1997) during a precision grip task. This task required that two levers were squeezed between index finger and thumb, and precisely held in position for one second. Oscillations occurred preferentially during the hold phase after a latency of a few hundred milliseconds and they disappeared 65 milliseconds after the end of the hold period. And during these oscillations the coherence between cortical LFP and the rectified EMG activities was increased. These results have been replicated in human subjects using EEG or magnetoencephalogram as a measure of the cortical activity (Salenius et al., 1997, Halliday et al., 1998).

The motor unit, i.e. one alpha motor neuron and the muscle fibers it innervates, can be easily recorded in human subjects. During a steady isometric contraction, motor units synchronize

and can exhibit an oscillatory pattern at a frequency of 20-30 Hz, probably because of a common input from the motor cortex (Datta and Stephens, 1990; Farmer et al., 1993)

A similar temporal pattern of oscillations has been evidenced in the granular layer of the monkey cerebellum during a task requiring an arm movement one second after an auditory cue (Pellerin and Lamarre, 1997). The oscillations occurred 200-300 ms after the cue and stopped 50-100 before movement onset. Immobile alertness was also reported to promote cerebellar oscillations. Timofeev and Steriade (1997) also showed that stimulation of the cerebellofugal axons in the brachium conjunctivum evokes cortico-thalamic oscillations, and that their destruction abolishes or strikingly reduces their spontaneous occurrence. Maex and De Schutter (1998) proposed a model of the granule layer that exhibits fast oscillations due to the massive and regular recruitment of the inhibitory Golgi cells[2].

Cortical, thalamic and cerebellar disruption of the oscillatory dynamics with the movement onset does not necessarily mean a cellular desynchronization. Cell discharges are probably time-locked on the movement onset, exactly as visual cells were time-locked on stimulus velocity variations. When a movement starts, the regular oscillatory process becomes superfluous because the information has to be processed as fast as possible toward the motoneurones.

3.4 Olfactory system

The cortex (telencephalon) is composed of three different cyto-architectures: the oldest one is the hippocampus (archicortex) and is heavily involved in memory and learning. Next to the hippocampus is another type of cortex, which has only two or three layers of cortical cells, the olfactory cortex (paleocortex). In mammals, the olfactory cortex is devoted to olfaction, but in reptiles it receives also different kinds of input. The last cyto-architecture – the neocortex – has many cell layers and is found only in mammals.

[2] This network is somewhat particular in the sense that Golgi cells are not interconnected and are excited mainly by the granular cells that they inhibit. Once the granule cells are activated, the Golgi cells produce a large feedback inhibition. If excitation is maintained, the granule cells discharge when the effects of inhibition vanish, and they trigger the Golgi cells once again. The absence of inhibitory connections between Golgi cells allows *all* the Golgi cells to fire at each cycle, synchronizing the granule cells by a large inhibitory reset. This global synchrony relies on the small number of Golgi cells (30) of which 17 were connected to each granule cell by delayed excitatory connection (0-5ms).

From mollusks like the *Limax* slug to insects and vertebrates, the structure of the olfactory system is remarkably similar. For the sake of simplicity, the terminology related to vertebrates will be described and used to explain results from other phyla. Transduction of the odor signal molecules into action potentials is performed by the olfactory receptor neurons situated in the olfactory epithelium, high up in the nasal cavity. Each cell projects into one or a few of the numerous clusters of synapses called glomeruli in the olfactory bulb. The neurons in the olfactory bulb that project into higher structures (the olfactory and piriform cortex and the olfactory tubercule) are simply called the projecting neurons (or mitral-tufted cells).

The locust – a grasshopper – has 50,000 olfactory receptors on two antennae (Laurent, 1996). Each olfactory receptor terminates in one, two or three of 1,000 glomeruli in the ipsilateral olfactory bulb (the "antennal lobe"). A glomerulus thus contains the axon terminals of 50-150 olfactory receptor cells. In each olfactory bulb, there are about 830 projecting neurons and 300 local inhibitory neurons. The dendritic arbor of projection neuron originates in 10 to 20 glomeruli. Projection neurons are excitatory and locally connect to both other projection and local neurons. They send projection to higher structures (the "mushroom body" and the "protocerebral lobe"). Local neurons in the olfactory bulb are GABAergic and they project throughout the entire bulb on to both GABAergic and non-GABAergic cells, forming a network of interconnected inhibitory cells...

Coherent 20-30 Hz oscillations in population activities can be detected in the olfactory bulb and piriform cortex in response to odor presentation. If the olfactory receptors are cut or the olfactory bulb severed, oscillations disappear. After ablation of the piriform cortex (mushroom body), oscillations still occur in the olfactory bulb. Intracellular recording in projection and local neurons show alternating EPSPs and IPSPs whose timing is phase-locked on to the local field potential. The phase of the projecting and local neurons activity is odor-independent, which indicates that odor quality is not encoded in the phase of firing of individual neurons (Laurent and Davidowitz, 1994). Projecting neurons discharge on average 90° in advance of local neurons maximal activity (one phase quarter; local neurons are axonless and connect their targets through slow dendro-dendritic connections).

The interesting part of the work is that oscillatory events are generated by odors, but are also compatible with the activation of odor-specific neural assemblies. Neurons have different patterns of activation, but each pattern is consistent for each neuron and odor. When a neuron synchronizes to the population, it usually produces only one action potential per cycle. Neurons form an oscillatory assembly that is coherent on a cycle-by-cycle basis, and not

simply on average, as would be calculated over many successive representations. Oscillations are therefore proposed to be a timed resetting that would limit the representation of the stimuli to the combinations of a determined number of neurons selected amongst 830 possible projection neurons.

3.5 Hippocampus

If a rat is placed in a radial arm maze which is composed of a central platform and radiating passageways, it quickly learns to go down the arms of the maze to eat the food placed there. Moreover, it does not go twice into one of the arms. If the hippocampus is destroyed, the rats can still learn the task, but go down the same arms more than once, as if they cannot remember which arms they have already been down (Olton et al., 1976,1979). Moreover, if a rat explores a small box for 10 minutes, some hippocampal cells discharge specifically for one location. Such cells are called "place cells", and the location that evokes the greatest response is called the neuron's place field. If the light is turned off, place cells still map the space in the same way, suggesting that place cells are related to where the animal thinks it is. And if an opening let the rat explore an adjacent box, the place fields are re-mapped over the two box space within 20 minutes. (Wilson and McNaughton, 1993).

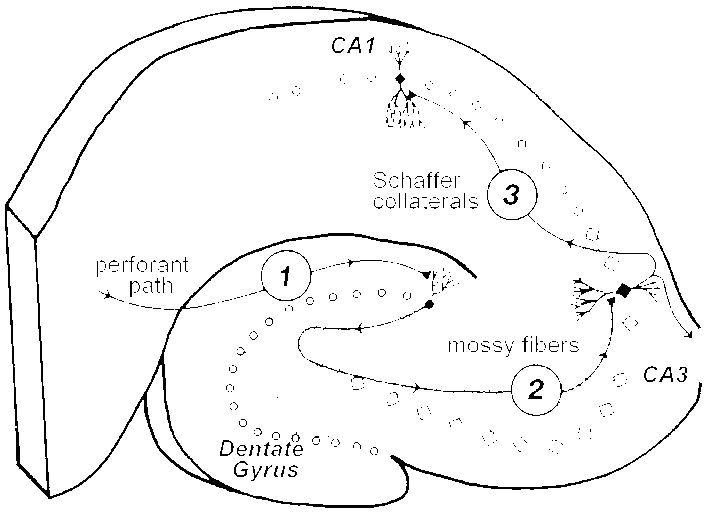

Figure 10. Some hippocampus microcircuits. The hippocampus includes two cellular sheets, the dentate gyrus (circles) and the Ammon's horn (cornu Ammonis, Latin for "Ammons's horn") that has four division of which the famous CA3 and CA1. Granule cells are localized in the dentate gyrus, receive inputs from the entorhinal cortex by perforant path and send projections – called the mossy fibers – to the CA3 pyramidal cells. The CA3 cells connect the CA1 pyramidal cell through the Schaffer collateral and project with them to the subiculum via the fornix. (Modified from Brown and Zador, 1990)

From these experiments, it appears that the hippocampus is involved in a special kind of memory that has been qualified as spatial, working, or even relational memory. The basic idea

of relational memory is that the hippocampus stores patterns of highly processed sensory information coming from multiple parts of the brain. A classical example would be the simultaneous occurrence of a smell and a visual object. Mechanisms and neuronal circuits to do so have been extensively studied because slice preparations of the hippocampus can be easily obtained. Some microcircuits of the hippocampus are shown in Fig. 10. Some of the most studied cells are the CA1 pyramidal cells. A high frequency stimulation of afferent Schaffer collateral induces an increase in the post-synaptic potential that lasts for hours and that could be the support of memory. This phenomenon – called long term potentiation – is specific to a pattern of stimulation. It relies on NMDA receptors and on calcium accumulation in the postsynaptic elements, which in turn results from the repeated and simultaneous activation of both pre- and postsynaptic cells.

If a low-frequency stimulation is applied, the opposite phenomenon – called long term depression – could take place. The role of these mechanisms in learning spatial locations has been demonstrated by injecting NMDA-receptor blocker into the hippocampus of rats performing behavioral tasks (Morris et al., 1986) and by studying the performance of rats with genetically deleted enzymes and receptors that are critical for synaptic plasticity.

In this context, it is very interesting to study the dynamics of the hippocampal network in the behaving rat. During space exploration, hippocampus electroencephalogram exhibits theta rhythms (4-12Hz), and on each cycle of this oscillation high frequency subcycles in the gamma range are superposed. Lisman and Idiart (1995) have proposed that each subcycle stores different patterns which are repeated at the theta frequency. Each pyramidal cell would fire only once per theta cycle and an afterdepolarization would promote firing at the next theta cycle. By this means, a pattern could be maintained for many cycles as a short-term memory. Since psychological experiments in humans showed that humans can store 5 to 9 short-term memories, it is suggested that it is due to the limited number of gamma subcycles that could take place in a theta cycle. Although appealing, this hypothesis requires that pyramidal cells are intrinsically tuned to the theta oscillations, a property that could be induced by cholinergic inputs (Andrade et al., 1991), but which is probably absent in other cortical cells.

The mechanism for gamma oscillations in hippocampal slices has been elucidated by Miles Whitington, Roger Traub and John Jefferys (1995). After a conditioning, 40Hz oscillations occur in CA1 pyramidal cells following the excitation of the Schaffer collaterals. The application of a $GABA_B$ receptor antagonist greatly prolongs the oscillations, whereas the application of $GABA_A$ receptor antagonist suppresses the oscillations. This demonstrates the

role of fast $GABA_A$ inhibitory post-synaptic potentials. The collective behavior of the interneuron network was further demonstrated in a simulated network of 128 realistic hippocampal interneurons. This network oscillated at a 40 Hz frequency as long as the interneurons were interconnected by fast $GABA_A$ inhibitory synapses and received tonic excitation. The oscillation frequency depended on the $GABA_A$ conductance and decay time constant (Traub et al., 1996; Wang an Buszaki, 1996; White 1997) and the interneurons were shown to be able to pace the pyramidal cells (Traub et al., 1996)

3.6 Thalamo-cortical system

3.6.1 Sleep

Cerebral and thalamic activities are synchronized at different levels of vigilance (Steriade, 1997). The state of resting sleep is characterized by low-frequency oscillations (<15 Hz) which extend over the whole hemisphere. The spindle oscillations (7-14 Hz) characterize early stages of resting sleep. Their mechanism includes relay and reticular cells, and if the cortex is removed, spindle oscillations persisted locally within the thalamus (< 1mm) but were no more synchronous over the whole structure. The coherence of thalamic oscillations during resting sleep was thus determined by corticothalamic projections (Contreras et al, 1996). The slow frequency is achieved by means of a loop of sequential activation: reticular cells are mutually interconnected inhibitory neurons that inhibit the thalamocortical cells. The $GABA_A$-mediated inhibition in thalamocortical cells results in the activation of low-threshold calcium current and further in a burst of action potentials. This burst of activity excites the GABAergic reticular cells, starting a new cycle. The period is mainly due to the required time for the thalamocortical cells to produce a rebound burst (Mc Cormick and Bal, 1997). Since the reticular cells form an interconnected inhibitory network, the number of cells that will be activated depends on the strength of the inhibitory synapses. It has been shown recently (Huntsman et al., 1999) that if the $GABA_A$-mediated inhibition was selectively suppressed between reticular cells in knock-out mice[3], the spindle oscillations amplitude dramatically increase, probably because all reticular cells are heavily recruited, as predicted by numerical

[3] A knock-out mouse is a mouse that has a specific gene mutated, so that the corresponding protein is no more produced. The knock-out mice used by Huntsman et al. (1999) exhibits many neurological impairments : hyperactivity, myoclonus and occasional epileptic seizures (it is considered as a model of Angelman's syndrome in human; Homanics et al, 1997; Deloray et al., 1998). The impaired fast $GABA_A$ receptor sub-unit is thus required for normal brain function, but this sub-unit is also present in other cerebral structures, but not in the thalamo-cortical cells.

simulation performed by Wang et al. (1995). Spindle oscillations are not an emergent phenomenon, they are the product of a loop of sequential activations since $GABA_A$-mediated inhibition in thalamocortical cells resulted, in the end, into a burst of activity.

3.6.2 Wakefulness

Now that the scene is set, what is going on during wakefulness? Cortical stimulation at 30-50 Hz leads to a large increase of the excitatory post-synaptic potentials in related thalamocortical cells, waiving the requirement of calcium current to be activated. Moreover, thalamocortical cells receive direct afferent input from the periphery that can be transmitted very efficiently, as previously described for retinal afferent (Alonso et al., 1996). Fast oscillations were shown in the thalamic reticular nucleus, coherently with other thalamic nuclei and the EEG (Steriade, 1996b). Reticular cells, receiving excitatory inputs from corticothalamic and thalamocortical cells, display tonic discharge at 30-40 Hz of single spikes (Steriade et al., 1986). This suggests that thalamocortical cells act as relay cells between the periphery and the cortex and between cortical sites (via common projections and intralaminar nuclei, Steriade et al., 1996a), and that reticular cells probably play a role in promoting fast synchrony amongst thalamocortical cells through a fast excitato-inhibitory loop.

This last example of the reticular cells involvement in synchronizing thalamocortical cells both during sleep spindles and wakefulness ends our overview of the evidence for synchrony and temporal coding in the central nervous system. The next section is dedicated to some techniques that are widely used to assess the existence of such synchronization between two spike trains.

4. Superior colliculus

The superior colliculus (SC) is located in the roof the mesencephalon, which is a much more primitive structure than the cortex. In the goldfish, the SC (optic tectum) has roughly the same size as the cortex. It is involved in orientation movements as demonstrated by the movements of the eyes and tail evoked by local electrical microstimulation (Herrero et al., 1998).

In mammalians, the SC is known to be involved in rapid orientation movements for a long time. Hess et al. (1946) explained these movements as being the result of a “visual grasp

reflex"[4] taking place in the mesencephalon. In small animals like rats, stimulation of the SC by local microinjections of picrotoxin or by other stimulating agents can also elicit movements resembling avoidance, defense or escape (Dean et al, 1989). This suggests that the SC is capable of producing fully integrated responses when appropriately triggered.

In humans, the SC is particularly involved in gaze orientation movements during early infancy (Johnson, 1995) because of the slow maturation of several cortical pathways. Four collicular pathways proposed by Schiller (1985) and Johnson (1995) are reproduced here:

1. *A direct pathway from the retina to the superior colliculus, involved in rapid input-driven (exogenous) eye movements toward simple, easily discriminable stimuli and fed mainly by the temporal visual field.*
2. *A cortical pathway that goes to the superior colliculus both directly from the primary visual cortex and also via the middle temporal area (MT). This pathway is largely driven by the broadband or magnocellular stream.*
3. *A cortical pathway that combines both broadband and color-opponent streams of processing in the frontal eye fields (FEFs) and that is involved in the detailed and complex analysis of visual stimuli, such as the temporal sequencing of eye movements within complex arrays and anticipatory saccades.*
4. *A final pathway for the control of eye movements involving tonic inhibition of the colliculus via the substantia nigra and basal ganglia.*

In accordance with this description, the visually guided behavior of the newborn is under predominant subcortical control. The newborn follows a moving object in a saccadic manner and is incapable of smooth pursuit. Moreover, the eyes always lag behind the stimulus movement rather than predicting its trajectory. Newborns also orient much more readily toward stimuli in the temporal visual field (rather than in the nasal visual field), and toward large objects or moving stimuli. A similar oculomotor behavior has been described in an adult subject with accidental damage to the left geniculostriate projection (Barbur et al., 1988).

The direct retinal pathway is also involved in the production of saccades with short latency. These saccades are called "express saccades" and can be reliably produced when a temporal

[4] This emphasizes the view of Mountcastle (1995) about the understanding of the brain function after Sir Sherrington as a set of intermingled reflex loops.

gap is introduced between the disappearance of an initially fixated light spot and the appearance of a new eccentric target (Fischer and Ramsperger, 1984). During this gap, the level of activity in the SC is correlated with the shortening of the saccade latency (Dorris et al., 1997). Accordingly, express saccades in the monkey are abolished after ablation of the SC (Schiller at al., 1987).

Other afferent connections also involve the cerebellum, and the efferent pathway is a complex pattern of termination sites in the brainstem and in the cervical spinal cord (Grantyn and Grantyn, 1982; Grantyn 1988 for review).

Experiments in adult cats emphasize the relationship between the SC, the retina and the visual cortex, whereas experiments in monkeys demonstrate the effect of attention and the influence of non-visual cortical areas on the SC activity.

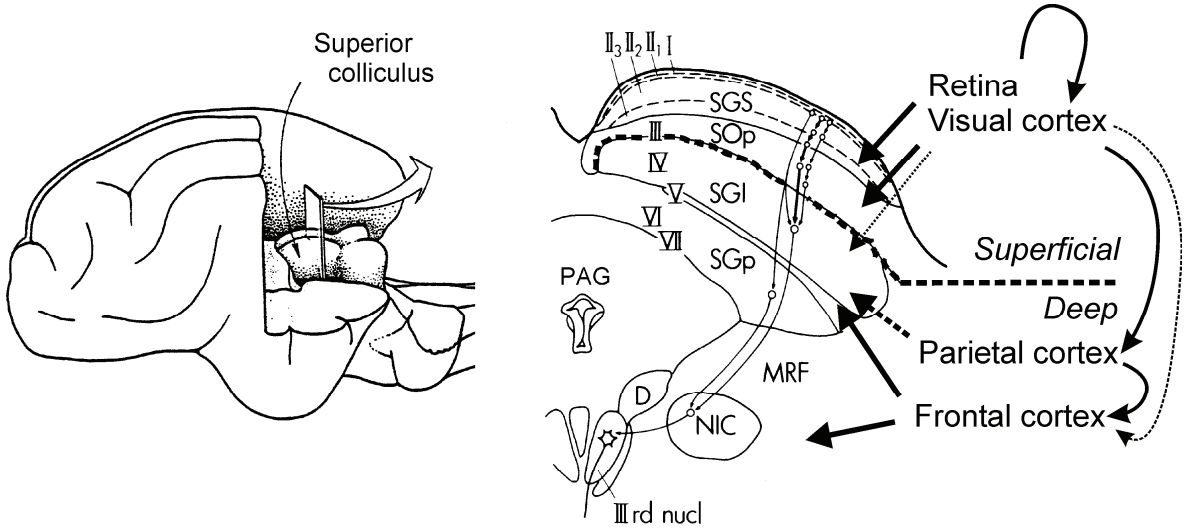

Figure 11. Laminar organization of the superior colliculus. I stratum zonale; II_1, II_2, II_3, sublaminae of stratum griseum superficiale (SGS); III, stratum opticum (SOp); IV, stratum griseum intermediale (SGI); V, stratum album intermediale (SAI); VI, stratum griseum profundum (SGP); VII, stratum album profundum (SAP). Abbreviations : periaqueducal gray (PAG); mesencephalic reticular formation MRF), nucleus interstitialis Cajal (NIC), nucleus Darkschewitsch (D).

The SC is a multi-layered structure presented in Fig.11. Each layer can be further divided in sub-layers. They are functionally grouped into the visual layers which are superficial (stratum zonale, stratum griseum superficiale, and stratum opticum), and the motor layers which are deeply located (stratum griseum intermediale, stratum album intermediale, stratum griseum profundum, and stratum album profundum). The transition between visual and motor layers occurs between the stratum opticum, and the stratum griseum intermediale (Sparks, 1986; Grantyn, 1988).

The study of the afferent and efferent terminals and of the neuronal histochemistry revealed that the superficial layers consist of two different subsystems (Mize, 1996). The division of the visual pathway into two components is supported by the bimodal distribution of the response latencies obtained after electrical stimulation of the optic nerve (Hoffman, 1973).

4.1 The superficial layers

4.1.1 The slow visual pathway

The most superficial part of the SC visual layers receives input from the slow W retinal pathway. Retinal W ganglion cells represent in cats up to 50% of the retinal ganglion cells (Spear et al., 1989). They have a slow axonal conduction velocity, large receptive field, poor spatio-temporal resolution and poor contrast sensitivity (Sur and Sherman, 1982, Sherman and Koch, 1989). Their response to visual stimulation is reported to be "characteristically sluggish" (Sur and Sherman, 1982; Spear et al.1989) and is optimal to diffuse illumination or slowly moving stimuli. They form a heterogeneous group and very little is known about their function. Freeman and Singer (1983) even proposed dividing the W-afferent into two sub-groups according to their graded conduction velocity. The slowest fibers were indeed located in the upper part of the visual layers.

Mize (1996) reports that the dense band of W retinal input to SC overlaps with the most superficial layers of small interneurons containing the calcium-binding protein calbindin. These cells apparently do not send any efferent collateral except toward the C laminae of dorsal lateral geniculate nucleus, which is known to receive direct W retinal inputs. Some of these collicular cells are probably inhibitory cells (Mize et al, 1991) and that is the reason why Mize (1996) proposed that this circuit mediates some feed-forward inhibition to the C laminae.

These cells are the first ones to be recorded when the electrode is lowered into the SC. As the room was dimly illuminated during the experiments presented in Chapter 4, these cells discharged spontaneously, making the identification of the SC easier. Their small size prevented the isolation of individual spike waveforms, so that we did not record their activities. Nevertheless, the population activity could be strongly modulated by the movement of large objects.

4.1.2 The fast visual pathway

The lowest part of the visual layers receives inputs from the Y retinal cells. These cells represent less than 10% of the retinal ganglion cells but they have the best temporal resolution, contrast sensitivity, and conduction velocity. They were studied extensively in the primate and were called M-type ganglion cells, after the magnocellular layer of the lateral geniculate nucleus to which they project. They respond to the appearance of stimulus by a transient burst and are involved in motion processing. The Y- or magnocellular pathway is classically distinguished from the parvocellular pathway, related to the slower but tonically responsive X retinal ganglion cells and to the processing of contours (and of colors in the primate).

The collicular neurons receiving Y retinal afferents seems to contain parvalbumine (Mize, 1996) and to project to the lateral posterior nucleus of the thalamus and sometimes to the dorsal lateral gray pontine nucleus.

These cells receive strong excitation from cortical visual areas 17 and 18. Most of the cortical neurons from the visual areas that project to the SC have Y-like receptive properties (Palmer and Rosenquist, 1974). They are binocularly driven and are particularly sensitive to a stimulus moving toward the periphery of the controlateral half of the visual field. Interestingly, it was shown by Wickelgren and Sterling (1969) that after lesions of the ipsilateral visual cortex, most SC cells were no longer direction selective and were driven only by the controlateral eye. Moreover, if the visual cortex was cooled, SC cells became unresponsive. In the primate, only 10% of the SC cells do show direction selectivity (Golberg and Wurtz, 1972a). However, as in the cat, inactivation of the cortical magnocellular pathway disrupts the visually driven activity in the fast SC visual cells (inactivation of the magnocellular laminae in the lateral geniculate nucleus and cortical cooling, Schiller et al., 1979).

These SC cells also exhibit an enhanced response when the animal is going to perform a saccade toward a visual target in comparison with passive viewing, as shown in Fig. 12 (Goldberg and Wurtz, 1972b) This enhancement was interpreted as related to an attentional phenomenon. It is interesting to notice that this enhancement usually persists until the saccade starts and even after the end of the eye movement.

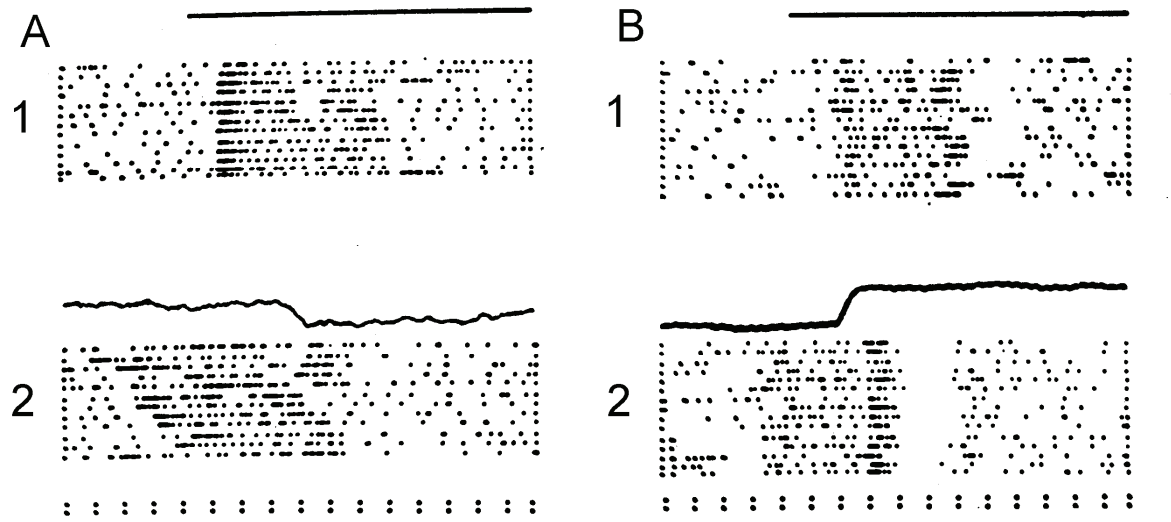

Figure 12. *Comparison of the temporal relationship of cell responses to the receptive-field stimulus and to eye movement made to the receptive-field stimulus. Responses of two cells are shown in A and B. The cell response is aligned with the onset of the receptive-field stimulus (shown by indicator line) in the segment labeled 1 and is aligned with the eye movement (located by the sample eye movement) in the segment labeled 2. In A2, the response ended shortly after the eye movement started, and in B2 the cell gave a burst of discharges at the same time, and both these responses presumably resulted from the eye movement. The on-response is not well synchronized with the eye-movement in A2 or B2.* (from Goldberg and Wurtz, 1972b.)

After the saccade, the visual cells usually exhibit a suppression of the background rate. This suppression results from a "corollary discharge" occurring during the saccade in the oculomotor system, and consequently occurred in total darkness or when a retrobulbar block was induced (Richmond and Wurtz, 1980). The mean latency of this suppression was 50 ms in the light and 90 ms in the dark or during the block.

The last important fact concerns the topographic organization of the cell receptive fields. This organization is retinotopic, i.e. the relative position of each receptive field is conserved. The center and the first 10 degrees of the visual field are represented in the anterior third of the SC. Cortical afferents do respect this organization, so that cortical cells having a central receptive field project the anterior part of the SC.

Some of the SC neurons have very large receptive fields and are also responsive to auditory or tactile stimuli (Meredith and Stein, 1990), arising from both cortical and sub-cortical structures and preserving the topographical relationship over the receptive fields (Sparks, 1989).

4.2 The deep motor layers

The first kind of efferent neurons – called T neurons – is preferentially located in the intermediate layer, and is found sometimes in neighboring layers (ventral stratum opticum

and deep layers; Moschovakis and Karabelas, 1985; Olivier et al., 1998). These neurons provide a commissural branch (tecto-tectal) and also some recurrent collaterals in the deeper layers. They are composed of two different populations immunoreactive for glutamate or GABA in equal number (Olivier et al., 1999).

The second sort of efferent neurons – called X neurons – is located in the intermediate and deep layers of the SC, and is excitatory in nature (Moschovakis and Karabelas, 1985). These neurons project to the pontomedullar reticular formation and into the spinal cervical cord, and appear to lack totally intracollicular collaterals (Grantyn and Grantyn, 1982; Moschovakis and Karabelas, 1985).

The usual motor response of these neurons is characterized by a burst of activity that precedes the saccadic eye movement by 20 ms on average (Moschovakis et al., 1996). Moreover, electrical stimulation in the SC deep layers elicits short latency gaze movements. Both cellular discharges and electrically evoked saccades are organized according to the retinotopic map, i.e. large amplitude movements elicit a burst of activity in the posterior part of the SC, and are evoked by electrical stimulation of the same area. Cells in the anterior SC discharge for small amplitude movements, and if their receptive field includes the center, they discharge also during target fixation (fixation cells).

Population coding of the saccadic eye movements was demonstrated in the SC by local injection of lidocaine (Lee et al., 1988) which showed that the direction, amplitude and velocity of saccadic eye movements are determined by the entire population of active SC cells.

4.2.1 Cortical afferents

Cells in the deep SC (intermediary and deep layers) receive the same kind of magnocellular input from visual cortical areas as the cells described in the fast visual pathway, but to a considerably less extent (Harting et al., 1992). The main characteristic of the visual response is *a dramatic decrease of the response magnitude with repetitive stimulus presentation*. As in fast visual cells, no visual response can be elicited after ablation or cooling of the visual cortex. But in these conditions, the burst of activity related to the saccadic eye movements is still observed.

It is also possible to elicit saccadic gaze movement by electrical stimulation of the occipital, parietal or frontal cortices. Movements evoked by stimulation of the visual cortex are blocked

by lesions of the SC[5] (Keating and Gooley, 1988). However, the isolated lesion of the SC or of the frontal eye fields[6] (FEF) are unable to suppress saccades evoked by electrical stimulation of the parietal cortex. The proposed explanation is that there are two pathways from the visual cortex to the oculomotor structures: one through the SC, the other through the parietal cortex and the FEF[7]. Moreover, the FEF send axons directly to collicular neurons in the intermediate layer (Fries, 1984; Segraves and Goldberg, 1987). FEF microstimulations excite cells in the SC that code for the same vector and inhibit all others (Schlag-Rey, Schlag and Dassonville, 1992).

Neurons in the FEF are very active just before visually guided and memory guided saccades (Segraves and Goldberg, 1987). Some of them could also respond to visual stimulus, but this activity was not sustained (Schall and Hanes, 1993).

Another important cortical area playing a role in saccade production in the monkey is the lateral intraparietal area (LIP)[8]. These neurons discharge in response to the stimulus presentation and when the monkey waits for the eye saccade in the visual area corresponding to the cell visual field, even if the visual target has already disappeared (Martin and Wurtz, 1997).

4.2.2 Motor preparation

The involvement of the SC in the preparation of orientating movements is suggested in the primate by the discharge of some cells called "buildup cells" preceding the saccades to memorized targets as shown in Fig. 13 (Munoz and Wurtz, 1995). These cells discharge in response to the flashed target, but as fixation is still required, their discharge decreases slowly. When the fixation point disappears and the monkey is allowed to shift its gaze to the remembered flash location, the discharge of the buildup cell increases and eventually changes into a high frequency burst at saccade onset. The fact that the activity increases slowly –

---

[5] There is however a small area in the visual cortex which connects directly the FEF and from which electrical stimulation evokes saccadic eye movements.

[6] The frontal eye field is in the anterior bank of the arcuate sulcus in frontal cortex

[7] As pointed out by Grantyn (1988), saccadic eye movements elicited by stimulation of the ipsilateral frontal eye field are not prevented by SC ablation, indicating the existence of two independent cortico-oculomotor pathways: a striate-tecto-oculomor pathway, and a fronto-oculomotor pathway. Frontal eye fields do project to the SC although these connections are not required to elicit a saccadic eye movement.

[8] The lateral intraparietal area is located in the lateral bank of the intraparietal sulcus in posterior parietal cortex.

"builds up" – 100-150 ms before the saccade could be regarded as an argument for the movement preparation in the SC.

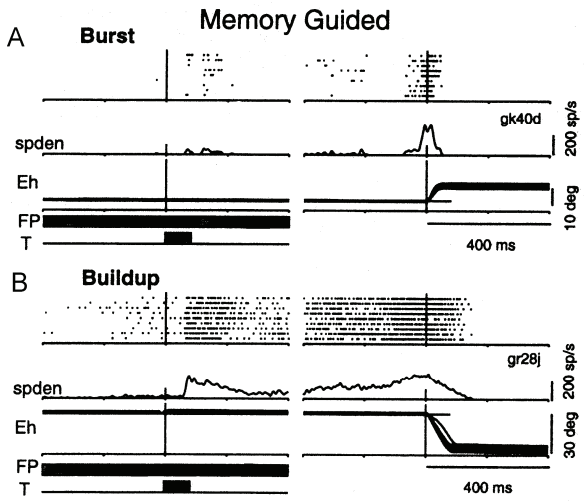

Figure 13. Burst and buildup discharges during memory guided saccades. In the upper panel is displayed the discharge of a burst cell, which is represented by a spike raster or by a spike density function (spden, σ=4 ms). The eye horizontal position (Eh) is shown below with a schematic representation of the behavioral paradigm. While the fixation point (FP) remained illuminated, the Target was flashed. After a random period of time (400-800 ms), the FP was turned off and the monkey was required to make a saccade in the direction of the remembered location of the T flash. On the left, the discharge of the burst cell is aligned with the T onset, whereas on the right, this discharge is aligned with the beginning of the eye movement. The burst cell discharged mainly just before and during the saccade. (B) In contrast, the buildup cell exhibited a sustained response after the presentation of the target and this discharge increased until the saccade was performed. (Modified from Munoz and Wurtz, 1995)

The buildup discharge was also shown to be modulated by the number of possible targets and the monkey's expectations (Basso and Wurtz, 1997). Similar modulations of the spike discharge were found in many cortical areas : the frontal cortex, but also the visual cortex, the medio-temporal and especially the lateral intraparietal areas (Schall et al., 1995; Moran and Desimone, 1985; Treue and Maunsell, 1996; Motter 1993; Paré and Wurtz, 1997). Most of the non-visual cortical projections are directed to the griseum intermediale and include also adjacent superficial and deep layers (Shook at al., 1990; Harting et al., 1992).

There is no experiment which definitively proves that the buildup cells are radically different from the fast visual cells with enhanced response described by Goldberg and Wurtz (1972b). Visual cells with enhanced response and buildup cells could belong to the same category, except for the more frequent presence of a saccade-related burst of activity in buildup cells and for their projections to the reticulo-spinal pathway. A definitive demonstration of the existence of motor preparation in the SC, would be the characterization of buildup cells in the decorticated animal during memory guided saccade, which is probably impossible to show. However, the distinction between attention shift and motor preparation could be impossible to draw. Mays et al. (1987) showed that electrically evoked saccades are modified when the monkey prepares an eye movement. Kustov and Robinson (1996) demonstrated that similar changes occur when the monkey simply fixated on a target and was required to respond only with hand movements to a color cue in the center of the visual field. Attention was shifted to

the right or to left, and electrically evoked saccades were subsequently modified. Attention shifts are definitely involved in this effect, but it is impossible to exclude the possibility that the monkey did not plan a gaze movement.

We could then assume a continuum of discharge patterns in SC from the simple fast visual cells to the burst cells according to their cortical inputs. Spikes emitted during the buildup response could simply be related to the afferent terminals originating from the cortex and mediating attentional enhancement. Indeed, attentional enhancement occurs during the period of target remembrance and long before the movement, simultaneously in the SC and in the lateral intraparietal area, whereas the burst related to the gaze movement occurs mainly in the SC and in the FEF (Paré and Wurtz, 1997).

The fact that buildup could be just the result of a cortical process does not contradict its possible importance in priming the SC activity and in the target selection process.

The SC could be understood as a visual and attentional filter on the cortico-tectal-oculomotor pathway, which ensures that, in the end, only one orientation movement is selected. Once the burst is triggered in the SC, the activity could be locally amplified by the local excitatory circuit located in the intermediate layers of the SC (Pettit et al., 1999) and dispatched to the brain stem and the spinal cord.

As expected from its presumed function of attentional filter, the SC is not essential for saccadic eye movements. Lesions in the monkey SC produce only minor deficit in saccadic accuracy for peripheral targets. SC lesions resulted in an increase in latency of saccadic movements in the days following the lesion (generally about 150-300 ms) and transient changes in eye velocity profiles (Wurtz an Golberg, 1972). Cats with unilateral SC lesions disregard the stimuli of the controlateral visual field much more than the monkeys and they walk in circles away from this field (Sprague and Meikle, 1965). However, this hemi-neglect syndrome is transient, emphasizing the power of the cortex in making up for the SC lesion.

4.2.3 Saccadic push-pull mechanism

The saccade is preceded by a burst of activity in about 15 different types of saccade related cells in addition of the oculomotor neurons (Moschovakis et al., 1996). As explained in the previous section, this burst can be elicited from stimulation of the SC, the visual cortical areas, the frontal eye fields, but also in the thalamus, cerebellum and various reticular areas (Grantyn, 1988). Saccades also interrupt the tonic activity of other kinds of cells, called pause neurons – a category to which the fixation cells in the anterior part of the SC and some other

inhibitory cells in the brain stem, called the omnipause neurons belong (see Moschovakis et al, 1996, for details).

During fixation, both the fixation cells in the rostral pole of the SC and the omnipause neurons discharge. They both inhibit the population of burst cells in the caudal part of the SC. Before a saccade, the background activity increases at one location on the SC sensori-motor map until a burst is triggered. During the burst, the omnipause neurons are inhibited until the end of the saccade. Fixation activity is then restored as well as the activity in the omnipause neurons, and burst cells are inhibited. Fixation cells are somewhat different from the omnipause neurons, because fixation cells could also discharge for small saccade amplitude (Munoz and Wurtz, 1993a,b; Gandhi and Keller, 1997).

4.3 Synchrony in the superior colliculus

Activity in SC can thus be divided into three categories: visual response, attentional-premotor discharge, and phasic movement-related burst.

The analysis of the coherence between two spike trains during the movement-related burst is expected to be trivial. The gaze movement would synchronize the spikes, just as in the visual cortex an external stimulus synchronized cell discharges. It would have been more interesting to look at the buildup discharge during the movement preparation. However, the training of behaving cats to a task with delayed or remembered targets seemed very demanding if not impossible. As demonstrated recently, the buildup activity depends on animals' expectations (Basso and Wurtz,1997). That would imply that the cat was sufficiently attentive to produce some expectation during a two-hour session. These are the main reasons why we choose the less demanding fixation task to analyze the visual response of cells in the SC.

Moreover, the similarity between SC and cortical responses to a moving stimulus led Neuenschwander and Varela (1993) to study the dynamics of the SC in the awake pigeon in response to moving light bars. The bars are well known to elicit maximal oscillatory response at the cortical level, whereas SC cells are not sensitive to their orientation. Using only one recording channel, they showed that both the multiunit activity response and the local field potential in the SC presented some oscillatory epochs. These oscillations had frequencies in the range 20-50 Hz and exhibited a great variability. It was suggested that these oscillations were the carrier for synchronization between cortical areas and the SC.

Brecht et al. (1998) examined this question in the anesthetized cat. Although they showed some cases of synchronized discharges between the visual cortex and the SC at 40 Hz, most of the recording exhibited a frequency of 10 Hz. Moreover, the synchronization was broadly tuned and the central peak in the CCH had a mean width of 51 ms, indicating that the cells were co-activated rather than finely synchronized.

Since attention was shown to be an important component in the SC discharge, we decided to study the SC dynamics in the awake cat. In order to assess the fine temporal synchronization between neighboring cells, we also used two independent electrodes.

5. Appendix: Technical background

Synchronization is quantified by means of cross-correlation histograms (CCH, Fig. 14). For each spike of the first spike train A, one assesses if some spikes occurred around the same time in spike train B. The time intervals between the reference A's spike and the B's spikes are counted in a histogram, the cross-correlation histogram (CCH). Such counts, when divided by the number of A's spikes, represent the conditional probability of the occurrence of a B's spike if an A's spike occurred. When two spike trains are independent, the CCH is flat, i.e. the conditional probability remains constant whatever the time interval.

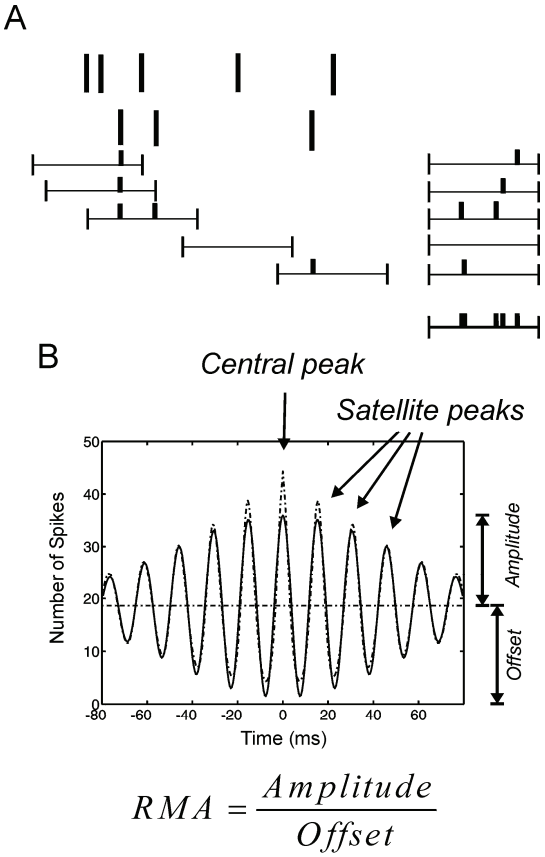

$$RMA = \frac{Amplitude}{Offset}$$

Figure 14. The counting process involved in the CCH, and related measures. (A) For each spike of the reference train, one counts the spikes occurring within a determined delay in the second train. The sum of all these histogram leads the CCH. (B) The CCH could then be quantified by fitting damped sine wave (Gabor function; König, 1994), and the parameter of this function are used to characterize the CCH. They are the amplitude, the offset, the frequency, the peak lag and the damping constant. Complementary parameter could be added in order to characterize the central peak individually. We uses this method to quantify the CCH of our simulated network in Chapter 2. The other way consists in calculating the expected CCH from the cell firing rates, and then to compare the value obtained to the predicted value, assuming either a normal distribution when this value is large, or a Poisson distribution when the value small or if the ISI is shorter than one bin and two or more spikes occur sometimes in the same bin for a single reference spike. Oscillations are then assessed by the existence of a second or a third peak next the central peak. This is the method we found appropriate for the data analyses presented in Chapter 4.

When two spike trains are synchronized with a zero-time lag, the conditional probability of a B's spike is higher at 0 ms than at other time lags. It is usually described as a "central peak".

Furthermore, if cells discharge regularly, the B's spikes tend to be locked on the simultaneous A's spike, but also to the preceding and following spikes. This is revealed by some peaks at a time lag corresponding to the cell period. These peaks are called "satellite peaks" and are the hallmark of synchronized oscillations.

The last situation is when cell A is serially connected to cell B. Then the CCH expresses the change in discharge probability due to that connection and the time interval at which the peak occurs correspond to the conduction delay. The influence of single connection requires many thousand spikes to be characterized and as two cells are usually part of the same network, it is mainly the influence of the network activity which determines the CCH profile.

From the central peak the peak lag, the amplitude, the width at half height, and the area are extracted. The amplitude is usually compared to the offset as a measure of the

synchronization strength (amplitude to offset ratio, also called the relative modulation amplitude RMA, Gray et al., 1990; Nelson et al., 1992)[9] .

These parameters can be extracted from the raw data if the spike trains are recorded in stationary conditions. When the spikes are produced in response to a stimulus, the stimulus could synchronize the recorded cells. This stimulus related synchronization is quantified by the shift- or shuffled-predictor (Perkel et al. 1967, Palm et al., 1988). As the CCH, the shift predictor is computed between train A and train B, except that the trains come from two different trials. In the shift predictor, if train A corresponds to the n^{th} trial, the correlation is computed with train B of the $(n+1)^{th}$ trial. In the shuffled predictor, the trial for train B is chosen randomly.

The use of the shift-predictor has severe limitations: it implies that the cell discharges are stationary. The mean firing rate and discharge variability are supposed to be identical for each stimulus presentation. This condition is probably fulfilled in the anesthetized animals if simple sensory paradigms are used. But in the awake animal, which is subject to attention fluctuations and fatigue, cell discharges could vary strongly from one trial to next, and worse than that, cell discharges often covary. Indeed, two simultaneously recorded cells tend to discharge at a high rate at the same time because their discharge is related to the experimental conditions. This can produce an underestimation of stimulus locked effect and of the expected number of coincident events, as discussed in Chapters 3&4.

Significance calculation of the CCH peaks are discussed by Palm et al. (1988), but all these tests assume that the PSTHs adequately represent the firing rate of each trials and that spike trains do not covary with trial repetition or with other poorly controlled parameters like attention and task performance.

Some authors developed some quantification methods to partially alleviate this problem, like the fitting a damped sine wave function on the CCH (Gabor function, Gray et al., 1989; Engel et al., 1990; König, 1994), or like Eckhorn et al. (1989) who compared the raw CCH to the filtered CCH (Eckhorn et al., 1988). Such methods, if the parameters are carefully checked,

[9] A lot of normalization methods were also developed that did not much improve the quality of the information ("Correlation index", where amplitude is replaced by half the distance from peak to trough, Livingstone, 1996; "Michelson contrast", Bringuier et al. 1997). Palm et al. (1988) encouraged the use of the correlation coefficient (the amplitude divided by the product of the spike count standard deviations). The strength of the interaction was also estimated by measuring the areas rather than the amplitudes (Toyama et al, 1981ab; Ts'o et al., 1986; Schwarz and Bolz, 1991), which is less descriptive than the combination of amplitude, width, and lag.

ensure that only narrow peaks are quantified. If the CCH is calculated during stable conditions (a moving stimulus at constant velocity) and if the shift predictor does not exhibit a narrow peak, then the narrow peak in the CCH is probably due to emergent network synchronization.

REFERENCES

Abeles M (1982) Role of the cortical neuron: integrator or coincidence detector ? *Isr. J. Med. Sci.* 18:83-92.

Abeles M (1991) Corticonics: neural circuits of the cerebral cortex. Cambridge University Press, Cambridge.

Abeles M, Bergman E, Margalit E, Vaadia E (1993) Spatiotemporal firing patterns in the frontal cortex of behaving monkeys. *J. Neurophysiol.* 70:1629-1638.

Abeles M, Gerstein GL (1988) Detecting spatiotemporal firing patterns among simultaneously recorded single neurons. *J. Neurophysiol.* 60 : 909-924.

Abeles M, PrutY, Bergman H, Vaadia E (1994) Synchronization in neuronal transmission and its importance for information processing. *Prog. Br. Res.* 102:395-404.

Alonso JM, Usrey WM, Reid RC (1996) Precisely correlated firing in cells of the lateral geniculate nucleus. *Nature* 383:815-819.

Amzica F, Neckelman D, Steriade M (1997) Instrumental conditioning of fats (20- to 50-Hz) oscillations in corticothalamic networks. *Proc. Natl. Acad. Sci. USA* 94:1985-1989.

Baker SN, Olivier E, Lemon RN (1997) Coherent oscillations in the monkey motor cortex and hand muscle EMG show task-dependent modulation. *J. Physiol.* 501:225-541.

Baker, S.N. and Lemon, R.N. (1999). Precise repeating neuronal patterns are not evidence for temporal coding. *Science* (submitted).

Barbur JL, Forsyth PM, Findlay JM (1988) Human saccadic eye movements in the absence of the geniculocalcarine projection. *Brain* 111:63-82.

Basso MA, Wurtz RH (1997) Modulation of neuronal activity by target uncertainty. *Nature* 389:66-69.

Bishop CM, Svensen M, Williams CKI (1998) GTM: The generative topographic mapping. *Neural Comput.* 10:215-234.

Brecht M, Singer W, Engel AK (1998) Correlation analysis of corticotectal intercations in the cat visual system. *J. Neurophysiol.* 79:2394-2407.

Bringuier V, Frégnac Y, Baranyi A, Debanne D, Shulz DE (1997) Synaptic origin and stimulus dependency of neuronal oscillatory activity in the primary visual cortex of the cat. *J. Physiol.* 500:751-774.

Brown TH, Zador AM (1990) Hippocampus. In: The synaptic organization of the brain (Shepherd GM, ed.), pp 346-388. New York: Oxford University Press.

Burchell TH, Faulkner MA, Whittington MA (1998) Gamma frequency oscillations gate temporally coded afferent inputs in the rat hippocampal slice. *Neurosci. Lett.*255:151-154.

Bush P, Sejnowski T (1996) Inhibition synchronizes sparsely connected cortical neurons within and between columns in realistic network models. *J. Comput. Neurosci.* 3:91-110.

Contreras D, Destexhe A, Sejnowski TJ, Steriade (1996) Control of spatiotemporal coherence of a thalamic oscillation by corticothalamic feedback. *Science* 274:771-774.

D

Datta AK, Stephens JA (1990) Short-term synchronization of motor unit activity during voluntary contractions in human. *J. Physiol.* 422:397-419.

Dayhoff JE, Gerstein GL (1983) Favored patterns in spike trains. I. Detection. *J. Neurophysiol.* 49:1334-1348.

Dayhoff JE, Gerstein GL (1983) Favored patterns in spike trains. II. Application. *J. Neurophysiol.* 49:1349-1363.

Dean P, Redgrave P, Westby GWM (1989) Event or emergency? two response systems in the mammalian superior colliculus. *Trends Neurosci.* 12:137-147.

deCharms RC, Merzenich MM (1996) Primary cortical representation of sounds by the coordination of action-potential timing. *Nature* 381:610-613.

Donoghue JP, Sanes JN, Hatsopoulos NG, Gaal G (1998) Neural discharge and local field potential oscillations in primate motor cortex during voluntary movements. *J. Neurophysiol.* 79:159-173.

Dorris MC, Paré, M, Munoz DP (1997) Neuronal activity in monkey superior colliculus related to the initiation of saccadic eye movements. *J. Neurosci.* 17:8566-8579.

Eckhorn R (1994) Oscillatory and non-oscillatory synchronizations in the visual cortex and their possible roles in associations of visual features. *Prog. Brain Res.* 102:405-426.

Engel AK, König P, Kreiter AK, Schillen TB, Singer W (1992) Temporal coding in the visual cortex: new vistas on integration in the nervous system. *Trends Neurosci.* 15:218-226.

Engel AK, König P, Kreiter AK, Singer W (1991a) Interhemispheric synchronization of oscillatory neuronal responses in cat visual cortex. *Science* 252:1177-1179.

Engel AK, König P, Schillen TP (1992) Why does the cortex oscillate ? *Curr. Biol.* 2:332-334.

Engel AK, König P, Singer W (1991b) Direct physiological evidence for scene segmentation by temporal coding. *Proc. Natl. Acad. USA* 88:9136-9140.

F

Farmer SF, Bremmer FD, Halliday DM, Rosenberg JR, Stephens JA (1993) The frequency content of common synaptic inputs to motoneurones studied during voluntary isometric contraction in man *J. Physiol.* 470:127-155.

Fischer B, Ramsperger E (1984) Human express saccades: extremely short reaction times of goal directed eye movements. *Exp. Brain Res.* 57:191-195.

Freeman B, Singer W (1983) Direct and indirect visual inputs to superficial layers of cat superior colliculus: a current source-density analysis of electrically evoked potentials. *J. Neurophysiol.* 49:1075-1091.

Fries W (1984) Cortical projections to the superior colliculus in the macaque monkey: a a retrograde study using horseradish peroxidase. *J. Comp. Neurol.* 230:55-76.

Fukai T (1996) Competition in the temporal domain among neural activities phase-locked to subthreshold oscillations. *Biol. Cybern*. 75:453-461.

Gabbiani and Koch (1998) Principles of spike train analysis. In : Methods in neuronal modeling: from ions to networks (Koch C and Segev I ed.), pp 313-360. Cambridge: MIT Press.

Gandhi NJ, Keller EL (1997) Spatial distribution and discharge characteristics of superior colliculus neurons antidromically activated from the omnipause region in monkey. *J. Neurophysiol.* 78:2221-2225.

Georgopoulos AP (1995) Current issues in directional motor control. *Trends Neurosci.*13:2758-71.

Georgopoulos AP, Lurito JT, Petrides M, Schwartz AB, Massey JT (1989) Mental rotation of the neuronal population vector. *Science* 243:234-236.

Gerstner W (1996) Rapid phase locking in systems of pulse-coupled oscillators with delays. *Phys. Rev. E* 76:1755-1758.

Ghose GM, Freeman RD (1997) Intracortical connections are not required for oscillatory activity in the visual cortex. *Vis. Neurosci.* 14:963-979.

Goldberg ME, Wurts RH (1972a) Activity of superior colliculus in behaving monkey. I. Visual receptive fields of single neurons. *J. Neurophys.* 15:542-559.

Goldberg ME, Wurtz RH (1972b) Activity of superior colliculus in behaving monkey. II. Effect of attention on neuronal responses. *J. Neurophys.* 15:560-574.

Grantyn A, Grantyn R (1982) Axonal patterns and sites of termination of cat superior colliculus neurons projecting in the tecto-bulbo-spinal tract. *Exp. Brain Res.* 46:243-256.

Grantyn R (1988) Gaze control through superior colliculus: strucutre and function. In: Neuroanatomy of the oculomor system (Büttner-Ennever, ed.), pp 273-333. Elsevier.

Gray CM, Engel, AK, König P, Singer W (1990) Stimulus-dependent neuronal oscillations in cat visual cortex: receptive field properties and feature dependence. *Eur. J. Neurosci.* 2:607-619.

Gray CM, Singer W (1989) Stimulus specific neuronal oscillations in orientation columns of cat visual cortex. *Proc. Natl. Acad. Sci. USA* 86:1696-1702.

Gray CM, Viana Di Prisco G (1997) Stimulus-dependent neuronal oscillations and local synchronization in striate cortex of the alert cat. *J. Neurosci*. 17:3239-3253.

H

Hansel D, Mato G, Meunier C (1995) Synchrony in excitatory neural networks. *Neural Comput.* 7:307-337.

Hebb DO (1949) The organization of behavior: a neuropsychological theory. Willey. New York.

Herrero L, Rodriguez F, Salas C, Torres B (1998) Tail and eye movements evoked by electrical microstimulation of the optic tectum in goldfish. *Exp. Brain Res.* 120:291:305.

Hess WR, Bürgi S, Bucher V (1946) Motor function of tectal and tegmental area. *Mschr. Psychiat. Neurol.* 112:1-52.

Halliday DM, Conway BA, Farmer SF, Rosenberg JR (1998) On the use of the EEG to explore functional aspects of correlations between cortical recordings and muscle EMG during voluntary contractions in human. *Neurosci. Let.* 241:5-8.

Harting JK Updyke BV, Van Lieshout DP (1992) Corticotectal projections in the cat: anterograde transport studies of twenty-five cortical areas. *J. Comp. Neurol.* 324:379-414.

Hoffmann KP (1973) Conduction velocity in pathways from retina to superior colliculus in the cat: a correlation with receptive fields properties. *J. Neurophysiol.* 36:409-424.

Hopfield JJ (1995) Pattern recognition computation using action potential timing for stimulus representation. *Nature* 376:33-36.

Hopfield JJ (1995) Transforming neual coputations and representing time. *Proc. Natl. Acad. Sci. USA* 93:15440-15444.

Hopfield JJ, Brody CD, Roweis S (????) Computin with action potentials. ????

Huntsman MM, Porcello DM, Homanics GE, DeLorey TM, Huguenard JR (1999) Reciprocal inhibitory connections and network synchrony in the mammalian thalamus. *Science* 283:541-543.

Jagadeesh B, Gray CM, Ferster D (1992) Visually evoked oscillations of membrane potential in neurons of cat striate cortex studied with in vivo whole cell patch recording. *Science.* 257:552-554.

Johnson MH (1995) The development of visual attention: a cognitive neuroscience perspective. In: The cognitive neurosciences (Gazzaniga MS, ed.), pp 735-747. Cambridge: MIT Press.

Jones KR, Berkley MA (1983) Loss of temporal sensitivity in dorsal lateral geniculate nucleus and area 18 of the cat following monocular deprivation. *J. Neurophysiol.* 49:254:268.

K

Keating EG, Gooley SG (1988) Disconnection of parietal and occipital access to the saccadic oculomotor system. *Exp. Brain Res.* 70:385-398.

Kempter R, Gerstner W, van Hemmen JL, Wagner H (1998) Extracting oscillations: neuronal coincidence detection with noisy periodic spike input. *Neural Comp.* 10:1987-2017.

Koch (1997) Computation and the single neuron. *Nature* 385:207-210.

Koch C, Rapp M, Segev I (1996) A brief history of time (constants). *Cereb. Cortex* 6:93-101.

Kohonen T (1982) Self-organized organized of topologically correct feature maps. *Biol. Cybern.* 43:59-69.

Kohonen T (1995) Self-organizing maps. Berlin. Springer-Verlag.

Kohonen T, Kaski S, Lappalainen H (1997) Self-organized formation of various invariant feature filters in the adaptive-subspace SOM. *Neural Comp.* 9:1321-1344.

König P (1994) A method for the quantification of synchrony and oscillatory properties of neuronal activity. *J. Neurosci. Meth*. 54:31-37.

König P, Engel AK, Löwel S, Singer W (1993) Squint affects synchronization of oscillatory responses in cat visual cortex. *Eur. J . Neurosci.* 5:501-508.

König P, Engel AK, Singer W (1994) Integrator or coincidence detectors ? The role of cortical neuron revisited. *Trends Neurosci.* 19:130-137.

König P, Engel AK, Singer W (1995) Relation between oscillatory activity and long range synchronization in cat visual cortex. *Proc. Natl. Acad. Sci. USA* 92:290-294.

Kreiter AK,Singer W (1994) Global stimulus arrangement determines synchronization of neuronal activity in the awake macaque monkey. *Suppl. Eur. J. Neurosci.* 7:153.

Kruse W, Eckorn R (1996) Inhibition of sustained gamma oscillations (35-80 Hz) by fast transient responses in cat visual cortex. *Proc. Natl. Acad. USA* 93:6112-6117.

Larkum ME, Zhu JJ, Sakmann B (1999) A new cellular mechanism for coupling inputs arriving at different cortical layers. *Nature* 398:338-341.

Lee C, Rohrer WH, Sparks DL (1988) Population coding of saccadic eye movements by neurons in the superior colliculus. *Nature* 332:357-360.

Lisman JE, Idiart MA (1995) Storage of 7±2 short-term memories in oscillatory subcycles. *Science* 267:1512-1515.

Livingstone MS (1996) Oscillatory firing and interneuronal correlations in squirrel monkey striate cortex. *J. Neurophysiol.* 75:2467-2485.

Löwel S, Singer W (1992) Selection of intrinsic horizontal connections in the visual cortex by correlated neuronal activity. *Science* 255:209-212.

M

Maex R, De Schutter E (1998) Synchronization of Golgi and granule cell firing in a detailed network model of the cerebellar granule cell layer. *J. Neurophysiol.* 80:2521-2537.

Mc Cormick DA, Bal T (1997) Sleep and arousal: thalamocortical mechanisms. *Annu. Rev. Neurosci.* 20:185-215.

Meredith MA, Stein BE (1990) The visuotopic component of the multisensory map in the deep laminae of the cat superior colliculus. *J. Neurosci.* 10:3727-3742.

Metherate R, Cox CL, Ashe AH (1992) Cellular bases of neocortical activation: modulation of neural oscillations by the nucleus basalis and endogenous acetylcholine. *J. Neurosci.* 12:4701-4711.

Mirollo RE, Stogatz SH (1990) Synchronization of pulse-coupled biological oscillators. *SIAM J. Appl. Math.* 6:1645-1657.

Mize RR (1996) Neurochemical microcircuitry underlyning visual and oculomotor function in the cat superior colliculus. *Prog. Brain Res.* 112:35-55.

Mize RR, Jeon CJ, Butler G, Luo Q, Emson PC (1991) The calcium binding protein calbindin-D28K reveals subpopulations of projection and interneurons in the cat superior colliculus. *J. Comp. Neurol.* 307:417-436.

Moran J, Desimone R (1985) Selective attention gates visual processing in extrastriate cortex. *Science* 229:782-784.

Morris RGM, Anderson E, Lynch GS, Baudry M (1986) Selective impairment of learning and blockade of long-term potentiation by an N-methyl-D-aspartate receptor antagonist, AP5. *Nature* 319:774-776.

Moschovaki AK, Karabelas AB (1985) Observations on the somatodendritic morphology and axonal trajectory of intracellularly HRP-labeled efferent neurons located in the deeper layers of the superior colliculus of the cat. *J. Comp. Neurol.* 239:276-308.

Moschovakis AK, Scudder CA, Highstein SM (1996) The microscopic anatomy and physiology of the mammalian saccadic system. *Prog. Neurobiol.* 50:133-254.

Motter BC (1993) Focal attention produces spatially selective processing in visual cortical areas V1; V2, and V4 in the presence of competing stimuli. *J. Neurphysiol.* 70:909-919.

Mountcastle V (1995) The evolution of ideas concerning the function of the neocortex. *Cereb. Cortex* 5:289-295.

Munoz DP, Wurtz RH (1993a) Fixation cells in the monkey superior colliculus. I. Characteristics of cell discharge. *J. Neurophysiol.* 70:559-575.

Munoz DP, Wurtz RH (1993b) Fixation cells in the monkey superior colliculus. II. Reversible activation and deactivation. *J. Neurophysiol.* 70:576-589.

Munoz DP, Wurtz RH (1995) Saccade-related activity in monkey superior colliculus I. Characteristics of burst and buildup cells. *J. Neurohysiol.* 73:2313-2333.

Murthy VN, Fetz EE (1992) Coherent 25- to 35-Hz oscillations in the sensorimotor cortex of awake behaving monkey. *Proc. Natl. Acad. Sci. USA* 89:5670-5674.

Murthy VN, Fetz EE (1996a) Oscillatory activity in sensorimotor cortex of awake monkeys: synchronization of local field potentials and relation to behavior. *J. Neurophysiol.* 76:3949-3976.

Murthy VN, Fetz EE (1996b) Synchronization of neurons during local field potential oscillations in sensorimotor cortex of awake monkeys. *J. Neurophysiol.* 76:3968-3982.

Nelson JI, Salin PA, Munk MHJ, Arzi M, Bullier J (1992) Spatial and temporal coherence in cortico-cortical connections: a cross-correlation study in areas 17 and 18 in the cat. *Vis. Neurosci.* 9:21-37.

Neuenschwander S, Singer W (1996) Long-range synchronization of oscillatory light responses in the cat retina and lateral geniculate nucleus. *Nature* 379:728-733.

Neuenschwander S, Varela FJ (1993) Visually triggered neuronal oscillations in the pigeon: an autocorrelation study of the tectal activity. *Eur. J. Neurosci.* 5:870-881.

Olivier E, Chat M, Grantyn A (1991) Rostrocaudal and lateromedial density distributions of superior colliculus neurons projecting in the predorsal bundle and to the spinal cord: a retrograde HRP study in the cat. *Exp. Brain Res.* 87:268-282.

Olivier E, Corvisier J, Pauluis Q, Hardy O (1999) Evidence for Glutamate-positive commissural neurons in the cat superior colliculus. *Submitted.*

Olivier E, Grantyn A, Chat M, Berthoz A (1993) The control of slow orienting eye movements by tectoreticulospinal neurons in the cat: behavior, discharge patterns and underlying connections. *Exp. Brain Res.* 93:435-49.

Olivier E, Porter JD, May PF (1998) Comparison of the distribution and somatodendritic morphology of tectotectal neurons in the cat and monkey. *Vis. Neurosci.* 15:903-922.

Olton DS, Becker JT, Handelman GE (1979) Hippocampus, space, and memory. *Behav. Brain Sci.* 2:313-365.

Olton DS, Samuelson RJ (1976) Remembrance of places passed: spatial memory in rats. *J. Exp. Psychol.* 2:97-116.

Palm G, Aertsen AMHJ, Gerstein GL (1988) On the significance of correlations among neuronal spike trains. *Biol. Cybern.* 59:1-11.

Palmer LA, Rosenquist AC (1974) Visual receptive fields of single striate cortical units projecting to the superior colliculus in the cat. *Brain Res.* 67:27-42.

Paré M, Wurtz RH (1997) Monkey posterior parietal cortex neurons antidromically activated from superior colliculus. *J. Neurophysiol.* 78:3493-3497.

Parodi O, Combe P, Ducom JC (1996) Temporal coding in vision: coding by the spike times arrival leads to oscillations in the case of moving target. *Biol. Cybern.* 74:497-509.

Pettit DL, Helms MC, Lee P, Augustine GJ, Hall WC (1999) Local excitatory circuits in the intermediate gray layer of the superior colliculus. *J. Neurophysiol.* 81:1424-1427.

Pellerin JP, Lamarre Y (1997) Local field potential oscillations in primate cerebellar cortex during voluntary movements. *J. Neurophysiol.* 78:3502-3507.

Prechtl JC (1994) Visual motion induces synchronous oscillations in turtle visual cortex. *Proc. Natl. Acad. Sci. USA* 91:12467-12471.

R

Richmond BJ, Wurtz RH (1980) Vision during saccadic eye movements. II. A corollary discharge to monkey superior colliculus. *J. Neurophysiol.* 43:1156-1167.

Rock I, Palmer S (1990) The legacy of Gestalt psychology. *Scient. Am.* 263(6):48-61.

Roelfsema PR, König P, Engel AK, Sireteanu R, Singer W (1994) Reduced synchronization in the visual cortex of cats with strabismic amblyopia. *Eur. J. Neurosci.* 6:1645-1655.

Roelfsema PR, Singer W (1998) Detecting connectedness. *Cereb. Cortex* 8:385-396.

Salenius S, Portin K, Kajola M, Salmelin R, Hari R (1997) Cortical control of human motorneuron firing during isometric contraction. *J. Neurophysiol.* 77::3401-3405.

Sanes JN, Donoghue JP (1993) Oscillations in local field potentials of the primate motor cortex during voluntary movement. *Proc. Natl. Acad. Sci. USA* 90:4470-4474.

Schall JD, Hanes DP (1993) Neural basis of saccade target selection in frontal eye field during visual search. *Nature* 366:467-469.

Schall JD, Hanes DP, Thompson KG, King DJ (1995) Saccade target selection in frontal eye field of macaque. I. Visual and premovement activation. *J. Neurosci.* 15:6905-6918.

Schiller PH (1985) A model for the generation of visually guided saccadic eye movements. In: Models of the visual cortex (Rose R, Dobson VG, eds) Chicester: Wiley.

Schiller PH, Malpeli JG, Schein SJ (1979) Composition of geniculostriate input to superior colliculus of the rhesus monkey. *J. Neurophysiol.* 35:915-924.

Schiller PH, Sandel JH, Maunsell JHR (1987) The effect of frontal eye field and superior colliculus lesions on saccade latencies in the rhesus monkey. *J. Neurophysiol.* 57:1033-1049.

Schlag-Rey M, Schlag J, Dassonville P (1992) How the frontal eye field can impose a saccade goal on superior colliculus neurons. *J. Neurophysiol.* 67:1003-1005.

Schwartz AB (1993) Motor cortical activity during drawing movements: population representation during sinusoid tracing. *J. Neurophysiol.* 70:28-36.

Schwartz AB (1994) Direct cortical representation of drawing. *Science* 265:540-542.

Segraves MA, Goldberg ME (1987) Functional properties of corticotectal neurons in the monkey's frontal eye field. *J. Neurophysiol.* 58: 1387-1419.

Seidemann E, Meilijson I, Abeles M, Bergaman H, Vaadia E (1996) Simultaneously recorded single units in the frontal cortex go through sequences of discrete and stable states in monkeys performing a delayed localization task. *J. Neurosci.* 16:752-768.

Shadlen MN, Newsome WT (1998) The variable discharge of cortical neurons: Implications for connectivity, computation, and information coding. *J. Neurosci.* 18:3870-3896.

Shadlen, M.N., & Newsome, W.T. (1994). Noise, neural codes and cortical organization. *Curr Opin. Neurobiol.*, *4*, 569-579.

Sherman SM, Koch C (1989) Thalamus. In: The synaptic organization of the brain (Shepherd GM, ed.), pp 246-278. New York: Oxford University Press.

Shook BL, Schlag-rey M, Schlag J (1990) Primate supplementary eye field: I. Comparative aspects of mesencephalic and pontine connections. *J. Comp. Neurol.* 301:619-642.

Sillito AM, Jones HE, Gerstein GL, West DC (1994) Feature-linked synchronization of thalamic relay cell firing induced by feedback from the visual cortex. *Nature* 369:479-482.

Singer W, Gray CM (1995) Visual feature integration and the temporal correlation hypothesis. *Annu. Rev. Neurosci.* 18:555-86.

Sparks DL (1986) Translation of sensory signals into commands for control of saccadic eye movements: role of the primate superior colliculus. *Physiol. Rev.* 66:118-171.

Spear PD, McCall MA, Tumosa N (1989) W- and Y-cells in the C layers of the cat's lateral geniculate nucleus: normal properties and effects of monocular deprivation. *J. Neurophysiol.* 61:58-73.

Sprague JM, Miekle TH (1965) The role of the superior colliculus in the visually guided behavior. *Exp. Neurol.* 11:115-146.

Steriade M (1997) Synchronized activities of coupled oscillators in the cerebral cortex and thalamus at different levels of vigilance. *Cereb. Cortex* 7:583-604.

Steriade M, Amzica F, Contreras D (1996) Synchronization of fast (30-40 Hz) spontaneous cortical rhythms during brain activation. *J. Neurosci.* 16:392-417.

Sur M, Sherman M (1982) Linear and nonlinear W-cells in C-laminae of the cat's lateral geniculate nucleus. *J. Neurophysiol.* 47:869-884.

T

Timofeev I, Steriade M (1997) Fast (mainly 30-100 Hz) oscillations in the cat cerebellothalamic pathway and their synchronization with cortical potentials. *J. Physiol.* 504:153-168.

Toyama K, Kimura M, Tanaka K (1981a) Organization of cat visual cortex as investigated by cross-correlation technique. *J. Neurophysiol.* 46: 202-214.

Toyama K, Kimura M, Tanaka K (1981b) Cross-correlation analysis of interneuronal connectivity in cat visual cortex. *J. Neurophysiol.* 46:191-201.

Traub RD, Whittington MA, Colling SB, Buzsáki G, Jefferys JGR (1996) Analysis of gamma rhythms in the rat hippocampus in vitro and in vivo. *J. Physiol.* 493:471-484.

Treue S, Maunsell JH (1996) Attentional modulation of visual motion processing in cortical areas MT and MST. *Nature* 382:539-541.

Ts'o DY, Gilbert CD, Wiesel TN (1986) Relationships between horizontal interactions and functional architecture in cat striate cortex as revealed by cross-correlation analysis. *J. Neurosci.* 6:1160-1170.

Tsodyks M, Mitkov I, Sompolinski H (1993) Patterns of synchrony in integrate and fire network. *Phys. Rev. Lett.* 71:1280-1283.

Vaadia E, Haalman I, Abeles M, Bergaman H, Prut Y, Slovin H, Aertsen A (1995) Dynamics of neuronal interactions in monkey cortex in relation to behavioural events. *Nature* 373:515-518.

van Vreeswijck C, Sompolinski H (1996) Chaos in neuronal networks with balanced excitatory and inhibitory activity. *Science* 274 : 1724-1726.

van Vreeswijck C, Sompolinski H (1998) Chaotic balanced state in a model of cortical circuits. *Neural Comput.* 10:1321-1371.

van Vreeswijk C, Abbott LF, Erementrout GB (1994) When inhibition not excitation synchronizes neural firing. *J. Comput. Neurosci.* 1:313-321.

Von der Malsburg C, Schneider W (1986) A neural cocktail-party processor. *Biol. Cybern.* 54:29-40.

Wang X, Merzenich MM, Beitel R, Schreiner CE (1995) Representation of a species-specific vocalization in the primary auditory cortex of the common marmoset: temporal and spectral characteristics. *J. Neurophysiol.* 74:2685-2706.

Wang XJ, Buzsáki G (1996) Gamma oscillation by synaptic inhibition in a hippocampal interneuron network model. *J. Neurosci.* 15:6402-6413.

Wang XJ, Golomb D, Rinzel J (1995) Emergent spindle oscillations and intermittent burst firing in a thalamic model: specific neuronal mechanisms. *Proc. Natl. Acad. Sci. USA* 92:5577-5581.

White JA, Chow CC, Ritt J, Soto-Treviño C, Kopell N (1997) Synchronization and oscillatory dynamics in heterogeneous, mutually inhibited neurons. *In press*.

Whittington MA, Traub RD, Jeffereys JGR (1995) Synchronized oscillations in interneuron networks driven by metabotropic glutamate receptor activation. *Nature* 373:612-615.

Wickergen BG, Sterling P (1969) Influence of visual cortex on receptive fields in the superior colliculus of the cat. *J. Neurophysiol.* 32:16-23.

Willshaw D, Hallam J, Gingell S, Lau SL (1997) Marr's theory of the neocortex as a self-organizing neural network. *Neural Comput.* 9:911-936.

Wilson HR, Cowan JD (1972) Excitatory and inhibitory interactions in localized populations of model neurons. *Biophys. J.* 12:1-24.

Wilson MA, McNaughton BL (1993) Dynamics of the hippocampal ensemble code for space. *Science* 261:1055-1058.

Wollman DE, Palmer LA (1995) Phase locking of neuronal responses to the vertical refresh of computer display monitor in cat lateral geniculate nucleus and striate cortex. *J. Neurosci. Meth.* 60:107-113.

Wurtz RH, Goldberg ME (1972) Activity of superior colliculus in behaving monkey. IV. Effect of lesions on eye movements. *J. Neurophysiol.* 15:587-596.

Chapter 2 Simulations

EMERGENT OSCILLATIONS IN A REALISTIC NETWORK : THE ROLE OF INHIBITION AND THE EFFECT OF THE SPATIOTEMPORAL DISTRIBUTION OF THE INPUT

Journal of Computational Neuroscience (1999) 6:27-48

ABSTRACT

We have simulated a network of 10 000 two-compartment cells, spatially distributed on a two dimensional sheet; 15 % of the cells were inhibitory. The input to the network was spatially delimited. Global oscillations frequently were achieved with a simple set of connectivity rules. The inhibitory neurons paced the network, whereas the excitatory neurons amplified the input, permitting oscillations at low input intensities. Inhibitory neurons were active over a greater area than excitatory ones, forming a 'ring of inhibition'. The oscillation frequency was modulated to some extent by the input intensity, as has been shown experimentally in the striate cortex, but predominantly by the properties of the inhibitory neurons and their connections : the membrane and synaptic time constants and the distribution of delays.

In networks which showed oscillations and in those which did not, widely distributed inputs could lead to the specific recruitment of the inhibitory neurons and to near zero activity of the excitatory cells. Hence the spatial distribution of excitatory inputs could provide a means of selectively exciting or inhibiting a target network. Finally, neither the presence of oscillations nor the global spike activity provided any reliable indication of the level of excitatory output from the network.

Keywords

Oscillations, gamma range, synchronization, visual cortex, inhibition

1. Introduction

Spike trains recorded from two or more neurons in the central nervous system often show temporal correlation, such that spikes are synchronized more often than expected by chance. Recent work in the visual cortex has shown that this synchronization frequently is accompanied by oscillations around the gamma frequency range of 20-70 Hz (Singer and Gray, 1995). Most of these studies are concerned with long range synchronization between different cortical columns, or even different cortical areas. Cell populations responding to different features of the same object are proposed to synchronize, thereby reflecting the higher order structure of the visual scene. As the object changes, new combinations of synchronized populations will emerge.

A prerequisite for such long range oscillatory synchronization is that the local neuronal populations should be able to oscillate. In the visual cortex of both anesthetized (Gray et al., 1990) and awake cats (Gray and Viana Di Prisco, 1997), adjacent neurons engage in highly synchronous oscillatory discharges when presented with their preferred stimulus. These oscillations appear because the time intervals between synchronized events are regular (15 to 30 ms). The oscillation frequency is modulated by the stimulus features; for example, changes in the velocity of a moving bar can change the oscillation frequency by up to 20 Hz (Gray et al., 1990; Gray and Viana Di Prisco, 1997).

Two main mechanisms have been advanced to explain the generation of synchronized oscillations. The first assumes that the recorded population is driven by a common oscillatory input (Perkel et al., 1967). Afferents from the lateral geniculate nucleus are a good candidate as they project to the visual cortex and convey oscillatory input from the retina (Neuenschwander and Singer, 1996; Alonso et al., 1996; Ghose and Freeman, 1997). However, cells in striate and extrastriate cortex (posteromedial lateral suprasylvian sulcus) can synchronize despite the fact that their retinal afferents are largely relayed through different thalamic nuclei (Engel et al., 1991b). Moreover, inter-hemispheric synchrony can be abolished by section of callosal fibers (Engel et al. 1991a), suggesting that corticocortical connections are critically involved in this process. Finally, if normal development of

corticocortical projections is prevented by early strabismus, synchronous oscillations are abolished (Roelfsema et al., 1994).

The second possible explanation is that oscillations are an emergent property of the active network. Wilson and Cowan (1972) proposed a simple model of this which used two coupled differential equations to represent excitatory and inhibitory neuronal populations. More recently, in a rat hippocampus model (Traub et al., 1996) with multicompartment sparsely connected excitatory and inhibitory cells, oscillations are produced in the gamma range by rhythmic synchronized IPSPs, and modulated by the parameters regulating the inhibitory coupling between interneurons. Bush and Sejnowski (1996) simulated a sparsely connected network of 100-1000 excitatory and inhibitory cells, each with nine compartments. They found that the oscillatory frequency could be modulated by the network input and by the global conduction delay distribution. This work was preceded by studies of an isolated network of inhibitory neurons which are able to oscillate synchronously in response to constant input in the hippocampus (Whittington et al., 1995; Wang and Buzsáki,1996; White et al., 1997) or when the cells had a post-inhibitory rebound response as in the thalamic reticularis nucleus (Wang and Rinzel, 1993). Because of this post-inhibitory rebound and the lower oscillation frequency ($GABA_A$ and $GABA_B$-mediated), the thalamic model constitutes a special case of synchrony (Wang et al., 1995). In all these studies, strong mutual inhibition was important to achieve stable oscillations. However, most of them did not investigate the spatial distribution of the input, and oscillations were only seen when the input magnitude was relatively similar for all cells (<10% variability, Traub et al., 1996; Wang and Buzsáki, 1996; White et al., 1997).

The present study investigated the emergence of stable local network oscillations. We have simulated a network of 10 000 excitatory and inhibitory cells. Such a number allowed the connectivity to be sparse, with realistically small post-synaptic potentials. Each neuron had two compartments, permitting effective somatic inhibition, whilst remaining computationally tractable, thus allowing extensive investigation of the network properties. Neurons were identified by a location on a two dimensional sheet, and conduction delays between cells were determined from the conduction distance and velocity. Particular care was taken over delays, as recent studies have shown that intracortical conduction velocities are slower for inhibitory neurons than for excitatory ones (Salin and Prince, 1996; Murakoshi at al., 1993). Inputs were

temporally Poisson distributed, and varied spatially according to a centered Gaussian distribution.

The results show that local synchronization could be an emergent and stable feature of such a realistic network in response to non-oscillating excitation. The oscillation frequency was modulated as in reported experiments (Gray and Viana Di Prisco, 1997). Moreover, the major role played by the inhibitory neurons was carefully examined. With higher levels of input, identical oscillations were reproduced in a network having only inhibitory cells. We show that axonal delays in inhibitory neurons partially determine the oscillation frequency and that, by contrast, axonal delays in excitatory neurons do not. There was a similar sensitivity of the oscillation frequency to inhibitory, but not excitatory, synaptic time constants. We describe two other emergent properties. Firstly, a spontaneous ring of inhibition surrounding the activated neurons was seen, which depended on the relative properties of excitatory and inhibitory cell types. Secondly, only inhibitory neurons were activated when the input spanned over a large area. Such a mechanism could act to gate out the long range excitatory output of any cortical network. These latter properties did not depend on the oscillatory state and were also present in a non-oscillating network formed by removing the inhibitory connections directed to inhibitory neurons.

A preliminary account of some of the results described in the present paper has been published previously (Pauluis et al., 1997).

2. Methods

2.1 Computer Simulations

Equations providing precise specification of the model are given in the Appendix. Most of the parameters described in this section were varied; the values given below were the default, and were used unless others are specifically described in the text.

2.1.1 Neurons

Each neuron was composed of a dendritic and a somatic compartment (initial potential : 70 ± 3 mV SD). The passive properties of the membrane (App. Eq. 1) were simulated by a leak conductance with a resting membrane potential fixed at -70 mV (± 1 mV SD). Reversal potentials were 0 mV for the EPSPs, and -80 mV for the IPSPs. The soma included the trigger zone with a fixed threshold at -55 mV for action potential initiation. In excitatory neurons, the membrane time constant was 2 ms (± 5 % CV) in the dendritic compartment and 10 ms (± 5 % CV) at the soma (Koch et al., 1996). Somatic membrane resistance (R^s_m) was 600 MΩ (± 5 % CV). Inhibitory cells had smaller membrane time constants (1.5 and 7.5 ms ± 5 % CV in the dendrite and the soma respectively) and also a somatic membrane resistance of 800 MΩ (± 5 % CV). The dendritic compartment had a high resistance (R^d_m= 3.0 R^s_m) to approximate the current spread along a single ended cable, producing large voltage changes in the dendrite and current flowing mainly towards the soma with voltage attenuation (Fig. 1A&B). The resistance between the dendrite and the soma was calibrated to achieve a realistic attenuation of the dendritic postsynaptic potentials (PSPs; R_{ds}= 2.4 R^s_m). Membrane capacitances were calculated from the set of conductances and time constants.

Analytical resolution of these differential equations with a stepwise constant approximation was used (App. Eq. 2), since it is computationnally faster and provides better precision than purely numerical integration (MacGregor, 1993). This method supposes that all the parameters remain approximately constant during each time step.

During the rise time of the postsynaptic potentials, the change of conductance followed an alpha function (App. Eq.3). The rise time was 1 ms for all the EPSPs and for the IPSPs on the dendrite, which corresponded to a conductance peak and a time constant of 0.25 ms (t_{peak}).

On the soma, the IPSPs had a rise time of 3 ms, corresponding to a t_{peak} of 0.75 ms. Conductance peaks were calibrated to produce realistic PSPs at the soma (Fig. 1A&B; mean EPSPs and IPSPs had a peak conductance change of 0.5 nS and 1 nS respectively, leading to amplitudes of 1 mV or less; Thomson et al., 1993, 1995; Buhl et al., 1997; Tamàs et al., 1997). The distribution of the conductance peak was calculated as the difference of two exponential curves, chosen to bias the distribution towards lower conductance peaks (App. Eq. 4; range 12-381% of the mean, peak at 36%).

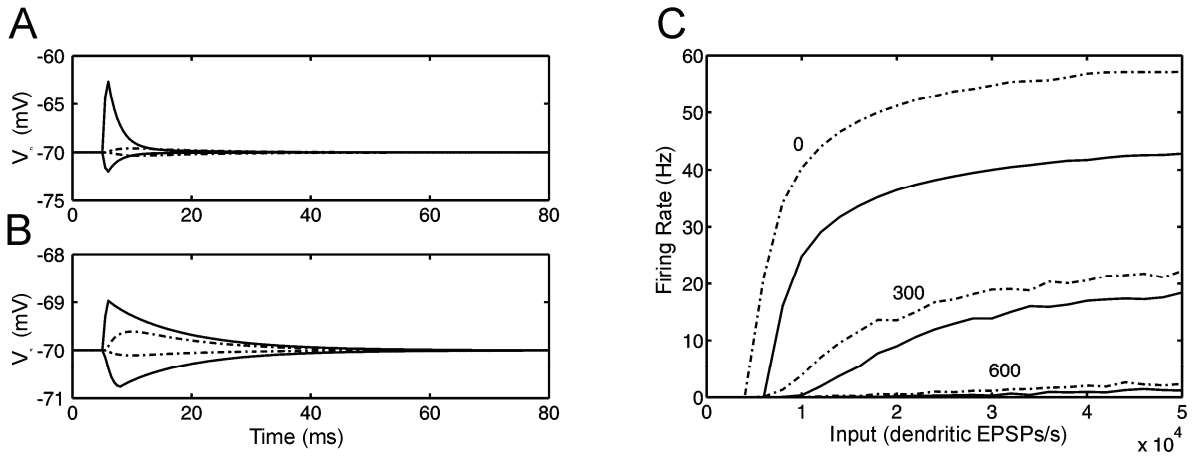

Figure 1. (A&B) Excitatory and inhibitory post-synaptic potentials on the dendritic (V_D) and somatic compartments (V_S). Solid lines represents PSPs applied directly on the compartment, while dotted line are the PSPs applied on the other compartment. (C) Response curves corresponding to different levels of somatic inhibition : 0, 300, and 600somatic IPSPs/s. An excitatory cell is represented by the solid lines and an inhibitory cell by the dash-dotted lines. Parameters : conductance peak in EPSP (g_{syn}) = 0.5 nS, in IPSP = 1 nS; current time constant (t_{peak}) = 0.25 ms (except in somatic IPSPs : 0.75 ms) with rise time = 1 ms (except in somatic IPSPs : 3 ms); somatic resistance (R^s_m) = 0.6 GΩ; dendritic resistance (R^d_m) = 1.8 GΩ; resistance between dendrite and soma (R_{ds}) = 1.4 GΩ.

Following a threshold crossing, the somatic membrane potential was reset to -90 mV for 1 ms (action potential and absolute refractory period), and then it was released from this value (relative refractory period). Temporal buffers stored the spike initiation times until the end of the conduction delays.

To silence a cell whatever the input, more than 600 somatic IPSPs/s were needed (Fig.1C). There has been recent controversy over whether inhibition has a subtractive or divisive effect (Holt and Koch, 1997). The curves of Fig. 1C show a combination of these two mechanisms. With increasing inhibition, the threshold to begin firing was raised (subtractive), the initial slope was decreased (divisive), and the maximal firing rate was reduced (subtractive). It is important to note that the excitatory input in this figure was only dendritic. If somatic excitatory input were added, in the proportion of 10% for example, the maximal firing rate did not stabilize: it continued to increase to 240 Hz at 50 000 EPSPs/s and up to 475 Hz at

200 000 EPSPs/s. Moreover, in this case, 1200 somatic IPSPs/s decreased the firing frequency by only 50 and 15 Hz respectively.

2.1.2 Network

The network contained 10 000 cells, of which 85% were excitatory (Beaulieu and Colonnier, 1983; Peters et al, 1985; Peters and Yilmaz, 1993). It spanned a square of 500x500 μm and some elementary rules determined the connection and delay distributions (for review, White, 1989; Salin and Bullier, 1995).

All cells had a circular pattern of uniform connectivity with a range of 300 μm; connections directed outside the network (typically 45% of the total) were disregarded in agreement with the open boundary condition. A cell in a corner therefore connected to about four times fewer cells in the network than a cell in the center. Excitatory cells contacted 500 other cells of both types, and inhibitory neurons 1250. These figures reflected the fact that layer II-III pyramidal cells send more long range collaterals than inhibitory cells which have more local projections (Thomson and Deuchars, 1997; Kisvárday and Eysel, 1992).

Neurons receiving inputs from a given cell were determined at random (uniform probability) in the 300 μm connection range of the presynaptic cell. After each connection was so defined, its location, either on the dendrite or on the soma, was determined at random, using the following probabilities: probability for an inhibitory synapses to connect the soma if the target is excitatory : 0.76, if the target is inhibitory : 0.77; probability for an excitatory synapse to connect the soma if the target is inhibitory : 0.13. There were no excitatory connections directed to the soma of excitatory cells (White, 1989). Excitation directed to excitatory neurons was thus only through dendritic synapses. However, when the input ceased, it was sufficient to induce a self-sustained activity if inhibition was absent (strong coupling conditions). The previous figures produced a mean number of 30 somatic excitatory connections to inhibitory neurons, and 80 somatic inhibitory connections to both cell types.

A conduction velocity was attributed to each neuron from a normal distribution (Press et al., 1992) with a mean of 0.18 m/s for excitatory cells and 0.06 m/s for inhibitory cells (Murakoshi et al., 1993 ; Salin and Prince, 1996); their coefficients of variation were always maintained constant at 20% and 18% respectively. The distance divided by the conduction velocity gave the conduction time (minimum one time step) and 0.5 ms was added for the synaptic transmission. Therefore, minimal delays were 1 ms.

Each cell received a random train of dendritic EPSPs which followed a Poisson distribution (Press et al., 1992). The cell location determined the mean rate of this train, accordingly to a normal spatial distribution (± 18 cells SD), maximum in the center (App. Eq. 5). In this paper, input intensity will always refer to the mean input received by a central cell. The EPSP trains were therefore more regular in the center than in the periphery. It should be emphasized that inputs were not oscillatory, but Poisson.

Simulations were performed on a microcomputer (Intel Pentium Pro 200 MHz with 128 MB RAM). Programs were written in C (Linux gcc) and in Matlab languages (Version 4.2c). All the random number generators were designed to produce sequences of very long period (Press et al., 1992). Time steps were usually 0.5 ms and some control simulations were run with 0.1 ms time steps without noticeable changes to the global dynamics.

2.2 Analysis.

To assess the activity of the network, a spike histogram showing the summed activity of all the cells as a function of time was computed. Its auto-correlation histogram was calculated on the steady state period, after the initial 200 ms. Such a global auto-correlogram is the average of all the possible cross-correlograms and auto-correlograms for all the active cells in the network. It represents the number of spikes at a particular lag which are expected in the network given the presence of a spike.

A Gabor function was fitted to the auto-correlogram with a Levenberg-Marquardt algorithm (modified from Matlab 4.2c). The fit was visually inspected and adjusted by hand if necessary before a final minimization to ensure that a global minimum was found. Following Engel et al.(1990), we extracted from the fitted function the ratios between the amplitude and the offset (Fig. 2E), and between the decay constant and the oscillation period. The covariance matrix calculated by the Levenberg-Marquardt algorithm was used to assess the standard error of the Gabor fit. A peak of the Gabor function was significant if it was larger than the offset plus three standard errors (König, 1994; Baker et al., 1997) Using a fast Fourier transform, we tested the criteria used by Gray and Viana Di Prisco (1997): the ratio of the peak value to the DC component and the signal to noise ratio. Although all these methods were used systematically, the aim of this study was not a comparison of their relevance. In the end, results related to the oscillation features were displayed if the fit was visually correct and at least the central and first sub-peak were significant (> 3 SD).

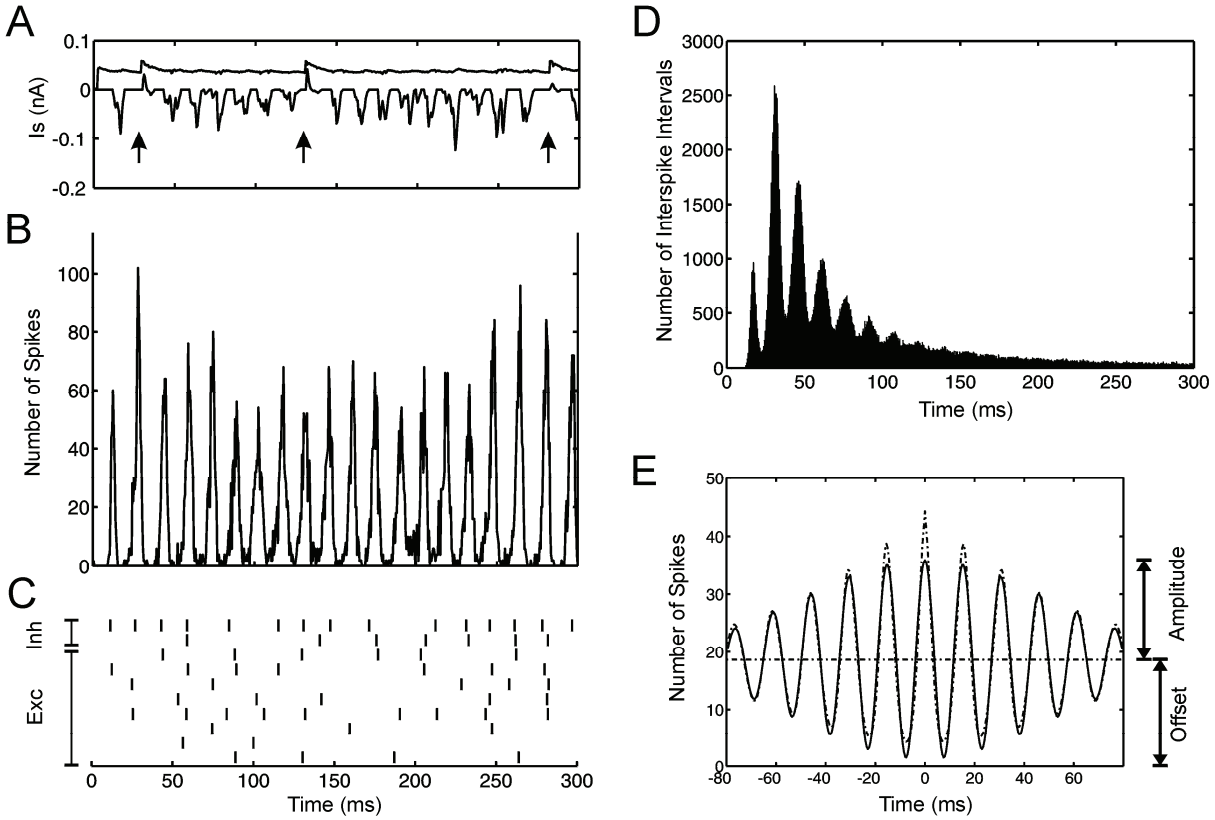

Figure 2. Example of a simulation with the reference parameters. (A) Currents flowing from the dendrite to the soma (upper trace, depolarizing), and from somatic inhibitory synapses (lower trace, hyperpolarizing). (B) Spike histogram computed for all the cells during the first 300 ms. (C) Rasters of 10 active cells. The top two cells were inhibitory, whereas the remaining eight neurons were excitatory. (D) Interspike interval histograms summed across all the cells in a 10 s long simulation (bin width : 0.5 ms). (E) Auto-correlogram of the global spike histogram (dotted) and its fitted Gabor function (solid). Parameters : maximum input in the center : 50 000 EPSPs/s per cell; spatial standard deviation (σ) : 18 cells; 500 connections per excitatory cell, 1250 connections per inhibitory cell, somatic inhibition : 80 connections, somatic excitation : 0 and 30 connections on excitatory and inhibitory cells, inhibitory mean delay : 3.9 ms, excitatory mean delay : 1.8 ms, synaptic time constant for somatic IPSPs (t_{peak}) : 0.75 ms, other PSPs : 0.25 ms. Simulation duration : 10 s. Compiled from 185 000 spikes in 3336 active cells (mean firing rate of 5.5 Hz). Oscillation frequency : 65 Hz, Amplitude to offset ratio after fitting : 0.92.

Besides the oscillatory frequency, we monitored the amplitude of the fitted function and the ratio of its amplitude to its offset, a commonly used physiological measure (Engel et al., 1990; Fig. 2E). We tested this measure on a network of 10 000 unconnected cells. With spatially diffuse inputs, significant oscillations were obtained (80 Hz), but their amplitude to offset ratio was never higher than 0.01. In particularly well synchronized networks, this ratio was larger than one, reflecting a best fit which crossed the null line of the auto-correlogram. This corresponded to synchronized events separated by silent pauses. In the case of perfect synchronization with a zero phase lag between all the cells, a spike synchronization index (Wang and Buzsáki, 1996) would give a value of one and the method used here would yield

an amplitude to offset ratio of two. The same value will be obtained with this method if the cells were synchronized with some sinusoidal phase distribution.

The mean phase of an individual cell discharge was calculated with reference to peaks of the all-spike histogram. This was checked by animated sequences showing the activity propagation across the network.

To test the response to an increasing input or to changes in the synaptic time constant, the same network with parameters fixed at realistic values was tested. To test the other parameters, a new network was built at each change.

3. Results

3.1 Oscillatory state

These simulations often produced networks which exhibited synchronous oscillatory activity, an example of which is given in Fig. 2&3. The network activity was entirely dependent on the input; when this ceased, the cells became inactive. Figure 2B shows a histogram of total network spike activity for the first 300 ms of the simulation. Rasters of individual cell activity are presented in Fig. 2C. The top two cells were inhibitory, and the first one had the highest firing rate during this simulation (53.3 Hz). In the excitatory population (remaining rasters), the fastest cell discharged at 35.2 Hz. The inhibitory neurons were more active than the excitatory ones. Of the 1.8 $x10^5$ spikes, 41% were produced by the inhibitory cells. All cells showed phase locking to the global oscillation (65 Hz), although in no case did a single cell fire in every cycle. Figure 2A shows the depolarizing current flowing from the dendrite (upper trace) in an excitatory cell close to the center of the input. The lower trace represents the inhibitory current due to somatic IPSPs, which occur repetitively after each synchronous event.

Interspike interval (ISI) histograms were computed for each cell over the 10 s simulation and then summed across all cells. This is shown in Fig. 2D. The smallest ISI was 10 ms, corresponding to an instantaneous frequency of 100 Hz. The ISI histogram computed in this way exhibits two features: an oscillatory modulation superimposed on a broad distribution with a long tail. The tail results partly from variability in single cell ISIs, due to the random nature of the external input. Individual cells showed an ISI distribution which had one or two

sharp peaks, at sub-harmonics of the network frequency. In addition, the wide distribution of firing rates seen across cells contributed to the long tail in this population measure. We have verified that a population of cells with an exponential distribution of firing rate (Baddeley et al., 1997) and individual cell ISIs following a sharp gamma distribution (integral order of 10) also show a population ISI which also has a long tail.

Figure 2E shows the global cross-correlation for this simulation, with the superimposed Gabor fit (Engel et al. 1990). Damped oscillations are clearly present here.

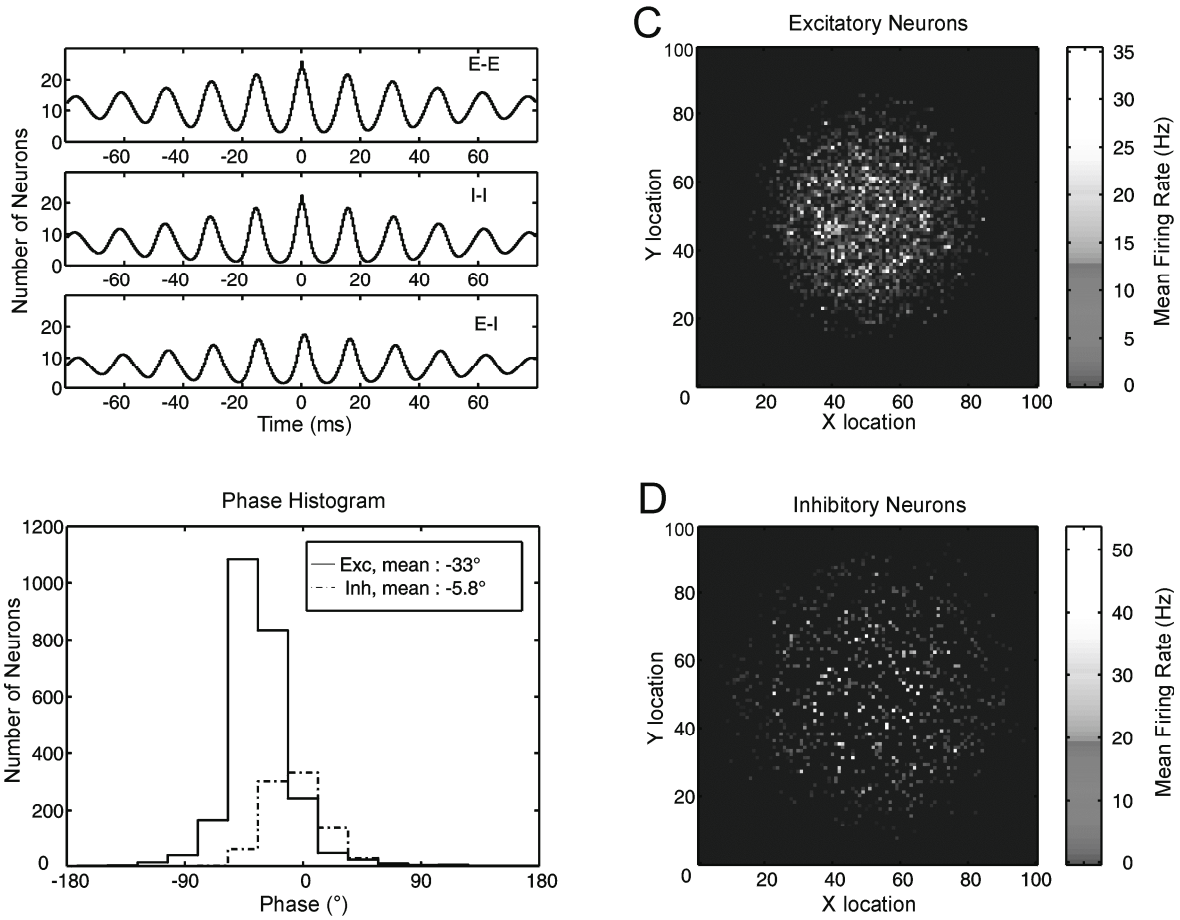

Figure 3. Same simulation as in Fig. 2. (A) Auto-correlogram computed from the spike histograms during the steady state (>200 ms) for the excitatory neurons (top), the inhibitory neurons (middle) and a cross-correlation histogram between the spike histograms of both populations (bottom). (B) Distribution of the phase of cell firing relative to the global oscillations. Dash-dotted line : inhibitory cells. Solid line : excitatory cells. Phase is indicated in degrees, and the mean phase is noted in the upper right corner. Cells which did not discharge during the simulation were not incorporated in the analysis. (C&D) Maps of the activity in the excitatory and in the inhibitory subpopulations. The inhibitory neurons were active over a larger area than the excitatory cells.

Figure 3A presents global auto-correlation histograms computed separately for excitatory and inhibitory populations. They confirm the presence of clear oscillations at a frequency of 65 Hz. The cross-correlation histogram between the two populations is presented at the bottom and exhibits no time shift larger than 1 ms.

The average phase at which each neuron fired relative to the global oscillations was determined; the distribution of this phase is plotted separately for the inhibitory and excitatory cell sub-populations in Fig. 3B. Whilst these distributions are heavily overlapping (5-95% confidence interval : [-151°,+86°] and [-126°,+90°] in excitatory and inhibitory sub-populations respectively), on average the excitatory cells showed a slight phase lead (-33°, equivalent to approximately 1.4 ms) over the inhibitory cells (-5.8°, 0.25 ms). In such a diagram, each cell is weighted equally regardless of its firing rate. For the most active cells in the population, the phase was more negative, and the phase difference between excitatory and inhibitory cells was smaller (firing rate higher than 25 Hz : -1.96 ms and -1.27 ms for excitatory and inhibitory cells respectively, compared with firing rate lower than 2.5 Hz : -1.2 ms and +0.6ms).

The phase shift between excitatory and inhibitory populations was small (33°) compared with the phase variability (5-95% confidence interval [-143°,+87°]). This could reflect a relatively small effect, or alternatively, that whilst the two sub-populations show variability, the phase shift between them is always present. These two possibilities were investigated by calculating the mean phase difference between excitatory and inhibitory cells for each cycle; this was 20 ±6° (0.86 ±0.25 ms). In addition, the mean phase of excitatory and inhibitory cells calculated for each cycle showed a highly significant positive correlation ($r= 0.64$, $P<0.001$). These results suggest that the temporal shift in activation of each cell class remains whatever the variability in single cycle cell timing.

Both populations had a mean phase in advance of the peak of activity probably because of the shape of the synchronous event. This comprised a slow but exponential increase followed by a sudden collapse of the activity (Fig. 2B). It was possible to produce a phase plane diagram of excitatory firing rate versus inhibitory firing rate (not shown). This diagram exhibited a limit cycle if the firing rate was calculated on an appropriate time interval (1.5-2 ms), exactly as shown by the simpler model of Wilson and Cowan (1972). This suggests that the population dynamics are the same in both models. Although the simple differential equations of Wilson and Cowan (1972) do summarize the main phenomenon, they do not reflect the spatial dynamics and the single cell complexity with delayed PSPs described here. As described in section 3.3, our network was able to produce oscillations with only inhibitory neurons under constant excitation. This feature can not be described by the model of Wilson and Cowan (1972) because their set of two differential equations with ‘time coarse graining’ reduces to a single differential equation, which has no oscillatory solution (trajectories in first-

order systems either approach a fixed point or diverge to ±∞). In such a case, explicit account of the inhibitory delays would have produced an oscillatory solution.

Consideration of the animated sequence and the phase map (not shown, but download available : see details in the Appendix) revealed that the first cells to be activated lay in the center.

Figures 3C&D show the location and magnitude of activity in the network separately for excitatory and inhibitory cells. In each case, activity was largest in the center, and declined towards the edges of the network. This reflected the Gaussian distribution of the input to the cells (App. Eq. 5). However, closer examination revealed that the radius of the active inhibitory cell population was greater than that of the excitatory cells. Hence the active excitatory cells were surrounded by a ring of inhibition. Indeed, the membrane potential of silent cells in the corner of the network was clearly hyperpolarized relative to the mean field potential and to their resting potential. This ring of inhibition depended on the response curve of the inhibitory relative to excitatory cells. The ring of inhibition surrounding the central activity was due to the recruitment of small inhibitory neurons in the input periphery. Such a ring could be inverted in a ring of active excitatory cells if the response curves of inhibitory and excitatory cell types were exchanged by a change of the somatic membrane resistance (see next section). A normally distributed input and smaller inhibitory cells with subsequent higher membrane resistance provided a mechanism for the lateral inhibition phenomenon, the ON-OFF response in the visual system.

Naturally, we do not expect to find more complicated features in this network because connections were random and not subjected to learning or to a geometric organization. In order to uncover a specific temporal relationship among the cells, their spike train was converted into a binary sequence according to the odd or even synchronous events to which the spikes belonged. The means were calculated for each cell and for different epoch duration, and compared to those obtained from random spike trains. Although the variance increased with small epochs in our simulation as in the control, there was no hint of bimodal distribution. In the same way, a search for groups of three cells discharging together during the same synchronous event (triplet; Abeles and Gerstein, 1988) showed few groups a bit more repeating than the maximum found in control trains (probability of occurrence : 0.045 versus 0.040 maximum in control). These groups contained some inhibitory neurons connected by a strong somatic excitatory synapse, forming a pair of excitatory and inhibitory

cells (doublet). We concluded that most of the activity in this simulation did not exhibit any strong organization of patterns.

Some simulations were run with a uniform input and wrap-around boundary conditions (torus surface). They showed the same oscillatory activity, but no differences in the distributions of active excitatory and inhibitory cells.

3.2 Somatic membrane resistance and time constant

The effect of changing the somatic membrane time constant was investigated separately in excitatory and inhibitory cells, varying the membrane capacitance (C_s) whilst keeping the other parameters the same (R^s_m). Although changing the membrane time constant altered the shape of PSPs, oscillations were still a stable feature and occurred in the gamma range for longer somatic membrane constants.

Changes in the somatic time constant of excitatory cells did not influence the oscillation frequency. When the somatic time constant of excitatory neurons exceeded 20 ms, brief epochs of desynchronization appeared, increasing the oscillation frequency. These epochs disappeared if we allowed a compensatory increase in conductance of the somatic IPSPs.

On the contrary, changing the somatic membrane time constant of inhibitory neurons did influence the oscillation frequency : the longer the time constant, the lower the frequency (Fig. 4A&B). Moreover, the somatic time constant had to be lower in inhibitory cells than in excitatory ones to prevent most of the latter from firing at each cycle, a situation reminiscent of an epileptic discharge (Fig. 4C). Figure 4B shows that at low input levels there was a region of relative instability for short and long time constants (less than 12 ms and higher than 25 ms). This instability disappeared at higher input intensities. The transient region of high stability could be related to the dramatic increase of excitatory output to inhibitory cells due to a prolongation of the burst activity. The longer membrane time constant of inhibitory cells acted to increase the effect of the mutual inhibition and hence decrease the recruitment of the inhibitory cells. An increased duration of the activity burst compensated for this by increasing the excitatory output. When the size of the burst saturated because of the spatially limited input and the inability of the cells to fire at high frequency, this network excitation failed to compensate for further increases in the somatic membrane time constant, and oscillations again became unstable.

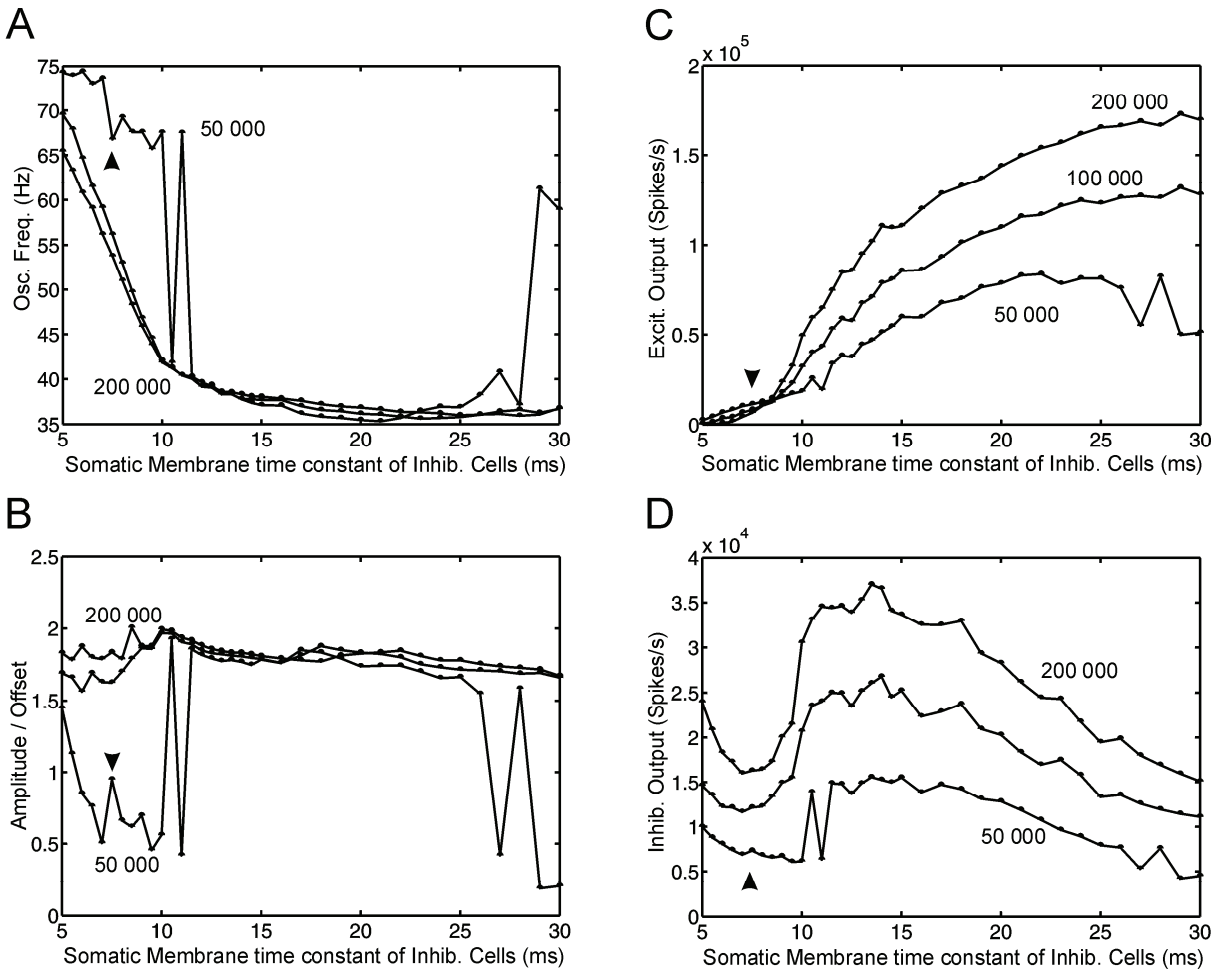

Figure 4. The somatic membrane time constant in inhibitory neurons was varied for three different input intensities (50 000, 100 000 and 200 000 EPSPs/s). (A) The frequency of the fitted Gabor function is modulated by the somatic membrane time constant of the inhibitory cells. (B) For large inputs, the amplitude to offset ratio (Fig. 2E) remained high across the full range of time constants tested. (C&D) The firing probability of any given cell in the network increased dramatically when the somatic membrane time constant in inhibitory neurons was larger than 10ms, its value in excitatory cells. The net effect of increasing the somatic membrane time constant in inhibitory neurons is firstly an inhibition of their discharge (higher sensitivity to somatic IPSPs; D), further compensated by a larger recruitment of the excitatory cells (C). Arrow heads indicate the simulation with the same parameters as in Fig. 2.

If the somatic resistance of the inhibitory cells was decreased from 800 to 400 MΩ, the active excitatory cells spanned over a larger area than the active inhibitory cells, forming a ring of excitatory cells. Although the network still produced oscillations at the same frequency, the amplitude to offset ratio was decreased to 0.26.

Both the somatic membrane resistance and time constant could alter the response curve of the individual cells and were thus important parameters to fix before testing the network connectivity. The membrane resistance was chosen to be higher in inhibitory cells because of their smaller size. By contrast, their membrane time constant was fixed at a lower value to provide them with a response curve shifted upward when compared to the excitatory cells

(Fig. 1C). As shown in Fig.4, this prevented most of excitatory cells from firing during the activity burst.

3.3 Connection characterization

To determine the underlying mechanism of the network oscillations, simulations were run with one or more connection types deleted. Figure 5A presents simulations where excitatory neurons were prevented from discharging by an artificially high threshold and hence the only effective connections were between inhibitory cells. At an input level (50 000 EPSPs/s) where oscillations were present in the complete network, there were no oscillations in the isolated inhibitory population. Oscillations only appeared for much higher inputs (140 000 EPSPs/s, an increase of 180%); however, they had the same frequency as in the intact network.

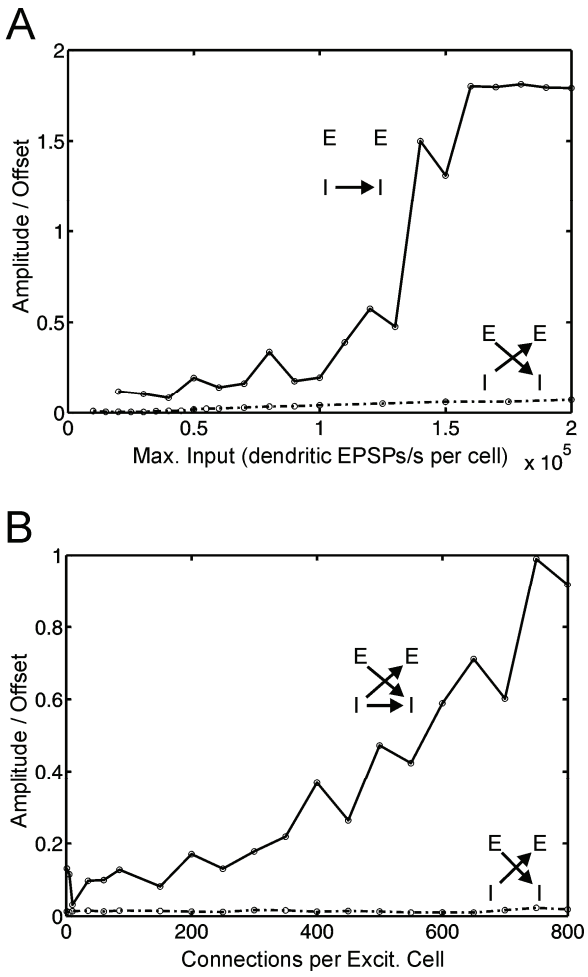

Figure 5. Characterization of the connection types. (A) A network where the only effective neurons were inhibitory and the only effective synapses were those from the input and between inhibitory cells. The network was thus a set of interconnected inhibitory neurons, without any excitatory cells. The amplitude to offset ratio increased suddenly when the input was larger than 140 000 EPSPs/s. Oscillations were then similar to those found in the entire network. Dotted line indicates the result obtained for a network without mutual inhibition; only excitatory to inhibitory and inhibitory to excitatory connections were present. Oscillations never became as strong as in the I->I network case. (B) In a network where excitatory to excitatory synapses were removed, the number of excitatory connections to the inhibitory cells was progressively increased. The input was fixed at 50 000 EPSPs/s on the center. When the number of excitatory synapses became sufficient, the oscillations appeared and the amplitude to offset ratio increased. Same parameters as in Fig. 2. Dotted line again shows the results in a network without mutual inhibition.

By contrast, no subset of the complete pattern of connectivity could produce strong oscillations if it omitted inhibitory to inhibitory connections. The possible role of interactions between the excitatory and the inhibitory populations was investigated in a network without

recurrent excitation or inhibition. The only connections were inhibitory to excitatory, and excitatory to inhibitory. In such a network, the amplitude to offset ratio increased slowly for large inputs, but at the maximum tested of 200 000 EPSPs/s, it reached at most 0.08, the highest value obtained from networks without inhibitory to inhibitory connections (dotted line in Fig.5A).

Figure 5B shows results from a network with inhibitory to inhibitory connections and inhibitory to excitatory connections. Excitatory to excitatory connections were removed and the number of excitatory connections directed to the inhibitory population was varied. In such a network, around 500 excitatory to inhibitory connections were needed before the amplitude to offset ratio became larger than 0.4. The number of excitatory connections needed to achieve such oscillations decreased for higher inputs, when excitatory to excitatory connections were present, or when the EPSP conductance peak was increased.

3.4 Local connectivity

In order to investigate the effect of changes in connection density on the oscillatory activity, the number of local inhibitory and excitatory connections per cell was varied, whilst respecting the spatial connectivity rules described in the Methods and scaling the conductance peak to avoid changes in the total level of excitation and inhibition. The relative distribution of the connections between somas and dendrites was also maintained the same as in the previous simulations.

Figure 6A shows the amplitude to offset ratio as a function of the number of connections made by each excitatory cell. The three curves represent three input levels. For sufficiently large inputs, no excitatory connections were required for strong network oscillations. For the standard input of 50 000 EPSPs/s, a few very strong excitatory connections can supply the inhibitory cells with the missing excitation. Figure 6B shows a similar plot where the number of connections established by the inhibitory cells was varied. There was a clear minimum in the number of inhibitory connections required to achieve strong oscillations; this was around 150. Such a number represented a connectivity of 1.5 percent for the whole network and corresponded to 23 connections emitted by each inhibitory neuron to other inhibitory cells (17 of which were somatic, 6 dendritic). Wang and Buzsáki (1996) found in an inhibitory network of 100 to 500 neurons a minimal number of 60 connections. Unfortunately, quantitative

comparison of minimum connectivity in these two different models is meaningless, and reflects probably the use of somatic inhibition in the present study.

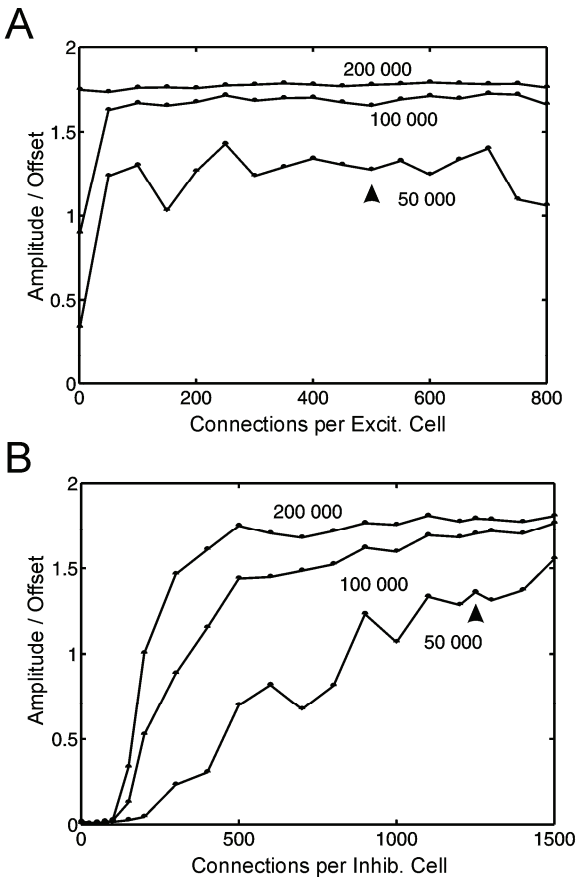

Figure 6. The number of local connections emitted by each cell type was varied, using the connectivity rules described in Methods and the same proportions of somatic connections. The synaptic conductance peaks were adjusted to keep the total excitation and inhibition constant. (A) The amplitude to offset ratio versus the number of local connections emitted by each excitatory cell. Each curve represents a different input level : 50 000, 100 000 and 200 000 EPSPs/s on the central cell. With high input, oscillations could be obtained even with no excitatory connections. (B) The amplitude to offset ratio versus the number of local inhibitory connections. A minimum of around 150 connections was needed to produce oscillations. This corresponded to 23 inhibitory connections directed towards other inhibitory cells. Same parameters as in Fig. 2; the level of connectivity and input used in that figure is indicated by an arrow head.

3.5 Conduction delays and synaptic time constant

To test the effect of changes in the conduction delays, the mean conduction velocities were changed whilst maintaining the coefficient of variation constant (see Methods).

In Fig. 7A, the oscillation frequency is plotted versus the mean delay of inhibitory connections. A different curve is drawn for three mean excitatory conduction velocities. The oscillation frequency was mostly influenced by the inhibitory mean delay, independently of the excitatory mean delay. Short inhibitory delays (2 ms) resulted in high frequency oscillations (120 Hz) whereas the longer ones (10 ms) produced a frequency around 30 Hz. The amplitude to offset ratio (Fig 7B) showed that oscillations became more prominent as the mean inhibitory delay increased above 2 ms. In addition, for a given mean inhibitory delay, oscillations were stronger the shorter the mean excitatory delay. However, a plot of the difference between the mean inhibitory and excitatory delays failed to show a clear tendency to have strong oscillations for positive differences (not illustrated). The stronger the

oscillation, the lower was the frequency, and the higher the proportion of active inhibitory neurons. High oscillation frequency around 70 Hz were achieved with individual cell firing rates smaller than 50 Hz.

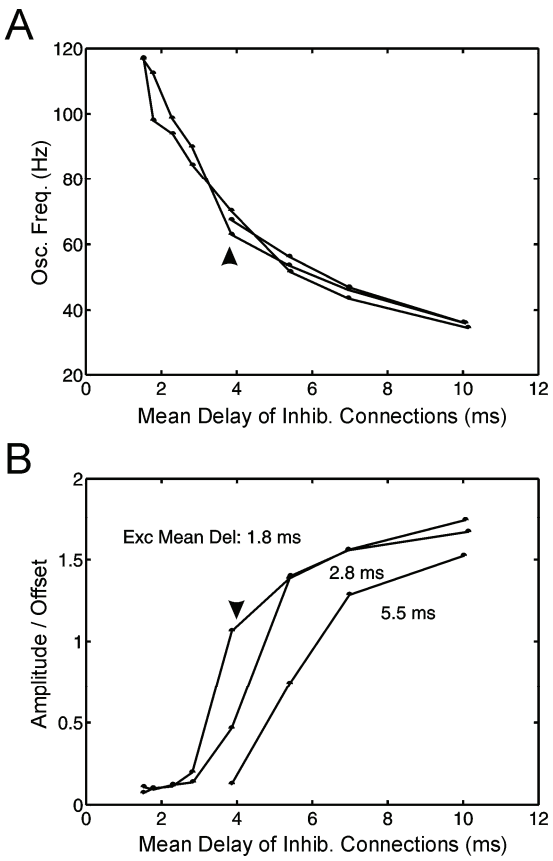

Figure 7. The effect of synaptic delays. (A) Oscillation frequency versus the mean delay in inhibitory connections. The three curves represent results with three different excitatory mean delays. They lay close to each other, indicating a very small effect on the oscillation frequency by the excitatory mean delay. By contrast, the oscillation frequency was strongly modulated by the inhibitory mean delay. (B) Amplitude to offset ratio versus the mean delay in inhibitory axons. The stronger oscillations occurred for the lower frequencies. Parameters: Excitatory conduction velocity =4.5, 9, 18 cm/s; Inhibitory conduction velocity = 2, 3, 4.5, 6, 9, 12, 18, 24 cm/s. Arrow head denotes the simulation with the same parameters as in Fig. 2.

Figure 8 demonstrates the effect of changing the time course of the different post-synaptic currents (PSCs). Each postsynaptic potential was simulated by a conductance change which followed an alpha function (App. Eq. 3). The rise time of the potential was four times longer than the time constant of this function. Whereas this time constant (t_{peak}) was varied, the amplitude of the conductance peak (g_{syn}) was maintained constant. In Fig. 8A, the oscillation frequency can be seen to depend mainly on the time constant of the IPSCs. By contrast the oscillation frequency was relatively insensitive to changes in the dendritic EPSC time constant. The amplitude to offset ratio remained constant in both cases. Figures 8B&C illustrate the desynchronization obtained on increasing the synaptic time constant of the somatic EPSCs (which were present on the inhibitory cells only); the amplitude to offset ratio decrease was accompanied by a decrease in the oscillation frequency. This is unusual : in the other simulations, desynchronization occurred concurrently with an increase of the oscillation frequency due to a weaker recruitment of the inhibitory cells. Here, the somatic current was the only one able to counteract the somatic inhibition and to force the neuron to discharge

even during an incoming IPSP volley. The desynchronization is therefore due to a stronger and less coordinated recruitment of inhibitory cells by an excess of excitatory input to the soma.

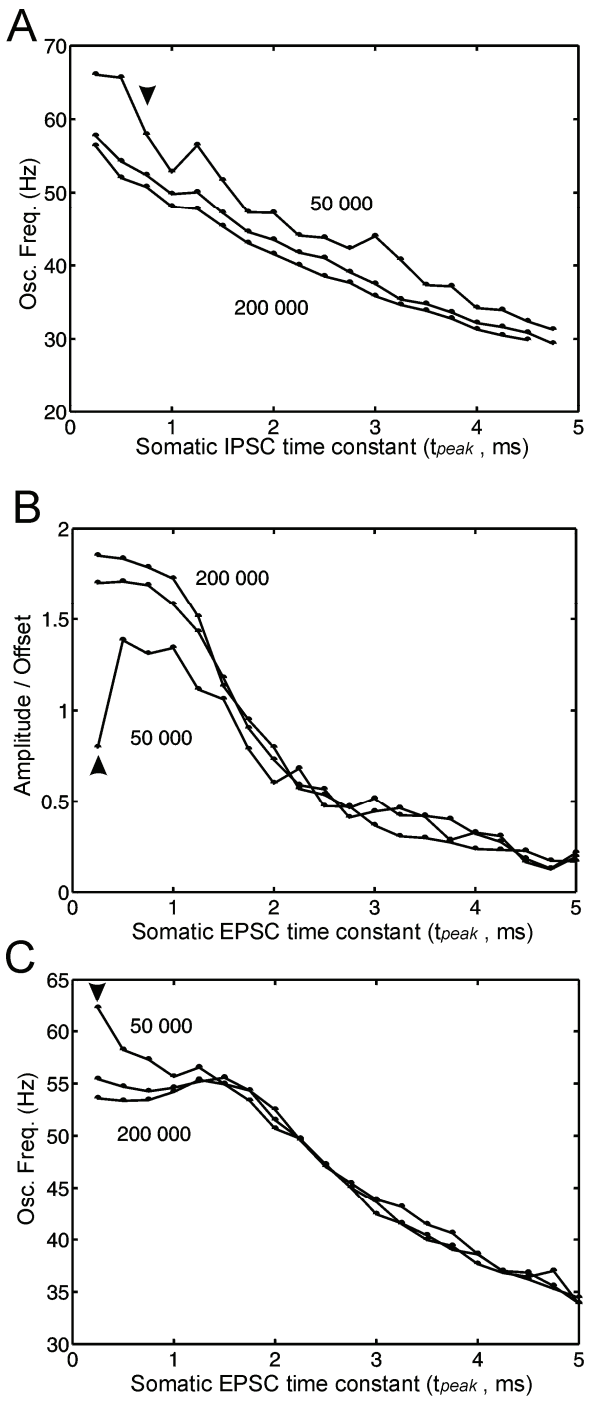

Figure 8. Synaptic time constant testing (t_{peak} in App. Eq. 3). (A) Effect of time constant in somatic IPSCs on the oscillation frequency for three different input intensities (50 000, 100 000 and 200 000 EPSPs/s on the central cell). The oscillation frequency decreased for slow IPSCs. The amplitude to offset ratio was stable for all the simulations and depended mainly on the input level (not shown). (B&C) The changes in the amplitude to offset ratio and in oscillation frequency are illustrated the time constant in somatic EPSCs was varied. The increase of the time constant of somatic EPSCs, directed only to the inhibitory cells, had a desynchronizing effect, as shown by the decrease of the amplitude to offset ratio (B). This desynchronization was accompanied by a decrease of the oscillation frequency (C). Arrow head denotes the simulation with the same parameters as in Fig. 2.

Prolonging the time course of dendritic IPSCs resulted in a slight desynchronization (lower amplitude to offset ratio, higher oscillation frequency), which could be counteracted by an increase in the input. Longer dendritic IPSPs actually resulted in a subtraction of the dendritic input. If the time course of the dendritic IPSCs was changed along with the somatic IPSCs, the changes were similar to those obtained in Fig. 8A for the somatic IPSCs alone. Somatic

inhibition thus influenced the network dynamics, whereas dendritic inhibition acted simply to cancel a proportion of the excitatory input.

Use of alternative shapes, other than alpha functions, for the PSPs did not alter the global dynamics of the network, provided that the inhibition was strong and the inhibitory delays were long enough. Particularly, if IPSPs had an abrupt onset and a slow exponential, a desynchronized state could be obtained for very long decay time constant (τ = 20 ms ; Wang and Buszáki, 1996, Fig.10A ; White et al., 1997, Fig.6). We reproduced this condition, and after the inhibitory delays were increased, the network oscillated regularly with a period of 65 ms.

3.6 Input sensitivity

The effects on the network dynamics of the input strength and spatial distribution were systematically investigated; the results are shown in Fig. 9. The input was characterized by the maximum intensity delivered to the center cell (shown on the abscissa) and its spatial distribution (shown as different lines).

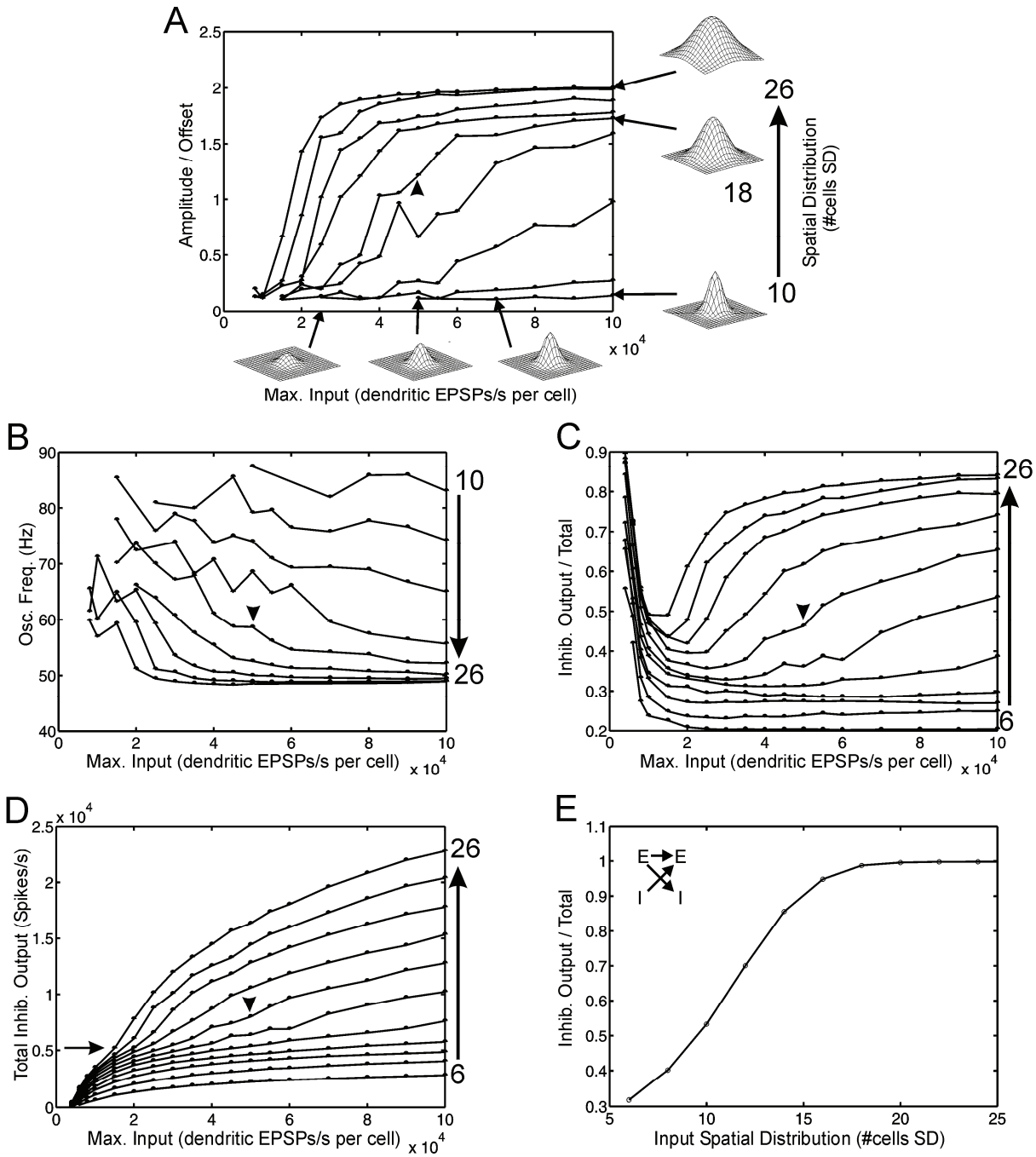

Figure 9. Effect of modulating the network input. Maximal input on the central cell was varied between 0 and 100 000 EPSPs/s. Each curve represents a different value of spatial standard deviation; the abscissa shows the input magnitude. The maximum and minimum spatial standard deviations tested are indicated on the right side of the graph. (A) Amplitude to offset ratio. The inset 3D curves show a schematic representation of the spatial distribution of input across the network for the indicated simulations. (B) Oscillation frequency. For large spatial SD, the oscillations appeared for small inputs and their frequency stabilized quickly to 50 Hz. (C) Fraction of the total spikes produced by the inhibitory cells. (D) The total number of spikes emitted by the inhibitory cells. When oscillations appeared, the inhibitory cells accentuated their discharge (arrow). If the input was then increased, the inhibitory cells became the most active. (E) Input sensitivity in a non-oscillatory network, where inhibitory to inhibitory connections where removed and the number of inhibitory connections directed toward excitatory cells was reduced to 255 to permit excitatory cells to be active. In this network, the amplitude to offset ratio remained below 0.02. Input was fixed at 50 000 EPSPs/s per cell whilst the spatial standard deviation of the input was varied. The fraction of spikes emitted by inhibitory cells is plotted versus the spatial distribution of the input.

Firstly, oscillations were not present for the narrowest input distributions (< 12 cells SD, Fig. 9A). Thereafter, there was a threshold of input intensity required before strong oscillation occurred. This threshold was lower for wider spatial distributions. This could not be explained simply as a function of the total input received by the network (data not shown).

A plot of oscillation frequency shows its high variability (Fig. 9B); however most of this variability related to smaller oscillations, whereas the frequency was constant for strong oscillations (comparison with Fig. 9A).

Figure 9C plots the fraction of total spikes emitted by inhibitory neurons. Because the inhibitory neurons had a higher somatic resistance than the excitatory ones, they began to discharge at lower input. Hence most active cells were inhibitory when the input was only just strong enough to elicit a few spikes. However, this situation was transient and the ratio decreased quickly, as the first excitatory neurons were recruited. The number of active neurons increased until the oscillations began (not shown). The moment at which this occurred depended on the spatial distribution of the input, as a larger spatial distribution recruited inhibitory neurons more effectively. With the oscillation onset, the firing rate of the inhibitory neurons suddenly rose more steeply (arrow in Fig. 9D), while the firing rate of excitatory neurons began to fall (not shown).

Figure 9E presents evidence that this change in the proportion of inhibitory to total spikes with spatial distribution of input was not dependent on the oscillatory state. In these simulations, the connections between inhibitory cells were absent; no oscillations were therefore seen. As a consequence, it was necessary to decrease the number of inhibitory connections to excitatory cells to 255 per inhibitory cell, as the inhibitory cells were firing more strongly. The presence of a modulation of the inhibitory and excitatory outputs similar to Fig. 9C suggests that the progressive recruitment of inhibitory neurons was caused by the geometric arrangement of the network rather than by the oscillatory state itself. Moreover, it also depended on the respective input/firing curves of both cell types. It was impossible to achieve a total absence of active excitatory cells, unless the inhibitory cells responded at lower input levels.

The oscillations were very stable. In an attempt to disrupt the periodic bursts, simulations were run with an input as high as 10^6 EPSPs of 100 nS conductance peak per cell; the same oscillations with the same frequency were still observed. The only manipulation which disrupted oscillations was to direct the excitatory input to the soma, a completely aberrant

connectivity. This produced very high firing rates in an uncorrelated fashion. Adding a few percent of somatic input to the inhibitory cells increased their excitability and favored oscillations at low input, but at much higher input this led to a desynchronization (data not shown).

In some ranges of parameters close to the emergence of oscillations, the oscillation frequencies of different networks could differ by up to 15 Hz for the same input level. Moreover, when oscillation did appear, they were not always fully stable, such oscillation amplitude waxed and waned over a few hundreds of milliseconds.

In all of these simulations, all active cells discharged at low mean frequencies (< 65 Hz) and were unable to burst. Bursting could have led to higher discharge rates during a synchronous event. In fact, the major cause of the firing frequency limitation was the neuron architecture itself, which was designed to produce realistic PSP amplitudes and membrane time constants. The selected configuration determined the input-output curve (Fig. 1C). Hence, under maximal dendritic stimulation, the cells were unable to discharge at a higher rate than 60 Hz because the dendritic tree was unable to provide more current to the soma. Such a limitation of the dendritic current was probably not realistic: it has been shown that, in presence of $GABA_A$ antagonist, the firing frequency in fast-spiking neurons could reach 650 Hz after orthodromic stimulation (McCormick et al., 1989). For this reason, we ran some simulations using cells which were able to discharge at 120 Hz under maximal stimulation. However, as we lowered the resistance between the dendrite and the soma (R_{ds}), the dendrite reflected more the somatic potential and its longer time constant. If we adjusted the synaptic conductance to reproduce the same PSPs amplitude, and if we kept the same network configuration, the network oscillations appeared at a frequency around 80 Hz. To constrain these oscillations to 50 Hz, we changed the local connectivity of the network to increase the inhibitory drive. The oscillation frequency was still modulated by the input as in Fig. 9. Another way to increase the maximal firing rate was to decrease the firing threshold. Although individual cells became able to fire at more than 90 Hz, the oscillation frequency remained stable at 70 Hz.

3.7 Damped versus stable oscillation

All of the analysis shown above was performed during the steady state, after an initial period of 200 ms. Results were similar if a progressive increase of the input during the first

100 ms was used. Interestingly, in the normal arrangement of input, the sudden appearance of the input in the first 200 ms sometimes evoked an damped oscillation of higher amplitude and lower frequency than during the steady state. During this transient, the proportion of active inhibitory neurons was also higher than later on. Moreover, the number of active cells per millisecond could be around twice as large, as if the inhibition was not yet fully effective. To investigate the initial transient more fully, two auto-correlation histograms were computed on each simulation : one from simulation time 0-200 ms, the other from 300-500 ms. These were essentially the same, in simulations where oscillation amplitude was either negligible or very strong. At intermediate levels of amplitude to offset ratio, oscillations were stronger during the transient. Some control simulations performed with cells capable of higher maximum firing rate showed that the transient frequency was influenced by the maximal cell firing rate, whereas stable oscillations depended on the network configuration (inhibitory delay distribution and the duration of the IPSPs). The intrinsic cell properties were indeed better assessed when all connections were absent and the input was applied suddenly. In this case, the oscillations at the input onset reflected the intrinsic cell frequencies (data not shown).

4. Discussion

4.1 Model assumptions

4.1.1 *Cell structure*

As described earlier, our cells had one dendritic compartment which received most of the excitatory input. This arrangement provided the cell with new dynamical features accentuating the difference between somatic IPSPs and dendritic EPSPs when compared with a classical one compartment model, as already shown by MacGregor (1987). In response to dendritic stimulation (Fig. 1C), our cells never discharged at higher rate than 60 spikes/s, but during a simulation, the instantaneous frequency in an inhibitory neuron (which also received somatic excitation) could reach 100 spikes/s. They were also unable to burst or to accommodate. However most of the available physiological studies have been done using somatic current injection or electrical stimulation and it is very difficult to estimate the firing range of cortical interneurons in vivo. In the monkey prefrontal cortex, Wilson et al. (1994) have shown that the spontaneous firing rate of fast-spiking cells (interneurons) was 17 ± 10.8 spikes/s and of regular-spiking cells (pyramidal) 5 ± 5.5 spikes/s. The maximum firing rate of

a fast-spiking cell to the most effective stimulus was 72 spikes/s with an instance of instantaneous firing rate reaching 140 spikes/s. Such data support the notion that, in the cerebral cortex, cells rarely achieve very high firing rate (see also van Vreeswijck and Sompolinski, 1996).

Most of the model neurons used in the present study had a small somatic time constant compared to figures given in the literature. However, simple measurements of time constants by current injection give a poor indication of how rapidly the membrane can respond and do not consider the important effect of background activity (Koch at al., 1996). The use of a short time constant permitted a close approximation to real neuronal dynamics with the computationally simple integrate and fire model. In those simulations where time constants were varied, oscillations remained robust (Fig. 4).

4.1.2 Connectivity

In the Methods, we described the set of simple connectivity rules used in this model. They can be summarized as follows : Firstly, no excitation was directed to the soma of excitatory cells. This rule is well established and confirmed by many anatomical studies (White, 1989). Secondly, no distinction was made between dendrites belonging to inhibitory or excitatory neurons, and connections were established on a simple probability rule (Abeles, 1991). Thirdly, there was somatic inhibition on both types of cells, without distinction and in the same proportion (Kisvárday et al., 1993).

By respecting these rules, self-sustained activity could be avoided. A prime problem for such a network with strong excitatory coupling is to block the propagation of the recurrent excitation, which would lead to the full activated state with abnormally high firing rates. Sparse random connectivity was another way to prevent strong activity propagation to immediate neighbor cells, but it was insufficient to prevent self-sustained activity.

4.1.3 Delay distributions

The delay distributions may seem very wide, with long means. However, it is necessary to remember that experimental quantification of these parameters is always biased towards the faster components. A mean delay is difficult to evaluate, especially if this mean is very long and if the network is intricate. Accordingly, we tested extensively the lower portion of the reported values (Salin and Prince, 1996; Murakoshi at al., 1993).

4.2 Oscillation Stability

In most of our simulations, we obtained repetitive events of synchronous activity. Somatic inhibition was of overriding importance in permitting a stable oscillating state. It was essential that this inhibition was strong enough to cancel the excitation from the input and from the excitatory synapses, thereby resetting the whole network on each cycle by synchronous IPSPs. Thus oscillations required both enough inhibitory cells to be active, and sufficient connections from these cells. In Fig. 9A, an input with small spatial distribution was unable to excite sufficient inhibitory cells to propagate synchronous IPSPs to the whole network; the consequence was that oscillations were never established. Likewise, even with a large, spatially distributed input, no oscillations could occur below a critical level of inhibitory connectivity (Fig. 6B). However, this mechanism relied upon the existence of a sufficient delay in inhibitory connections (Fig. 7A). Short excitatory delays favored small oscillation amplitude of high frequency while long inhibitory delays improved the oscillation stability and determined lower oscillation frequency. The total inhibitory delay was in fact the sum of the conduction delay, the synaptic delay (a constant plus the alpha function) and a possible integration delay depending on the model implementation (null in our model).

The ratio of the inhibitory delays to the IPSC decay time constant seems to be an important parameter to explain why IPSPs with abrupt onset and very slow decay produce desynchronization (Wang and Buszáki, 1996 ; White et al., 1997). Indeed, we have reproduced those conditions and shown that increasing the inhibitory delays could restore the oscillations. Accordingly, the use of an alpha function, which delayed the peak of inhibitory conductance, prevented the occurrence of the desynchronization . Moreover, very long IPSPs with abrupt onset and offset (pulse function) do synchronize the network, ruling out the IPSP duration as a desynchronizing parameter. Long decay time constant slowed down the release of the inhibition, allowing some cells to lead the others over a long lag. As the duration of a synchronous event depended on the inhibitory delays, if not enough cells were recruited during this period, the next event would be less synchronized.

A second factor influencing oscillation stability was the level of input to the inhibitory cells. This comprised both the external input and the EPSPs from the excitatory cells; the latter acted to amplify the input. Thus without excitatory cells, a considerably larger input was

needed to achieve stable oscillations (150 000 EPSPs/s in Fig. 5A compared with 60 000 in EPSPs/s Fig. 9A).

The structure of our cells, with two compartments, guarantees that the cells will be correctly inhibited by the synchronous somatic IPSPs whatever the input they receive on the dendrite. It is for this reason that increasing the time constant of the somatic EPSCs produced a desynchronization (Fig. 8B) – the input was then simply too strong. It is also possible that the cell structure, which produces response curves with an asymptotic maximal firing rate, promotes a uniform response in the inhibitory cells although they receive very different inputs.

Initial simulations used a different spatial arrangement of the input from the main body of the work reported here; the input was uniform, with wrap-around boundary conditions (i.e. a torus). Such a network also exhibited oscillations, which ceased when the input was stopped. We choose the current, spatially delimited input configuration, to approximate more closely localized input arriving in a cortical column, and to allow study of the spatial stability of the activity. We showed that activity remained local, and did not propagate to the rest of the network (Fig. 3C&D).

Experimental support for the critical features of our model exists. The somatic inhibition of inhibitory cells is now well accepted, even between large basket cells (Kisvárday et al., 1993), although its usual functional interpretation has been the disinhibition of the adjacent pyramidal neurons. Also, the recruitment of inhibitory neurons in an oscillatory manner has been illustrated when $GABA_A$-mediated inhibition is slightly reduced with low doses of bicuculline methiodide (Chagnac-Amitai and Connors, 1989). In phase with each synchronous event, most regular spiking cells (i.e. pyramidal and excitatory) are strongly inhibited, while intrinsically bursting (middle layer pyramids and spiny stellate) and fast cells (inhibitory) are strongly activated. We parallel this experiment with simulations using the wide input distribution, roughly equivalent to a global decrease of the inhibition.

Inhibition has been proposed for a long time to be one of the mechanisms to achieve synchrony. Hansel et al. (1993, 1995) showed with phase models in the weak coupling limit that a network with only excitatory connections exhibited a desynchronized state of high activity, and they predicted the synchronizing effect of inhibitory synapses. In a model of pyramidal neuron with 406 compartments and 11 different ionic channels, a somatic

inhibitory synapse produces phase-locking 100 times more powerfully than an excitatory one on a distant dendrite (Lytton and Sejnowski, 1991). Our results are similar to those found for a simple pair of coupled cells (van Vreeswijck et al, 1994). Indeed, we have verified that two of our neurons synchronize if they are connected through delayed inhibitory synapses and fail to do so if there was no delay or if the synapses were excitatory.

Whittington et al. (1995) have also shown that a network of inhibitory cells diffusely stimulated exhibited gamma range oscillations due to high amplitude synchronous IPSPs. This phenomenon was observed in a network of inhibitory cells modeling spindle generation in the thalamic reticular nucleus (Wang and Rinzel, 1993) and further extended to the hippocampus (Wang and Buszáki, 1996; White et al., 1997). However, in the reticular nucleus, the 7-14 Hz spindle oscillation depends on the slow $GABA_B$-mediated IPSPs, on postinhibitory rebound responses, and also is affected by some cellular autorythmic abilities (Wang and Rinzel, 1993). Our simulations of a network consisting only of interconnected inhibitory neurons (Fig. 5A) are in accordance with this previous work which always relies on strong, recurrent, and somewhat delayed inhibition.

Traub et al. (1996) have reproduced these oscillations in a network of excitatory and inhibitory cells, pointing out the importance of the total input to inhibitory cells and of an homogeneous somatic input, whereas Bush and Sejnowski (1996) reported that any input (which was somatic) directed to inhibitory cells degrades synchrony. It is interesting to note that these two studies use multi-compartment cells, unlike the more simple model used in the present work. We obtained strong oscillations with a large distribution of conduction delays in agreement with Bush and Sejnowski (1996). The major difference from this study is that, in our simulations, cells receiving very different input could synchronize due to the dendritic location of the input, which permitted somatic inhibition to play its dominant role.

In a population of excitatory and inhibitory non-linear oscillators, with all-to-all coupling, van Vreeswijck (1996) has shown that, for fast inhibition, the number of synchronized clusters tends to be large, whereas this number is smaller for slow inhibition. This is consistent with our results. Nevertheless, we did not test a network large enough to examine the possible desynchronization with very widely distributed input, and we did not characterize

the number of synchronous clusters present in the network when the activity was desynchronized.

The present simulations illustrate clearly how the oscillations in the gamma range are an emergent and stable property of a local network. Oscillations terminated when the input ceased and did not propagate across the whole network, they were thus *temporally* and *spatially* stable. Moreover these oscillations persisted in the face of large increases in the input and various changes in the connectivity and delay distribution.

4.3 Oscillation frequency

In determining the oscillation frequency, we have shown that the input to inhibitory cells is a factor that can produce a modulation of this frequency in parallel with a change in its amplitude. *In vivo*, this input is the parameter that changes the most quickly and contributes to the variability of the observations.

Gray and Viana Di Prisco (1997) have shown that the oscillation frequency increases with the speed of the moving bars in the awake cat. However, the real *input* received by the network during such a stimulus is unknown. For the *output*, it is known that slower velocities evoke a lower oscillation frequency and larger cross-correlation peaks (Gray et al., 1990). In our simulations, the oscillation frequency covered the same range, and diminished while the driving input increased. This leads us to suppose that the unknown input to the cortical network is higher at lower velocity. When excited with a fast moving light bar, the cortical network exhibits a higher firing rate of shorter duration and the oscillation frequency is higher. This could be explained by a decrease of the recruited inhibition due to a narrower or a smaller driving input or an input of shorter duration, which evokes more spikes. This situation could be compared with the network in Fig. 9 (line of 18 cell spatial SD), when it received a maximal input of 60 000 or 50 000 EPSPs/s (hypothetically, low and high stimulus velocity). The reduction of the input intensity led to a global higher firing rate but a less synchronized activity.

On the contrary, Traub et al. (1996) describe, in a network of 96 basket interneurons, an increase in the oscillatory frequency when the driving current rise. In this case, simulated electrical stimulation probably overdrives most of the somatic inhibition. Note that inhibition is imposed by a long IPSP time constant rather than by a delay distribution. Bush and

Sejnowski (1996) have found that increasing the strength of external driving permitted an increase of the oscillation frequency. This apparent conflict with our study suggests that the use of a dendritic input instead of a somatic injected current could be an important feature when characterizing the network response. In our two-compartment cells, the depolarizing current flowing from the dendrite saturates at a certain level, ensuring the firing rate stability.

At a longer time scale, learning mechanisms such as long term potentiation can change the amount of excitatory input received by the inhibitory neurons by increasing the input amplification done by the excitatory cells (Whittington et al., 1997). After potentiation, the network frequency decreased, as expected from an increase in dendritic input.

All of the parameters related to the propagation of inhibition among the inhibitory neurons can influence the oscillation frequency. Most of them are fixed *in vivo*: the somatic membrane time constant of inhibitory neurons, the conduction delays of IPSPs, their current time constant on the soma, and the inhibitory connectivity.

While Traub et al. (1996) already pointed out three of them, namely the driving current to the interneurons, the inhibitory conductance and decay time constant of IPSPs, Bush and Sejnowski (1996) reported that the conduction delays can change the oscillation frequency markedly. We have shown that a model as simple as a network of two compartment cells produced the same relationships.

4.4 Output

The spatial distribution of the input was able to recruit preferentially excitatory or inhibitory cells. Indeed, the spatial distribution of the input could enormously alter the excitatory component of the synchronous activity. In Figure 9C, if the Gaussian input spanned too much of the network, it silenced the excitatory cells. Although the strong inactivation of the excitatory cells with spatially extended input was not a generic feature, it could be achieved in most cases with moderate tuning of the connectivity and of the response curve of both cell types. Oscillations were not needed to produce this effect (Fig. 9E), which seemed to rely on the geometric arrangement of the network and on the relatively higher input sensitivity of inhibitory cells. When the input extended spatially, the ring of active inhibitory neurons grew and these cells became able to inhibit more powerfully the neurons in the center. The duration of the synchronous event decreased and fewer excitable cells had an opportunity to discharge.

A consequence of this effect is that the network could produce no long range output. An input could therefore act to gate network output depending on its 'focus'. This finding indicates that great care is required in interpreting high metabolic activity in networks which have inhibitory interneurons. The fundamental hypothesis of blood flow measures such as fMRI and PET is that activated cortical areas are excited and relevant for cognitive behavior. Our results indicate that these areas could just be inhibited by an inappropriately widespread excitatory input. If this is the case, global activity measures are of limited value, and the number of active excitatory cells is the only parameter which reliably estimates the contribution of an area to a global cognitive process. Unfortunately, at the moment, there is no technique able to separate the activity of the excitatory from inhibitory subpopulations.

Tonic inhibition has been proposed to gate the excitatory neurons in the somatosensory cortex (Wilson et al, 1994; Lebedev and Nelson, 1995), but the explanation provided relies on many selective connections between different cell types of excitatory and inhibitory populations, not on a simple dynamic recruitment of inhibitory neurons. Except for the absence of excitatory synapses on the soma of inhibitory cells, it is unlikely that selective connectivity exists in the neocortex; the current work presents the more parsimonious hypothesis

When the input was narrow, excitatory cells were highly excited and poorly inhibited due to the lack of active inhibitory cells and their sparse connectivity. This high excitation led to slightly synchronized activity. However, our network had only two dimensions. In a real 3D cortical column, the radially oriented interneurons could synchronize such a narrow activity with a few milliseconds of delay between different layers, as has been shown *in vivo* (Livingstone, 1996). This kind of radial inhibition could be tuned to permit the discharge of the excitatory cells.

5. Perspectives

We have documented here the importance of somatic inhibition for local synchronization, and the importance of a slow dynamic of IPSPs (conduction velocity and synaptic time constant). There is no need for an exact balance between excitation and inhibition since they occur *sequentially* in most of the activated cells. The only restriction is that inhibition must be stronger than excitation, which is achieved by somatic inhibition. Sparse connectivity offers the possibility to activate a large number of cells before the inhibition silences the network.

On the other hand, cell response curves could be tuned according to the range of connection, so that widely distributed inputs recruit massive inhibition.

In the oscillatory state, about the same number of cells will discharge synchronously whatever the input level. It is thus a mechanism which could serve to select in a given population the k most responding neurons. This kind of 'winner-takes-all' property has a special feature which is the concomitant processing of the network by some sparse inhibition, which will exclude some possible 'winners'. This inhibitory frame depended on the sparse connectivity and on the different response curves of both cell types.

Abeles (1991) has proposed a pattern of activity whereby successive sets of neurons discharge synchronously, one node after another; this is referred to as a synfire chain. In such synfire chains, local oscillations could be also a natural means for selecting or completing a local node of a given size. Indeed in this network, the maximal number of responding cells during a burst of activity was securely fixed by the local connectivity. Synchronous IPSPs acted as a temporal reset of all the local network; this could permit a new node selection on the next cycle. This node could be completely different and determined by the new inputs and incoming feedback. This idea is also very close to the sequential configuration model (MacGregor, 1991) which could be embedded in a burst of activity. However, most of the activity in our simulation was due to the random connectivity and to the random input.

As we have shown, the output of the excitatory cells depended on the spatial input distribution. Hence, two nodes projecting to exactly the same area will elicit a response, but if their inputs diverge too much, the final response will be inhibitory. This provides a logical 'exclusive or' and an inhibitory mechanism which relies on long range excitatory fibers between active networks.

In conclusion, interconnected inhibitory interneurons are able to pace a whole network of excitatory cells. At low input levels, oscillations which originated in the inhibitory population became a cooperative property of the network as the input amplification provided by the excitatory neurons compensated for the small input. The slow propagation of the inhibition and sparse connectivity permitted the number of active excitatory cells to increase. The spatial distribution of the non-specific incoming excitation could determine the effective activation or inhibition of the pyramidal cells, and thereby dramatically alter the contribution of this network to the global processing of the information. An increase of activity in a particular

area of the brain does not therefore imply that this area produces a long range excitatory output.

LIST OF ABBREVIATIONS

C_d : dendritic capacitance.

C_s : somatic capacitance.

E_{exc} : reversal potential of excitatory ionic channels.

E_{inh} : reversal potential of inhibitory ionic channels.

E_{rest} : resting membrane potential.

g^d_{exc} : total conductance due to dendritic EPSPs.

g^d_{inh} : : total conductance due to dendritic IPSPs.

g^d_{leak} : dendritic leak conductance.

g_{ds} : conductance between the soma and the dendrite

g^s_{exc} : total conductance due to somatic EPSPs.

g^s_{inh} : total conductance due to somatic IPSPs.

g^s_{leak} : somatic leak conductance.

I_{ds} : current flowing from the dendrite to the soma.

R^d_m: membrane resistance of the dendritic compartment.

R_{ds}: resistance between the dendrite and the soma.

R^s_m: membrane resistance of the somatic compartment .

t_{peak}: time constant of the alpha function, time of the conductance peak.

V_d : dendritic membrane potential.

V_s : somatic membrane potential.

APPENDIX

The details of the model are presented in this appendix. Passive membrane properties in the somatic and dendritic compartments are governed by the equations shown in Eq. 1 :

$$C_s \frac{dV_s}{dt} = g^s_{leak}(E_{rest} - V_s) + g^s_{exc}(E_{exc} - V_s) + g^s_{inh}(E_{inh} - V_s) + I_{ds}$$
$$C_d \frac{dV_d}{dt} = g^d_{leak}(E_{rest} - V_d) + g^d_{exc}(E_{exc} - V_d) + g^d_{inh}(E_{inh} - V_d) - I_{ds}$$
$$I_{ds} = g_{ds}(V_d - V_s)$$

(Eq. 1)

First order integration and stepwise constant approximation of Eq. 1 leads to :

$$V_s(t + \Delta t) = V_s(t)\exp(-A_s \Delta t) + \frac{B_s}{A_s}[1 - \exp(-A_s \Delta t)$$
$$V_d(t + \Delta t) = V_d(t)\exp(-A_d \Delta t) + \frac{B_d}{A_d}[1 - \exp(-A_d \Delta t)$$
$$A_s = \frac{g^s_{leak} + g^s_{exc} + g^s_{inh} + g_{ds}}{C_s}$$
$$B_s = \frac{g^s_{leak} E_{rest} + g^s_{exc} E_{exc} + g^s_{inh} E_{inh} + g_{ds} V_d(t)}{C_s}$$
$$A_d = \frac{g^d_{leak} + g^d_{exc} + g^d_{inh} + g_{ds}}{C_d}$$
$$B_d = \frac{g^d_{leak} E_{rest} + g^d_{exc} E_{exc} + g^d_{inh} E_{inh} + g_{ds} V_s(t)}{C_d}$$

(Eq. 2)

The time course of the conductance change followed an alpha function with normalized peak. Discretization of this function *g(t)* was done using the alpha function integral.

$$\alpha(t) = \frac{t}{t_{peak}} \exp\left(1 - \frac{t}{t_{peak}}\right)$$

$$g(t + \Delta t) = g_{syn} \frac{1}{\Delta t} \int_{t}^{t+\Delta t} \alpha(t) dt$$

(Eq. 3)

The following function gives the distribution of the conductance peaks, with mean conductance $\bar{g}$, where the parameter i varies from 1 to 32.

$$P\left(g_{syn} = \frac{\bar{g}\, i}{7.4}\right) = \frac{1}{4.43}\left[\exp\left(\frac{-i}{6}\right) - \exp\left(\frac{-i}{1.5}\right)\right]$$

(Eq. 4)

Equation 5 characterizes the mean number of dendritic EPSPs received by the cell i according to its distance from the center d_i (normal distribution).

$$Input_i = M \exp\left(\frac{-d_i^2}{2\sigma^2}\right)$$

(Eq. 5)

An animated sequence showing the activity pattern of the first simulation (Fig. 2&3) is available at the FTP site lewsun.ucl.ac.be (130.104.5.1, directory /pub/JCNS) under anonymous login. It requires Matlab or Octave to be installed.

ACKNOWLEDGMENTS

We thank David Hansel for critical discussion of these simulations, and the two referees for their helpful comments.

Q.P. acknowledges the hospitality of the 1997 Crete Course, where part of this work was concluded, and the Applied Computational Mathematics of FORTH for funding. This work was partly supported by a British Council - CGRI travel grant. S.N.B is funded by the UK MRC.

REFERENCES

Abeles M (1991) Corticonics: neural circuits of the cerebral cortex. Cambridge University Press, Cambridge.

Abeles M, Gerstein GL (1988) Detecting spatiotemporal firing patterns among simultaneously recorded single neurons. *J. Neurophysiol.* 60 : 909-924.

Alonso JM, Usrey WM, Reid RC (1996) Precisely correlated firing in cells of the lateral geniculate nucleus. *Nature* 383:815-819.

Baddeley R, Abott LF, Booth MCA, Sengpiel F, Freeman T, Wakeman EA, Rolls ET. (1997) Responses of neurons in primary and inferior temporal visual cortices to natural scenes. *Proc. R. Soc. Lond. B.* 264 :1775-1783.

Baker SN, Olivier E, Lemon RN (1997) Task dependent coherent oscillations recorded in monkey motor cortex and hand muscle EMG. *J. Physiol.* 50:225-241.

Beaulieu C, Colonnier M (1983) The number of neurons in the different laminae of the binocular and monocular regions of area 17 in the cat. *J. Comp. Neurol.* 217:337-344.

Buhl EH, Tamàs G, Szilàgyi T, Stricker C, Paulsen O, Somogyi P (1997) Effect number and location of synapses made by single pyramidal cells onto aspiny interneurons of cat visual cortex. *J. Physiol.* 500:689-713.

Bush P, Sejnowski T (1996) Inhibition synchronizes sparsely connected cortical neurons within and between columns in realistic network models. *J. Comput. Neurosci.* 3:91-110.

Chagnac-Amitai Y, Connors BW (1989) Synchronized excitation and inhibition driven by intrinsically bursting neurons in neocortex. *J. Neurophysiol.* 62:1149-1162.

Engel AK, König P, Gray CM, Singer W (1990) Stimulus-dependent neuronal oscillation in cat visual cortex : Inter-columnar interaction as determined by cross-correlation analysis. *Eur. J. Neurosci.* 2:588-606.

Engel AK, König P, Kreiter AK, Singer W (1991a) Interhemispheric synchronization of oscillatory neuronal responses in cat visual cortex. *Science* 252:1177-1179.

Engel AK, Kreiter AK, König P, Singer W (1991b) Synchronization of oscillatory neuronal responses between striate and extrastriate visual cortical areas of the cat. *Proc. Natl. Acad. Sci. USA* 88:6048-6052.

Ghose GM, Freeman RD (1997) Intracortical connections are not required for oscillatory activity in the visual cortex. *Vis. Neurosci.* 14:963-979.

Gray CM, Engel AK, König P, Singer (1990) Stimulus-dependent neuronal oscillations in cat visual cortex : Receptive field properties and feature dependence. *Eur. J. Neurosci*. 2:607-619.

Gray CM, Viana Di Prisco G (1997) Stimulus-dependent neuronal oscillations and local synchronization in striate cortex of the alert cat. *J. Neurosci*. 17:3239-3253.

Hansel D, Mato G, Meunier C (1995) Synchrony in excitatory neural networks. *Neural Comput.* 7:307-337.

Hansel D, Mato G, Meunier C (1993) Phase reduction and neural modelling. In *Functional Analysis of the Brain Based on Multiple-Site Recordings, October 1992. Concepts Neurosci.* 4 :192-210.

Holt GR, Koch C (1997) Shunting inhibition does not have a divisive effect on firing rates. *Neural Comput.* 9:1001-1014.

Kisvárday ZF, Beaulieu C, Eysel UT (1993) Network of GABAergic large basket cells in cat visual cortex (area 18) : Implication for lateral desinhibition. *J. Comp. Neurol.* 327:398-415.

Kisvárday ZF, Eysel UT (1992) Cellular organization of reciprocal patchy networks in layer III of cat visual cortex (area 17). *Neurosci.* 46:275-286.

Koch C, Rapp M, Segev I (1996) A brief history of time (constants). *Cereb. Cortex* 6:93-101.

König P (1994) A method for the quantification of synchrony and oscillatory properties of neuronal activity. *J. Neurosci. Meth*. 54:31-37.

Lebedev MA, Nelson RJ (1995) Rhythmically firing (20-50 Hz) neurons in primary somatosensory cortex : Activity patterns during initiation of vibratory-cued hand movements. *J. Comput. Neurosci.* 2:313-334.

Livingstone MS (1996) Oscillatory firing and interneuronal correlations in squirrel monkey striate cortex. *J. Neurphysiol.* 75:2467-2485.

Lytton WW, Sejnowski TJ (1991) Simulations of cortical pyramidal neurons synchronized by inhibitory interneurons. *J. Neurophysiol*. 66:1059-1079.

MacGregor RJ (1987) Neural and Brain Modeling. Academic Press, London.

MacGregor RJ (1991) Sequential configuration model for firing patterns in local neural networks. *Biol. Cybern*. 65:339-349.

MacGregor RJ (1993) Theoretical mechanics of biological neural networks. Academic Press, London.

McCormick DA, Connors BW, Lighthall JW, Prince DA (1989) Comparative electrophysiology of pyramidal and sparsely spiny stellate neurons of the neocortex. *J. Neurophysiol.* 54:782-806.

Murakoshi T, Guo JZ, Ichinose T (1993) Electrophysiological identification of horizontal synaptic connections in rat visual cortex in vitro. *Neurosci. Let.* 163:211-214.

Neuenschwander S, Singer W (1996) Long-range synchronization of oscillatory light responses in the cat retina and lateral geniculate nucleus. *Nature* 379:728-733.

Pauluis Q, Olivier E, Baker SN (1997) Long axonal delay could explain local firing rate oscillations in the gamma frequency range. *Soc. Neurosci. Abstr.* 27:499.9.

Perkel DH, Gerstein GL, Moore GP (1967b) Neuronal spike trains and stochastic point process. II. Simultaneous spike trains. *J. Biophys*. 7:419-440.

Peters A, Kara DA, Harriman KM (1985) The neuronal composition of area 17 of rat visual cortex. III. Numerical considerations. *J. Comp. Neurol.* 238:263-274.

Peters A, Yilmaz E (1993) Neuronal organization in area 17 of cat visual cortex. *Cereb. Cortex* 3:49-68.

Press WH, Teukolsky SA, Vetterling WT, Flannery BP (1992) Numerical recipes in C: The art of scientific computing. Cambridge University Press, Cambridge, MA. pp. 274-295.

Roelfsema PR, Konig P, Engel AK, Sireteanu R, Singer W (1994) Reduced synchronization in the visual cortex of cats with strabismic amblyopia. *Eur. J Neurosci*. 6:1645-1655.

Salin PA, Bullier J (1995) Corticocortical connections in the visual system : Structure and function. *Phys. Rev.* 75:107-154.

Salin PA, Prince DA (1996) Electrophysiological mapping of $GABA_A$ receptor-mediated inhibition in adult rat somatosensory cortex. *J. Neurophysiol*. 75:1589-1600.

Singer W, Gray CM (1995) Visual feature integration and the temporal correlation hypothesis. *Annu. Rev. Neurosci.* 18:555-86.

Tamàs G, Buhl EH, Somogyi P (1997) Fast IPSPs elicited via multiple synaptic release sites by different types of GABAergic neurone in cat visual cortex. *J. Physiol.* 500:715-738.

Thomson AM, Deuchars J (1997) Synaptic interactions in neocortical local circuits: Dual intracellular recordings in vitro. *Cereb. Cortex* 7:510-522.

Thomson AM, Deuchars J, West DC (1993) Single axon excitatory postsynaptic potentials in neocortical interneurons exhibit pronounced paired pulse facilitation. *Neuroscience* 54:347-360.

Thomson AM, West DC, Deuchars J (1995) Properties of single axon excitatory postsynaptic potentials elicited in spiny interneurons by action potentials in pyramidal neurons in slices of rat neocortex. *Neuroscience* 69:727-738.

Traub RD, Whittington MA, Colling SB, Buzsáki G, Jefferys JGR (1996) Analysis of gamma rhythms in the rat hippocampus in vitro and in vivo. *J. Physiol.* 493:471-484.

van Vreeswijk C (1996) Partial synchronization in populations of pulse-coupled oscillators. *Phys. Rev. E* 54:5522-5537.

van Vreeswijk C, Abbott LF, Erementrout GB (1994) When inhibition not excitation synchronizes neural firing. *J. Comput. Neurosci.* 1:313-321.

van Vreeswijck C, Sompolinski H (1996) Chaos in neuronal networks with balanced excitatory and inhibitory activity. *Science* 274 : 1724-1726.

Wang XJ, Buzsáki G (1996) Gamma oscillation by synaptic inhibition in a hippocampal interneuron network model. *J. Neurosci.* 15:6402-6413.

Wang XJ, Golomb D, Rinzel J (1995) Emergent spindle oscillations and intermittent burst firing in a thalamic model: specific neuronal mechanisms. *Proc. Natl. Acad. Sci. USA* 92:5577-5581.

Wang XJ, Rinzel J (1993) Spindle rhythmicity in the reticularis thalami nucleus: synchronization among mutually inhibitury neurons. *Neuroscience* 53:899-904.

White EL (1989) Cortical circuits. Synaptic organization of the cerebral cortex. Structure, function and theory. Birkäuser, Boston. pp. 46-82.

White JA, Chow CC, Ritt J, Soto-Treviño C, Kopell N (1997) Synchronization and oscillatory dynamics in heterogeneous, mutually inhibited neurons. *In press*.

Wilson FAW, Scalaide SP, Goldman-Rakic PS (1994) Functional synergism between putative γ-aminobutyrate-containing neurons and pyramidal neurons in prefrontal cortex. *Proc. Natl. Acad. Sci.* 91:4009-4013.

Wilson HR, Cowan JD (1972) Excitatory and inhibitory interactions in localized populations of model neurons. *Biophys. J*. 12:1-24.

Whittington MA, Traub RD, Jeffereys JGR (1995) Synchronized oscillations in interneuron networks driven by metabotropic glutamate receptor activation. *Nature* 373:612-615.

Whittington MA, Traub RD, Faulkner HJ, Stanford IM, Jefferys JGR (1997) Recurrent excitatory postsynaptic potentials induced by synchronized fast cortical oscillations. *Proc. Natl. Acad. Sci. USA* 94 :12198-12203.

Chapter 3 Experimental Methods

An Accurate Measure of the Instantaneous Discharge Probability, with Application to Unitary Joint-Event Analysis

Neural Computation, In press.

ABSTRACT

We present an estimate for the instantaneous discharge probability of a neurone, based on single trial spike train analysis. By detecting points where the neurone abruptly changes its firing rate and treating them specially, the method is able to achieve smooth estimates whilst avoiding the blurring of significant changes. This estimate of instantaneous discharge probability is then applied to the method of Unitary Event Analysis. We show that such analysis as originally conceived is highly sensitive to firing rate non-stationarities and covariations, but that it can be considerably improved if calculations of statistical significance use an instantaneous discharge probability, instead of a firing rate estimate based on averaging across multiple trials.

1. Introduction

Over the last few years, a large number of new techniques have been developed for the analysis of single unit neuronal discharge. The increasing mathematical complexity of these techniques permits maximal information to be extracted about how these signals are being used by the brain. However, most new techniques are developed and tested on the assumption that neurone spikes resemble stationary Poisson processes. This often yields mathematical tractability, but at the expense of grossly oversimplifying the statistics of the target spike trains.

Non-stationarity in cell discharge can occur in a number of ways. Firstly, the firing rate often changes following delivery of a stimulus or performance of a behavioural task by the experimental animal. These changes can be profound (from no firing to >100 Hz) and rapidly occurring. In order to account for such rate modulation, many analysis techniques estimate the firing rate on a single trial from the peri-stimulus time histogram (PSTH; Gerstein & Kiang, 1960; Lemon, 1984), derived by summing together the discharge on a number of repeats of the same trial. The underlying model for the spike train then becomes a Poisson process with instantaneous firing rate on any one trial modulating as the all-trial PSTH (Aertsen, Gerstein, Habib & Palm, 1989; Grün, 1996).

More complex non-stationarities occur when the firing rate modulation is not the same from one trial to the next. Firstly, there may be a jitter in the time of occurrence of a rise in rate relative to the alignment event; this is common in work on awake, behaving animals, where a trial lasting several seconds must be aligned to one point in the performance (Seidemann, Meilijson, Abeles, Bergmann & Vaadia, 1996; Munoz & Wurtz, 1993). Secondly, the overall shape could differ from one trial to the next, depending on uncontrolled external or random events such as attentional shifts. These two forms of non-stationarity may show no co-variation between simultaneously recorded cells. However, since such variation is often not simply noise in the system, but instead reflects genuine variation in the task performance of the animal from trial to trial, it is more likely that the times, the magnitudes or the overall

shape of rate changes will be correlated. The difference between these two situations is of great importance for methods that seek to estimate the expected number of synchronous discharges between two cells; unfortunately, the PSTH can only reflect the mean firing rate profile, and gives no clue to its variability or correlation structure from trial to trial.

Brody (1997,1998a,b) proposed a method of overcoming these problems by fitting the cell discharge on a single trial to a function which had the same shape as the mean PSTH, but was shifted by an adjustable latency and scaled by a multiplicative gain. This estimate of the single trial firing rates permitted a better prediction of the cross-correlation histogram between two units than one derived from the PSTH alone. However, the all-trial PSTH reflects only the mean change in rate, taking no account of the variability of this profile among trials, so that this technique is probably limited in its applicability to experimental data.

In this report, we present a method for estimating the instantaneous discharge probability density of a neurone in a single trial. We then apply it to the method of Unitary Event Analysis pioneered by Grün (1996), and recently applied to data recorded in the motor cortex of awake monkeys (Riehle, Grün, Diesmann & Aertsen, 1997). We show that this method as originally conceived is highly sensitive to the non-stationarities described above, but that it can be considerably improved using single trial firing rate estimates.

2. Measurement of Instantaneous Discharge Probability

We wish first to draw a distinction between instantaneous discharge probability density and the instantaneous firing rate. We view the latter as an output, which may be read by a neurone further downstream. By contrast, we view the discharge probability density as an input function which could be fed into a neuronal model to generate a spike train similar to the one observed. Generation of such a measure requires allowance to be made for the delayed response of the neuronal integrator to changes in its inputs. The discharge probability density should be smooth, and not replicate the variability that is typically seen in interspike

intervals (Softky & Koch, 1992; Shadle & Newsome, 1994). However, in conflict with this, the function should also be able to identify and vary abruptly with sudden firing changes. Finally, since the only data available is the spike train, the method has to start with a measure of the instantaneous firing rate.

Two distinct methods exist in the literature for estimation of the instantaneous firing rate of a spike train. In one, pulses produced at the spike times are low pass filtered (French & Holden, 1971), either using analogue filters (eg Houk, Dessem, Miller & Sybirska, 1987), or by convolution with a smoothing function (often a Gaussian, eg MacPherson & Aldridge, 1979; Richmond, Optican, Podell & Spitzer, 1987). The closer together the spikes, the more summation of the smoothed waveforms which occurs, and hence the larger the output signal. However, this method requires that the cut off of the low pass filter is adjusted to be appropriate for the firing rate under study. If it is too low, a highly smoothed signal is obtained which cannot follow rapid rate changes; if it is too high, periods of zero estimated firing rate are interposed between spikes with long intervals. Adaptive Kernel methods (Silverman 1986 ; Richmond, Optican & Spitzer, 1990) represent an attempt to adjust the amount of smoothing depending on the local density, so that these two extremes are avoided. More sophisticated techniques such as orthogonal series estimates and maximum penalised likelihood estimates (Silverman, 1986) can suffer from the need to tune smoothing parameters to find the optimal representation of the data.

An alternative is to use the reciprocal of the inter-spike interval (ISI) as an estimate of the firing rate during the time spanned by that interval. Such a method is often implicitly employed using 'frequencygram' plots, where a point is plotted at the time of each spike with a height of the reciprocal of the preceding interval (Matthews, 1963; Bessou, Laporte & Pagès, 1968; Awiszus, 1988). It is similar to the use of 'fractional intervals' (eg Schwartz, 1992). This technique has the advantage that it never has periods of zero estimated rate; however, in its raw form the estimate shows great variability. Any subsequent smoothing will necessarily be a trade-off between the need to reducing this variability without removing rapid fluctuations.

A means of avoiding this trade-off would be to detect rapid changes in firing rate and to treat them as a special case. This is essentially the same problem as detection of bursts in a spike train, and a number of techniques have been suggested in the literature for doing this. The first was the CUMSUM technique (Hurst, 1950), which has been applied to both averaged PSTH (Ellaway, 1978) and also to single trial analysis (Butler et al.,1992a,b). The CUMSUM involves subtraction of a control reference level from a series of datum points and adding cumulatively. However, when the goal is the formation of a continuous estimate of discharge probability, it is not clear where the control level should be placed. CUMSUM methods are also very sensitive to small variations during the control period and require excessive parameter tuning (Churchward et al., 1997). An alternative has been proposed by Cocatre-Filgien & Delcomyn (1992), who first identified ISI sub-populations using an ISI histogram, and then tested identified bursts against the mean firing frequency with a chi-square test. This method is well suited to a spike train where firing is at a constant level for most of the time, with occasional high frequency bursts; it is much less suitable for neurones where the firing rate changes continually over a wide range. Other methods in the literature suffer from similar problems – ISIs are always compared with the mean ISI for the whole recording, making the assumption that intervals are Poisson distributed (Legendy and Salcman, 1985; Eggermont et al., 1993).

Our proposed technique is a variation of these methods. The first difference is that we work with ISIs locally. In this way, a change in firing rate is identified relative to the firing of the cell close to the time of interest, rather than by comparison to the global ISI statistics. Three consecutive intervals are used, since a single interval shorter than the preceding one could simply represent the tail of the ISI distribution, even if firing rate were constant. Two consecutive ISIs significantly shorter than the ISI preceding are much less likely without a change in firing rate. The same limit to the smallest detectable burst has been used by Cocatre-Zilgien & Delcomyn (1992). Secondly, we assume that the ISIs follow a gamma density. This allows for an absolute refractory period and for the relative refractory period produced by after-hyperpolarisation, and is a more realistic description of interval statistics than the more commonly used Poisson process (for discussion, see Berry and Meister, 1998; de Ryuter van Steveninck, Lewen, Strong, Koberle & Bialek, 1997). Moreover, by changing the order parameter of the gamma density, it can be adjusted to fit interval statistics from a wide range of experimental data.

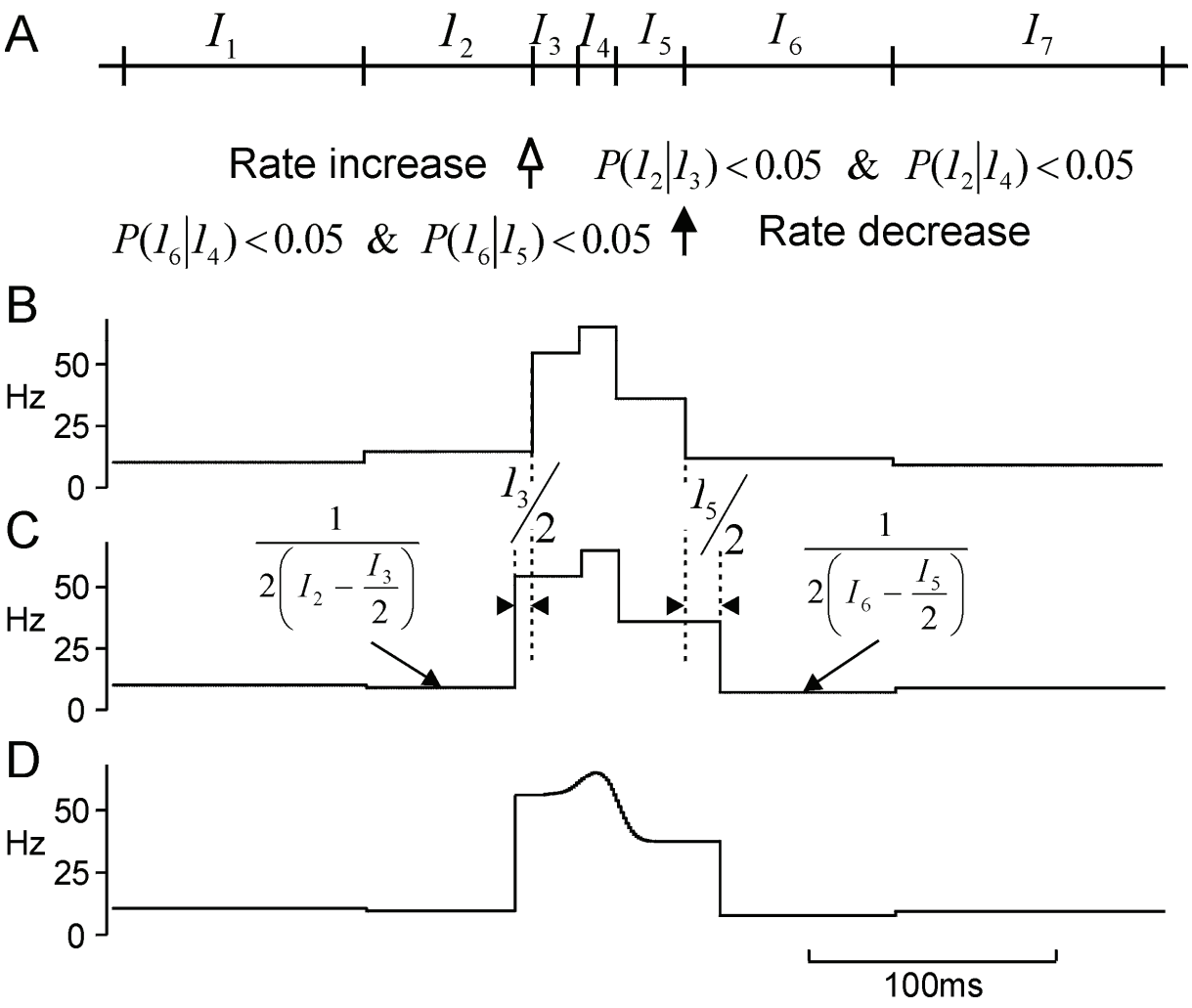

Figure 1. Reconstruction of the instantaneous frequency. (A) The original spike train. (B) The inverse of the interspike intervals (ISIs). Statistical tests detect points of rate increase (empty arrow), or decrease (filled arrow). (C) The high estimated firing rates are extended out half an interval, to the best estimate of the time of the rate change. In order to maintain the overall mean rate, the firing rate before or after these rate change points is reduced (D) The signal is smoothed by convolution with a Gaussian. No smoothing is performed across the rate change points. Full details are given in the text.

The first step is to generate an instantaneous firing rate function F(t), sampled at an appropriately fine temporal resolution, whose value at any point is simply the reciprocal of the ISI which spans it (Fig. 1B). The series of ISIs is then scanned to determine times at which the firing rate abruptly changes. To do this, we make the assumption that, at constant firing rate, ISIs are distributed according to a gamma density. The probability that, if the mean interval is μ, an interval *i* will be larger than some value *I* is then:

$$P(i > I \mid \mu) = \int_{\cdot}^{\infty} \left(\frac{a}{\mu}\right)^{a} \frac{1}{(a-1)!} t^{a-1} e^{-ta/\mu}\, dt$$

(1)

where *a* is the order of the gamma process used to model the intervals. In the remainder of this paper, we use *a*=4, although this can be adjusted to fit the interval statistics for a given cell (*a*=1 would correspond to a Poisson process). As illustrated in Fig. 1A, the *n*'th interval was accepted as the onset of an increase in rate if the following two criteria were both fulfilled:

$$P(i > I_n \mid \mu = I_{n+1}) < 0.05$$
$$P(i > I_{n-1} \mid \mu = I_{n+1}) < 0.05 \quad (2)$$

Likewise, the *n*'th interval was accepted as the onset of a decrease in rate if the following two criteria were both met:

$$P(i > I_n \mid \mu = I_{n-1}) < 0.05$$
$$P(i > I_{n+1} \mid \mu = I_{n-1}) < 0.05 \quad (3)$$

The longest of the three intervals under consideration is always the one tested. As noted above, the requirement that the interval should be significantly bigger than both of the intervals preceding it (for a rate fall) or succeeding it (for a rate rise) ensures that only genuine rate changes are detected, and not anomalous intervals arising from the tail of the ISI distribution.

Changes in rate can thus be detected; the next stage is to determine at what precise time the change occurs. One possibility would obviously be at the time of the first spike contributing to the changed interval. However, this is likely to be biased. A neurone which suddenly receives a higher rate of input will not fire immediately; the moment of firing probability rise is therefore likely to be some time prior to the first spike of the shortened interval. The best solution can be appreciated by the following formalism.

Let the long interval I_n be divided into two parts: one lasting T_{Lo} in which the discharge probability density is F_{Lo}, and another lasting T_{Hi} in which the discharge probability density is F_{Hi}. We have therefore that:

$$T_{Lo} + T_{Hi} = I_n \tag{4}$$

Since one spike in total resulted from the interval I_n, the sum of the firing probability density must be 1 over this time:

$$T_{Lo}F_{Lo} + T_{Hi}F_{Fi} = 1 \tag{5}$$

Finally, in the absence of any more information about the timing of the change in discharge probability, we assume that the change occurs independently from the spike process. Had the firing probability density not changed, the interval would have been $1/F_{Lo}$. We therefore assume that on average, T_{Lo} is half of this value:

$$\begin{aligned} T_{Lo} &= \frac{1}{2F_{Lo}} \\ T_{Lo}F_{Lo} &= 0.5 = T_{Hi}F_{Hi} \end{aligned} \tag{6}$$

F_{Hi} is assumed to be equal to the reciprocal of the short interval I_{Short} either preceding (for a rate fall) or succeeding (for a rate rise) I_n. Hence Eqs 4-6 provide a unique solution which is:

$$\begin{aligned} T_{Hi} &= \frac{1}{2F_{Hi}} = \frac{1}{2} I_{Short} \\ T_{Lo} &= I_n - \frac{1}{2F_{Hi}} = I_n - \frac{1}{2} I_{short} \\ F_{Lo} &= \frac{1}{2T_{Lo}} \end{aligned} \tag{7}$$

The high discharge probability density calculated from the short interval is therefore extended out for half of this interval into the adjoining long interval, as shown in Fig. 1C, for both rate increases and rate decreases. This is compensated for by reducing the discharge probability density in the remainder of the long interval to a value close to half of the original (Fig. 1C). A probability density function of this form is exactly normalised, in the sense that its integral from time zero to a given time, rounded down, gives the number of spikes which have occurred up to that point. This function can therefore be seen as the input to an integrate and fire neurone, which would thereby generate the observed spike train.

The discharge probability density of Fig. 1C still exhibits high variability, due to high variance in intervals even if the underlying rate remains constant (Shadlen & Newsome, 1994; Softky & Koch, 1992). In order partially to remove this unwanted variability, intervals between abrupt firing changes are then smoothed by convolution with a Gaussian kernel (standard deviations : 10 ms, chosen to be in the range of the somatic time constant; Koch, Rapp, & Segev, 1996). This smoothing is not carried out across boundaries of rate changes as defined above, producing a measure which varies smoothly between rate change points but abruptly at them. This is illustrated in Fig. 1D. It is the explicit identification and localisation of abrupt firing probability changes which confer to this measure the most tangible advantage over other techniques. Without such a step, there is necessarily a trade-off between over-smoothing rapid changes, and high variability, which cannot be satisfactorily resolved.

The method described above produces an estimate of the discharge probability density function which can be computed without averaging across trials. The next section investigates an application of this method to the assessment of significance of unitary joint-events.

3. Application to Unitary Joint Event Analysis

The aim of the unitary joint-event method is to detect discharges of two neurones which are synchronous within an allowed jitter, and occur more often than expected by chance. The technique, similar to that proposed by Grün (1996; 'UEMWA' method) but with minor changes to avoid unnecessary binning, is reviewed in Fig. 2A-G. From the repeated trials (Fig. 2A&C), PSTHs for the two cells are built up, and these are smoothed with a moving window (here chosen to be 101 ms wide, Fig. 2B&D). Spikes from the two cells occurring at times t_1 and t_2 are designated coincident events (CEs) if:

$$|t_1 - t_2| < \Delta \tag{10}$$

where Δ was in this study taken as 5 ms. We conventionally place the occurrence time of the CE halfway between the two coincident spikes, at $(t_1+t_2)/2$. The number of CEs is counted in

successive bins, and the count is plotted as dots in Fig. 2E. The number of these raw CEs rises as the cell discharge rates increase. The expected number of coincidences is approximately:

$$E(CEs\ in\ bin\ T) = 2w\Delta\ N\overline{F_1}(T)\overline{F_2}(T) \tag{11}$$

where N is the number of trials, w is the bin width used to count the CEs (here 1 ms), and $\overline{F_1}, \overline{F_2}$ represent the firing rates of the cells estimated from the smoothed PSTHs. Computation of the expected number of CEs is made more complex than Eq. 11 because the bin width w is in general larger than the precision to which spike times are recorded. If a CE falls into the bin centred on time T, then:

$$\left|\frac{(t_1 - t_2)}{2} - T\right| < \frac{w}{2} \tag{12}$$

Suppose as an example that t_1 is in the bin centred on T-w, and t_2 in the bin centred on T+w. For some possible combinations of t_1 and t_2, Eq. 12 could still be left unfulfilled (eg $t_1 = T-0.7w$ and $t_2 = T+1.3w$). This is shown schematically by Fig.3A: CEs generated by spikes each confined to one bin may fall into two adjacent bins.

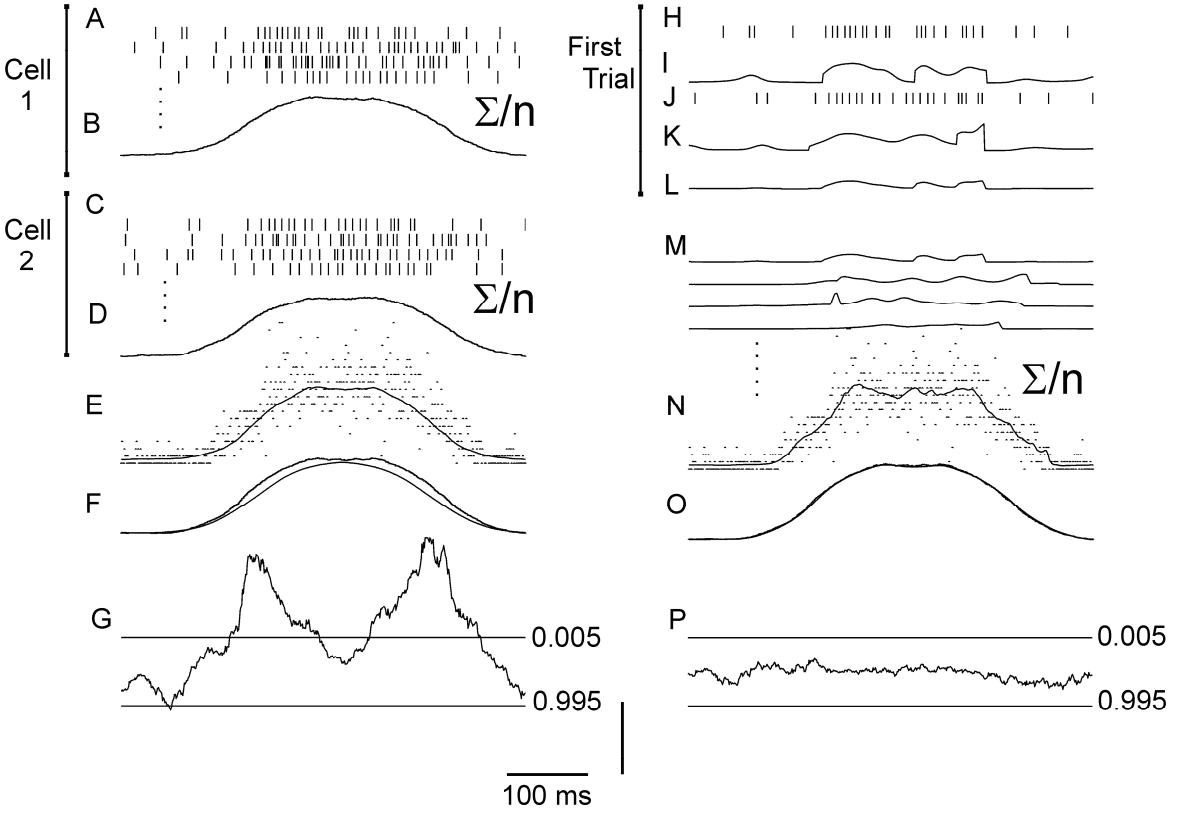

Figure 2. Comparison of significance calculation for coincident events using the method of Grün (1996) and the novel method proposed here. One hundred trials, each lasting 500 ms, were generated with a central 250 ms burst of activity (firing rate rose from 25 Hz to 75-125 Hz) which began with a temporal jitter of 100 ms.
(A-G) Methods based on the peri-stimulus time histograms (PSTH). For each cell (A&C), the mean firing rates are computed by compiling PSTHs across trials; these are smoothed by a 101 ms moving window (B&D). (E) The expected coincidence rate (solid line) is calculated by multiplying the two mean firing rates, with a correction for the size of the window within which coincidences are detected. Dots show the actual coincidences detected in this simulation. (F) Actual and expected coincidence rates are smoothed with a 101 ms moving window. (G) The probability P to find as many or more CEs as observed is calculated from the expected rate assuming a Poisson distribution. P is displayed as $\log_{10}((1-P)/P)$, facilitating visualisation of high and low values of P.
(H-P) Method based on the single trial firing rate estimate. For each cell (rasters for the first trial shown in H&J), the instantaneous frequency is reconstructed on a trial-by-trial basis (I&K ; filter SD between rate change points = 10 ms). Then the rate of expected CEs is calculated (L: first trial; M: four other trials). A bin per bin summation of the single trial CE expectancy curves produces the global CE expectancy (N, solid line), plotted with the number of CEs detected (dots). (O) Both rates are then filtered using a 101 ms moving window. (P) Significance of departures from the expected rate are assessed as in (G), and plotted in the same way
Vertical bar : (B&D) 100 $sp.s^{-1}$; (E,F,N,O) 100 $CE.s^{-1}.trial^{-1}$; (I,K) 500 $sp.s^{-1}$; (L,M) 1667 $CEs.s^{-1}$; (G,P) 5.

Extending these considerations to all possible combinations of bin occupancy for t_1 and t_2 which could fulfil Eqs 10 and 12 leads us to an exact solution for the case of Δ=5 ms shown in Fig.3B and which is described numerically below:

$$E(CEs\ in\ T) = w^2 N\left(\sum_{j=-3}^{+3} \left(\overline{F_1}(T + jw) . \sum_{k=-3}^{+3} M_{j,k}\, \overline{F_2}(T + kw) \right) \right) \tag{13}$$

$$M_{j=-3..3,k=-3..3} = \begin{bmatrix} 0 & 0 & 0 & 0 & 0 & 1/4 & 0 \\ 0 & 0 & 0 & 0 & 2/4 & 4/4 & 1/4 \\ 0 & 0 & 0 & 2/4 & 4/4 & 2/4 & 0 \\ 0 & 0 & 2/4 & 4/4 & 2/4 & 0 & 0 \\ 0 & 2/4 & 4/4 & 2/4 & 0 & 0 & 0 \\ 1/4 & 4/4 & 2/4 & 0 & 0 & 0 & 0 \\ 0 & 1/4 & 0 & 0 & 0 & 0 & 0 \end{bmatrix} \tag{14}$$

Figure 2E plots the expected number of coincidences *E* as a solid line. The number of observed coincidences is then smoothed with a 101 ms moving window, yielding the plot in Fig. 2F. Finally, the probability that the number of coincidences *c* will be at least as many as the number observed, *C*, given that *E* are expected, is calculated assuming that they follow a Poisson distribution:

$$P(c \geq C) = 1 - \sum_{i=0}^{i=C-1} \frac{e^{-E} E^i}{i!} \tag{15}$$

This probability is plotted in Fig. 2G as $log_{10}\ ((1\text{-}P)/P)$, thereby permitting bins with a significant excess, or a significant deficit of CEs to stand out. The horizontal lines mark the 99% confidence limits (two tailed).

The modification to this technique which we now propose is illustrated in Fig. 2H-P. For each trial (Fig. 2H&J), the instantaneous discharge probability density is calculated (Fig. 2I&K). This is used to calculate the expected number of coincidences in a single bin, in one trial; summing over all trials yields the approximate number of coincidences in a given bin:

$$E(CEs\ in\ T) = 2w\Delta \sum_{n=1}^{N} F_1^n(T) . F_2^n(T) \tag{16}$$

where F_1^n, F_2^n represent the instantaneous discharge probability density during trial *n*. Once again, however, the situation is made more complex by the binning used. By similar considerations to those above, we find the exact formula for when Δ=5w to be:

$$E(CEs\ in\ T) = w^2 . \sum_{n=1}^{N} \left(\sum_{j=-3}^{+3} \left(\overline{F_1^n}(T + jw) . \sum_{k=-3}^{+3} M_{j,k}\, \overline{F_2^n}(T + kw) \right) \right) \quad (17)$$

where $M_{j,k}$ is as defined in Eq. 14. This measure is plotted as a solid line in Fig. 2N, overlain with the observed number of coincidences (dots). The moving window smoothed traces are shown in Fig. 2O, and the significance plot, calculated according to Eq. 15, is illustrated in Fig. 2P.

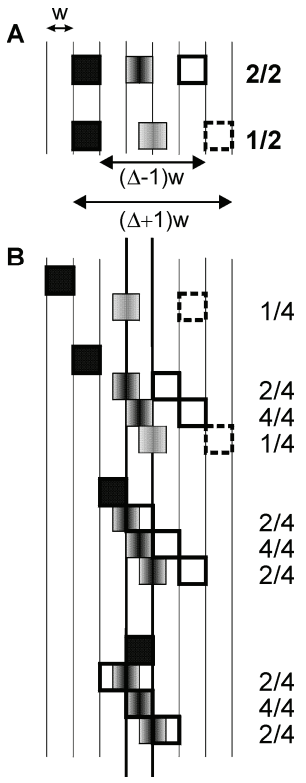

Figure 3. Schematic illustration of CE binning. Calculation of the CEs before the binning step ensures their exact determination, but renders complex the calculation of their expectancy. Black squares represent a bin containing spikes from one unit, white squares represent a bin containing spikes from the other. The grey squares code on a grey scale the density of CEs resulting from spikes in the black and white squares. White bins with dotted outlines indicate a situation where not all of the possible combinations of spikes will lie within the coincidence detection interval Δ. (A) The CE distribution resulting from the combination of spikes in two bins has a triangular shape. If bins are separated by (Δ-1)w, half the spike combinations do not verify the coincidence criterion of Eq. 10 and the number of CEs is reduced by two. (B) The problem is solved extensively for Δ=5 w. Figures on the right represent the fraction of spikes from these bins which would form CEs within the central bin of interest (shown with thick vertical lines).The values given are used to construct the matrix $M_{j,k}$ in Eq 14.

The crucial difference between the two methods lies in the order in which averaging across trials is performed. In the original method proposed by Grün (1996), firing rate is first averaged across trials, and then the expected number of coincidences is calculated as a product of firing rates. In the current method, the expectation product is calculated on a single trial, and this is then summed. These will produce different results if the firing rate shows any covariation from trial to trial about the mean.

In agreement with this, Table 1 presents data which shows that both methods are indeed similar if data are stationary. Two spike trains were generated as independent Gamma processes, order 4, with constant firing rate. Simulations were run for 1500 ms, with 100 trials per simulation; 400 simulations were run for each set of conditions. The number of simulations with significant CEs in the central 500 ms was counted using both of the methods described above, for two different significance criterion levels α. At the more relaxed criterion of α=0.025, a large number of false positives occur with each method, although the situation is slightly better for the instantaneous discharge probability technique. With the more rigorous criterion of α=0.005, the two methods give comparable numbers of false positives.

Frequency (Hz)	IDPM α=0.005	IDPM α=0.025	PSTHM α=0.005	PSTHM α=0.025	Diff. α=0.005	Diff. α=0.025
10	6	26.3	6.5	26	-0.5	0.3
30	2	15.8	3.3	20	-1.3*	-4.3*
50	0.5	8.3	0.5	12.5	0	-4.3*
70	0	2.3	0.3	4	-0.3	-1.8*

Table 1. Evaluation of the numbers of false positive CEs occurring in randomly simulated independent spike trains. 100 trials, 1 500 ms long, were simulated at a constant firing frequency for the two cells. CEs were counted within the central 500 ms of the simulation. The table shows the percentage of simulations with significant CEs in a sample of 400 simulations with the same firing frequency. Two values for the criterion level α were used. Results for the methods using instantaneous discharge probability (IDPM) and normalisation by the PSTH (PSTHM) are presented. The PSTH normalisation method gives more false positives, although false positive rates are high for both methods with α=0.025. * denotes a significant difference between the two methods (binomial test, $P<0.05$).

Figure 4 illustrates the performance of the two algorithms on simulated data, which have a covariation in the timing of the firing rate modulation. The spike trains were independent, apart from the rate covariation, so that no significant CEs should be detected. For a particular trial, the underlying firing rate profile of the two cells was the same. Figure 4A shows how the underlying firing rate changed with time; the onset of the two periods of increased firing rate was uniformly distributed over the times shown by the black bars; the timing of the two bursts were independent. One hundred such trials were simulated.

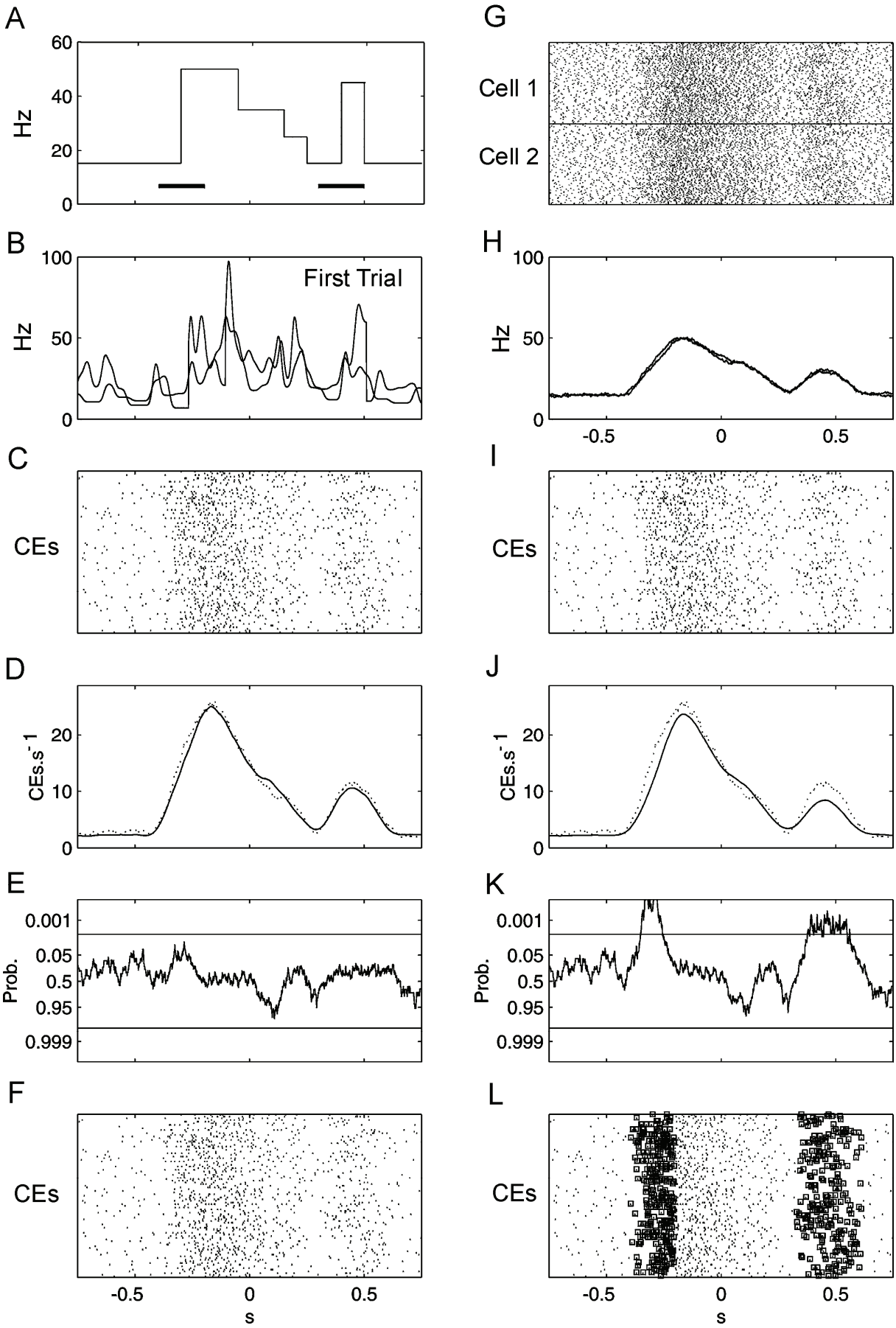

Figure 4. Performance of the two methods on spike trains with firing rate changes which covary in their timing.

One hundred trials were generated following the sequence of firing rate changes shown in (A). The black bars indicate the time range over which the rate changes began (uniform probability distribution). The first column shows the results obtained with the single trial expectancy calculation, and the second column with the method based on the mean firing rate. (G) Rasters of activity over the 100 trials for both cells. (B) Reconstructed instantaneous frequency for both cells during the first trial (filter SD between rate change points : 10 ms) and (H) mean firing rates assessed over all trials. (C&I) CE rasters. (D&J) CE expectancy (solid) and CE observed rate (dots) smoothed with a 101 ms moving window. (E&K) Probability plot (same display as Fig. 3G,P). (F&L) CE rasters. The CEs in windows which exceed the 0.5% confidence limits are marked by a square. A large number of false positives occur with the mean firing rate method.

Figure 4G shows rasters of the unit activities simulated according to the firing rate profile illustrated in Fig. 4A. The estimated instantaneous discharge probability density of the first trial (Fig. 4B) can be compared with the firing rate derived by averaging across all trials in Fig. 4H. Spikes which were coincident within 5 ms are shown in Fig. 4C&I. The number of CEs, counted in a 101 ms wide moving window, is plotted as dots in Fig. 4D&J. Overlain as a solid line is the expected number of coincidences, calculated according to the instantaneous discharge probability method (Fig. 4D), or the PSTH method (Fig. 4J). Whilst the two plots closely follow one another in Fig. 4D, there are discrepancies in Fig. 4J associated with the changes in firing rate. These differences reach significance on the calculation of Eq. 5, such that the significance plot of Fig. 4K goes outside the 0.5% confidence intervals. In Fig. 4F&L, following the display convention established by Grün (1996), we display rasters of the CEs in which all events falling within a window which tested as significant are highlighted by a square.

It is clear that use of a trial averaged firing rate estimate can lead to errors in significance testing of unitary events when the neurone firing rates show a temporal jitter relative to the analysis alignment point, and that jitter is not independent between the two units. Our method based on single trial discharge probability estimates is capable of alleviating this problem. The improvement primarily results from the changed order of the operators (multiply, then sum, *versus* sum, then multiply). It is likely that almost as much of an improvement would be obtained with simpler estimates of the instantaneous discharge probability, such as the ISI reciprocal (smoothed or not) or a low-pass filtered spike train. Our method however is capable of following both fast discharge probability changes (via insertion of breakpoints), and slow ones (via the smoothing of the ISI reciprocal); it is therefore to be preferred.

Figure 5 illustrates the results of analysis on spike trains simulated to display variation in firing rate from trial to trial. The underlying rates of the two neurones on a given trial were the same, allowing the effect of rate covariation to be examined. The simulated rate profiles are shown schematically in Fig. 5A. The remainder of Fig. 5 follows the same display conventions as Fig. 4. It can be seen that the trial averaged firing rates (smoothed PSTH) in Fig. 5H show no modulation: this is expected from Fig. 5A, since the *mean* firing rates do not change. However, the increase in firing rate variability brings about a rise in the number of CEs, shown by the dots in Fig. 5D&J. This cannot be predicted by the trial averaged measure, which therefore assigns a high significance level to these extra events. By contrast, the expected and observed curves show good agreement using the instantaneous discharge probability method of Fig. 5D, such that no CEs reach significance.

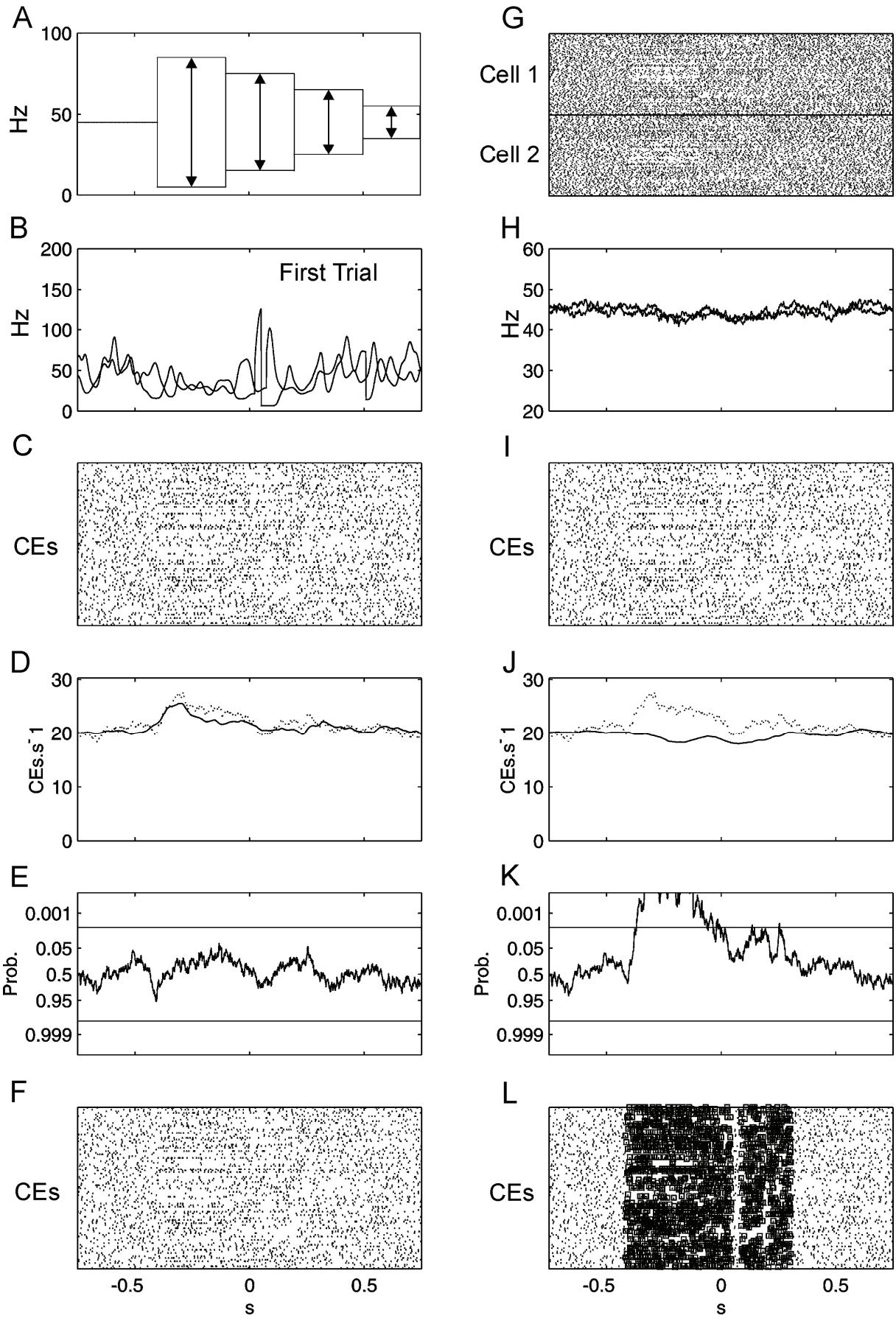

Figure 5. Performance of the two methods on spike trains which show covariant firing rates. (A) Schematic

indicating the simulated firing rate profiles. After an initial period of constant rate, the rate changed to a value chosen at random from the range shown. Three further rate changes occurred. The organisation of the panels is the same as in Fig. 4, with the methods based on the single trial expectancy in the left column, and the mean firing rate approximation on the right. Since the mean firing rate does not change in these simulations, the PSTH based method cannot predict the increased number of CEs expected, and a large number of false positives result.

Figure 6 examines the detection of genuine excess CEs by the new algorithm. Figure 6A-F follow the same format as Fig. 4&5. One spike train was simulated as previously by a simple Gamma process (order 4). Some of these spikes were selected at random to become 'imposed CEs'. The second spike train was also initially simulated as a Gamma process; the spike closest to each imposed CE was then moved to be at the same time as this event. This produced an increased number of CEs above the chance level, but maintained the firing rate of the two units. In Figs. 6E&F, the CEs injected between -0.4 and 0.25 s were accurately detected. During this period, the firing rate was constant at 30 Hz and there were 38% more CEs than expected by chance (893 CEs vs. 643 in a control simulation; 2.5 extra CEs per trial spread over 650 ms).

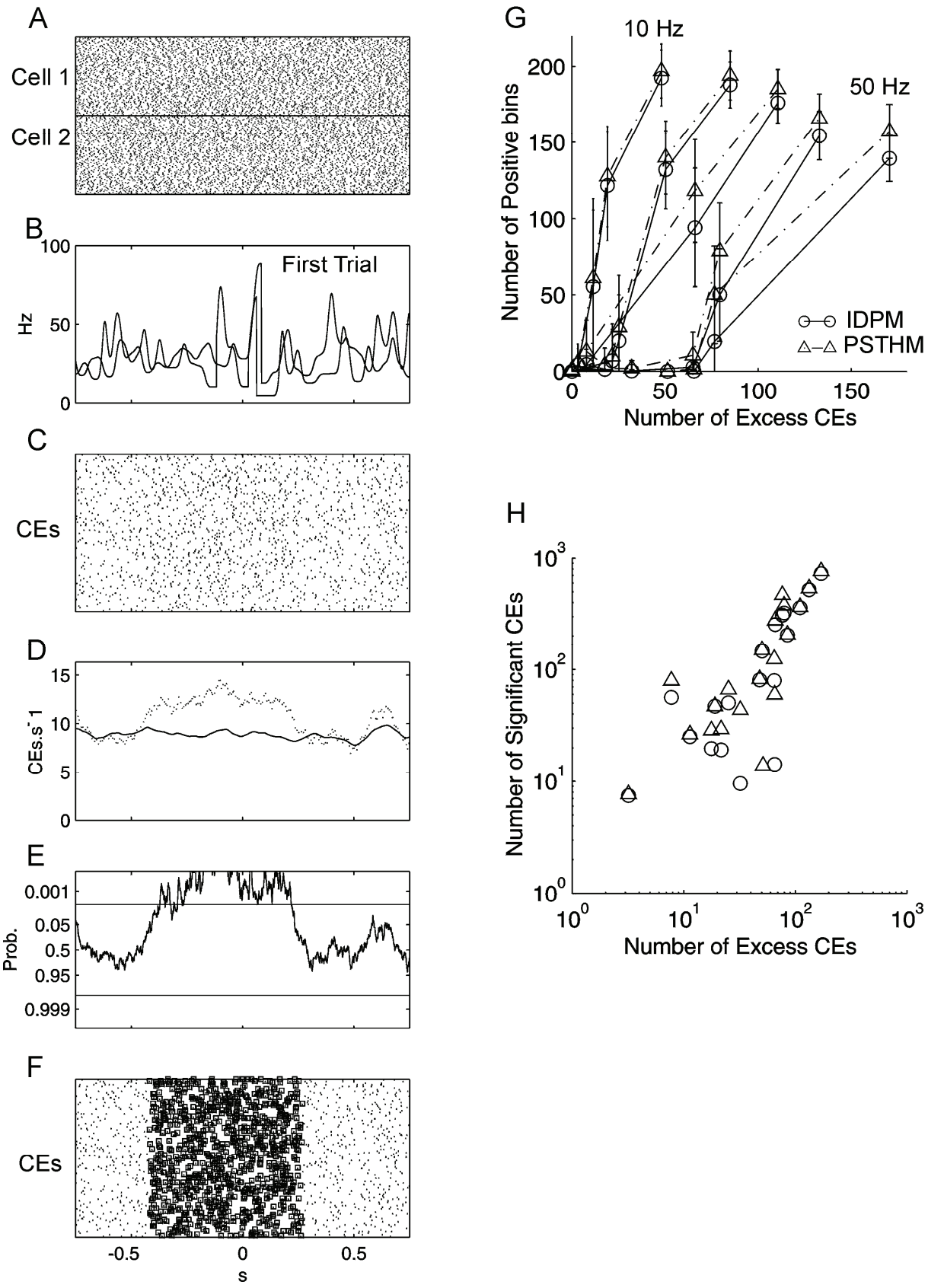

Figure 6. Detection of injected CEs by the method based on the single trial CE expectation, and comparison of the sensitivity of the two methods. One hundred trials were simulated with a constant firing rate of 30 Hz; between -0.4 and 0.25s, 371 coincident events were imposed on the spike train of the second cell (20% of the spikes of cell 1; this yielded 893 CEs in total, 250 more than the 643 CEs expected from a control simulation). (A-F) Detection of imposed CEs (same display conventions as Figs 4, 5, left column). (G) Data from

simulations of 100 trials at constant firing rate, which investigated the sensitivity of the two methods. Trials lasted 500 ms; CEs were imposed during the central 150 ms. The number of windows which exceeded significance is plotted versus the number of excess CEs. Different curves show results for different simulated background firing rates. Circles represent the method based on single trial expectancy (instantaneous discharge probability method, IDPM), and triangles the method based on the mean firing rates (PSTHM). Bars indicate one standard deviation in a sample of 20 simulations. The methods show similar sensitivity; the decrease seen for high firing rates is due to the high level of chance coincidences expected. (H) Number of CEs within windows which tested as significant, versus the number of excess CEs, for the same simulations as shown in (G). The correlation is good, indicating that many of the injected CEs are retrieved. Filter SD between rate change points: 10 ms.

The right hand side of Fig. 6 compares both methods for CE detection in stationary spike trains at different firing rates. This was investigated by simulations similar to the one illustrated in Fig. 6A, except that the firing rate and number of imposed CEs were varied systematically. Figure 6G plots the number of bins which tested as having a significant excess of CEs versus the number of excess CEs (calculated as the difference between the mean number of CEs observed and the mean number of CEs during control simulation without imposed CEs) . The curves for the two methods lie close together at all tested firing rates, indicating a similar sensitivity for each method. The decline of apparent sensitivity at high firing rates is due to the high number of CEs which would be expected by chance at these rates; larger numbers of excess CEs are therefore necessary before significance is reached

Figure 6H plots the number of detected CEs (the number of CEs in the significant bins) versus the number of excess CEs; for both methods there is a good correlation. Points lie above the identity line because significance is attributed to all the CEs in the 101 ms window; there is no means of dissociating the injected CEs from those which occurred by chance. The similar performance when conditions of firing rate stationarity are fulfilled indicates that the different results in more complex situations cannot be simply explained by a difference in overall sensitivity between the two methods.

4. Discussion

4.1 Instantaneous Discharge Probability Density Calculation

The instantaneous discharge probability density function described above has a number of attractive features, which make it a useful measure for single trial analysis. It is able to cope well with a large range of firing rates, unlike methods which smooth pulses derived from the spike train (French & Holden, 1971; Houk, Dessem, Miller & Sybirska, 1987). It is locally smooth, except at a few points of rapid change, and does not show great fluctuations simply due to the variable nature of ISIs. However, by explicitly detecting points of rate change, blurring of rapid changes is avoided. The probabilistic framework for the detection of rate changes means that it is an entirely objective method in application. Finally, the use of a general Gamma distribution as the underlying spike train model permits accurate representation of neurones with many different firing characteristics, simply by changing the order parameter *a*.

4.2 Unitary Event Significance Testing

The results presented above demonstrate that the current methods used for assessing the significance of unitary events can lead to errors when there is variability in the firing rate of the neurones from trial to trial. Such variation in responses from one trial to the next is less likely in sensory systems where the response to a stimulus is measured under anaesthesia, since relatively few synapses are interposed between peripheral receptor and recorded neurones. By contrast, in awake animals subject to attentional fluctuations, trial-to-trial variation is the norm. Animals can never be trained to produce precisely reproducible behaviour, and even if the overt output appears similar, it is likely that there are many different redundant patterns of neural activity which will lead to the same goal. Lee, Port, Kruse & Georgopoulos (1998) showed that single trial firing rates often show correlation (‘noise correlation’ in their terminology), which is strongest for cells close together. The situations presented in Figs 4&5 are therefore not artificially contrived to test current methods to their limits, but rather represent realistic possibilities which will be commonly encountered in experimental recordings. Other methods which rely on trial averaged measures, such as the joint peri-stimulus time histogram (JPSTH) of Aertsen, Gerstein, Habib & Palm (1989), or which assume inter-trial constancy, such as the widely used shuffle predictor (Perkel, Gerstein

& Moore, 1967; Engel, Konig, Gray & Singer, 1990; Lee, Port, Kruse & Georgopoulos, 1998) are also vulnerable to error in such situations. When there is little variation in firing rate from trial to trial, the proposed method based on instantaneous discharge probability has similar sensitivity to use of the PSTH (Table 1; Fig. 6). The novel method is therefore to be preferred in analysis of a wide range of empirical data.

Any technique for significance testing of CEs will make assumptions (the null hypothesis); whenever a significant excess of CEs is found, it indicates a region of the data where these assumptions do not hold. Normalisation using the PSTH makes the assumption that each trial is a realisation of a random process whose discharge probability changes as the PSTH. This will detect as significant all correlation between the two spike trains, both over the short-term, and also longer time course covariation of the firing rates about the trial-averaged level. Our method assumes that the neurones fire at random in response to an input which either changes smoothly over time or makes abrupt jumps in magnitude. CEs which are assigned significance using this approach result from transient input fluctuations which are correlated between the two neurones, and occur over a time scale briefer than that implied by the assumed smooth changes in input. We consider that this is appropriate, since we are interested in short-term synchronisation which may reflect processes of temporal coding, rather than longer-term co-modulation of firing rate. Artefactual CEs could be produced, however, if other assumptions of the method are violated. For example, consider the situation where the neurone is more regular in its response than assumed in the algorithm used to position breakpoints (eg the cell fires as a gamma process of order 4, but we test it against a Poisson process). In this case, the algorithm will fail to detect most of the step changes in input undergone by the cell; if these input changes covary between the two neurones investigated, an artefactual excess of CEs will be detected. It is therefore important to adjust the assumed order of the gamma distribution to agree with the observed inter-spike interval distribution in experimental data.

There is one interesting circumstance in which our method will fail to assign significant CEs; it is debatable whether this is desirable or not. If a neurone fires brief bursts of only a few spikes, breakpoints will be set to delimit the bursts. The instantaneous discharge probability will therefore show a sharp increase closely surrounding the burst. If two neurones burst simultaneously, the expected CE count will rise sharply during the burst, such that any CEs

which do occur are unlikely to reach significance. Whether such CEs should be treated as significant is an open question. Some other instantaneous discharge probability estimates could be proposed which would smooth across the burst limits; they would result in a measure of burst coincidence between the two trains, rather than a measure of spike coincidence inside synchronous bursts. Alternative measures more suited to the data, such as the correlation between neurones of burst onset latency measured on single trials, would probably be simpler to interpret.

The one report to date which has applied unitary joint-event analysis to experimental data demonstrated that significant CEs were seen both in association with rate changes, and during periods of constant firing rate (Riehle, Grün, Diesmann & Aertsen, 1997). No data were presented on the variability of firing rate around rate changes, but it is likely that some of these CEs would not be significant using our improved technique. In the instances where significant CEs occurred without a modulation in firing rate, it is possible that there was nevertheless a change in the variability of discharge, as simulated in Fig. 5. This could also lead to erroneous acceptance of chance CEs as significant.

The unitary joint-event method has received considerable interest, since it appears to allow the detection of synchronous firing on single trials (Fetz, 1997). However, as made clear by section 3, determination of the significance of CEs requires averaging across trials; this report has been concerned primarily with the best way in which to do this. Formally, therefore, the unitary joint-event method is similar to time-resolved cross-correlation methods, such as the JPSTH (Aertsen, Gerstein, Habib & Palm, 1989), except that it concentrates only on the central portion of the cross-correlation histogram, and then identifies the moment and the trials where synchronous firings occurred which contributed to significant cross-correlation peaks. Whether this trial identification is useful depends on our underlying model for how synchrony occurs and is used in information processing in the brain. If we postulate that synchrony *between the two recorded neurones* is itself an important event, then knowing the trials on which it occurs is of obvious value to investigate the relationship between the CEs and, for example, task precision or reaction time. However, we may alternatively assume that the brain is composed of many small assemblies of neurones, and that information is carried by the synchronous firing of a random subset of cells in one assembly (e.g. the synfire chain

hypothesis of Abeles, 1991; Pauluis, Baker & Olivier, 1998). This seems likely, since at any moment some cells of a given assembly may be refractory or otherwise non-excitable due to their recent participation in other assemblies. If this is the case, trials on which the two cells whose discharge is monitored fire synchronously are those trials where not only this assembly was active, but also where both cells were (by chance) able to participate in it. Knowing which trials contained the synchronous events is, on this model, less useful than knowing where, within the task, there was on average an excess of CEs.

In conclusion, we have shown that modification of unitary event analysis to use an instantaneous discharge probability density measure can compensate accurately for changes in the occurrence rate of CEs produced by firing rate covariation. It is anticipated that this technique, or others based on the instantaneous discharge probability density, will find wide applicability in the analysis of synchronisation amongst neural populations recorded from awake behaving animals.

Acknowledgements

We thank Sonia Grün for helpful discussions. This work was supported by a British Council –CGRI travel grant. S.N.B. is supported by the UK MRC and Christ's College, Cambridge.

REFERENCES

Abeles, M. (1991). *Corticonics.* Cambridge: Cambridge University Press.

Aertsen, A.M.H.J., Gerstein, G.L., Habib, M.K., & Palm, G. (1989). Dynamics of neuronal firing correlation: modulation of "effective connectivity". *J Neurophysiol.*, *61*, 900-917.

Awiszus, F. (1988). Continuous functions determined by spike trains of a neuron subject to stimulation. *Biol. Cybern., 58*, 321-327

Berry, M.J., & Meister, M. (1998). Refractoriness and neural precision. *J. Neurosci., 18*, 2200-2211.

Bessou, P., Laporte, Y., & Pagès, B. (1968). A method of analysing the response of spindle primary endings to fusimotor stimulation. *J. Physiol.*, *196*, 37-45.

Brody C.D. (1997) Latency, excitability, and spike timing correlations. *Soc.Neurosci. Abstr. 23,*14.

Brody C.D. (1998a) Disambiguating different covariation types. *Neural Comput. (submitted).*

Brody C.D. (1998b) Latency, excitability, and spike timing correlations. *Neural Comput. (submitted).*

Butler, E.G., Horne M.K., Hawkins N.J. (1992a) The activity of monkey thalamic and motor cortical neurones in a skilled, ballistic movement. *J. Physiol. ,442,* 25-48.

Butler, E.G., Horne M.K., Rawson J.A. (1992b) Sensory characteristics of monkey thalamic and motor cortex neurones. *J. Physiol. 442,* 1-24.

Churchward P.R., Butler E.G., Finkelstein D.I., Aumann T.D., Sudbury A., Horne M.K. (1997) A comparison of methods used to detect changes in neuronal discharge patterns. *J. Neurosci. Meth. 76,* 203-210.

Cocatre-Filgien J.H., Delcomyn F. (1992) Identification of bursts in spike trains. *J. Neurosci. Meth. 41,*19-30.

de Ruyter van Steveninck, R.R., Lewen, G.D., Strong, S.P., Koberle, R., & Bialek, W. (1997). Reproducibility and variability in neural spike trains. *Science, 275*, 1805-1808.

Eggermont J.J., Smith G.M., Bowman D. (1993) Spontaneous firing in cat primary auditory cortex: Age and depth dependence and its effect on neural interaction measures. *J. Neurophysiol. 69*, 1292-1313.

Ellaway P.H. (1978) Cumulative sum technique and its application to the analysis of peristimulus time histograms. *Electroenceph. Clin. Neurophys.45,* 302-304.

Engel, A.K., Konig, P., Gray, C.M., & Singer, W. (1990). Stimulus-dependent neuronal oscillations in cat visual-cortex - intercolumnar interaction as determined by cross-correlation analysis. *Europ. J. Neurosci., 2*, 588-606.

Fetz, E.E. (1997). Temporal coding in neural populations? *Science, 278*, 1901-1902.

French, A.S., Holden, A.V. (1971). Alias-free sampling of neuronal spike trains. *Kybernetik*, *8*, 165-171.

Gerstein, G.L., & Kiang, N.Y.S. (1960). An approach to the quantitative analysis of electrophysiological data from single neurons. *Biophys. J.*, *1*, 15-28.

Grun, S. (1996). *Unitary Joint-Events in Multiple-Neuron Spiking Activity.* Thun, Frankfurt am Main: Harri Deutsch.

Houk, J.C., Dessem, D.A., Miller, L.E., & Sybirska, E.H. (1987). Correlation and spectral analysis of relations between single unit discharge and muscle activities. *J. Neurosci. Methods*, *21*, 201-224.

Koch, C., Rapp, M., & Segev, I. (1996). A brief history of time (constants). *Cereb. Cortex* 6:93-101.

Lamarre, Y., Spidalieri, G., & Lund, J.P. (1981). Patterns of muscular and motor cortical activity during a simple arm movement in the monkey. *Can. J. Physiol.. Pharmacol., 59*, 748-756.

Lee, D., Port, N.L., Kruse, W., & Georgopoulos, A.P. (1998). Variability and correlated noise in the discharge of neurons in motor and parietal areas of the primate cortex. *J. Neurosci.*, *18*, 1161-1170.

Legéndy C.R., Salcman M. (1985) Bursts and recurrences of bursts in the spike trains of spontaneously active striate cortex neurons. *J. Neurophysiol. 53,* 926-939.

Lemon, R.N. (1984). *Methods for neuronal recording in conscious animals. IBRO Handbook series: Methods in Neurosciences Vol.4*. London: Wiley.

MacPherson, J.M., & Aldridge, J.W.A. (1979). A quantitative method of computer analysis of spike train data collected from behaving animals. *Brain Res., 175*, 183-187.

Matthews, P.B.C. (1963). Apparatus for studying the responses of muscle spindles to stretching. *J. Physiol.*, *169*, 58-60P.

Munoz, D.P., Wurtz, R.H. (1993). Fixation cells in monkey superior colliculus. I. Characteristics of cell discharge. *J. Neurophysiol.* 70:559-575.

Pauluis, Q., Baker, S.N., & Olivier, E. (1999). Emergent oscillations in a realistic network: the role of inhibition and the effect of spatiotemporal distribution of the input. *J. Comput. Neurosci.,* 6:27-48.

Perkel, D.H., Gerstein, G.L., & Moore, G.P. (1967). Neuronal spike trains and stochastic point processes. II. Simultaneous spike trains. *Biophys. J.*, *7*, 419-440.

Richmond, B.J., Optican, L.M., Podell, M., & Spitzer, H. (1987). Temporal encoding of two-dimensional patterns by single units in primate inferior temporal cortex. I. Response characteristics. *J. Neurophysiol.. 57*, 132-146.

Richmond, B.J., Optican, L.M., & Spitzer, H. (1990). Temporal encoding of two-dimensional patterns by single units in primate primary visual cortex. I. Stimulus-response relations. *J. Neurophysiol. 64*, 351-369.

Riehle, A., Grün, S., Diesmann, M., & Aertsen, A. (1997). Spike synchronization and rate modulation differentially involved in motor cortical function. *Science*, *278*, 1950-1953.

Seidemann, E., Meilijson, I., Abeles, M., Bergman, H., & Vaadia, E. (1996). Simultaneously recorded single units in the frontal cortex go through sequences of discrete and stable states in monkeys performing a delayed localization task. *J. Neurosci. 16*, 752-768

Schwartz, A.B. (1992). Motor cortical activity during drawing movements: single-unit activity during sinusoid tracing. *J. Neurophysiol.*, *68*, 528-541.

Shadlen, M.N., & Newsome, W.T. (1994). Noise, neural codes and cortical organization. *Curr Opin. Neurobiol.*, *4*, 569-579.

Silverman, B.W. (1986). *Density estimation for statistics and data analysis*. London: Chapman & Hall.

Softky, W.R., & Koch, C. (1992). Cortical cells should fire regularly, but do not. *Neural Comput.*, *4*, 643-646.

Chapter 4 Recordings

Temporal Coding in the Superior Colliculus of the Awake Cat during Moving Stimulus Presentation

To be submitted in Journal of Neuroscience

ABSTRACT

In response to a visual stimulus, neighboring cells in the superior colliculus are shown to synchronize their discharge with a few-millisecond precision. We propose a new method to assess significance of coincident spikes, which permits analysis of non-stationary data and direct quantification of the shift predictors. Two coincident spikes were termed a coincident event (CE) when they were part of the cross-correlation central peak. CEs are shown (1) to cluster in 8-14ms packets separated by a variable delay (10-70 ms), (2) to be sometimes oscillatory at 65 Hz, and (3) to be time locked to the stimulus presentation, whereas usual cross-correlation shift predictors were flat. We show that most of these findings could simply be related to the presence of bursts in the spike trains and not to synchronous discharges.

These data suggests that in other structures and in the absence of bursting cells, temporal coding could simply be demonstrated by the fact that CEs could code information locked to the stimulus presentation more reliably than any single spike train. But when cells are bursting, great care must be provided for the analysis of the CE trains.

Key words:

superior colliculus; correlation analysis; coincident event; fast oscillations; burst; motion-processing; stimulus-locked responses

1. Introduction

For more than thirty-five years, synchronous neuronal activity at the millisecond time scale has been described in the mammalian visual cortex (Griffith and Horn, 1963). Recently, it has been demonstrated in many other regions of the brain (Singer and Gray, 1995), and even in the three layer visual cortex of the reptile (Prechtl, 1994). Although this phenomenon has aroused interest for some time, its functional significance remains uncertain and became an object of speculation and controversy (Usrey and Reid, 1999). Synchrony could be related to information transfer by synfire chains (Abeles, 1991), information storage in potentiated synapses (Singer, 1995; Whittington et al., 1997), time advance coding scheme (Hopfield 1995), tag transmission in binding theory (Roelfsema and Singer, 1998), or to timed neuronal selection for temporal pattern recognition (Laurent, 1996; Parodi et al., 1996). Moreover, coincident bursts have also been suggested to play a relevant role in synaptic plasticity and information processing (Lisman, 1997).

The question of temporal coding by coincident events (CEs) is difficult to answer because it relies on the existence of methods able to quantify the CE excess even if the firing rates covary with the animal performance, behavior or attention (Pauluis and Baker, 1999). Precise excess quantification is absolutely required in order to show that the temporal coding contains more (or different) information than the firing rate.

The superior colliculus (SC) has long been known as a sensory-motor interface which controls rapid orientation movements (Sparks, 1986; Grantyn, 1988). The ventral part of the superficial laminae of the SC receive direct afferent from the retina and visual cortex layers V and VI pyramidal cells (magnocellular pathway). Cortical projections maintain topographic alignment with the retinal input, so that the central 10° of the visual field are represented proximally by >30% of the SC. Cells in superficial and intermediate layers are all visually responsive, exhibit a phasic response to onset and offset of stationary spot of light, and respond vigorously to stimuli moving at 0.5 to 30°/s (sometimes up to 800°/s). On the contrary, the response of cells in deep layers exhibits dramatic adaptation with repetitive stimulus. In the cat, direction selectivity and binocularity are dependent on cortical input (Wickelgren and Sterling, 1969).

The involvement of the SC in visual processing of moving visual stimuli makes the SC a possible network where synchrony could be demonstrated. However, collicular and cortico-

tectal correlations observed in the anesthetized cat exhibit much broader peaks than in the cortex (average width at half height: 51 ms, Brecht et al., 1998). Such broad temporal dispersion are thought to be related to simultaneous activation, but not especially to temporal coding ("castle-type", Nelson et al., 1992). Given the major role of the SC in gaze and attention orientation (Goldberg and Wurtz, 1972; Wurtz et al., 1982), we studied spike train correlations in SC of the *awake* cat during the presentation of moving visual stimuli. The cat was performing a fixation task to a central target while a light spot was moving in its visual field. We used new quantification methods which relied on instantaneous discharge probability estimates to calculate the expected correlation on a single trial basis (Pauluis and Baker, 1999). The experiment was designed to assess and characterize synchrony in superior colliculus during presentations of visual moving stimuli.

2. Methods

Experiments were performed on two adult cats selected after a few weeks of training on gaze orientation tasks. The care and use of animals was in accordance with the guidelines of the Society for Neuroscience and the American Physiological Society. Couldn't you list the European/Belgium equivalent instead?

2.1 General

Two cats were prepared for chronic gaze recording by undergoing a first surgery. Anesthesia was induced with xylazine (2 mg/kg IM) and, after 20 minutes, with ketamine hydrochloride (10 mg/kg IM). Deep anesthesia was maintained throughout with additional injections of both drugs. A scleral search coil (3 turns of Teflon insulated stainless-steel wire, 20 mm diam., Cooper Wire Co. CA) was implanted under the conjunctiva (Judge et al., 1980). The animal was placed in a Horsley-Clarke apparatus and a head implant was constructed from dental cement and anchored to the skull with stainless steel screws. A fixation device was embedded in dental cement in order to fix the head during experiments.

After recovery from the surgery, cats underwent a second stereotaxic procedure under deep anesthesia. A craniotomy was performed to allow access of microelectrodes into both SC and a stainless steel recording chamber was added to the head implant on the midline at stereotaxic coordinates A2.

2.2 Behavioral paradigms

Cats were trained to perform fixation and saccade tasks for food reward. The target spots were projected on a tangent screen by oscilloscopes controlled with a 80486 personal computer (digital to analog converter frequency : 100 Hz). When stable recording was obtained on both channels, cell preferences were rapidly determined with a manually driven laser beam.

moving distracter paradigm All trials started with an auditory click followed after 300 ms of the appearance of a small fixation point (FP) and a larger distracter (DS) both at the center of the visual field. The cat had 1200 ms to begin fixating and it was required to maintain fixation for 500-1200 ms. Then the DS moved slowly towards the periphery with determined velocity (5-70°/s), amplitude (5-35°), and direction, which could be chosen either specifically or randomly. At the end of the ramp, the DS was switched off for 300 ms. A new cycle with a required fixation duration of 60 ms was then repeated for 2 or 3 times. During all this paradigm the cats were not allowed to follow the distracter and had to maintain fixation within 3° of the FP in order to receive food reward.

Typically cats were capable of two hour sustained task performance, carrying out a total of 300 to 600 trials.

2.3 Recording and data collection

Neuronal discharge was recorded extracellularly with commercially available tungsten microelectrodes (Frederick Haer) that had impedance of 0.15-0.6 MΩ at 1kHz (IMP-1, Bak Electronics). The electrodes were mounted on a double hydraulic microdrive (Narashige, MO-95B) fitting the same recording chamber. Electrode penetration were made vertically through a single guide tube (21G, horizontal distance between electrode tips : > 300 μm). The guide tube was inserted afresh each session through the dura 5 mm above the SC. Neural activity was conventionally amplified 5 000-10 000 times (Neurolog NL-100 & NL-104, Digitimer), filtered (300-6 000 Hz, Neurolog NL-125, Digitimer), and displayed. System noise level was 30 μV because of the magnetic search coil fields. Cross talk between the two channels was never observed.

Eye position was measured with the magnetic search coil technique (Robinson, 1963; magnetic field frequencies : 50 and 75 kHz) . The target and distracter positions were controlled by a 80486 personal computer (National Instrument AT-MIO-16E) that drove the

food reward pump. The computer also controlled a constant current stimulus isolator (WPI) for electrical stimulation.

All the data related to the gaze and distracter positions, to the stimulation, and to the reward were digitized at 2 kHz, while the extracellular activities were digitized at 20 kHz (Pentium-Pro 200 MHz, National Instruments AT-MIO-64-E3). Some data files were transferred immediately after the series of trials onto another computer (Pentium-Pro 200 MHz) to assess fine temporal relationship between the spike trains.

The two independent electrodes were positioned in the SC just after the first layer of spontaneously active cells in dim light, so that it was possible to isolate one to three spike waveforms. As the track was continued deeper, cell discharges became more and more adaptive, preventing any reliable recording for more than a few trials. For this reason, most of the cells were recorded in the superficial and intermediate layers (<2 mm depth).

After a recording session, if electrodes were placed in a new location or if the location was uncertain, we used a *stimulation paradigm*. After an initial fixation of a single FP in the center, the FP was turned off and, after a gap of 50 ms, a stimulation train was delivered (500μs pulse width, 200 Hz, 200 ms duration, 20 μA). In order to distract cat's attention to both sides of the visual field, at the end of the stimulation train a new target appeared randomly 10° to the right or to the left of the FP, and the cat had to fixate this new target for food reward. The direction and amplitude of evoked short-latency saccadic eye-movements permitted precise assessment of the electrode position (Roucoux and Crommelinck, 1976).

At the end of the day, raw data were stored on digital compact disks for further off-line analysis.

At the last recording session, electrolytic lesions were made with stainless steel electrodes in order to mark the SC (20s-20μA anodal pulse). The animal was then anesthetized with xylazine (2 mg/kg IM) followed by pentobarbital sodium (IP XX). After transcardiac injection of heparine, the animal was perfused with 0.9% saline and neutral formalin with potassium ferrocyanate to color iron deposits. The brain was removed and placed into a solution of formalin with 15 and then 30% sucrose until it sank. The SC was blocked, frozen, and cut into 30 μm transversal sections. One section out of three was mounted onto chrom-alun-coated slides and stained. *Post mortem* histological processing confirmed that the sites were located in the half anterior part of the SC.

2.4 Data Analysis

To remove artifacts and to sort two or more spike waveforms, we used routinely a program based on multiple level discriminators set sequentially on a plot of superposed spike waveforms (Matlab 5.0). This simple strategy has been compared to a more time-consuming principal component analysis and was identically efficient. To assess the number of cells recorded, an auto-correlation histogram (ACH) was systematically constructed for each waveform (0.1 ms bin width). The waveform was attributed to a single cell only if an absolute refractory period could be measured within 0.75 ms (SC cells could discharge at frequency as high as 1200 Hz). All the waveforms that did not satisfy this criterion were pooled in a multi-unit activity. From this processing, it was usually possible to extract one or more cell activities from a single channel and to classify them as originating from a single or multiple units.

Before considering the temporal relationship of two different cell discharges, we investigated if the same cells could have been recorded on both electrodes simultaneously. This was achieved by a high-precision CCH (0.1 ms bin width, within –2 and 2 ms). The recording was excluded from the analysis if one or two bins were significantly different from the mean ($p<0.0001$, assuming a Poisson distribution, see below).

Other analysis always took place during a period which started 80 ms after the movement beginning, that is after the strongest effect due to movement onset, and ended at the movement offset, that is before the offset response. Offline, cells were characterized by their responsiveness, calculated as the difference between the maximum frequency obtained from the PSTH (> 80ms) and the mean frequency preceding the presentation (-0.2 to -0.05s).

As the cat attention was heavily changing, there was some trial to trial co-variation in the firing rate. Consequently, usual methods based on the JPSTH or on a shuffled predictor were inadequate to estimate the number of coincident events expected by chance. We used in this study a method that we described previously for the calculation of the expected number of coincident events (Pauluis and Baker, 1999).

2.4.1 Instantaneous discharge probability

Instead of assuming a discharge probability equal to the PSTH, the method uses the second alternative (Palm et al., 1988) i.e. to estimate the instantaneous discharge probability directly from the spike train. This estimate is plotted in Fig.1G and compared with other common

estimates. Figure 1A shows DS displacement and Fig. 1B, the spot onset. The cat was already performing fixation when the DS was turned on because it was the third repetition of the stimuli. The spike train recorded during the presentation is shown in Fig. 1C (same cell as cell 1 in Fig. 2). The first estimate in Fig.1D is the reciprocal of the interspike interval (ISI-Reciprocal). For each interspike interval (ISI), the reciprocal is calculated and extended over the interspike duration. This estimate could be further smoothed by a convolution with a Gaussian curve (SD 10 ms) leading to the estimate presented in Fig. 1E (Filtered ISIR). Fine temporal graining due to bursts of spikes has disappeared. Our estimate (Pauluis and Baker, 1999) starts with the ISI reciprocal (Fig. 1D). In order first to determine points of abrupt change in firing rate, a statistical test was performed on three consecutive ISIs. The statistical test assumed a gamma ISI density function and required a long ISI to be significantly larger (α=0.05) than two consecutive short ISIs that preceded (decrease) or followed (rate increase). The probability that an interval was larger than some value *I* was calculated as Eq.1 :

$$P\left(i > I \middle| \mu\right) = \int_{I}^{\infty} \left(\frac{a}{\mu}\right)^{a} \frac{1}{(a-1)!} t^{a-1} e^{-ta/\mu} dt \qquad (1)$$

where μ is the expected ISI duration and *a* the order of the gamma process used to model the intervals. In this experimental study, we kept *a* constant at 4, since it allows for a reliable refractory period. This model was also quite regular with respect to the usual Poisson model and thus permitted detection of smaller firing rate changes.

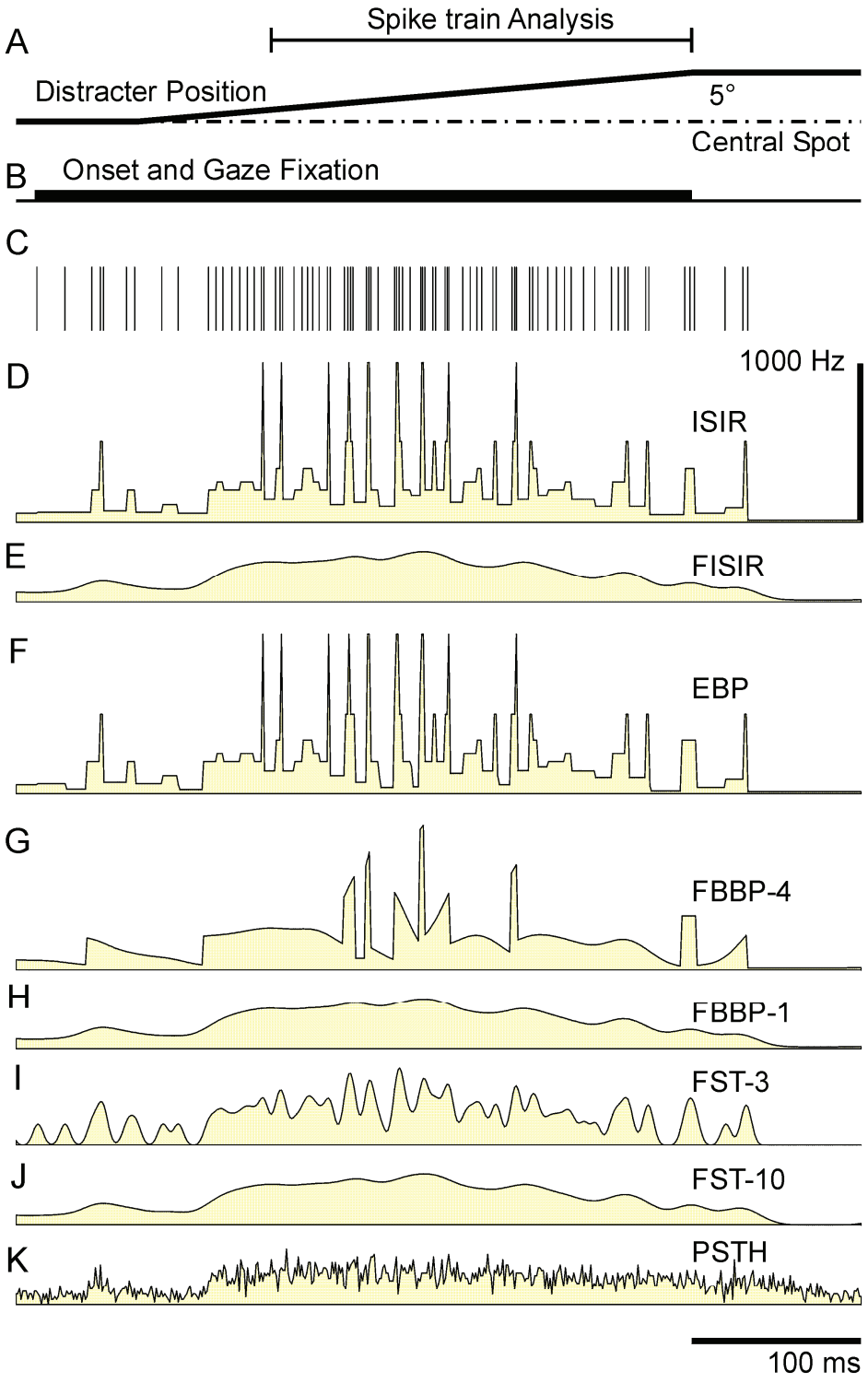

Figure 1. Instantaneous discharge probability estimates. A light spot was presented in the center of the screen and was moved at a uniform velocity (15°/s) toward the periphery while the cat was continuously fixating another central point. The distracter position is shown in (A) and its onset in (B). A train of action potentials recorded during the presentation of a moving stimuli is shown in (C) above various instantaneous discharge probability density estimates. The first one (D) is the ISI reciprocal (ISIR), also known as 'frequencygram', and was calculated simply by extending the reciprocal of the ISI over its duration. This estimate could be filtered with a Gaussian kernel (10 ms SD, FISIR) as shown in (E), or could be further processed for determination of rapid firing rate change points. Once such points were determined, the high discharge probability epochs were slightly extended to better reflect the exact moment of discharge probability increase or decrease (Extended

BreakPoints, F; see Methods for details). Only after precise determination of rapid variations, the estimate is filtered between them with a Gaussian kernel (10 ms SD) but never across them. Determination of rapid discharge probability changes assumed a ISI distribution in stationary conditions: in (G) it was a gamma distribution of order 4 (FBBP-4), and in (H) it was a Poisson distribution (FBBP-1). If a Poisson distribution was assumed, no rapid discharge probability changes were detected. Other commonly used estimate are filtered spike train, shown in (I&J) with a 3 ms or 10 ms Gaussian kernel respectively (FST-3 and FST-10). But the most used estimate was the PSTH (K) which, in this case, underestimates the discharge probability since data were not stationary like in most experiments on awake animals.

The occurrences of rapid firing rate changes were so determined, but their most probable location does not correspond exactly to the time of the first or last spikes. Time of the rapid firing changes were calculated, leading to a slight increase of the duration of the high frequency epochs and to a further decrease of the adjacent low discharge rate (Extended Break Points, Fig.1F). The last steps is a convolution of this estimate with a Gaussian curve (10 ms SD), *exclusively* between points of rapid firing changes, not across them (Filtered Between Break Points, FBBP-4 in Fig. 1G). A similar estimate using a Poisson ISI density function (order 1) is plotted in Fig. 1H (FBBP-1). No rapid firing changes are further recognized because the model of the discharge is far less regular than a gamma process of order 4, and the results are similar to curve 1E. The only difference between our previously published algorithm (Pauluis and Baker, 1999) and the one we used in this study lies in the moment at which the spike times are binned. Indeed we found much more reliable in case of fast firing rate to first bin the spike time and then to calculate the ISI reciprocal. Exact solution could be calculated, but were time consuming and prone to errors when two events occurred at exactly at the same time (see below).

Figure 1J&K show the spike train filtered by convolution with a Gaussian function (SD = 3 ms, filtered spike train FST-3 in Fig. 1G, and SD = 10 ms, FST-10 in Fig. 1H), and the last estimate is simply the raw PSTH (Fig. 1I). Although it could also be filtered, the PSTH underestimates the number of spikes generated during this trial because data were not stationary, as often is the case when recording from awake animals. The use of this latter estimate for cross-correlation significance testing corresponds to the JPSTH method (Palm et al., 1988). Analyses described in this study were performed with most of these estimates, and comparative results are presented in Tables 1&2 for respectively the FST-10, FBBP-4, and EBP estimates.

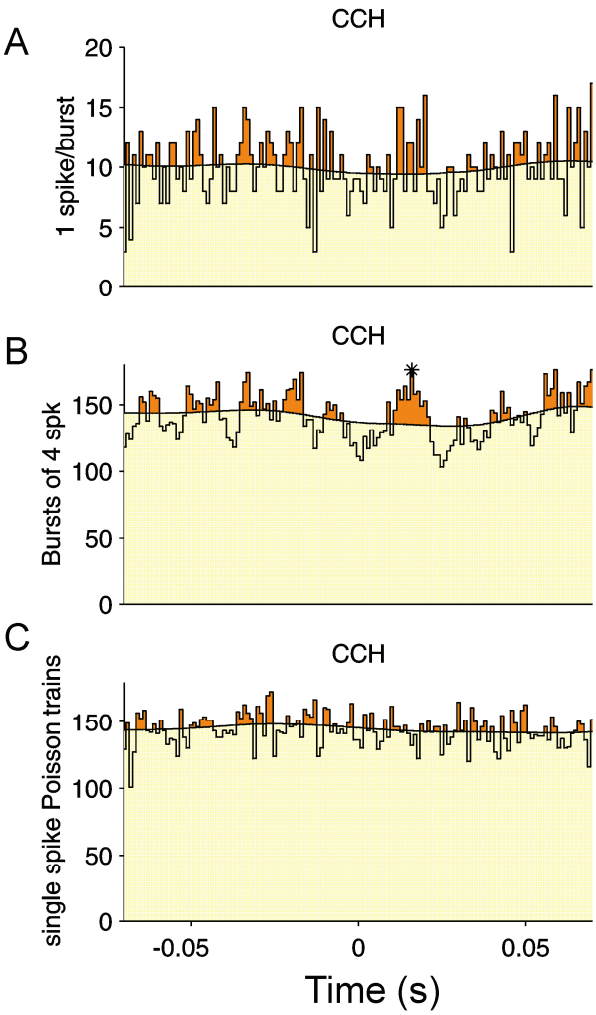

Figure 2. Effects of spike bursts on CCH statistics. (A) Two Poisson processes are simulated, having a frequency of 30 Hz. Their CCH exhibits a high frequency noise. If the instantaneous discharge is estimated by filtering the spike train with a Gaussian kernel (10 ms SD, Fig. 1E) and the expected CCH constructed, no significant peak is found after filtering ($p<0.001$ in two consecutive 5 ms windows, see Methods for details). (B) The same spike trains are then used to produce burst of 4 spikes chosen in a uniform distribution of 0.15 and 3 ms and then sorted in ascending order (burst frequency: 30 Hz, spike frequency: 120 Hz). The CCH has much less noise in the high frequency band. As a consequence, one peak is now significant. This peak occurs at a location that could be predicted when looking at A. (C) For comparison, two Poisson trains were simulated with a frequency of 120 Hz. The CCH has the same offset, but the noise is less correlated between adjacent bins. Although none of the recorded cells exhibited such caricatured bursting discharge, we concluded that bursts could induce artifactual peaks in the CCH. If we used an instantaneous discharge estimate which is able to detect the rapid firing rate changes like the one we proposed (FBBP-4, Fig. 1G), no significant peak was found in the CCH of the burst trains.

2.4.2 Time-resolved cross-correlation

For each trial, we calculated the time resolved cross-correlation (TXC) and its expectation function, using the instantaneous frequency estimate. The TXC and expected TXC were then summed across trials and compared (1 ms bins). Summed TXC (Fig. 2D) has a stimulus related time axis (X) and a spike related time axis (Y).

2.4.3 Cross-correlation histogram

The cross-correlation histogram could be extracted from the TXC by summing along the stimulus related time axis X. Filtering was performed by means of a moving window average on 5 ms. All further analyses were related to the filtered CCH Significance was then assessed assuming that spike distribution in each window followed a Poisson distribution ($p<0.001$). The probability that the number of coincidences c will be at least as many as the number observed, C, given that E are expected, was calculated as Eq.2 :

$$P(c \geq C) = 1 - \sum_{i=0}^{i=C-1} \frac{e^{-E} E^i}{i!}$$

(2)

This method for significance quantification is independent from the bin width, on the contrary of the usual binomial test, which assumes that there is only one spike per bin.

Two successive significant windows ($p<0.001$) accounted for a "peak", of which the width was determined by intersections of observed and expected count curves. The peak closest to 0 ms lag was called the "central peak" and was characterized after filtering by the relative modulation amplitude (RMA), calculated as the ratio of the peak amplitude to the expected value: *(max-expect.)/expect.*, and by the peak width at half-height

The time lag of the CCH peaks occurring within ± 70 ms were also characterized relative to the maximum count. If there were more than one central peak, the other significant peaks were called "satellite peaks" and accounted for an oscillatory correlation. We did not use the Gabor curve fitting to characterize CCHs (König, 1994), because the criteria of 15% variance accounted for was dependent on the CCH width, and the fitting algorithms we used previously on our simulations (Pauluis et al, 1999) were not able to fit accurately the data.

The shift predictor (SP, Perkel et al., 1969) was calculated in order to assess the influence on stimulus presentation on the occurrence of spike correlation. The expectation of the SP was calculated on a single trial basis, as explained for TXC and permitted to investigate the occurrence of possible significant peaks in the SP which were not related to the cellular firing rate but to precise time locking with the stimulus presentation.

2.4.4 Auto-correlation histogram

Auto-correlation histograms were also computed for each spike train in order to quantify the oscillatory discharge. Statistical requirements for significance were similar to the CCH. We characterized also the ISI distribution by two proportions. The first one is the proportion of ISIs shorter than 8 ms and refers to the classical criteria used to define a bursting cell (> 25%,Cattaneo et al. 1981). The second one is proportion of ISIs shorter than 3 ms which was used to characterize chattering cells (> 50%, Gray and McCormick, 1995). Although that these proportions were previously applied to single unit recordings, we extended their use to the multi-unit activities for descriptive purpose only, because the number of different recorded cells remained limited.

In order to investigate how the timing of the cell discharge was locked on the stimulus presentation, an ACH-SP was systematically computed. The expectation was calculated on a single trial basis, using the instantaneous discharge probability; as explained for the TXC.

2.4.5 Coincident events

If a central peak was observed in the CCH, we used the number of significant windows to define the time delay during which a spike occurring in both cells will be called a coincident event (CE). In the example of Fig. 9, four windows centered at –1, 0, 1, and 2 ms were significant, so that all the spikes of the second cell occurring 1.5 ms before to 2.5 ms after a spike of cell 1 were considered as CEs. The CE definition was thus directly related to the CCH peak, contrarily to previous arbitrary definition (Riehle et al., 1997).

Considering a CE as an event, we calculate the ACH and the ACH-SP for the CE train. This allowed the characterization of the CE dynamics, i.e. the oscillations and stimulus time-locking of the CE train. To perform those analysis, the moment of each CE was determined as the mean time between both spikes of cell 1 and 2 : *(t1-t2)/2* (Pauluis and Baker, 1999). This definition permitted two CEs to occur by chance exactly at the same moment, and forced spike binning before the calculation if the ISI reciprocal and discrete adaptation of the firing rate if two spikes were found in the same bin.

To investigate if averaging the CEs across trials blurs the stimulus-locked properties of the CE train or if the CEs were clustered during a portion of the stimulus presentation, we computed an equivalent of the post-stimulus time histogram, and quantified the bumps of the average CE count. CEs were extracted from the TXC by summing the related central bins along the Y time axis. Filtering was performed as previously with a 9-ms moving window. A further convolution with a wide Gaussian curve (50 ms SD) provided a smoothed average of the CE count and also permitted us to delimitate the largest period of interest with a mean count larger or equal to 6 CEs per window. We had to choose a lower limit in order to ensure that statistical tests were performed on a minimal number of events. Assuming a Poisson distribution in each time window, significance was tested against predicted CE count (Eq. 1, $p<0.005$) and against the smoothed curve of the observed count ($p<0.05$) to assess the CE excess and its time variability. Time variability – the number of expected bumps during this period - was further quantified by comparison with 400 simulations of the CE count (Silverman 1986), which assumed a probability density curve for each trial similar to the smoothed observed count and a non-homogeneous Poisson process. The number of trials to be

simulated was equal to the number of experimental presentations multiplied by the number of significant windows in the CCH peak used to determined the CEs (this ensured the smallest CE probability < 0.067 $ms^{-1}trial^{-1}$). Filtering procedure was performed on the simulations exactly as on real data.

Because the firing rate was not uniform during the trials, the expected CE count could also exhibit some bumps which required to be quantified. The expected CE count was thus tested against its smoothed estimate (50 ms SD). If some bumps were detected, they were added to the number of bumps found in simulated CE counts to compensate for possible firing rate variability (which was not taken into account in the smoothed observed CE count). We counted the number of simulations that presented at least the same number of bumps as the data, corrected for possible bumps in the expected CE count. If less than 20 simulations over 400 exhibited at least the same number of bumps as the data, then the probability that the CEs are more clustered than expected by chance is less than 0.05. Bumps were then characterized by the maximum CE count and the moments at which the expected CE count crossed the observed CE count.

Regarding trial to trial analysis, we compared the observed number of CEs for each trial with the expected value.

2.4.6 Control analyses

Control analyses were performed on spike trains after that the bursts were filtered out. This was achieved by iterative suppression of the second spike in each burst until no ISI smaller than 3 ms were found.

A second kind of control analysis was implemented by simulating some spike trains according to the instantaneous discharge probability estimate. Because we wanted to control for the influence of bursts on the results of the preceding analysis, we used a filtered spike train (FST-10) as an imprecise instantaneous discharge probability estimate. This estimate was divided by n, the number of spikes per burst, and a gamma process was simulated accordingly. Each event was then replaced by a burst of n spikes. These spikes were chosen in a uniform distribution ranging from 0.15 ms to 3 ms, in order to simulate a multi-unit activity. ISI in the same burst were then sorted in ascending order. Analyses were then performed as with real data.

Finally we also used a counting model to illustrate the effect of delayed inhibitory feedback on the CCH of two cells. The model itself is extensively described by Shadlen and Newsome

(1998) and consists simply in counting the inputs until a fixed threshold is crossed. Details of the modifications we made are given in the figure legend.

3. Results

All the recordings were pooled for quantitative analysis and results are reported in Table 1. In this table, a pair could be represented more than once. The best sessions with a significant cross-correlation peak were chosen for each site and were compiled in Table 2. Criteria used to formally distinguish to sites were the depth (required difference > 300µm) and changes in spike waveforms and ACHs. Each cellular activity pair was represented in this table only once. Careful examination of both tables does not reveal great differences. Because recordings at the same site could differ within a few minutes after smaller changes in electrode depth, we feel justified to present analysis on the largest data pool, treating each recording session as a single entity, even if they were not all truly independent.

	FST-10	FBBP-4	EBP	No ISI < 3ms FST-10	Sim. Bursts FST-10
spike>500 & offset>15	181	181	181	165	175
# pairs with CCH peak	116	111	100	87	169
# CCH with sign satellite peak :	**11**	**12**	**11**	**1**	**572**
# CCH with significant trough(s)	**43**	**38**	**33**	**21**	**157**
# troughs in CCH	94	81	67	42	555
# cells ACH peaks > 8 ms	34	28	29	28	691
# CCH-SP offset > 15 :	114	109	98	85	166
# peaks CCH-SP	0	0	0	0	161
# peaks Cell ACH-SP	1	3	0	0	331
# CE-ACH-SP offset > 15 :	63	61	52	26	62
# CE-ACH-SP with central peak	**41**	**24**	**2**	**0**	**62**
# ACH-CE with satellite peaks	**38**	**28**	**8**	**1**	**148**
# ACH-CE peaks > 8ms (all rec.)	168	114	28	2	924
# txc analysis performed	99	94	82	62	145
% recordings with txc bumps	**0.3333**	**0.1064**	**0.02439**	**0**	**0.7793**
sign txc :	<10E-9	0.02221	0.9155	1	0
mean # predicted bumps due to FR :	**0.1313**	**1.617**	**2.659**	**0.01613**	**0.6207**
mean # obtained bumps vs filt. :	5.798	5.691	5.463	2.694	8.572
mean # obtained bumps vs exp. :	9.182	7.649	4.598	4.048	9.124

Table 1 shows the main results for pooled recordings. The measurement which best mirrors the spike train was the ISI reciprocal extended over the rapid firing change points to best reflect the changes in discharge probability (EBP). Changing the instantaneous firing rate estimate has serious consequences for the statistics performed on the CEs. Most of CE shift predictors could be predicted by an accurate EBP estimate. The number of bumps found on the expected CE count also changed dramatically, modifying the results of the statistical test on the number of CE bumps.

3.1 Cross-Correlation Histograms

To justify the great care provided for burst analysis in spike trains, we first show the raw CCHs for three pairs of simulated spike trains (Fig. 2). The first trains are simply two Poisson processes with a frequency of 30 Hz, simulated during 10 s. The CCH is noisy but no significant peak was found. The second ones were constructed from the first ones. The Poisson processes were transformed into a train of bursts by replacing each spike by 4. The ISIs within the burst were chosen in a uniform distribution (0.15-3 ms) and sorted in ascending order. The resulting spike frequency was 120 Hz. The CCH noise seems to be low-pass filtered and a peak was now significant. For comparison, two Poisson processes with a frequency of 120 Hz were simulated. Their CCH is shown in Fig. 2C and exhibits high frequency noise. Although no spike train in the SC exhibited so much bursts, we concluded that bursting cells requires much more spikes than usual cells to average the low frequency noise. Further simulations showed that about 20000 spikes could be a safe amount of data, but we were not able to collect so much spikes for a single recording site.

	FST-10	FBBP-4	EBP	No ISI < 3ms FST-10
# of pairs	79	79	79	79
spike>500 & offset>15	58	58	58	56
# pairs with CCH peak	**52**	**51**	**44**	**39**
# CCH with significant trough(s)	**23**	**21**	**19**	**12**
# troughs in CCH	54	45	38	24
# cells ACH peaks > 8 ms	12	12	14	7
# CCH-SP offset > 15 :	51	50	43	38
# peaks CCH-SP	0	0	0	0
# peaks Cell ACH-SP	2	3	0	0
# CE-ACH-SP offset > 15 :	32	31	27	18
# CE-ACH-SP with central peak	**18**	**13**	**2**	**0**
# ACH-CE with satellite peaks	**19**	**17**	**7**	**1**
# ACH-CE peaks > 8ms (all rec.)	68	46	14	2
# txc analysis performed	47	46	41	31
% recordings with txc bumps	**0.2979**	**0.04348**	**0**	**0**
sign txc :	2.03E-07	0.6691	1	1
mean # predicted bumps due to FR :	**0.1915**	**1.848**	**2.439**	**0**
mean # obtained bumps vs filt. :	5.702	5.391	4.878	2.677
mean # obtained bumps vs exp. :	10	9.217	6.122	6.032

Table 2. shows the main results when only one file is considered for each recording site. Choosing EBP or FST-10 as instantaneous discharge probability estimates has a dramatic influence on the proportion of recording exhibiting more bumps than their related simulation. This is due mainly to an increase in the number of bumps found on the expected CE count.

Of 686 recordings tested for cross-correlation testing, 181 were selected for having a fair amount of data (>500 spikes in each train, mean cross-correlation count > 15). A significant central peak in the CCH was found in 111 recordings (100 to 116, see Table 1 for dependence on instantaneous discharge probability estimate calculation, and Table 2 for site based analysis). 14 recordings involved two single units.

Properties of CCH central peaks are detailed in Fig. 3. The relative amplitude modulation (RMA) is plotted in Fig. 3A. RMA exceeding 0.8 are plotted as circles in Fig. 3B, RMA smaller than 0.3 are represented by a dot, and RMA between 0.3-0.8 were not drawn for clarity concern. Consequently, Fig. 3B shows the distribution of the RMA as a function of responsiveness of both spike trains. It appears that the most responding cells do not have the

largest ratio, although they produce the largest amplitude peak when expressed in raw spike count (data no shown).

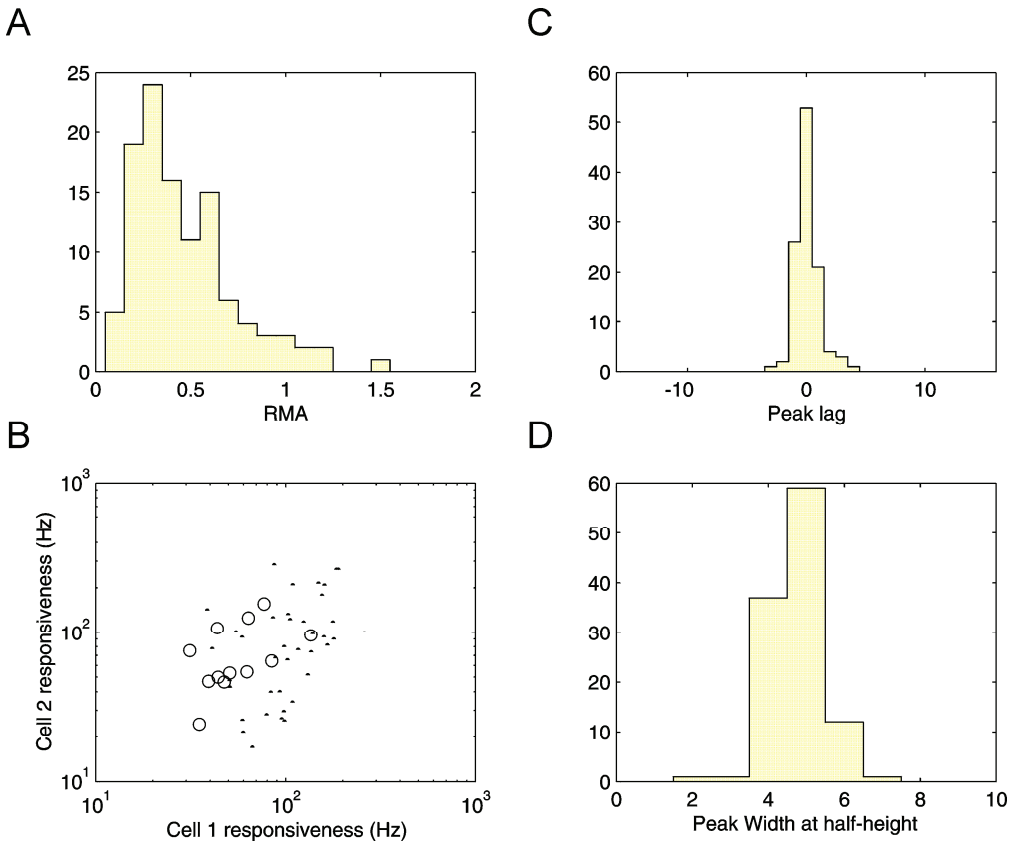

Figure 3. CCH. After filtering, central peaks on cross-correlation histograms were quantified by their relative modulation amplitude (RMA): *(max-expect.)/expect.* The RMA distribution is shown in (A). Cell responsiveness is the difference in the PSTH between the maximum firing rate during the stimulus presentation (>80 ms) and the average frequency before the presentation. (B) shows that pairs which exhibited the highest relative modulation amplitude (circles, RMA > 0.8) were probably not as responsive as pairs with smaller RMA (dots, RMA<0.3). Peak lag distribution is displayed in (C) (mean : 0.06 ms +/- 2.20 ms, n=285) and peak width at half height in (D).

The distribution of the central peak time lag is shown in Fig. 3C and is well centered on 0 ms (mean : 0.06 ms +/- 2.20 ms, n=285). Figure 3D displays distribution of the central peak width at half height. Only 12 recordings (11-13) showed some significant satellite peaks (Fig. 5A, dark gray). Shift predictors were constructed as a correlation histogram, but with spike trains from two successive trials. The use of an instantaneous discharge probability estimate allowed direct significance quantification for each kind of shift predictors. All the CCH-SP were flat. In conclusion, most recordings exhibited a central peak, showing that cells were synchronized. Only a few recordings showed an oscillatory synchronization and since no peak was found in the CCH-SP, no CCH feature was time-locked on stimulus presentation. Tables 1&2 show also that about one third of central peaks were flanked by some significant troughs, indicating that these CCHs were not characterized only by an isolated central peak.

Figure 4 summarizes the modest influence of the stimulus velocity on cellular synchronization for 13 tested pairs. With increased velocity, the maximum firing rate increased slightly (mean difference : 14.6 Hz +/- 9.8 SE, p = 0.068). Raw CCHs obtained for the lowest velocity are displayed in the left column. Visual inspection reveals that peak shapes are remarkably constant. Although changes were globally not significant, a high velocity stimuli decreased the RMA (displayed in the upper left corner) in 6 pairs (maximal decrease : -0.06), but increased markedly (>0.06) the RMA for 4 out of 7 pairs, and a significant satellite peak appeared for the eleventh one (arrow).

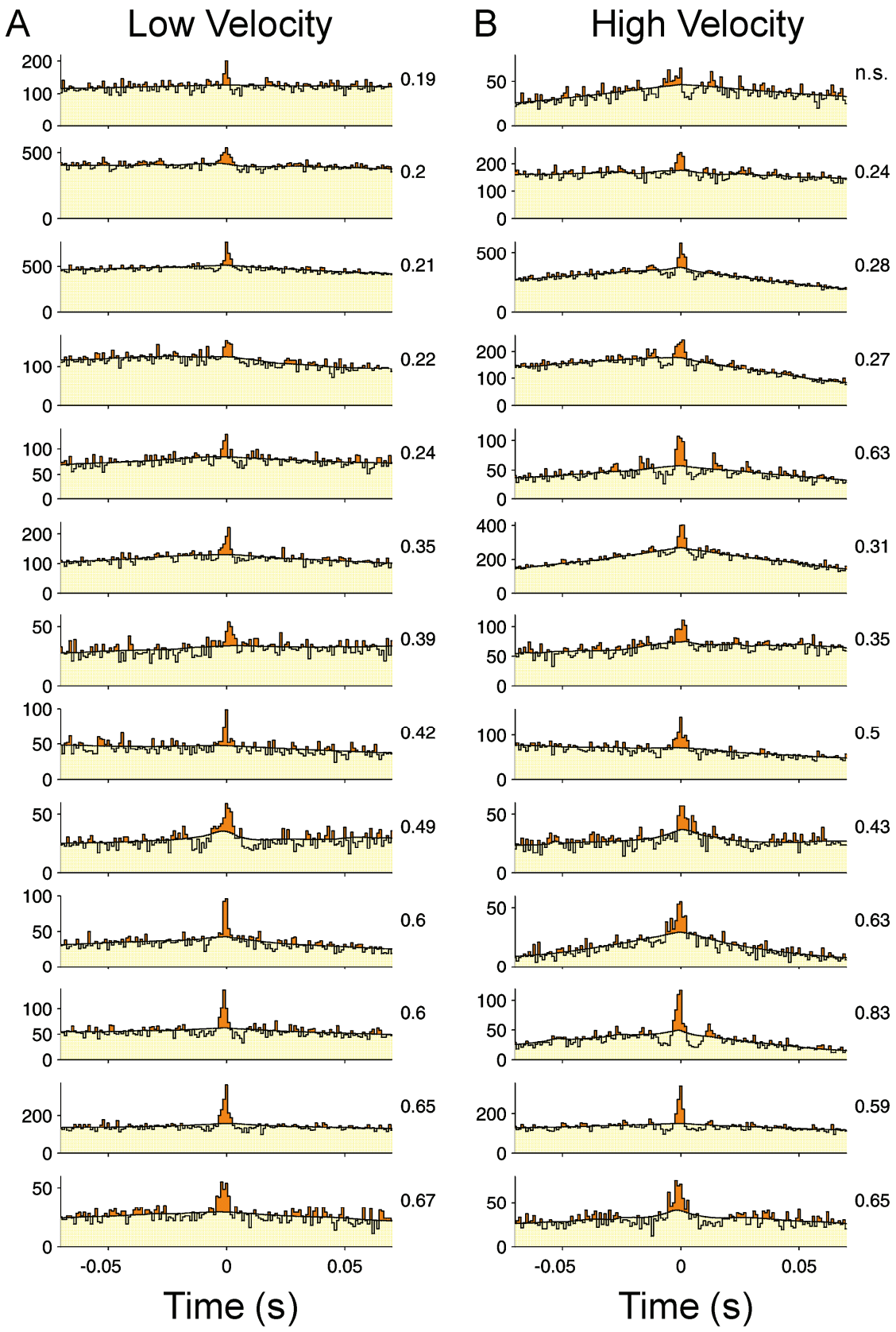

Figure 4. Stimulus velocity testing. Thirteen pairs were tested for low (A) and high (B) stimulus velocities and resulting cross-correlation histograms were compared. Nine out of 13 peaks increased their relative modulation amplitude when the stimulus velocity increased. Cross-correlation shift predictors remained flat.

3.2 Auto-Correlation histograms

A significant peak within 8 ms of zero lag in the ACH was found in 6-29 recordings. The proportion of cells which presented more than 50% of their ISIs shorter than 8 ms (bursting train) was 33.4 % (n=362)in the set of recordings presenting enough data. In the same set, the proportion of cells which presented more than 25% of their ISIs shorter than 3 ms (chattering train) was equivalent (32.6%). These proportions were not significantly different if the CCH was peaked.

Satellite peaks in auto-correlation histograms were found in 28 cells (28-31). Figure 5A shows the distribution of their time lags in light gray, which has a clear mode centered around 16 ms (63 Hz). A similar distribution was found for the CCH satellite peaks (dark gray). Only 3 spike trains exhibited a significant peak in the ACH-SP (Table 1), illustrating that some cells had a discharge which was time-locked on the stimulus presentation.

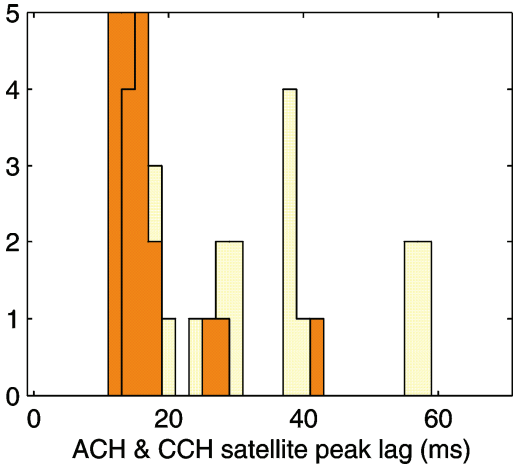

Figure 5. ACH. Satellite peaks were identified on ACHs and their delay distribution is shown in (A) in light gray. Some satellite peaks were also found in the CCHs and are displayed in dark gray. Most peaks are found between 12 and 18 ms (55-85 Hz) but they represent less than 10 percent of the recordings (see Table 1).

CEs were defined as spikes falling within the central peak of the cross-correlation histogram. Considering these CEs as simple events, we calculated the CE shift predictors for each experiment (CE-ACH-SP). Surprisingly we found some significant peaks, showing that CEs could be locked to the stimulus presentation. This is contrasted by the fact that no cross-correlation shift predictor and only a three auto-correlation shift predictor were peaked (see Table 1). This could mean that CEs are better locked to the stimulus presentation than single spikes. Figure 6 shows the correlation analysis performed on CEs. 24 (2-41) recordings exhibited both a peaked CCH and a positive CE auto-correlation shift predictor. The RMA of the central peak of the shift predictor is shown in Fig. 6A and was smaller than for CCH (Fig. 3A). Since correlation concerns two different kinds of event, no direct comparison could be made; CCH has to be compared to CCH-SP which were all flat, and CE-ACH to the CE-ACH-SP.

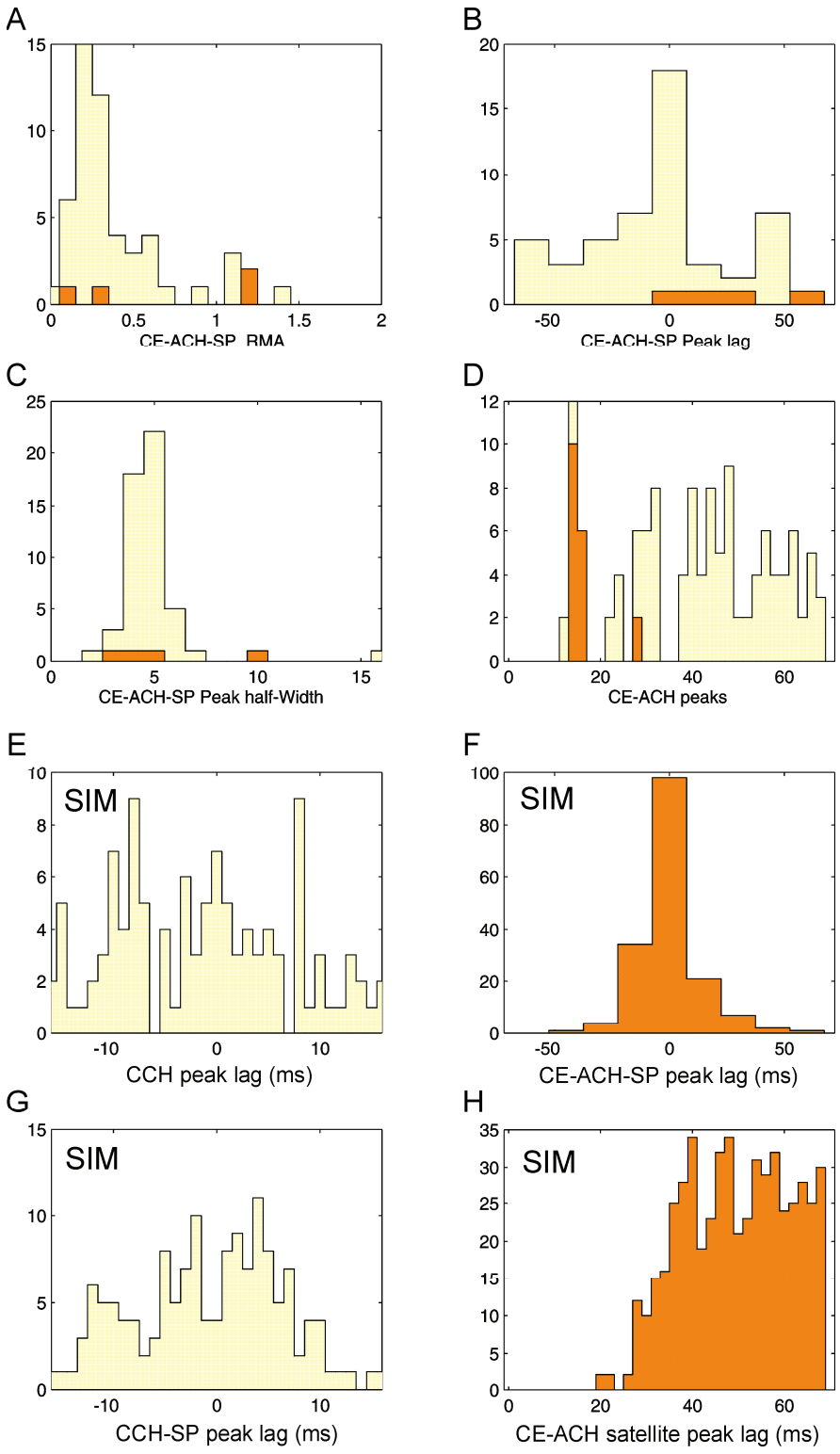

Figure 6. CE-ACHSP and CE-ACH. Shift predictors were calculated for the recording with significant CCH peaks. Most of them were flat, except when CEs were treated as events. As shown by their auto-correlation shift-predictor, CEs were found to be time-locked on the stimulus presentation in 51 recordings if the instantaneous discharge was evaluated by a filtered spike train (light gray; FST-10, Fig. 1J). The number of recordings with stimulus-locked CEs fell to 4 if we used the ISI reciprocal with a compensation for rapid firing changes (dark gray; EBP, Fig. 1F). (A) These peaks did not have a large amplitude (B) Peak lag distribution was broadly centered around 0 ms (2.0 ms +/-5.7 SE, n=49). (C) The peak width at half height was similar to CCH peaks. (D) Auto-correlation performed on CEs revealed much more satellite peaks than any other correlation measure, with a clear mode around 15, and then at 30 and 45 ms. The peak lag distribution obtained in simulated burst

trains matched with the data discharge probability are shown in figure E,F,G&H. The main difference are the wide distribution of the CCH peaks when compared to Fig. 3C, the occurrence of peak in the CCH-SP, and the absence of a peak below 20 ms in the distribution of the CE-ACH peak lags.

3.3 Coincident events are oscillatory distributed and time-locked on the stimulus presentation

We found 47 % of chattering spike trains in recordings with a significant peak on the CE-ACH-SP ($p<0.02$, n=62). This implies that epochs of high frequency discharge could be synchronized between cells and reproducible from trial to trial, but these peaks could also be artifacts due to the simple presence of clustered CEs, as shown for clustered spikes in Fig. 2.

The peak lag distribution is shown for different shifts in Fig. 6B. The peak lag of the CE-ACH-SP was centered on around 0 ms (2.0 ms +/-5.7 SE, n=49, shift=1). Since the peak closest to the center is chosen as the central peak, this centered distribution could also be artifactual. The CE-ACH-SP amplitude was not very high, but peaks had the same width as CCH peaks (Fig. 6C & 3D).

Finally, we performed auto-correlation analysis on CEs, and satellite peaks were found around 15, 30 and 45 ms (Fig. 6D), as for spike train auto-correlation (Fig. 5A), except that CE-ACH peaks were more frequent and regularly spaced. CEs in the SC were thus oscillatory at 65 Hz and could be locked to the stimulus presentation. This time-locking was much weaker when observed at the spike level and illustrated that information about the stimulus could be coded by coincident action potentials. These features were dependent on the instantaneous density estimate we used. Indeed, when the estimate based on extended breakpoint was used, only a four peaks were found (dark gray).

The importance of bursts was first tested by analyzing the spike trains after their bursts were filtered. Although, central peaks in the CCHs were still present, only oscillatory response was found and all the features related to CE train were absent (Table 1).

The second control analysis was performed after replacing the data by simulated burst trains. These trains were simulated according to a smooth instantaneous discharge probability estimate (the filtered spike train, FST-10 in Fig. 1J). In the most caricatured approximation, burst occurrences were determined randomly according to a gamma process of order 4. Each burst was composed of 4 spikes. The number of central peak in the CE-ACH-SP reaches the amazing number of 98 (Fig. 6F, to be compared to 18 in Fig.B), but the first satellite peaks in CE-ACH were found after 25 ms (Fig. 6H) and were not clustered as in Fig. 6D. CCH central

peak were broadly distributed around 0 ms (Fig. 6E, compare with Fig. 3C), as were CE-ACH peaks, and many CCH-SP were found to be significantly peaked (Fig. 6G). This suggests that centered CCH peaks (Fig. 3C) can not be accounted for by the bursts, but the peaks in CE-ACH-SP could well. Moreover the cluster below 20 ms in the distribution the CE-ACH satellite peak lags was not found in this and all other simulated burst trains with other gamma order and number of spikes per burst (data not shown).

3.4 Time resolved cross-correlation

To show how the CE density could vary from trials to trials, we present in Fig. 7, ten successive trials obtained from one pair of neurons. The stimulus presentation is symbolized in Fig. 7A with the stimulus motion starting at 0 s. The first five trials are plotted in the upper part of Fig. 7 (B,C,D), and the five next trials are mirrored in the lower part (E,F,G). Graphs 7B and 7G show the spike trains of respectively the first and second cells and the corresponding trains of CEs, defined as spikes falling within the central peak of the cross-correlation histogram (Figs. 7I&J). Time-resolved cross-correlation (TXC) is displayed in Figs. 7C&D. The abscissa corresponds to time relative to the stimulus movement onset, while the ordinate is the time relative to each spike of cell 1. It is exactly as if the cross-correlation histogram was plotted in a gray scale as a function of peri-stimulus time, like in a raw JPSTH. After testing for significance and filtering (two-dimensional Gaussian convolution 2 ms SD), the first percentile of smallest p is determined and highlighted by a white line. The raw CCHs are plotted in Figs. 7I&J and correspond to the sum of the time resolved cross-correlation along the stimulus locked time axis between 80 and 300 ms. CCH expectation is superposed in light gray. The number of adjacent significant windows in the cross-correlation histogram is shown by the two horizontal lines on both sides of the zero-ms lag in the time resolved cross-correlation histogram (-1 to +1 ms, Fig. 7C&F). All the points between these two-lines were called "coincident events" (CEs). They were summed and plotted in Figs. 7D&E as a PSTH (dark gray curve), on which is superposed the corresponding expectation (light gray). Significant excesses in two consecutive windows are reported on Fig. 7D&E by stars.

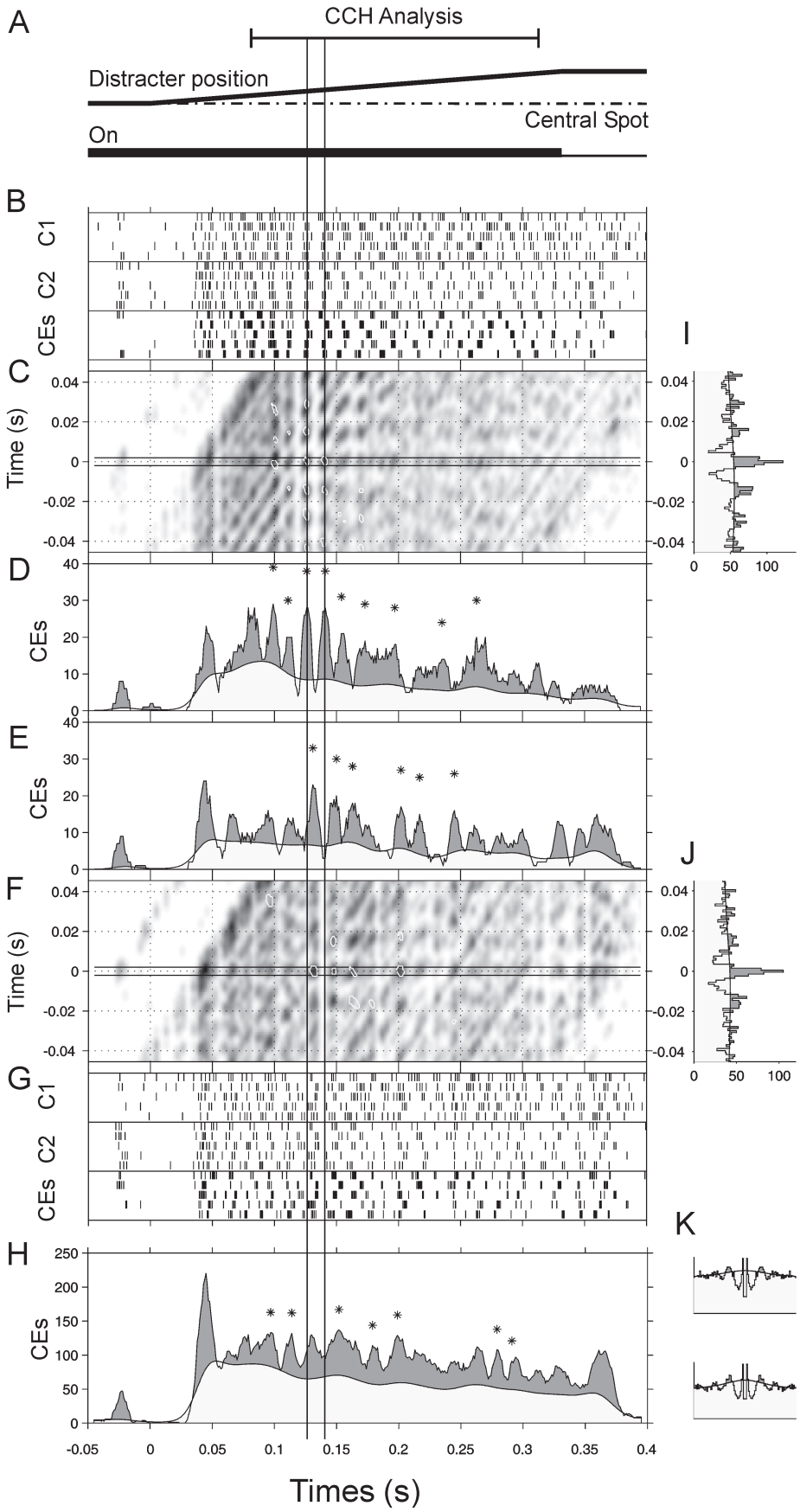

Figure 7. Example of trial by trial variations in a pair of oscillatory cells. Peak locations in the CE count could change within a few trials. The usual stimulus configuration is displayed in (A) relative to the movement onset. Notice that the light spot onset occurred at –60 ms and is not represented. Two sets of five consecutive trials are

compared. After off-line discrimination, action potentials are plotted in the two upper rasters (B). The texture is more patchy in the CE raster than in the spike rasters because CE calculation enhances burst coincidences. Their cross-correlation is shown in (I) and from the significant bins of the central peak, the delay defining a CE was determined (-1 to +1 ms). The corresponding CEs are shown in the lower raster in (B). (C) The raw time-resolved cross-correlation (TXC) is shown in a gray color scale. The CEs are shown inside the two horizontal lines. The expected value of the TXC was calculated from the instantaneous discharge probabilities for each trials, and then summed. The first percentile of most significant p after filtering is highlighted by white curves. wheres the white curves the first percentile of most significant bins. The CCH (I) was calculated as the bin sum along the abscissa between 80 and 330 ms. The TXC can also be summed along the Y-axis between –1 and +1 ms to give the CE count shown in D (dark gray). The expected CE count is calculated similarly and shown in light gray. The significant peaks are marked by a star($p<0.005$ in two consecutive windows). (E,F,G,J) follow the same display conventions as A,B,C, and I for the next five trials of the same experiment. (H) The CE count and its estimate are plotted for the complete experiment (80 trials), ant the ACH for each spike train is shown in (K). Two main peaks can be identified at 126 and 141 ms in the first five trials and were shifted to 132 and 148 ms in the second set (dashed lines). After averaging over all trials, it the second peak configuration which seems to come out, but the peak at 132 ms is no more significant. Cells were bursting and we used a filtered spike train (FST-10) as instantaneous discharge probability estimate. If another estimate which accounts for bursts as a change in firing rate was used, no significant peak was in the CE count (not shown).

Since cells were bursting, we avoided the use of our instantaneous discharge probability estimate which is able to detect fast changes in firing rates, and we preferred the filtered spike train (FST-10, Fig. 1J) because it permitted to assess coherence between bursts. Indeed, synchrony arises here from burst synchronization, as confirmed by examination of the rasters. If we used the EBP estimate (Fig. 1F, data not shown), no significant peaks were found. If the FBBP-4 was used, only three significant peaks were found in each data set (Fig. 1G, data not shown). Here, clear peaks in the CE count for both series were significant. However, peaks at 126 and 141 ms in the first data set were shifted to 132 and 148 ms in the second one. This shift of 6.5 ms represents 40 percent of a period, so that first peaks were blurred in the main average (one non-significant peak at 130 ms, Fig 7H).

This confirms that in bursting spike trains, CEs could be loosely time locked to the stimulus presentation, but that time locking is probably stronger for temporally close trials. To illustrate this point, various shift predictors (SP) were computed. Figure 8A&B show the ACH-SP for the first spike train calculated for the first and second sets of trials. Although some non-significant periodicity can be observed in Fig. 8A, it disappeared in Fig. 8B. The second spike train exhibited a significant peak centered at -2 ms (Fig. 8C), which again disappeared during the second set (Fig. 8D). CCH-SP (Fig. 8E&F) are completely flat. If no other test were performed, the conclusion would be that only the second spike train was weakly locked to the stimulus presentation during the first set of trials. However, if the auto-correlation shift predictor for CEs is examined (Fig. 8G&H CE-ACH-SP), it appears clearly that CEs are strongly locked to the moving stimuli from one trial to the next. The main peak is in fact centered at 12 ms, which is accounted for by a CE trend to shift from one CE cluster to

the following one when the trial was repeated. This suggests that stimulus locked information is encoded much more *precisely* by CEs than by any single spike train.

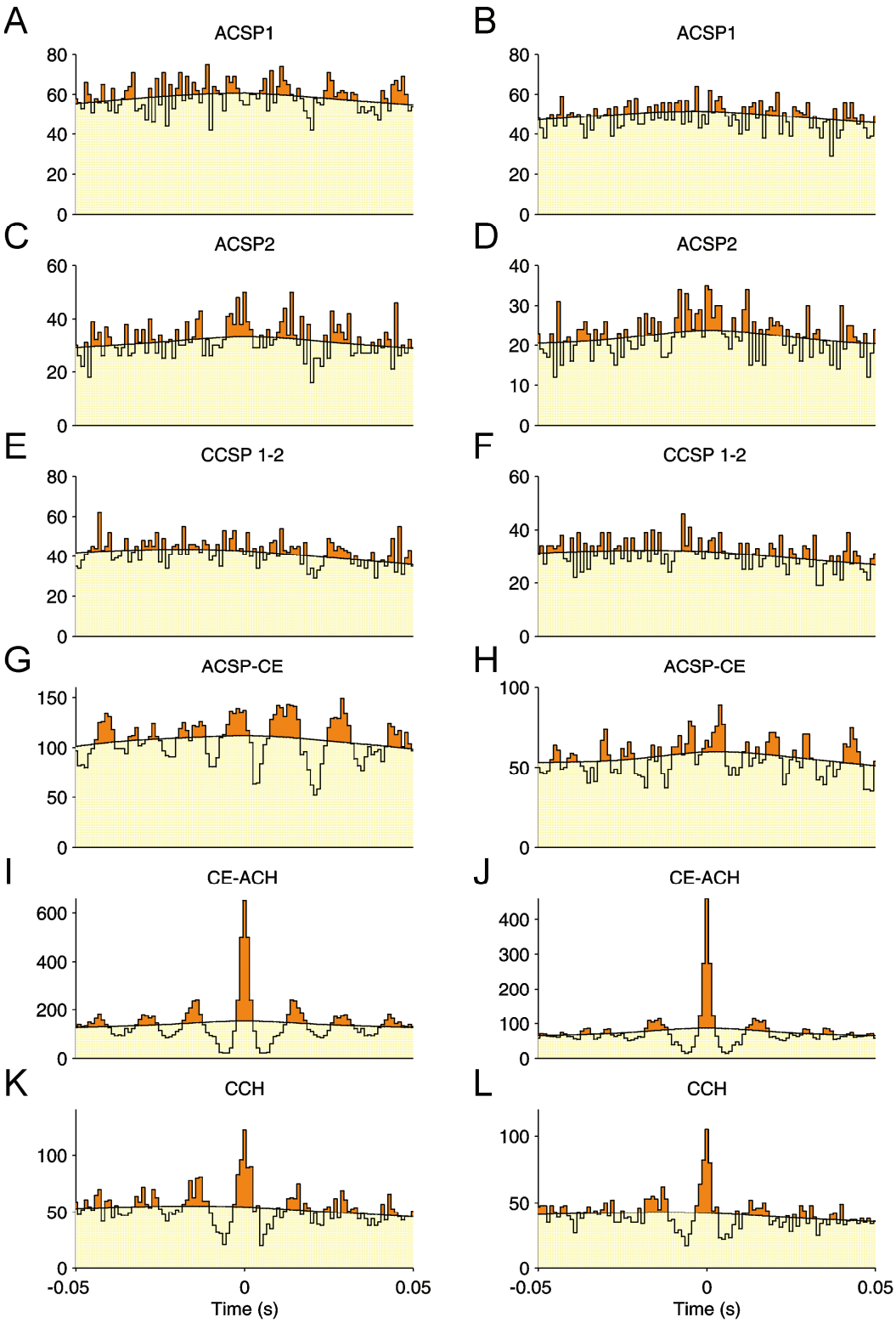

Figure 8. Correlation measures. CEs were better locked to the stimulus presentation during the first trials. Correlation measures are displayed on the left for the first set of trials and on the right for the second one. Auto-correlation shift predictors for each spike train (A,B,C,&D) show that only cell 2 is time locked on the stimulus presentation during the first 5 trials, but that during the second set, no peak was significant. (E&F) Cross-correlation shift-predictors were completely flat. (G&H) Considering CEs as usual events, we calculated an

instantaneous discharge probability (FST-10). Auto-correlation shift predictors of CEs clearly show that CEs are better time locked than any other kind of cellular event, and that it was better time locked during the first set of trials. (I&J) Moreover, the auto-correlation performed on CE train showed six and two significant satellite peaks, whereas only one was significant one each CCH (K&L).

Comparison between the spike cross-correlation histograms and the CE auto-correlation histogram is shown in Fig. 8 I,J,K&L. Although satellite peaks are significant on the CCH, they are much more evident on the CE-ACH. This fact suggests now that CEs encode information much more *regularly* than any spike train. Because the transformation of two spike trains in to one CE train multiplies the spikes when they are coincident and suppresses them when they are not, the actual number of CE could increase, leading to a CE-ACH smoother than the CCH. Once again, all these salient features were absent if an estimate accounting for bursts as firing changes was used (not shown).

The analyses performed to assess the possible clustering of CEs in the global post-stimulus time-average are shown in Fig. 9. Figure 9B shows the response of two cells and the raster of the corresponding CEs during the presentation of a moving stimulus represented in Fig. 9A.

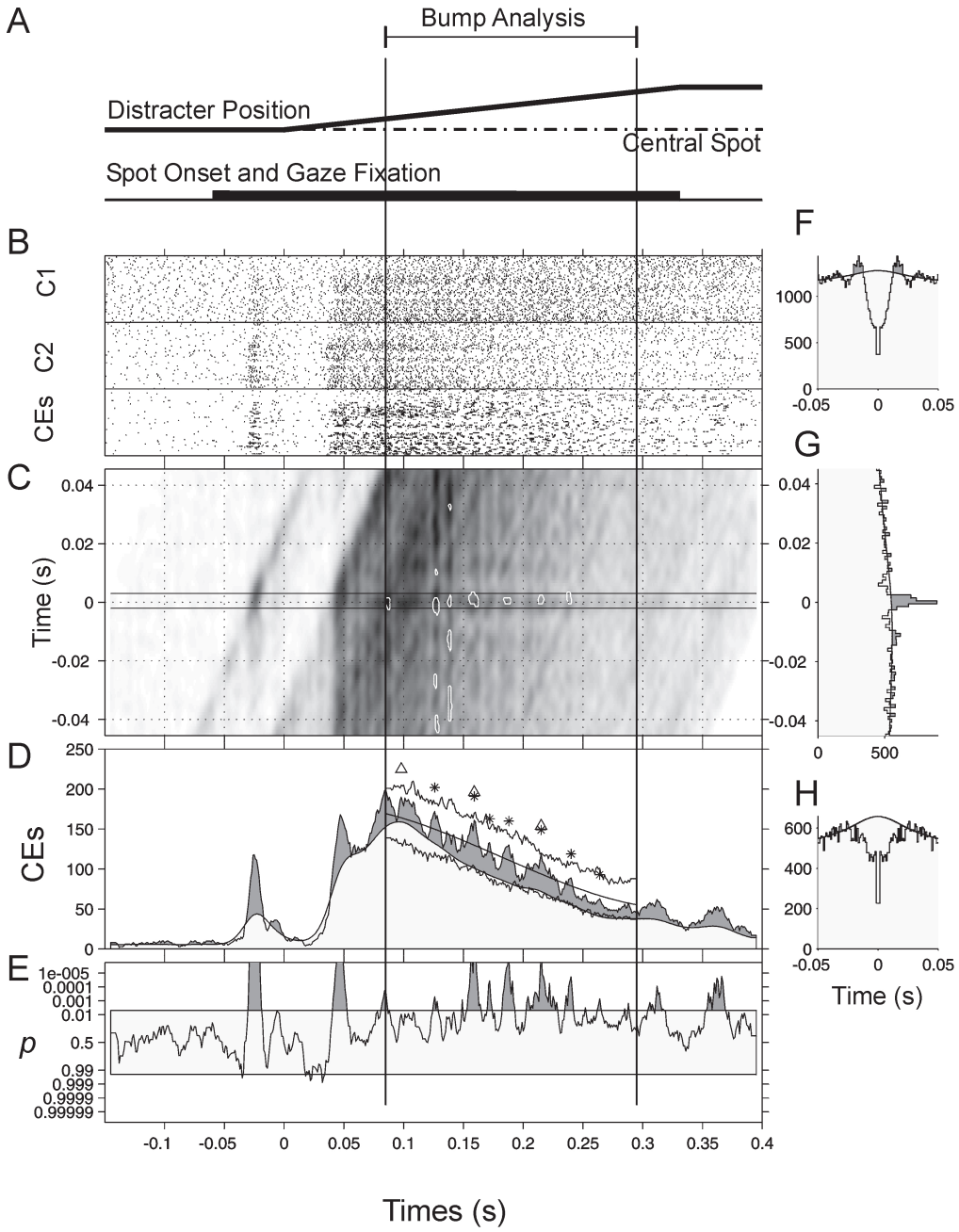

Figure 9. Bump analysis. This figure follows the same display convention as in Fig. 7, with the stimulus configuration (A), spike and CEs rasters (B), TXC in (C), CE count in (D) and the CCH in (G). The ACH for each whole spike trains are shown in (F) and (H). In (E), the significance test of the CE count is plotted as a surprise test : $log_{10}((1-p)/p)$. Each time p-values pass below 0.005, the curve is shaded in dark gray and the corresponding peak in D, receives a star. Superimposed on the observed and expected CE counts in D, are the smoothed estimate of the observed CE count and the envelop of 400 control simulation. Triangles represent peaks which are significant when compared to the filtered CE count ($p<0.05$). The number of simulations exhibiting at least 3 peaks was 77 over 400, showing that such a number of peak is quite common and could occur by chance.

The time-resolved cross-correlation histogram is displayed in Figure 9C. Around 130 ms until 250 ms, the central spots are surrounded by two brighter traces, resembling eraser marks, which are related to two troughs in cross-correlation histogram. Hot spots are well delimited on the zero-lag axis, but irregularly spaced leading to misalignment of the spots at other time

lags. The corresponding auto-correlation histograms are shown in figures 9F&H.The coincidence count (Fig. 9D) was then tested, assuming a Poisson distribution of the coincident events. This is plotted as a surprise measure in Fig. 9E. CE excesses occurred clearly at different moments during the visual stimulation and are represented by the stars in Fig. 9D.

After this, the CE curve is further filtered from 80 ms to the end of the stimulus presentation by convolution with a Gaussian kernel (50 ms SD), and the number of bumps is defined by testing the obtained CE count against its smoothed estimate (α=0.05). A bump was defined by the crossing of the CE count with its smoothed estimate. These bumps are signaled by triangles in Fig. 9D. To estimate the rate of occurrence of such bumps, 400 simulation of 4x60 Poisson trains were generated according to the smoothed CE count, and the bumps were identified for each simulation. The envelop of those simulations is represented in Fig. 9D by two curves starting 80 ms. In this case, 77 simulations out of 400 exhibited a larger or equal number of bumps (p=0.19).

Such a characterization of the temporal distribution of CEs was achieved on 94 pairs and, for each of them, 400 corresponding simulations. The same operation was performed on the expected count of CEs to assess the number of bumps that could be related to firing rate covariations locked on stimulus presentation. This expected number was added to the number of bumps in each simulation, and if the sum was equal or higher than the observed number of bumps in the data, the simulation was counted as positive. The probability to find an equal or higher number of bumps than observed could then be calculated as *n/400*. The expected number of peaks varied greatly with the measure chosen to estimate the instantaneous firing rate (see Table 1) since the more a measure resembled the spike train, the more similar were the expected and observed CE counts, and the more bumps were found in the expected CE count. The distribution of the probability to find more CE bumps in the simulations than in the data is shown in Fig. 10A for the EBP estimate (light gray; Fig. 1F) and the filtered spike train (dark gray, Fig. 1H, FST-10). The percentage of recordings with $p<0.05$ was 2.4 % and 33.3 % respectively. The differences with the expected 5 % were significant only for the second estimate ($p<10^{-9}$): the CEs tend to cluster at some moments during the stimuli presentation if rapid firing rate changes are present in the data. The values corresponding to the FBBP-4 estimate can be found in Table 1 and are intermediate.

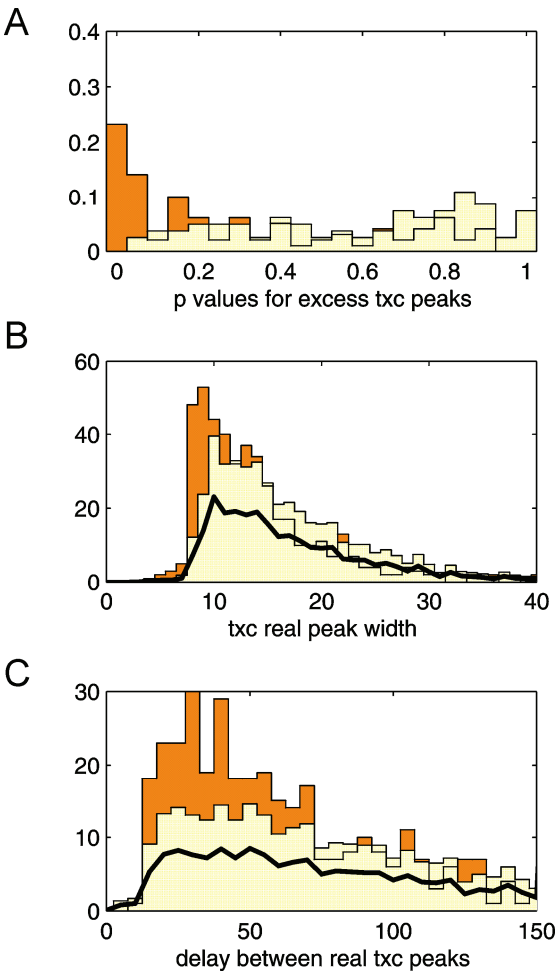

Figure 10. CE clustering. If the CE count exhibited one real peak, that is if it exceeded the CE smoothed count with significance level of 0.05, 400 simulations were run to estimate if such a number of peaks could have occurred by chance. The distribution of the significance levels on the number of peaks are displayed in (A) when the EBP estimate (light gray) or the FST-10 estimate were used to calculate the expected number of CEs. The differences between these distributions are due to the fact that EBP estimate partly accounts for bursts as firing rate changes, whereas the FST-10 estimate did not. (B) Peaks were characterized by intersections with the smoothed CE count (Gaussian SD 50ms, triangles in Fig. 9D). Dark gray histogram is the observed peak width distribution. Distribution from ten control simulations is represented by the solid line and scaled for compensation of the number of peaks found on the expected CE count (EBP; light gray). (C) Using the same conventions, the distributions of delays between peak maximums. Peaks in excess had a width ranging from 6 to 12 ms and they were separated by delays ranging from 15 to 70 ms. Although the number of peaks was not significantly increased in the data when compared to paired simulations, on average their distribution was different.

Distribution of bump width, defined by the closest intersections of the CE count with its the filtered count, is displayed in Fig. 10B. Dark gray histogram represents real data, while the solid line represents the mean value obtained for 10 simulations. The bump count of the simulated data was then increased for bumps observed in the expected CE count (obtained with EBP) and represented by the light gray histogram. Bump width in the data is clearly shifted toward 8 to 14 ms. Following the same conventions, the delays between two successive bumps are shown in Fig. 10C. Original bumps were separated more often by delays that spanned from 10 to 70 ms than bumps found in the simulations. Although CEs were more clustered because of the presence of bursts, they also exhibit another distribution than would a Poisson process.

In conclusion, most of our CCH peaks were isolated or flanked by significant troughs but only a few oscillatory patterns were found. Moreover CE clustering seems probably more dependent on the presence of bust discharge than on time locking on the stimulus presentation because no CE clustering can be found after burst filtering.

Since it is known for a long time that isolated CCH peak could be due to common input, we studied this possibility using the simple counting model proposed by Shadlen and Newsome (1998) in a regime of balanced excitation and inhibition. We reproduced the effect of shared excitation-inhibition on their model (Fig. 11A). Inputs were modeled by 300 Poisson trains of which 40 percent were common to both cells. Each excitatory event increased the cell count by one, and each inhibitory event decreased this count by one. As previously shown by Perkel et al. (1967), shared inputs produce a peak in the CCH. In this model, the peak width is similar to the input duration rather than to the membrane time constant (20 ms). We propose then that inhibition is mainly conveyed by a few somatic inputs. In Fig. 11B, the inhibitory inputs were totally shared and restricted to only 30 Poisson trains while the common excitatory drive was suppressed. Moreover, we increased the duration of the inhibitory inputs to 5 ms, which produced a broader CCH peak (strength: 2.2 counts). As expected from Perkel et al. (1967), the CCH exhibited a peak, but no trough. In order to imitate a delayed inhibitory feedback, the excitatory inputs to cell 1 were scaled, rounded, and delayed by 10 ms to produce the common inhibitory inputs. Next to the central peak appeared a trough (Fig. 11C). Meanwhile, the firing rate decreased because the variance of inhibitory inputs was reduced. If the inhibitory drive was constructed by averaging both excitatory sources, the central peak appeared to be surrounded by symmetrical troughs (Fig. 11D). Figure 11D suggests that oscillations are not required to produce collateral troughs in a CCH and that a common inhibitory feedback – probably mediated by local interneurons – could explain most of our CCH patterns. Oscillation could be added to the model if the inhibitory feedback becomes oscillatory, as is the case when inhibitory interneurons are connected (Whittington et al, 1995; Wang and Buszaki, 1996; Pauluis et al., 1999). Oscillations could also alleviate the problem of the variance on inhibitory inputs because oscillations would ensure a minimum input fluctuation.

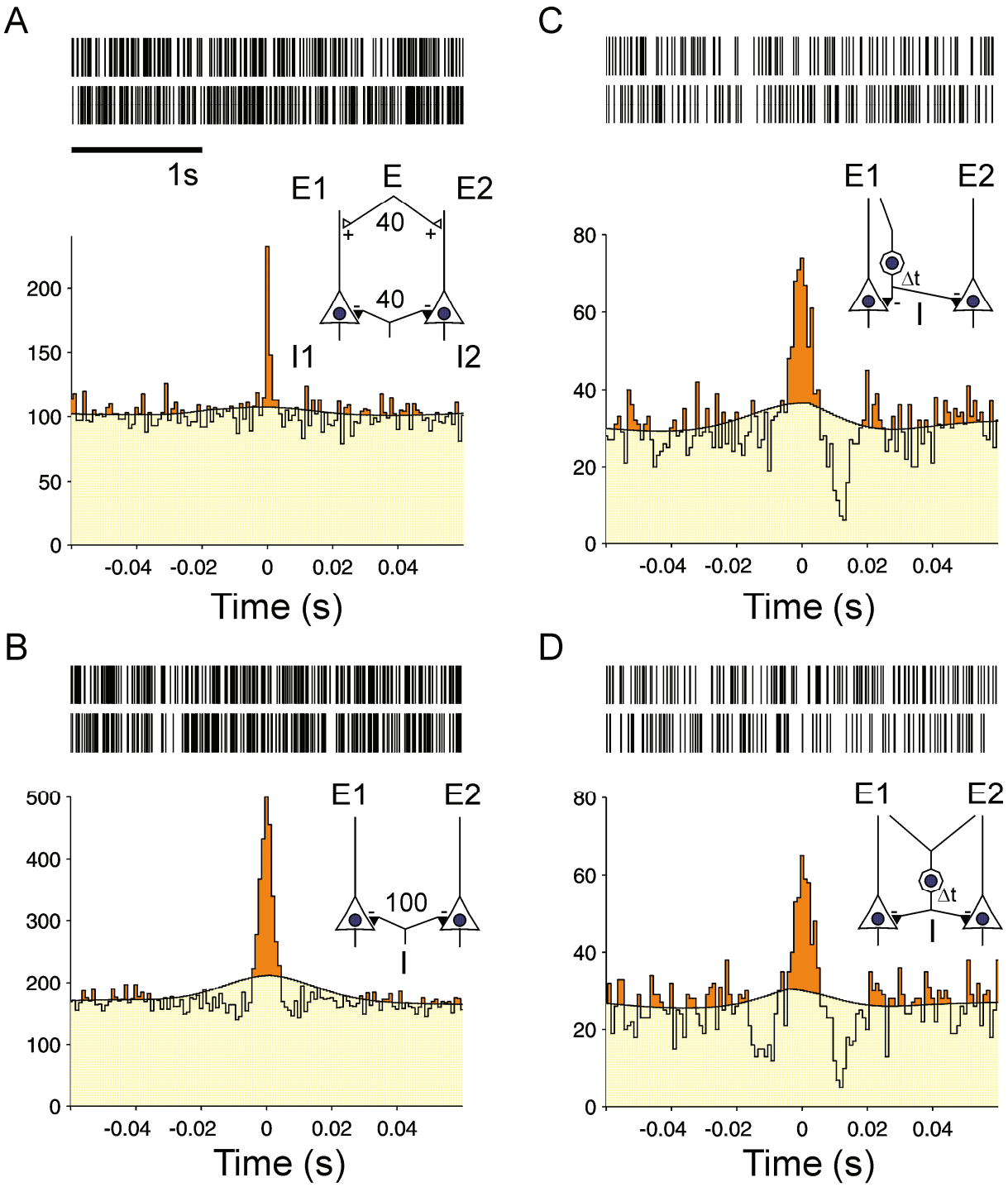

Figure 11. Balanced excitation-inhibition in simple counting neurons. Two cells are simulated after the simple counting model proposed by Shadlen and Newsome (1998). Inputs are modeled by independent random trains of events with an exponential distribution (Poisson process) and a frequency of 50 Hz. The cell receives these random excitatory and inhibitory inputs which increment or decrement the count by one unit. If the count reaches a threshold of 15, the cell is emitting a spike and the count is reset to zero. The count can not be negative and decays exponentially with a time constant of 20 ms. (A) This simulation reproduces the conditions of Fig.8E in Shadlen and Newsome (1998) except for the CCH bin width which here of 1 ms. Each cells receives a total 300 trains of excitatory inputs from two independent sources (E1,E2) and a common one. Among the 300 trains an average of 75 are identical for both cells (E, 40%), and 225 are different (E1, E2). Inhibitory inputs are constructed similarly. The resulting spike trains are shown in the upper part of the figure and represents the first three second of the 20 second stimulation (1 ms time step). The common excitatory and inhibitory inputs produce a sharp central peak. (B) The common source of excitatory inputs is removed and each cell receives 300 independent excitatory trains. There is only one source of common inhibitory inputs. In order to reflect the

somatic inhibition, the number of inhibitory trains is reduced to 30, the input duration is prolonged to 5 ms, and a single inhibitory input cancels now 2.2 excitatory ones at each time step. The resulting cell frequency is close to 90 Hz, and the central peak is now 9 ms broad. (C) As in a network of excitatory and inhibitory cells, the inhibition depends somehow on the network input, we used here the first source of excitatory inputs (E1) to produce the common inhibitory drive after linear scaling (1/10), rounding to the nearest integer, and adding some delay (10 ms). The inhibition is still a time series, but the variance is decreased, which decreased the firing rate of both cells to 37 and 38 Hz. Although the peak also decreased, there is now a clear trough after 10 ms. (D) If both independent excitatory sources are averaged to the produce the common inhibitory drive, the central peak is flanked of symmetrical troughs, as in many experimental CCHs which fail to have significant satellite peaks. This suggests that a common delayed inhibitory feedback could easily explain most of our data.

It is interesting to notice that the situation can be reversed. It has been suggested that inhibitory neurons could prime the network activity (Pauluis et al., 1999). If the inhibitory inputs preceded the excitatory ones, the peak in CCH was still flanked by two troughs (data not shown). The peak exhibited a slightly smaller amplitude (58 spikes.bin^{-1}) and troughs were restricted to +/-12 ms.

3.5 Single trial analysis

In the previous section, we have shown that CEs tended to be temporally clustered in 8-14 ms packets separated by delays varying from 10 to 70 ms. Our method allows inspection and significance assessment of single trial provided that enough spikes were collected.

Figure 12 illustrates how the CEs count varies with trial repetition for the experiment of Fig.7 (Fig. 12A&B) and for the other recordings (Fig.12C). Experiment presented in Fig. 7 was made up of 80 trials of 300 ms that were represented sequentially along the abscissa in Fig. 12A. The observed number of CEs is described by the dark gray histogram, and the expected CE count by the overlying light gray area. Obviously, cells discharged much during the first trials, as shown by the high expected CE count.

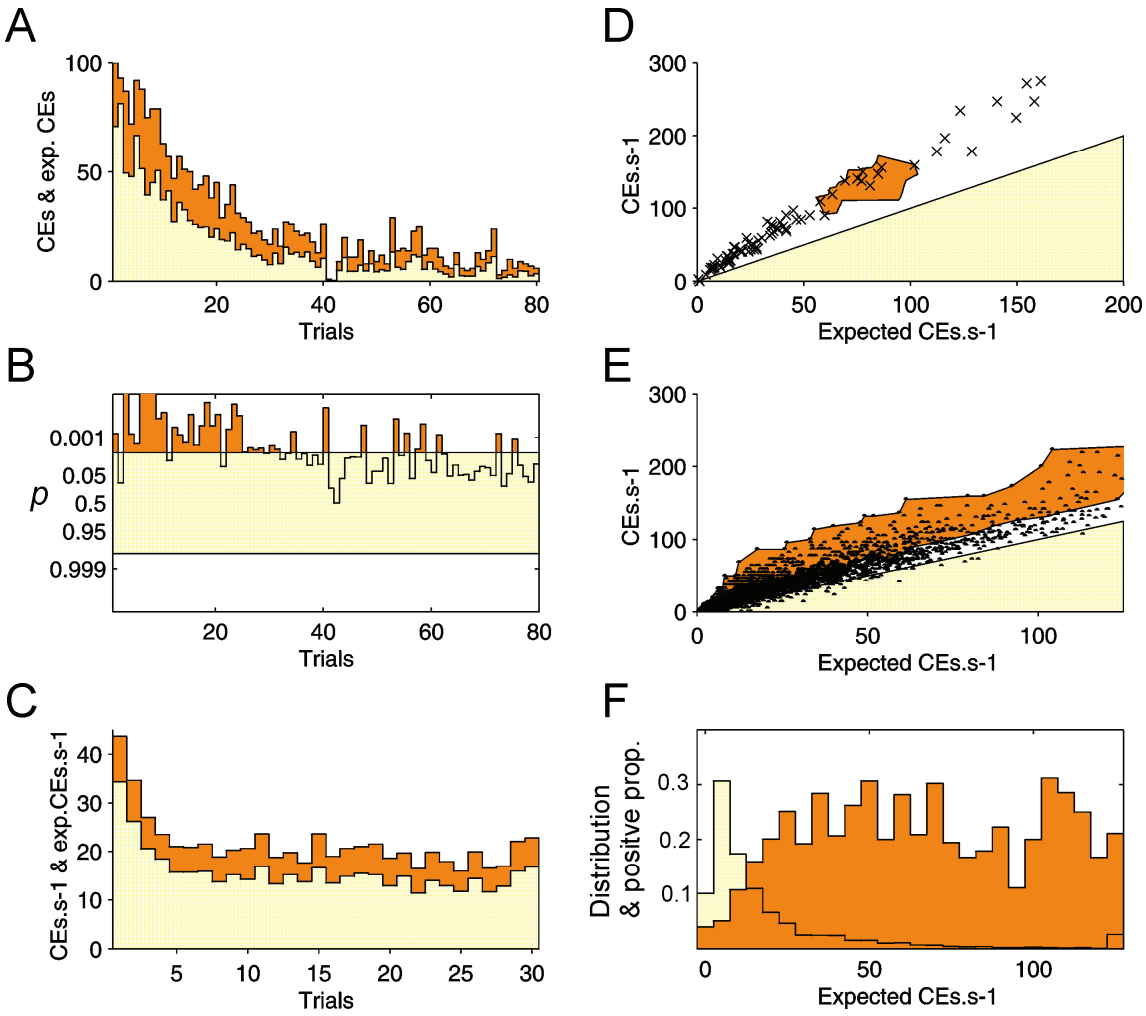

Figure 12. Trial repetition. Instantaneous discharge probability estimates allow quantification of the CE excess on a single trial basis. (A) CEs (dark gray) and expected CE count (light gray, FST-10) are shown for all trials of the experiment in Figs. 9&10. In these figures, the first set was composed of trial 5 to 9, and second one of trial 10 to 14. They were situated in the period during which the stimulus efficacy decreased. (B) The surprise test on each trial was positive more often during the first part of the experiment than during the second one. (C) CE count and expectation were averaged for all experiments presenting at least one CCH peak and composed of 31 to 40 trials. The decrease occurred within the first five trials. This contrasts with (A) but this experiment was the first of the day and uncontrol phenomenon like atention could have been longer sustained. (D) The relationship between the CE rate and the expected CE rate is represented by a cross for each trial. The dark gray area represents this relationship averaged across trials but varying during the presentation (like the curve of Fig.9D). The light gray triangular area corresponds a ratio less than one (unity line). (E) Dots represent each trials of all the experiments with at least one significant CCH peak. All the significant trials are regrouped in the shaded area. Since the CE rates are described, most but not all the dots in the shaded area were significant trials. (F) The global distribution of the expected CE rate is shown in light gray, and the corresponding proportion of positive trials is shown in dark gray. Whereas the trials were more often found positive if the expected firing rate was higher than 25 CEs.s^{-1}, most of the trials had an expected CE rate below 10 CEs.s^{-1}.

The surprise test for each trial is presented in Fig. 12B. This experiment was the first one of the day, so attention was probably long sustained at the beginning of the session. Attentional and related effects usually take place within a few seconds. CE rates from recordings with a significant cross-correlation peak were averaged sequentially trial by trial. Figure 12C shows this average for 108 experiments composed of 30 to 40 trials (average trial duration : 1s).

Cells are usually more responsive to the first five trials. However, these trials failed to be significant more often than the others. Even though, these results suggest that the more CEs were expected, the more CEs were obtained. There was always an excess of synchrony and, on the time scale of a single trial, CE count and expected CE count were related to each other. Such a strong relationship favors the hypothesis of a common input as responsible for both the cell discharges and their synchrony.

Figure 12D shows explicitly this relationship between observed CE and expected CE rate for the trials of Fig. 12A. Each cross represents one trial, and the dark gray area is spanned by the CE rate when averaged across trials (the equivalent of the gray curves in figure 7D). The relationship is fairly linear. This is further exemplified in Fig. 12E, where all the trials from recordings with a significant cross-correlation peak are plotted. The shaded area now represents part of the trials with a significant CEs excess. Not all trials in this area were significant since trial duration had also to be taken into account for significance calculation. The CE rate stayed below 100 Hz for most of the trials. Figure 12F plots the density histogram of the expected CE rate for each trial (light gray) and the corresponding proportion of significant trials (dark gray). This relationship shows that the expected CE rate influenced the chance to obtain a significant CE excess below a determined level, and consequently, chance to obtain a CE excess varied with cell firing rates under this level. Most of the recordings (78%) with a significant cross-correlation peak exhibited less than 20% of significant trials. Although, our simple sensory paradigm did not permit to relate those trials to any behavioral parameter, it is probable that it was simply related to the low expected CEs rate in most trials.

4. Discussion

4.1 Methodological considerations

The method developed in this study offers many advantages over the usual JPSTH method. Firstly it is able to cope with highly non-stationary data since the CE estimate is adjusted for each trial separately. Nearly every trial can be included securely to the raster, even if cells responded much less or much more than usual. Such trials with covariant and unexplained discharge variations are pernicious when included in JPSTH since they are not described adequately by the PSTH and consequently bias the CE expectation. This leads to the

assessment of large cross-correlation peaks due to patterns of covariant activities (Brody 1999a,b; Pauluis and Baker, 1999). A way to control for this problem is to show that the expected CCH offset fits well the observed CCH offset for the each period of the experiment. Even tough, this simple display is discarded in some CE analysis (Rhiele et al, 1997). The method used here is based on the calculation of the CE expectation for each single trial and compensates very simply for this kind of problems. Secondly, it also offers a quantitative approach of significance testing for any correlation measure, and for the first time for the shift predictor, which was quantified previously by recursion or by comparison with the shuffled predictor. Thirdly, the use of different instantaneous discharge density estimates permits to separate the effects on synchrony due to bursts from those due to single spikes. Table 1 shows that bursts influence indeed most correlation analysis. Fourthly, it allows trial by trial CE significance calculation, an ability that permitted to quantify the effect of trial repetition and of which more sophisticated paradigms could make use.

4.2 Synchronization in the superior colliculus

Brecht et al. (1996, 1998) reported previously that synchrony take place in the SC of the anesthetized cats on a wide temporal basis : the mean width at half height was of 51 ms for cortico-tectal interactions and similar values were reported for intra-collicular interactions (>20 ms). However, Brecht et al. (1998) assessed CCH peaks by fitting a generalized Gabor function on the CCHs (König et al., 1994) and excluded all the recordings with a non-flat CCH-SP. Broad peaks could possibly be better identified than thin ones because the fitted curves had to explain only 20% of the variance of the CCH.

Data in awake cats are much different since the peak width at half height was on average 5 ms. This is a change from one peak type to another (Nelson et al. 1992; Nowak et al., 1995): “hills” and “castle” structures in the anesthetized cat apparently become “towers” when the animal is awake, and temporal relationship changes from a co-activation pattern to real synchrony. In this study we never found a peak larger than 15 ms at half-height that was not expected by the firing rate.

Although we found oscillations in ACHs, and some regularity in CE patterns, most the CCHs exhibited a unique central peak. This would be interpreted, if recording were made in the visual cortex, as a lock-in state (Eckorn, 1994) which probably corresponds to sub-optimal stimuli. Because of constraints on the length of recordings in awake animals, our stimuli

parameters were only broadly tuned, if not fixed like the spot shape. Moreover, attention and motivation decreased during the experiment leading to a decrease of the response to the stimulus. Whereas attention modulates the visual response in the SC (Goldberg and Wurtz 1972), it has been shown that stimulation of the mesencephalic reticular formation increases visually evoked oscillation in anesthetized and awake cat (Metherate et al. 1992; Munk et al., 1996; Steriade et al., 1996). However habituation is probably also a potent phenomenon in the SC, which prevented recording of visual response of deep layers neurons. The visual response of such output neurons decreased dramatically at the second trial, as a consequence that stimuli had to be new and interesting on each presentation, and any response averaging was prevented.

The second explanation which could account for the absence of a regular oscillatory process, is that the input to the SC was varying strongly during the task. The oscillations could have occurred but their frequency would have been too irregular to be significant in the CCH. The third hypothesis refers to the connections between inhibitory interneurons, which are necessary to produce the oscillations (Whittington et al. 1995; Wang and Buzsaki, 1996; Pauluis et al., 1999). Their number could be smaller in the SC than in the visual cortex, possibly because the visual map in the SC is less complicated than the columnar organization of the visual cortex and because of the probable uselessness of coding simultaneously, and for a long duration, two different objects in the SC. Indeed the SC could function as an attentional filter which selects a single target for rapid orientation movement. As shown by Basso and Wurtz (1997), it could be achieved simply by a modulation of the firing rates.

4.3 Temporal coding by Coincident Events

In our study, all the CCH shift predictors were flat, meaning that cross-correlation peaks were due exclusively to neuronal connectivity and common input that was not time-related to the stimulus. This extreme interpretation has to be tempered by the fact that cross-correlation peaks could be not large enough to show weak locking on the stimulus presentation, or inversely, the effect of this locking could be too weak to be uncovered by the analysis of covariance between two cell discharges. We have shown that CEs could be time locked on the presentation since many of their auto-correlation shift predictors were significantly peaked. However it can not be decided to what extend these results were due to the bursting discharge of SC cells and the restricted amount of available data, or to real stimulus locking. One the one hand, this means that CEs could code stimulus locked information better than isolated

spikes, and thus this fact could provide a strong argument for temporal coding in the SC. On the other hand, it alerts on possible artifacts arising from bursting spike trains.

Time locking has been described in response to a sudden change in the stimulus presentation (Mainen and Sejnowski, 1995). It was also reported that most cells in the cat LGN and visual cortex could synchronize strongly on a 60 Hz monitor refresh rate (Wollman and Palmer 1995). Such evident causes of fast stimulus locking are unlikely during our stimulus presentation since we used an oscilloscope with a position increment rate of 100 Hz, and SC oscillations were described with a frequency of 65 Hz. We also took care to start analysis after the fast transient due to movement ignition and we also excluded the stimulus offset because such events would have locked the cell discharge. It was shown recently that fixational eye movements can cause large response modification in the firing rate of visual cells in the primary cortex and lateral geniculate nucleus (Gur et al, 1997). The are however no reason for these very small movements to occur in stimulus-locked fashion.

This implies that the distinction between stimulus locked synchronization and rhythmic stimulus-non-locked oscillations could be not as straightforward as previously thought (Eckorn 1994). The independence of oscillatory phases from the stimulus presentation were usually assessed by the shuffled or shift predictor of spike trains or by stimulus-locked temporal averaging of local field potentials (Eckhorn et al., 1988; Gray et al. 1989a&b; Neuenschwander and Singer 1996). Whereas oscillatory synchronization that are time locked on the stimulus presentation are quite common in the auditory and the olfactory system (Epping and Eggermont, 1987; Laurent 1996), this phenomenon was evidenced in the visual system on very few occasions by the shift predictor, but was discarded (Bringuier et al., 1997) or usually subtracted to the CCH (Schwartz and Bolz, 1991; Nowak et al., 1995). Kruse and Eckhorn (1996) isolated the oscillatory component using the cross-spectra of the shift-predictor calculated on the local field potential or on the multi-unit activity. They showed that in the anesthetized cat, the stimulus locked power spectrum is nearly flat for slow stimulus movements when compared to the power or cross-power spectra. This is the similar to comparing oscillations in the CE-ACH and in the CE-ACH-SP (Fig. 8G,I,H&J). It does not ensure of the absence of small significant peak in the shift predictor.

Although it is possible that, in the awake animal, cognitive processes or attention shifts over a few hundreds of milliseconds would produce transient responses which covary with the stimulus presentation, we point out that CE trains are much less linear than spike trains and local field potentials. Events are added if bursts coincide, and events disappear if no

correlation is present. CE train was thus constructed by creating new events and by deleting some others, leading to a high contrasted signal. As a consequence, correlation measures performed on CEs were probably much more sensitive to any periodicity or time locking. In a sense, MUA and LFP analysis corresponds to testing the hypothesis of population coding by averaging all activities, whereas CE testing implies coding by coincidence detection.

It CEs are really time-locked on the stimulus presentation, then action potential were not random variables and participated in a complex information processing which relied on reproducible CEs. Since, there could be a temporal code in the largest sense. Whether it really means something or is a by-product of a local selection or attentive process can not be decided.

4.4 Temporal pattern processing

Parodi et al. (1996) proposed that a temporal coding network needs, in the case of motion analysis, a periodical reset to avoid information jamming. This resetting could be performed via a delay loop of adjustable length. In our model (Pauluis et al. 1999), this reset would have been provided by a strong inhibitory feedback from interneurons. The existence and the effect of such strong inhibitory input compared to the excitatory conductance is a matter of debate (Douglas et al., 1995; Holt and Koch, 1997). Recently, *in vivo* whole cell voltage clamping showed a dramatic increase of the somatic input conductance in response to optimally oriented flashed light bars (Borg-Graham et al., 1998). This very potent mechanism mediated by the inhibitory interneurons produces a current shunt that decreases dramatically the amplitude of the excitatory response.

When repetitive comparison is required, information related to temporal pattern is discretized at a frequency that depends grossly on the network activation. Each phase becomes a way to select the best responsive cells and to limit combinatorial possibilities (Laurent, 1996). Such a selection could be related to the synfire chain theory (Abeles 1991) as a node selection process. Since we used a simple sensory paradigm, we are not allowed to extend our hypothesis further. Although binding theory itself remained unquestioned in this study, we shown that local networks tend to synchronize probably in response to a common feedback inhibition and that this synchrony could be stimulus related. Indeed, CEs seemed to be more often time locked on the stimulus presentation than single spikes. This could provide a new way to assess temporal coding by CE train analysis. However, bursting data must be handled

with great care and, in this study, prevented any definitive conclusion since CE time-locking was very sensitive to the use of precise instantaneous discharge estimates and to burst filtering.

List of Abbreviations

ACH: auto-correlation histogram

CCH: cross-correlation histogram

CE: coincident event

DS: distracter point

EBP: instantaneous discharge estimate with extended breakpoints

FISIR: filtered ISI reciprocal

FP: fixation point

FSP: filtered spike train

ISI: interspike interval

PSTH: post-stimulus time histogram

RMA: relative modulation amplitude

SBBP: instantaneous discharge estimate which is smoothed between breakpoints

SC: superior colliculus

SP: shift predictor

TXC: time-resolved cross-correlation

REFERENCES

Abeles M (1991) Corticonics: neural circuits of the cerebral cortex. Cambridge University Press, Cambridge.

Aertsen, A.M.H.J., Gerstein, G.L., Habib, M.K., & Palm, G. (1989). Dynamics of neuronal firing correlation: modulation of "effective connectivity". *J Neurophysiol.*, 61: 900-917.

Basso MA, Wurtz RH (1997) Modulation of neuronal activity by target uncertainty. *Nature* 389:66-69.

Borg-Graham LJ, Monier C, Frégnac Y (1998) Visual input evokes transient and strong shunting inhibition in visual cortical neurons. *Nature* 393:369-373.

Brody C.D. (1999a) Disambiguating different covariation types. *Neural Comput. (submitted).*

Brody C.D. (1999b) Latency, excitability, and spike timing correlations. *Neural Comput. (submitted).*

Bush P, Sejnowski T (1996) Inhibition synchronizes sparsely connected cortical neurons within and between columns in realistic network models. *J. Comput. Neurosci.* 3: 91-110.

Cattaneo A, Maffei L, Morrone C (1981) Patterns in the discharge of simple and complex visual cortical cells. *Proc. R. Soc. Lond. B* 212:279-297.

DeBusk BC, DeBruyn EJ, Snider RK, Kabara JF, Bonds AB (1997) Stimulus-dependent modualtion of spike burst length in cat striate cortical cells. *J. Neurophysiol.* 78:199-213.

Douglas RJ, Koch, C, Mahowald M, Martin KAC, Suarez HH (1995) Recurrent excitation in neocortical circuits. *Science* 269:981-985.

Eckhorn R (1994) Oscillatory and non-oscillatory synchronizations in the visual cortex and their possible roles in associations of visual features. *Prog. Brain Res*. 102:405-425.

Eckorn RE, Bauer R, Brosch M, Kruse W, Munk, M, Reitboeck HJ (1988) Coherent oscillations: A mechanism of feature linking in the visual cortex ? *Biol. Cybern.* 60:121-130.

Epping WJM, Eggermont JJ (1987) Coherent neural activity in the auditory midbrain of the Grassfrog. *J. Neurophysiol.* 57:1464-1483.

Goldberg ME, Wurtz RH (1972) Activity of superior colliculus in behaving monkey. II. Effect of attention on neuronal responses. *J. Neurophys.* 15:560-574.

Gray CM, Engel AK, König P, Singer (1990) Stimulus-dependent neuronal oscillations in cat visual cortex : Receptive field properties and feature dependence. *Eur. J. Neurosci*. 2: 607-619.

Gray CM, König P, Engel AK, Singer W (1989) Oscillatory responses in cat visual cortex exhibit inter-columnar synchronization which reflects global stimulus properties. *Nature* 338:334-337.

Gray CM, Mc Cormick DA (1996) Chattering cells: superficial pyramidal neurons contributing to the generation of synchronous oscillations in the visual cortex. *Science* 274:109-113.

Gray CM, Viana Di Prisco G (1997) Stimulus-dependent neuronal oscillations and local synchronization in striate cortex of the alert cat. *J. Neurosci*. 17: 3239-325.

Gur M, Beylin A, Snodderly DM (1997) Response variability of neurons in primary visual cortex (V1) of alert monkeys. *J. Neurosci.* 17:2914-2920.

Holt GR, Koch C (1997) Shunting inhibition does not have a divisive effect on firing rates. *Neural Comput.* 9:1001-1014.

Koch, C., Rapp, M., & Segev, I. (1996). A brief history of time (constants). *Cereb. Cortex* 6: 93-101.

König P (1994) A method for the quantification of synchrony and oscillatory properties of neuronal activity. *J. Neurosci. Meth*. 54: 31-37.

Laurent G (1996) Dynamical representation of odors by oscillating and evolving neural assemblies. *Trends Neurosci.* 19:489-496.

Lisman JE (1997) Burst as a unit of neural information: making unreliable synapses reliable. *Trends Neurosci.* 20:38-43.

Livingstone MS (1996) Oscillatory firing and interneuronal correlations in squirrel monkey striate cortex. *J. Neurphysiol.* 75: 2467-2485.

Lytton WW, Sejnowski TJ (1991) Simulations of cortical pyramidal neurons synchronized by inhibitory interneurons. *J. Neurophysiol*. 66: 1059-1079.

Mainen ZF, Sejnowski TJ (1995) Reliability of spike timing in neocortical neurons. *Science* 268:1503-1506.

Metherate R, Cox CL, Ashe AH (1992) Cellular bases of neocortical activation: modulation of neural oscillations by the nucleus basalis and endogenous acetylcholine. *J. Neurosci.* 12:4701-4711.

Munk MHJ, Roelfsema PR, König P, Engel AK, Singer W (1996) Role of reticular activation in the modulation of intracortical synchronization. *Science* 272:271-274.

Neuenschwander S, Singer W (1996) Long-range synchronization of oscillatory light responses in the cat retina and lateral geniculate nucleus. *Nature* 379:728-733.

Nowak LG, Munk MHJ, Nelson JI, JamesAC, Bullier J (1995) Structural basis of cortical synchronization. I. Three types of interhemispheric coupling. *J. Neurophysiol.* 74:2379-2400.

Nelson JI, Salin PA, Munk MHJ, Arzi M, Bullier J (1992) Spatial and temporal coherence in cortico-cortical connections: across-correlation study in areas 17 and 18 in the cat. *Visual Neurosci.* 9:21-37.

Palm G, Aertsen AMHJ, Gerstein GL (1988) On the significance of correlations among neuronal spike trains. *Biol. Cybern.* 59:1-11.

Parodi O, Combe P, Ducom JC (1996) Temporal coding in vision: coding by the spike times arrival leads to oscillations in the case of moving target. *Biol. Cybern.* 74:497-509.

Perkel DH, Gerstein GL, Moore GP (1967) Neuronal spike trains and stochastic point process. II. Simultaneous spike trains. *J. Biophys*. 7: 419-440.

Riehle, A., Grün, S., Diesmann, M., & Aertsen, A. (1997). Spike synchronization and rate modulation differentially involved in motor cortical function. *Science*, *278*: 1950-1953.

Ritz R, Sejnowski (1997) Syncronous oscillatory activity in sensory systems: new vistas on meachanisms. *Curr. Opin. Neurobiol.* 7: 536-546.

Roelfsema PR, Singer W (1998) Detecting connectedness. *Cereb. Cortex* 8:385-396.

Roucoux A, Crommelinck M (1976) Eye movement evoked by superior colliculus stimulus in the alert cat. *Brain Res.* 97:95-107.

Schiller PH, Stryker M, Cynader M, Berman N N (1974) Response characteristics of single cells in the monkey superior colliculus following ablation or cooling of the visual cortex. *J. Neurophysiol.* 37:181-194.

Schwartz C, Bolz J (1991) Functional specificity of a long-range horizontal connection in cat visual cortex: a cross-correlation study. *J. Neurosci.* 11:2995-3007.

Shadlen M.N, Newsome WT (1994) Noise, neural codes and cortical organization. *Curr Opin. Neurobiol.*, 4: 569-579.

Shadlen MN, Newsome WT (1998) The variable discharge of cortical neurons: implications for connectivity, computation, and information coding. *J. Neurosci.* 18:3870-3896.

Silverman BW (1986) Density estimation for statistics and data analysis. London: Chapman & Hall.

Singer W (1995) Development and plasticity of cortical processing architectures. *Science* 270: 758-764.

Singer W, Gray CM (1995) Visual feature integration and the temporal correlation hypothesis. *Annu. Rev. Neurosci.* 18: 555-86.

Sparks DL (1986) Translation of sensory signals into commands for control of saccadic eye movements: role of primate superior colliculus. *Physiol. Rev.* 66:118-170.

Steriade M, Amzica F, Contreras D (1996) Synchronization of fast (30-40 Hz) spontaneous cortical rhythms during brain activation. *J. Neurosci.* 16:392-417.

Traub RD, Whittington MA, Colling SB, Buzsáki G, Jefferys JGR (1996) Analysis of gamma rhythms in the rat hippocampus in vitro and in vivo. *J. Physiol.* 493: 471-484.

Vaadia E, Haalman I, Abeles M, Bergaman H, Prut Y, Slovin H, Aertsen A (1995) Dynamics of neuronal interactions in monkey cortex in relation to behavioural events. *Nature* 373:515-518.

van Vreeswijck C, Sompolinski H (1998) Chaotic balanced state in a model of cortical circuits. *Neural Comput.* 10:1321-1371.

Wang XJ, Buzsáki G (1996) Gamma oscillation by synaptic inhibition in a hippocampal interneuron network model. *J. Neurosci.* 15:6402-6413.

Whittington MA, Traub RD, Faulkner HJ, Stanford IM, Jefferys JGR (1997) Recurrent excitatory postsynaptic potentials induced by synchronized fast cortical oscillations. *Proc. Natl.Acad. Sci. USA* 94: 12198-12203.

Whittington MA, Traub RD, Jeffereys JGR (1995) Synchronized oscillations in interneuron networks driven by metabotropic glutamate receptor activation. *Nature* 373: 612-615.

Wickergen BG, Sterling P (1969) Influence of visual cortex on receptive fields in the superior colliculus of the cat. *J. Neurophysiol.* 32:16-23.

Wilson HR, Cowan JD (1972) Excitatory and inhibitory interactions in localized populations of model neurons. *Biophys. J.* 12: 1-24.

Wollman DE, Palmer LA (1995) Phase locking of neuronal responses to the vertical refresh of computer display monitor in cat lateral geniculate nucleus and striate cortex. *J. Neurosci. Meth.* 60:107-113.

Wurtz RH, Goldberg ME, Robinson DL (1982) Brain mechanisms of visual attention. *Sci. Am.* 246:124-135.

Chapter 5 Conclusion

The work presented in this thesis presents a startling contrast between today's opportunity to produce complex network models and the difficulty in analyzing information processing in real data.

The first part of this thesis demonstrated the major role of a few strong inhibitory connections in the dynamics of a large neural network. The amazing technical progress in computer science allows testing of precise hypotheses about neuronal network organization, but also the search for statistical evidence of coherence in real data, as exemplified by Chaps. 3 and 4. We developed a new method to assess significance of the coincident events. Recordings in the SC showed that during the presentation of a moving light spot, there was an excess of synchrony between neighboring cells. The original method allowed identification of the moment during the trial or the individual trials when the excess was more prominent, even if the data were non-stationary. By filtering the rapid cell discharge during bursts of activity or by simulating some spike trains paired with the data, we were also able to isolate the effects of isolated spikes and burst discharges on the coincident event detection and on the occurrence of oscillatory discharge in the SC. Oscillations and clustering of coincident events were indeed closely linked to the presence of high frequency bursts in the cell discharge.

1. Continuation

The method for assessment of coincidence in non-stationary data is expected to have a wide application in electrophysiology and cognitive neuroscience. It could be further developed in order to analyze more than two simultaneous spike trains and the repetition of complex spike patterns.

The possibility that coincident events are better time locked on the stimulus presentation than isolated spikes is an important argument in favor of precise spike timing in the SC. It deserves to be tested in the visual cortex and other well-studied preparations.

Other experiments worth doing are the reproduction of these result in the monkey which could sustain attention for a long period, and also the study of the SC dynamics during the

buildup discharge preceding a gaze movement. Indeed, attention could be involved in the increase of excitatory input and in the recruitment of local inhibitory interneurons, leading to synchrony, selection, and learning.

The high rate of synchrony occurrence between neighboring cells, the time lag of 0 ms between the two spike trains, and the narrow width of the CCH peaks are in favor of a local process that would synchronize the network repetitively. However, we were unable to prove conclusively that synchrony in the SC is an emergent and local phenomenon, as was the case in our simulated network. Simultaneous recordings in the visual cortex and in the SC could be a means of showing that collicular synchrony is the product of a common cortical input. But the recent developments of *in vivo* experiments in collicular slices (Pettit at al., 1999) should allow direct testing of the local network abilities to synchronize. Such quantification of the cellular dynamics would be also very helpful to simulate the SC system with the help of spiking neurons rather than with traditional mathematical components.

2. Applied Prospects

In the perspective of applied research, this work has wide implications in the fields of computational science and in medical research on epilepsy.

Once founded, the hypotheses of timed neuronal selection and of information propagation in synfire chains could transform the temporal pattern processing in voice recognition systems, motion analysis, meteorology, financial forecasts,… Temporal coding justifies the discretization of continuous data flows, their parallel processing, the local learning rules, and the repetitive selection of the most salient features in order to reduce the data complexity. Although none of these principles are new, the temporal binding theory allows their simultaneous implementation in a parallel network.

When I started my research in neurophysiology, I was “attracted” by the dynamic analysis of epileptic focus (Lopes da Silva et al., 1994), and the attempts made to control the network by electrical stimulation (Durand 1986; Kayyali and Durand, 1991; Durand and Warman 1994; Schiff et al., 1994; Jerger and Schiff, 1995). As other time series, the electroencephalogram could be analyzed to predict the occurrence of seizures. Then, it could have seemed paradoxical to propose a treatment based on electrical stimulation as electrical stimulations themselves can induce epileptic seizures. It would have seemed related to the archaic principle of similarity in the first pharmacopoeia where drugs producing determined

symptoms in healthy people were proposed to cure patients presenting the same symptoms. This was fanciful demagogy. Here, the proposition is based on two "scientific" ideas.

The first idea is the possible prediction of the network activity and the influence of small electrical stimulation on its dynamics. The question to be answered is whether or not the dynamics could be driven into a non-oscillatory state, exactly as some oscillatory systems are driven into a chaotic state with help of precise small perturbations (Schall et al, 1994). This point could gain deep insight from models of cortical networks. The recent demonstration of the cortical origin of spike-wave complexes makes these models even more valuable (Steriade and Contreras, 1998, Steriade et al., 1998; Neckelman et al., 1998; Timofeev et al., 1998).

The second idea is related to the network simulation we performed. We showed that a broad excitation is able to recruit specifically the inhibitory cells when they have a lower firing threshold than the excitatory population. It could be interesting to study this phenomenon in brain slices with arrays of low impedance electrodes. If specific stimulation of the inhibitory cells can be achieved in brain tissue, it could also be proposed when a seizure is predicted. This technique would be complementary to the traditional medical treatment which would be tailored to ensure that inhibitory cells indeed respond faster than excitatory cells to a widely distributed excitation.

REFERENCES

Durand D (1986) Electrical stimulation can inhibit synchronized neuronal activity. *Brain Res.* 382:139-144.

Durand DM, Warman EN (1994) Desynchronization of epileptiform activity by extracellular current pulses in rat hippocampal slices. *J. Physiol.* 480:527-537.

Jerger K, Schiff SJ (1995) Periodic pacing an in vitro epileptic focus. *J. Neurophysiol.* 73:876-879.

Kayyali H, Durand D (1991) Effects of applied currents on epileptiform bursts *in vitro*. *Exp. Neurol.* 113:249-254.

Lopes da Silva FHL, Pijn JP, Wadman WJ (1994) Dynamics of local neuronal networks: control parameters and state bifurcations in epileptogenesis. *Prog. Brain Res.* 102:359-370.

Neckelmann D, Amzica F, Steriade M (1998) Spike-wave complexes and fast components of cortically generated seizures. III. Synchronizing mechanisms. *J. Neurophysiol.* 80:1480-1494.

Schiff SJ, Jerger K, Duong DH, Chang T, Spano ML, Ditto WL (1994) Controlling chaos in the brain. *Nature* 370:615-620.

Steriade M, Amzica F, Neckelmann D, Timofeev I (1998) Spike-wave complexes and fast components of cortically generated seizures. II. Extra- and intracellular patterns. *J. Neurophysiol.* 80:1456-1479.

Steriade M, Contreras D (1998) Spike-wave complexes and fast components of cortically generated seizures. I. Role of neocortex and thalamus. *J. Neurophysiol.* 80:1439-1455.

Timofeev I, Grenier F, Steriade M (1998) Spike-wave complexes and fast components of cortically generated seizures. IV. Paroxysmal fast runs in cortical and thalamic neurons. *J. Neurophysiol.* 80:1495-1513.

INDEX

N

O

P

R

S

T

U

V

W

X